POWDER PRODUCTION IN AEROSOL REACTORS: PARTICLE STRUCTURE AND REACTOR OPTIMIZATION

Thesis by

Hung Viet Nguyen

In Partial Fulfillment of the Requirements

for the Degree of

Doctor of Philosophy

California Institute of Technology

Pasadena, California

1990

Submitted December 21, 1989

In memory of my grandmother and to my parents.

ACKNOWLEDGEMENTS

I would like to thank my advisor Dr. Richard C. Flagan. His guidance, unmatched physical insight, support, and encouragement will always be remembered. He, more than anyone else, has instilled in me the importance of "quality" versus "quantity" research.

I am deeply grateful to Dr. John Seinfeld and Dr. Manfred Morari for the helpful discussions about the optimization work. It was always fun and stimulating to discuss with Dr. William Johnson about phase transition and surface roughing. The advice of Dr. Kikuo Okuyama (University of Osaka Prefecture) during our collaboration are much appreciated. I am thankful to Dr. Arijit Bose (University of Rhode Island) for introducing me to the excitement of doing research, and for his continued moral support and friendship.

The financial support of the Caltech's Program in Advanced Technology and the National Science Foundation are gratefully acknowledged.

My thanks also go to Joe Fontana and Rich Eastvedt for their assistance in making experimental parts; Carol Garland for helping me with the TEM analysis; Rayma Harrison and Gunilla Hastrup for being such nice librarians; Joan Mathews, Elaine Granger, and Sandy Brooks for putting up with my petty nuisances; Melinda Hendrix-Werts and Evelina Cui for always doing their secretarial work with a smile.

It was a pleasure working with so many bright people in the lab – Mark Cohen, Gidi Sageev Grader, Dale Warren, Carol Jones, Jennifer Stern, Sonia Kreidenweis-Dandy, Yiannis Levendis, Ranajit Sahu, Brian Wong, Steve Rogak, Barbara Wylouzil. Chak Chan, Xiaoming Li, and Ken Wolfenbarger. The technical discussions and

daily joking around were fun and exciting. Thanks to Ken Wolfenbarger for his help with the DMA inversions and optimization work. The collaboration with Steve Rogak was fruitful and enjoyable. Shih-Chen Wang was a wonderful officemate, colleague, and friend. Thanks to her for providing the SEMS software, which was a big help in obtaining fast DMA data. I am particularly grateful to Jin Jwang Wu, a brilliant colleague and a dear friend. She helped me familiarized with Caltech and comforted me in many troubled times. Collaborating with her was very educating and productive.

The activities with the Vietnamese Student Association at Caltech made my stay here a more memorable one. The guitar and singing sessions on friday nights with the gang were great fun. Singing in the Vietnamese choir in Gardena was spiritually up-lifting. The choir members are fun and enjoyable.

The many ups and downs that Chris Guske and I shared together as room-mates in my first four years at Caltech have made us very special friends. Life at Caltech would be much less colorful without Chris. Thu Pham was a super room-mate during my last year at Caltech and continues to be a dear friend. The philosophical discussions with him have always been stimulating. An added benefit of coming to California was meeting Anh Hoan. He has educated me about the many valuable aspects of life not taught in the campus environment. The support of ThienNga and her family, especially during my final months of thesis writing, is deeply appreciated.

Finally, and most importantly, I would like to thank my family. The love and support of my parents and late grandmother are immeasurable. It is to them that I dedicate this thesis. Trang, Loan, Dung, Cuong, and Ben – Thanks for being wonderful sisters and brothers, and for bearing the burdens during hardtimes!

ABSTRACT

Powders consisting of dense, nonagglomerated, roughly spherical particles with a controlled size distribution are thought to be ideal for engineering applications of ceramic materials. The production of such powders in aerosol reactors is difficult due to the extreme difficulty of controlling particle formation by homogeneous nucleation of condensible vapors produced by gas phase chemical reactions. To generate the quality of powders necessary for engineering applications, one needs to understand the processes governing particle formation and growth in aerosol reactors.

Homogeneous and heterogeneous nucleation were studied in a laminar flow aerosol generator using dibutylphthalate vapor. Seed particles were found to suppress homogeneous nucleation to an extent depending on their concentration. With additional insights on nucleation and nucleation suppression, aerosol physics was applied to an effort to generate dense, spherical silicon particles in a single stage multi-zone externally heated aerosol reactor. Subsequent experiments revealed that the dense silicon particles generated resulted from the sintering of aggregates formed by coagulation of like-sized particles. While the production of dense particles by sintering of low density agglomerates are feasible for low melting materials, it is not practical for refractory materials due to the high sintering temperatures required for complete coalescence in the available residence time. To produce ideal refractory powder materials, growth must be limited to vapor and small cluster deposition. An optimization technique was applied to the highly nonlinear aerosol reactor system to directly derive optimal temperature profiles that maximizes seed growth while minimizing the amount of fine particles formed.

TABLE OF CONTENTS

LIST OF FIGURES

CHAPTER 2

CHAPTER 3

CHAPTER 4

LIST OF TABLES

CHAPTER 4

CHAPTER 1

INTRODUCTION

Engineering applications of ceramic materials are generally limited because of their unpredictable failures. The ultimate strength of ceramic materials is directly related to the flaws formed during fabrication, which can frequently be traced back to the basic building blocks, the starting powders (1). Large, dense particles tend to form green compacts with a small number of large pores. Powders containing low density agglomerates generate yet even larger pores and more inhomogeneity in the pore distribution in the green compact than dense, nonagglomerated particles of the same structure size. These large pores and nonuniformity in the pore distribution are a major cause of the lack of reproducibility of the structural properties of ceramic parts. Furthermore, large pores lead to long sintering times for complete densification. If the pores are too big, complete densification of the compact may not be feasible. Residual pores then become points of origins of cracks, causing failure of the part at stress levels far below those predicted for a homogeneous material.

Small particles result in smaller pore sizes in the green compact. However, handling of ultrafine particles is very difficult and expensive. Moreover, the high surface area to volume ratio of ultrafine particles makes them highly susceptible to surface contamination. Powders consisting of solid, roughly equiaxed, nonagglomerated, submicron particles with controlled size distribution are thought to be ideal for the formation of uniform, high density green compacts of ceramics and other powder based materials (1).

For these reasons, considerable efforts have been concentrated on the synthesis of ideal ceramic powders. A variety of process have been developed to generate such powders. Colloidal processes produce highly uniform, nonagglomerated particles, but the range of composition is limited to metal oxides (2,3). Here, the interparticle

forces can be manipulated, e.g., coulombic or steric repulsion, to retard agglomerate formation. Aerosol routes can be used to produce a wider range of powders than is possible with current colloidal processing techniques, but control of particle structure is much more difficult. Reasonably uniform silicon, silicon nitride, and silicon carbide have been generated by laser induced chemical reactions (4,5). Oxide particles have been produced by the vapor phase oxidation of metal halides (6-8). High quality silicon powders have been obtained from the pyrolysis of silane in an externally heated aerosol reactor (9). Silicon nitride have been produced by the reaction of silane and ammonia in a heated tube (10).

The use of gaseous precursors is particularly promising because virtually any material that can be deposited by chemical vapor deposition (CVD) can be produced by this method. Gas phase chemical reactions of these precursors generate condesible vapors. High supersaturations are readily achieved due to the low saturation vapor pressure of ceramic materials, and particles are formed by homogeneous nucleation in large numbers. These particles then grow by vapor deposition (condensation and surface reaction), cluster deposition, and coagulation with large clusters and like-sized particles. Growth by vapor and cluster deposition results in dense, nonagglomerated particles. Growth by coagulation produces low density flocs. These agglomerates can be sintered to densification if the temperature is sufficiently high. Thus, dense particles can be produced by vapor and cluster deposition and by sintering of aggregates to complete coalescence. The latter approach is not practical for refractory materials due to the very high temperatures required to achieve complete coalescence within the residence time available in aerosol reactors.

Homogeneous nucleation generally leads to the formation of high number concentrations of particles, which inevitablly leads to growth by coagulation. Since

coagulation is a second order process, the number concentration must be reduced to minimize its effects. Seed particles can be used to suppress the formation of new particles by homogeneous nucleation. They act as a source scavenging the condensible vapors, and thus, reducing the potential for homogeneous nucleation. To produce dense, nonagglomerated particles, these seeds must exist in low number concentration and grow by vapor and cluster deposition without further ge neration of particles by homogeneous nucleation.

Alam and Flagan (11) have shown that seed particles can be grown to supermicron sizes at constant apparent input-ouput number concentration, i.e., the number concentration at the reactor outlet is the same as that of seeds at the reactor inlet. Growth of large from small silicon seed particles was achieved by manipulating the rate of silane pyrolysis. Subsequent investigation revealed that the particles produced were low density aggregates, indicating growth by deposition of clusters too large to sinter completely before additional deposition took place. Wu et al. (12) have shown that the transition from successful seed growth at constant apparent input-ouput number concentration to runaway nucleation leading to high number concentrations at the reactor outlet is very sharp. The ability of the seed particles to suppress homogeneous nucleation depends on both their number concentration and size. Orders of magnitude change in the measured number concentration can result from a small change in the reactant concentration at a given set of operating conditions (12).

Dense, spherical silicon particles have been generated by Wu et al. (9) in a single stage, multizone, externally heated aerosol reactor. However, the mechanism of dense particle formation in their experiment was not known. Analysis indicates that growth of particles in those experiments was influenced by both vapor and clus-

ter deposition and coagulation of like-sized particles. The dense particles obtained may have resulted from the sintering of low density agglomerates formed earlier in the reactor because of the high peak temperature used in the final zone.

The goal of this thesis was to elucidate the growth and densification mechanism typical in externally heated aerosol reactor, and to develop methods to directly determine the control stategies, i.e., the operating conditions, that will produce dense, nonagglomerated particles.

To achieve this, we first took a step back and studied a much simpler system than material producing aerosol reactors to gain additional insight on nucleation and the role of seed to suppress homogeneous nucleation. In this work, described in Chapter 2, nitrogen gas saturated with dibutylphthalate (DBP) vapor at high temperature was cooled rapidly in a laminar flow aerosol generator (LFAG). Upon cooling, the DBP vapor became supersaturated and particles were formed by homogeneous nucleation. The effects of the saturation temperature, and thus initial vapor concentration, and the concentration and size of the NaCl seed particles on nucleation were studied.

With increased understanding on nucleation, we then applied aerosol physics principles to the generation of powder materials by gas phase chemical reactions. The production of dense silicon particles (Wu et al. (9), Appendix A) showed promise for the use of single stage, multizone, externally heated aerosol reactors to produce ideal refractory powder materials. However, it raised questions regarding the mechanism of dense particle formation. As mentioned earlier, dense particles can result from both vapor and small cluster deposition and sintering of low density agglomerates. The latter is not practical due to the high temperatures required to sinter refractory materials in residence times available in aerosol reactors. The

generation of dense, nonagglomerated refractory powder materials using a single stage aerosol reactor is practical only with the former mechanism of dense particle formation. It is, therefore, critical that the mechanism of growth and densification occuring in the experiments of Wu et al. (9) be determined. Chapter 3 is devoted to the discussion of experiments and model simulations performed for this purpose.

Finally, it was determined that the most viable means of dense particle production is the use of seed particles. As Wu et al. (12) have shown, control of nucleation is very difficult, and the transition from successful seed growth to runaway nucleation is very abrupt. Their experiments and those of Alam and Flagan (11) indicate that growth of seed particles at constant apparent input-ouput number concentration is necessary but not sufficient for dense particle production. The number concentration of clusters too large to completely sinter before additional deposition takes place must be limited to grow fully dense particles. Alternatives from qualitative recipes are needed to define the reactor operating conditions that would achieve this goal. No method has yet been proposed for direct determination of the optimal reactor design to meet these stringent requirements. Chapter 4 discusses a first attempt at applying optimization techniques to highly nonlinear aerosol reactor systems to derive the reaction rate schedule that would produce high quality refractrory powders under constraints of finite reactor volume, throughput, residence time, initial seed size, seed number concentration, and initial reactant concentration.

Studies in collaboration with Wu et al. (12) and Okuyama et al. (13) to evaluate the parameters important in and to determine control approaches that would produce ideal powders are reported in Appendices B and C, respectively.

References

1. Bowen, H.K., *Mater. Sci. Eng.*, 44, 1 (1980).
2. Barringer, E.A., and Bowen, H.K., *Comm. Am. Ceram. Soc.* , C-199 (1982).
3. Gobet, J., and Matejevic, E., *J. Colloid Interface Sci.* , 100, 555 (1984).
4. Cannon, W.R., Danforth, S.C., Flint, J.H., Haggerty, J.S., and Marra, R.A., *J. Am. Ceram. Soc.*, 65, 324 (1982).
5. Cannon, W.R., Danforth, S.C., Haggerty, J.S., and Marra, R.A., *J. Am. Ceram. Soc.*, 65, 330 (1982).
6. Ulrich, G.D., *Combust. Sci. Technol.* , 4, 47 (1971).
7. Ulrich, G.D., Ines, B.A.M., and Subramanian, N.S., *Combust. Sci. Technol.* , 14, 243 (1976).
8. Ulrich, G.D., and Subramanian, N.A., *Combust. Sci. Technol.*, 17, 119 (1977).
9. Wu, J.J, Nguyen, H.V., and Flagan, R.C., *Langmuir* , 3, 266 (1987).
10. Prochazka, S., Greskovich, C., *Am. Ceram. Soc. Bull.*, 57, 579 (1978).
11. Alam, M.K., and Flagan, R.C., *Aerosol Sci. Technol.*, 5, 237 (1986).
12. Wu, J.J., and Flagan, R.C., *J. Appl. Phys.*, 61, 1365 (1987).
13. Okuyama, K., Jeung, J., Kousaka, Y., Nguyen, H.V., Wu, J.J., and Flagan, R.C., *Chem. Eng. Science*, 44[6], 1369 (1989).

CHAPTER 2

HOMOGENEOUS AND HETEROGENEOUS NUCLEATION IN A LAMINAR FLOW AEROSOL GENERATOR

Published in the

J. Colloid Interface Sci.

119(2), 491 (1987)

HOMOGENEOUS AND HETEROGENEOUS NUCLEATION IN A LAMINAR FLOW AEROSOL GENERATOR

Hung V. Nguyen †, Kikuo Okuyama *, Tadaaki Mimura *,
Yasuo Kousaka *, Richard C. Flagan ‡ and John H. Seinfeld †◇

† Department of Chemical Engineering, California Institute of Technology, Pasadena, CA 91125.

* Department of Chemical Engineering, University of Osaka Prefecture, Sakai 591, Japan.

‡ Departmnet of Environmental Engineering Science, California Institute of Technology, Pasadena, CA 91125.

◇ To whom all correspondence should be addressed.

Published in the
J. Colloid Interface Sci.
119(2), 491 (1987)

Abstract

The formation of aerosol particles by homogeneous and heterogeneous nucleation has been studied experimentally using a laminar flow aerosol generator. Dry gas (N_2 or air) saturated with dibutylphthalate (DBP), either particle-free or containing an ultrafine monodisperse aerosol, was cooled well below the saturation temperature causing the highly supersaturated vapor to nucleate. The resulting particle number concentrations were observed under various conditions of the gas stream and properties of the introduced foreign condensation nuclei. The dependence of the nucleation rate on the vapor concentration, cooling rate, and seed aerosol concentration was studied. Comparisons of the measured number concentrations with predictions based on the model of Pesthy et al.(1981) showed good qualitative agreement when the classical homogeneous nucleation rates were enhanced by a factor of 10^5 - 10^7. The laminar flow aerosol generator is found to be a particularly effective system for the study of the influence of foreign particles on the rate of homogeneous nucleation of a vapor.

1. Introduction

Nucleation is the formation of new particles from a continuous phase and can occur heterogeneously and/or homogeneously. Heterogeneous nucleation in a gas can occur on foreign nuclei, such as aerosol particles, ions, or surfaces. Homogeneous nucleation, or self- nucleation, occurs by a vapor depositing on its own clusters or embryos without the presence of foreign substances serving as nucleation sites. The former requires a low degree of supersaturation, whereas, the latter requires much higher supersaturations. Homogeneous nucleation may be effected by cooling a vapor or by producing condensible species via chemical reactions.

Laboratory studies of homogeneous nucleation have been carried out by adiabatic expansion of room temperature vapor-gas mixtures(1-3) and by mixing of high temperature vapor with low temperature gas(4-8). Adiabatic expansion is usually carried out using the Wilson type fog chamber or high velocity nozzle flows. Nucleation by mixing has been done either in a laminar stream or in a laminar or turbulent jet, for which the mixing characteristics must be accurately known in order to theoretically predict the observed mixing rates. For each of these methods, fast and efficient mixing or expansion must be achieved to minimize spatial variation of the supersaturation.

We present in this paper a method for studying homogeneous nucleation using a laminar flow aerosol generator (LFAG) in which hot gas carrying a condensible vapor is cooled rapidly causing the vapor to be highly supersaturated. The advantage of this method over the others that have been used to study nucleation is that, under laminar flow, the mixing characteristics of the system are well characterized. As will be seen, a crucial requirement for effective operation of the LFAG is careful temperature control. A detailed theoretical analysis of aerosol nucleation and

growth in laminar flow was presented by Pesthy et al.(9), and the simulation of aerosol formation can be carried out based on that theory.

The objective of this paper is to evaluate the laminar flow aerosol generator as a means to study the fundamentals of homogeneous and heterogeneous nucleation. High temperature gas saturated with dibutylphthalate (DBP) vapor, either particle-free or containing an ultrafine aerosol, was introduced into the LFAG, and the resulting number concentrations of aerosol particles were measured under various conditions of the gas (temperature and flow rate) and properties of the introduced foreign condensation nuclei (number concentration and size). Dibutylphthalate was chosen as the condensing species because of its high boiling point, low diffusivity and its common use in aerosol generators(10-16). The measured number concentrations and size distributions were compared with those predicted using the theoretical analysis of aerosol nucleation and growth in laminar flow of Pesthy et al.(9).

2. The Laminar Flow Aerosol Generator

Two experimental systems were used to generate aerosol continuously in a well-characterized laminar pipe flow. Initial experiments were conducted at the California Institute of Technology using system A. Based upon the results and experience with this system, an improved version, system B, was constructed at the University of Osaka Prefecture, Japan . The former system was used for homogeneous nucleation experiments, while the latter was also used for studies of heterogeneous nucleation. In both kinds of experiment (homogeneous and heterogenous nucleation), a fully developed laminar pipe flow was subjected to a sudden drop in temperature. Well dried, particle-free carrier gas was passed through a saturator where it left saturated with DBP. It then flowed through the hot zone of the aerosol generator where it was heated to a uniform temperature. The uniform temperature gas then passed through a cooling zone where the supersaturated vapor nucleated. The aerosol flow leaving the cooling zone was introduced into instruments for measurements of the size distribution and number concentration of the generated droplets.

The two experimental systems are illustrated in Fig. 1. The aerosol generators were similar, but system B (Fig. 1(b)) incorporated improvements in the saturator, a seed aerosol preparation system, and the use of an ultramicroscope in addition to the condensation nuclei counter for particle measurements.

In system A, the flow rate of the nitrogen carrier gas was kept constant at 1.25 l/min. The preheater was a 150 cm copper coil heated by a heating tape. With a residence time of about two seconds, the gas was preheated to within two degrees of the temperature of the saturator. The saturator (Fig. 1(a)), based on the design of Okuyama et al.(17), consisted of a 2.54 cm i.d., 33 cm brass tube filled with a 30 cm column of DBP impregnated silica gel. The gas residence time in the saturator was

about four seconds. The temperature of the saturator was varied between 50 and 105 °C to obtain different saturation ratios in the cooling zone. The temperature of the gas leaving the the saturator was measured with a chromel-alumel thermocouple and was controlled to within ±0.6 °C.

The saturator of system B was mounted directly at the top of the aerosol generator, allowing for experiments with the saturator having the same temperatures as that of the hot zone, since vapor condensation in the transport line was eliminated. Figure 2 shows in detail the improved saturator used in system B. The saturator consisted of a 2.90 cm i.d., 30 cm long brass tube, heated by heating tapes, and filled with DBP impregnated silica gel. The preheater consisted of a 390 cm copper coil wrapped around the saturator, so that the gas was preheated to the same temperature as that of the saturator prior to its introduction into the saturator. The carrier gas for these experiments was dried and filtered air. The gas residence time in the saturator was about 4.0 seconds for the flow rate of 1 l/min, and 8.0 seconds for the flow rate of 0.5 l/min. The temperature of the saturator was varied between 70 and 120 °C. A high-performance temperature controller was used to maintain the temperature within ±0.1 °C, and the temperature of the gas leaving the saturator was controlled within ±0.3 °C. Under steady state conditions, the temperatures measured by the 0.1 mm diameter Chromel-Alumel thermocouples at the various positions shown in Fig. 2 were constant within ±0.3 °C.

The coil inside the saturator was used in the heterogeneous nucleation experiments. The seed aerosol was also preheated by flowing through the coil wrapped around the saturator before entering the internal coil. Seed aerosol at the same temperature as that of the vapor was mixed with the vapor at the exit of the saturator.

The laminar flow sections (LFAG) consisted of metal tubes (stainless steel for system A and brass for system B). The dimensions and experimental conditions used in the two systems are summarized in Table 1. The tube in system A was 1.73 cm i.d. and 118 cm long, while that in system B was 1.0 cm i.d. and 132 cm long. The aerosol generators were vertical with the heated inlets at the top to minimize buoyancy induced secondary flows. The hydrodynamic entry lengths were on the order of a few centimeters at the Reynolds numbers of interest($Re \leq 150$). Therefore, fully developed laminar flow was achieved well upstream of the cooling section. The effect of natural convection will be shown in a later section to be small for system A and negligible for system B. The upper hot zones were wrapped with heating tapes using variable spacing to achieve uniform wall temperature. In system B, two tapes were used, one wrapped along the entire pipe and the other wrapped around the lower part of the hot zone, as illustrated in Fig. 1. Electrically insulated Chromel-alumel thermocouples were cemented onto the outer surfaces of the tubes at the positions illustrated in Figures 3(a) and (b) for wall temperature profile measurements. The temperature inside the pipe was measured by inserting a thermocouple as described below.

As illustrated in Fig. 1, cooling was achieved by circulating cold water through a jacket surrounding the flow tube. The temperature of the cooling water was controlled to $\pm 0.3\,^{\circ}C$, and was constant during each run, but was varied between 8 and $25\,^{\circ}C$ in different experiments. Figures 4(a) and (b) show the exits of the laminar flow aerosol generators. System A was designed to extract the aerosol from the center core of the LFAG using a 0.62 cm i.d. brass probe. Aerosol samples were extracted isokinetically (based on the laminar pipe flow velocity profile), so only the aerosol from the central core of the LFAG was measured. A dilution system was used to reduce the number concentration for single particle count measurements.

The number concentations before and after dilution differed by a factor of two or less. Cooled and filtered air was used as dilution gas to avoid evaporation. Due to the low vapor pressure of DBP, evaporation of the aerosol droplets in the size range measured was calculated to be negiligible. The second LFAG was designed to study the entire aerosol flow, so the stream was split into two , one going to the measuring instruments and the other to the exhaust. All measurements with this system were made without dilution. The following particle counting and sizing instruments were used to characterize the DBP aerosol: (i) a TSI 3020 condensation nuclei counter (CNC); (ii) a Royco 226 laser optical particle counter; (iii) a TSI 3030 differential mobility analyzer(DMA); and (iv) an ultramicroscopic sizing apparatus capable of measuring the size distribution of particles larger than 0.3 μm by the sedimentation method.

Figure 5 shows the device used to measure the centerline temperature of the laminar flow section of system B. The device containing a 0.1 mm diameter Chromel-Alumel thermocouple was inserted from the bottom of the cooling zone. In order to minimize the influence of radiation from the wall, the thermocouple was shielded inside a stainless steel tube.

In the homogeneous nucleation experiments, the dry gas flow was set to the desired flow rate, and the temperature of the saturator was increased gradually to the desired value. The temperature of the hot zone of the generator was set so as to avoid premature vapor condensation on the tube wall. In system A, the temperature of the hot zone was kept constant and the temperature of the saturator was varied. In system B, however, the temperature of the hot zone was adjusted to that of the saturator, and both temperatures were altered simultaneously. Once steady state conditions were achieved, the number concentration and size distribution of the homogeneously nucleated DBP particles were measured.

In the heterogeneous condensation experiment, monodisperse NaCl seed particles (with diameters between 0.01 μm and 0.2 μm) were generated by the evaporation-condensation type generator(18) and were classified by the differential mobility analyzer (DMA)(19). The foreign condensation nuclei passed through the preheater pipe and the coil inside the saturator and were mixed with the vapor. The resulting number concentration of the aerosol produced by the combination of heterogeneous and homogeneous nucleation was monitored with the CNC. The particle number concentration generated by homogeneous nucleation in the absence of the seed nuclei was measured by simply setting the high voltage of the DMA to zero. After the temperature of the saturator was lowered to suppress DBP droplet formation by homogeneous nucleation, the number concentration of the seed aerosol was measured by re-introducing the aerosol from the DMA into the LFAG.

3. Experimental Results

3.1 Temperature Profiles

The influence of free convection on the laminar pipe flow will first be considered. The different flow regimes, forced convection, free convection, and mixed flow, depend on the values the Reynolds number ($Re = \bar{u}D\rho/\mu$), the Grashof number ($Gr = D^3\beta\rho^2 g(T_o - T_{wf})/\mu^2$), and the Prandtl number ($Pr = \hat{C}_p\mu/k'$). As Re is increased, force convection becomes dominant over free convection; whereas, free convection effects increase with the increase of the product of Gr and Pr. Evaluation using the physical properties of gas at 100 °C ($\rho = 0.946$ kg/m^3, $\mu = 2.176 \times 10^{-5}$ kg/m s, $k' = 0.0321$ J/m s, $C_p = 1.011 \times 10^3$ J/kg K) gives $Pr = 0.69$. With $T_o = 120$ °C, $T_{wf} = 20$ °C, $Q = 1.25$ l/min and $L = 30$ cm, system A was operating at $Gr = 3.37 \times 10^4$, $GrPr(D/L) = 1325$, and $Re = 137$. The correlations of Metais and Eckert(20) place this system in the mixed laminar flow regime where the buoyancy force influenced, but did not dominate, the flow. System B, with a smaller pipe diameter, Re = 54 for 0.5 l/min and 104 for 1 l/min, and Gr = 5993, GrPr(D/L) = 140 corresponding to $T_o = 100$ °C, $T_{wf} = 20$ °C, and L = 30 cm, operated in the forced convection dominant regime.

Figures 6(a) to (c) show typical steady state axial temperature profiles of the hot and cooling zones achieved after about three hours of operation. Both the wall and centerline temperatures are shown for system B. As can be seen, the hot zone temperature was kept very uniform. The wall temperature dropped rapidly to that of the cooling water at about 5 cm below the water level. The reproducibility of the aerosol generator temperature profile at different saturator temperatures was found to be very good. As expected, the centerline temperature of the gas decreased more slowly than that of the wall. This difference is more pronounced with larger flow

rates. Also shown in Figures 6(b) and (c) are the centerline temperature profiles predicted by solving the basic laminar flow energy equation(9), which were found to agree, within experimental error, with the measured ones. In the calculation, the wall temperature profiles were approximated by a third order cubic spline function.

3.2 Homogeneous Nucleation

The influence of the partial pressure of the vapor exiting the saturator was first studied in the particle-free experiments. In system A, keeping the hot zone temperature, T_1, constant, the temperature of the saturator, T_s, was increased, thereby increasing the partial pressure of the DBP vapor. In system B, the hot zone temperature was adjusted to that of the saturator. Figure 7 shows how the saturation mole fraction of DBP varies with temperature. The range of the saturator temperatures used in the LFAG experiments provided more than an order of magnitude variation in the amount of vapor available for nucleation and growth.

The number concentrations of the DBP droplets produced by homogeneous nucleation, N_{Jo}, are shown as a function of the saturator temperature in Fig. 8 for system A and Fig. 9 for system B. The black circles in Fig. 8 represent the measured number concentrations at the center core. The solid and broken lines show the centerline and tube average results, respectively, from the simulation corresponding to the experimental conditions using Pesthy's model(17) with classical nucleation rate enhancement factors, E_J, of 10^5 and 10^7. The open and darkened circles and squares in Fig. 9 are experimental data obtained with system B for two different flow rates and cooling water temperatures. The curves represent the simulation results corresponding to the experimental conditions indicated by the arrows. Also shown are the predictions of the Lothe-Pound and the nonenhanced classical nucleation theories(21). Results from system A show that the final center

core number concentration increased only slightly with increasing saturator temperature for $T_s \leq 86\,^{\circ}C$, rose sharply as T_s was raised to about $92\,^{\circ}C$, and then levelled off for $T_s \geq 92\,^{\circ}C$. The predictions using classical nucleation theory track very well the observed sharp rise and the levelling off in the final number concentration with increasing saturator temperature, but do not show the plateau observed for $T_s \leq 86\,^{\circ}C$. The experimental data fall between the predicted centerline and the tube average number concentrations, with the classical nucleation rates enhanced by a factor of 10^5. Results from system B (Fig. 9) show that the final tube average number concentration increased monotonically with increasing saturator temperature, T_s. As shown in Fig. 9, N_{J_o} increased only slightly with a factor of two increase in the total gas flow rate, while increases of two to three orders of magnitude resulted when the cooling water temperature was reduced from 21 to $9\,^{\circ}C$. This behavior is expected since a lower cooling water temperature results in a higher supersaturation, and homogeneous nucleation is extremely sensitive to the degree of supersaturation (expressed in terms of the saturation ratio, S). The model using enhanced classical nucleation rates predicts well the rising trends in the number concentration with increasing saturator temperature. The simulations again show that the average number concentration levels off at higher saturator temperatures, which, however, was not observed in system B for the conditions studied. Despite the differences between systems A and B, the results for comparable cooling water and saturator temperatures are in good agreement.

The histograms in Figures 10(a) and (b) represent the raw center core volume distributions, for saturator temperatures of 85.2 and $104.6\,^{\circ}C$ respectively, obtained from system A in the particle-free experiments with a Royco 226 laser optical particle counter. The dashed curves are plots of the simulated tube average distributions corresponding to the same experimental conditions and $E_J = 10^5$. It appears that

the predicted mass mean particle diameters are larger than the experimental ones, although calulations show that evaporation of the droplets in the size range measured is negligible due to the low vapor pressure of DBP. While the mass mean diameter changed negligibly, the number concentration jumped four orders of magnitude, from 55 to 1.6×10^5 cm^{-3}, as T_s was raised from 85.2 to 104.6 °C. Figures 11(a) and (b) present the tube average number size distributions, for $T_s = T_l$ of 102 and 80.5 °C, respectively, from system B. The points depict the experimental data and the smooth curves the simulation results with the indicated enhancement factors for the classical homogeneous nucleation rates. Again, there was essentially no change in the mean diameter corresponding to almost two orders of magnitude change in the number concentration. We see that the model results, with the aforementioned enhancement factors, agree closely with those observed experimentally. The mass fraction of DBP in the aerosol phase was found to vary from only a fraction of a percent at low T_s to about 40% at high T_s, with most of the DBP lost to the tube wall. This means that at high enough saturator temperatures, there was sufficient DBP to allow rapid growth of the many nucleated particles to the final sizes before the vapor had a chance to diffuse to the wall.

3.3 Heterogeneous Nucleation

Figures 12(a) to (c) show the total number concentration of particles resulting from homogeneous and heterogeneous nucleation, N_f, in the LFAG as a function of the number concentration of the NaCl seed particles, N_i. Curves corresponding to the total number concentrations assuming that homogeneous and heterogeneous nucleation took place independently are labeled $N_{Jo} + N_i$. The figures correspond to three cases in which, N_{Jo}, the number concentration produced by homogeneous nucleation in the absence of seed particles at the given conditions, was 1.05×10^5,

2.95×10^4, and 8.43×10^3 cm^{-3} respectively. The circles, squares, and triangles are measured experimental results. The singly dashed curves represent the simulation data using the enhancement factors, E_J, that were obtained by matching the homogeneous nucleation rates to fit the observed number of particles generated in the absence of seed nuclei at the same saturator and cooling water temperatures. The seed sizes used were 10.2, 43.3, and 185.5 nm. We see that homogeneous nucleation was suppressed by the introduction of the condensation nuclei at concentrations exceeding about 10^3 cm^{-3}. The size of the seed nuclei, for the range studied, however, did not have any effect on suppressing homogeneous nucleation. This is reasonable since the amount of vapor required for the seed paricles to grow from 10.2 to 185.5 nm is negligible compared to that required to grow the particles to the final sizes which were greater than 1 μm. Thus, the number concentration of the seed nuclei is the critical factor in suppressing homogeous nucleation. This fact can be seen more clearly from Table 3 which presents the simulated results ($2z/D\,Pe = 400$, z is the axial distance beginning at the point where the wall temperature begins to drop) for a seeded experiment, including the fractions of vapor lost to the wall, to the initial seeds, and to the homogeneously nucleated particles. We see that at a seed concentration of 1000 cm^{-3}, only 1.9% of the total vapor is predicted to be scavenged by the seed aerosol, and 7.7% by the homogeneously nucleated particles. Whereas, at $N_i = 1.7 \times 10^4 cm^{-3}$, the fraction of vapor predicted to be taken up by the seed is 24.3% and that by the homogeneously nucleated particles is only 0.1%, indicating almost complete suppression of homogeneous nucleation. Figure 13 shows the experimental and the corresponding predicted ratio of the final number concentration, N_f, to the sum of the initial seed concentration, N_i, and the number concentration, N_{Jo}, produced by homogeneous nucleation in the absence of seed nuclei as a function of the ratio N_i/N_{Jo}. Those values of $N_f/(N_i + N_{Jo})$ that

are less than unity indicate the suppression of homogeneous nucleation in terms of total number concentration due to the initial aerosol. The suppression is shown to be negligible for values of N_i/N_{J_o} much less than unity. The maximum percentage suppression in total number concentration occurred at those N_i/N_{J_o} in the range between 0.4 to 1.4, $(N_i/N_{J_o})_{max}$ decreasing with increasing N_{J_o}, for the cases studied. It is clear that with the enhancement factors used, the model overpredicts the degree of suppression.

4. Discussion

To understand the various processes that take place in the LFAG, we need to follow the gas stream as it is cooled. As the vapor-gas mixture enters the cooling zone, its temperature begins to drop with the coldest temperature at the wall. Vapor molecules near the wall diffuse to and condense on the cold surface. Concurrently the saturation ratio ($S = P_v/P_{sat}(T)$) increases throughout the entire cross section of the tube. Initially the maximum supersaturation occurs in the immediate vicinity of the wall. When a sufficiently high saturation ratio is reached, particles form by homogeneous nucleation and begin scavenging and competing for vapor to grow. As the vapor is depleted by the tube wall and the particles, the maximum saturation ratio begins to propagate away from the wall toward the center of the pipe, where the vapor content is still high while the temperature falls continuously to that at the wall. If there is a large amount of vapor available, particles would be generated at a high rate due to the high supersaturation achieved. The homogeneously nucleated particles quickly deplete the vapor as they grow and, with the additional vapor loss to the wall, eventually stop further nucleation. If there is very little vapor, the saturation ratio would be too low for significant nucleation to occur and most of the vapor is lost to the wall. The saturation ratio, therefore, increases axially to a maximum value and then decreases steadily due to the depletion of the vapor. It is reasonable that at sufficiently high vapor content, the large number of particles formed, together with the wall, can quickly quench nucleation, so that the net increase in the final number concentration becomes smaller with increasing initial vapor content.

The role of the seed particles is to reduce the vapor content in the gas before a high saturation ratio can be achieved. At low seed number concentrations, only a small amount of vapor is quickly scavenged by the seed in their growth to their

final sizes. Therefore, nucleation is quenched mainly by the wall and the seed nuclei, and by the wall and the homogeneously nucleated particles for low and high initial vapor content, respectively. At high seed concentrations, the seed nuclei immediately deplete a large amount of vapor, and nucleation is quenched by the initial seed particles and the cold wall.

The above described physical picture is supported, for the most part, by the simulation and experimental results. As observed in system A, the final number concentration increased sharply with increasing saturator temperature, i.e., initial vapor content, and levelled off at higher saturator temperatures confirming the quick depletion of the vapor by the nucleated particles. The results from system B also confirm the increase in the number concentration with increasing initial vapor content. The essentially negligible changes in the volume and size distributions with large changes in the number concentration attest to the ability of the particles to compete with the wall and quickly scavenge sufficient vapor to grow. However, the plateau for $T_s \leq 86\,^{\circ}C$ observed in system A and the continual steep increase in the number concentration at high saturator temperatures observed in system B are not reproduced by the simulations. It is seen that the number concentration of the particles produced by homogeneous nucleation changed very little with changes in the total flow rate keeping other parameters constant. Increases in the flow rate at a given saturator temperature only increase the total amount of vapor and not the degree of saturation. Fig. 13 shows that the temperature profiles at the two flow rates studied coincide when plotted in dimensionless units. It is reasonable, therefore, to expect similar number concentrations to be produced, with a higher total number of particles at a higher flow rate.

As shown by the heterogeneous nucleation experiments, suppression of homogeneous nucleation can be achieved by introducing seed particles into the LFAG.

The degree of suppression is higher at higher initial saturation of the gas leaving the saturator, $x_{A\circ}$ (higher saturator temperature), and thus higher homogeneous nucleation rate in the absence of seed particles. This is because vapor is being depleted faster by the seed nuclei at higher $x_{A\circ}$. This depletion reduces the saturation ratio thereby reducing the homogeneous nucleation rate. Since the reduction in the saturation ratio is higher at higher initial saturation, the suppression in the number concentration is correspondingly higher. Calculations using Pesthy's model show that 12.4% of the vapor still remains in the gas phase ($2z/D\,Pe = 400$) for $x_{A\circ} = 2.57 \times 10^{-5}$ and only 6.8% for $x_{A\circ} = 4.52 \times 10^{-5}$ at a total flow rate of 1 l/min and seed number concentration of 10^3 cm^{-3}. The percentage of vapor lost to the wall is about the same for the two cases. We see that the nucleation rate may be higher at a higher initial saturation, but the time for nucleation may actually be less in the laminar flow aerosol generator. This is in contrast to that observed by Warren et al.(8) in a mixing type system.

The overprediction of the suppression by the model, when the values of E_J obtained by matching the homogeneous nucleation rates to the observed number concentrations were used, is believed to be due to the following reasons. When supersaturated vapor condenses on a foreign particle whose substance is different from that of the vapor, the interactions between the vapor and the particle surface become important. Experiments by Kousaka et al.(22) had shown that higher supersaturation than that calculated from the Kelvin effect was required to activate heterogeneous nucleation of DBP on NaCl particles. The simulation did not take into account this effect. Also, the presence of the seed particles may affect the values of the enhancement factor.

Although the method used to achieve supersaturation in the previous DBP nucleation experiments using the particle size magnifier (PSM)(6-8) is different

from that used in the LFAG experiments, enhancement factors of approximately 10^7 over the classical nucleation rates were also found to be necessary to explain experimental observations. In the PSM experiments, the highly supersaturated atmosphere is formed instantaneously due to the rapid mixing of the hot and the cold gas streams. Homogeneous nucleation occurs quickly without the loss of vapor to the walls, and cannot be appreciably suppressed by the introduction of seed particles. Supersaturation in the LFAG is, on the other hand, gradually achieved by cooling the tube wall. Loss of vapor to the wall can be large, and the introduction of seed nuclei, in this case, can effectively suppress homogeneous nucleation. It is believed, therefore, that the PSM is more suitable for studying homogeneous nucleation and the LFAG for studying heterogeneous nucleation. Since both nucleation phenomena occur in real systems, research using both the PSM and the LFAG will be fruitful.

The fact that the observed homogeneous nucleation rates of DBP in several systems exceed those predicted on the basis of classical theory is no doubt due to weaknesses of the classical theory in describing DBP nucleation. In a broader sense, the resolution of theoretical predictions and experimental observations of nucleation rates represents a major unsolved problem in aerosol science.

5. Conclusion

Homogeneous and heterogeneous nucleation of aerosol particles in a laminar flow aerosol generator (LFAG) has been studied experimentally using two different systems. The behavior of the LFAG using DBP vapor can be explained using a model developed by Pesthy et al.(9). Experimental results are quite consistent with those predicted using the classical theory of homogeneous nucleation when the rates are enhanced by a factor of $10^5 - 10^7$. The particle number concentration can increase by orders of magnitude due to only a several percent increase in the vapor concentration. The mean size of the droplets produced does not change significantly with a correspondingly large increase in the particle number concentration, in the systems and for the conditions studied, because the particles produced by homogeneous nucleation can quickly scavenge sufficient vapor to grow to their final sizes. The introduction of seed particles into the LFAG can decrease the homogeneous nucleation rate to an extent depending on the seed particle concentration. The suppression due to the seed particles is found to be higher the higher the homogeneous nucleation rate in the absence of seed nuclei. Seed particle size in the range between 0.01 and 0.2 μm does not have any effect on the suppression of homogeneous nucleation. The LFAG can be used, especially if the dominant wall loss effects are minimized, to further understand the vapor scavenging ability of seed particles in suppressing homogeneous nucleation and to study the applicability of various nucleation theories.

Acknowledgment

This work was supported by National Science Foundation Grant ATM-8503103 and Japan Grant-in-Aid for Environmental Science.

6. Literature cited

1. Allen, L. B. and Kessner, Jr. J. L., *J. Colloid Interface Sci.*, 30, 81 (1968).
2. Wagner, P. E. and Strey, R., *J. Phys. Chem.*, 85, 2694 (1981).
3. Wilson, C.T.R., *Phil. Trans.*, 189, 265 (1987).
4. Anisimov, M. P. and Cherevko, A.G., *J. Aerosol Sci.*, 16, 97 (1985).
5. Higuchi, W. I. and O'Konski, C. T., *J. Colloid Interface Sci.*, 15, 14 (1960).
6. Okuyama, K., Kousaka, Y. Warren, D. R., Flagan, R. C. and Seinfeld, J. H., *Aerosol Sci. Technol.*, in press (1986).
7. Rybin, E. N., Pankratova, M. E., and Kogan, Y. I., *Russ. J. Phys. Chem.*, 51, 617 (1977).
8. Warren, D. R., Okuyama, K., Kousaka, Y., Seinfeld, J. H. and Flagan, R. C., *J. Colloid Interface Sci.*, in press (1986).
9. Pesthy, A. J., Flagan, R. C. and Seinfeld, J. H., *J. Colloid Interface Sci.*, 91, 525 (1983).
10. Chang, R. and Davis, E. J., *J. Colloid Interface Sci.*, 54, 352 (1976).
11. Davis, E. J. and Liao, S. C., *J. Colloid Interface Sci.*, 50, 448 (1975).
12. La Mer, V. K., Inn, E. C. Y. and Wilson, I. B., *J. Colloid Interface Sci.*, 30, 81 (1968).
13. Nicolaon, G., Cooke, D. D., Kerker, M. and Matijevic, E., *J. Colloid Interface Sci.*, 34, 534 (1970).
14. Nicolaon, G., Cooke, D. D., Davis, E. J., Kerker, M. and Matijevic, E. *J. Colloid Interface Sci.*, 35, 490 (1971).

15. Nicolaon, G., Kerker, M., Cooke, D. D. and Matijevic, E., *J. Colloid Interface Sci.,* 38, 460 (1972).

16. Nicolaon, G. and Kerker, M., *J. Colloid Interface Sci.*, 43, 246 (1973).

17. Okuyama, K., Kousaka, Y. and Motouchi, T., *Aerosol Sci. Technol.*, 3, 353 (1984).

18. Kousaka, Y., Niida, T., Okuyama, K. and Tanaka, H., *J. Aerosol Sci.*, 12, 231 (1982).

19. Knutson, E.O., and Whitby, K.T., *J. Aerosol Sci.*, 6, 443 (1975).

20. Metais, B. and Eckert, E. R. G., *Transactions of the ASME, J. Heat Transfer, Ser. C*, 86, 295 (1964).

21. Springer, G. S., in "Advances in Heat Transfer" (T. F. Irvine and J. P. Harnett, Eds.), Vol. 14, pp. 281-346. Academic Press, New York, 1978.

22. Kousaka, Y., Okuyama, K., Niida, T., Hosokawa, T. and Mimura, T., *Paraticle Characterization*, 2, 119 (1985).

Figure Captions

1. Schematic diagram of experimental apparatus.
   (a) System A.
   (b) System B.
2. Saturator of system B.

3(a). Sampling and dilution in system A.

3(b). Sampling in system B.

4(a). Measured wall temperature profile ($T_s = 105\,^{\circ}C$, $T_l = 120\,^{\circ}C$, $T_{wf} = 19.5\,^{\circ}C$, $Q = 1.25\ l\,min^{-1}$) (system A).

4(b). Measured and calculated temperature profiles ($T_s = T_l = 99.6\,^{\circ}C$, $T_{wf} = 22.8\,^{\circ}C$, $Q = 0.5\ l\,min^{-1}$) (system B).

4(c). Measured and calculated temperature profiles ($T_s = T_l = 99.5\,^{\circ}C$, $T_{wf} = 23.7\,^{\circ}C$, $Q = 1.0\ l\,min^{-1}$) (system B).

5. Measured and predicted center core and predicted tube average aerosol number concentrations generated in system A by homogeneous nucleation in the absence of seed aerosol ($T_l = 120\,^{\circ}C$, $T_{wf} = 20\,^{\circ}C$, $Q = 1.25\ l\,min^{-1}$).
6. Measured and simulated tube average number concentrations of aerosol generated in system B by homogeneous nucleation in the absence of seed aerosol (J_{LP} and J_{CL} denoting the Lothe-Pound and classical nucleation theories, respectively).
7. Measured and simulated aerosol volume distributions generated in system A by homogeneous nucleation in the absence of seed aerosol.

(a) $T_s = 104.6\,^{\circ}C$ and $N_{J_o} = 1.5 \times 10^5\ cm^{-3}$.

(b) $T_s = 85.2\,^{\circ}C$ and $N_{J_o} = 55\ cm^{-3}$.

8. Measured and simulated aerosol number distributions generated in system B by homogeneous nucleation in the absence of seed aerosol.

   (a) $T_s = T_l = 102\,^{\circ}C$, $T_{wf} = 21.4\,^{\circ}C$, $N_{J_o} = 8.16 \times 10^5\ cm^{-3}$, $Q = 1\ l\,min^{-1}$.

   (b) $T_s = T_l = 80.5\,^{\circ}C$, $T_{wf} = 8.7\,^{\circ}C$, $N_{J_o} = 2.33 \times 10^4\ cm^{-3}$, $Q = 1\ l\,min^{-1}$.

9. measured and simulated aerosol number concentrations generated in system B as a function of seed particle number concentration.

   (a) $T_s = T_l = 99\,^{\circ}C$, $T_{wf} = 22.2\,^{\circ}C$.

   (b) $T_s = T_l = 95.7\,^{\circ}$, $T_{wf} = 22.2\,^{\circ}C$.

   (c) $T_s = T_l = 93\,^{\circ}$, $T_{wf} = 22.3\,^{\circ}C$.

10. Measured and simulated relative aerosol number concentrations generated in system B as a function of the relative initial number concentration.

11. Dimensionless gas temperature profiles for two different flow rates as a function of dimensionless axial position.

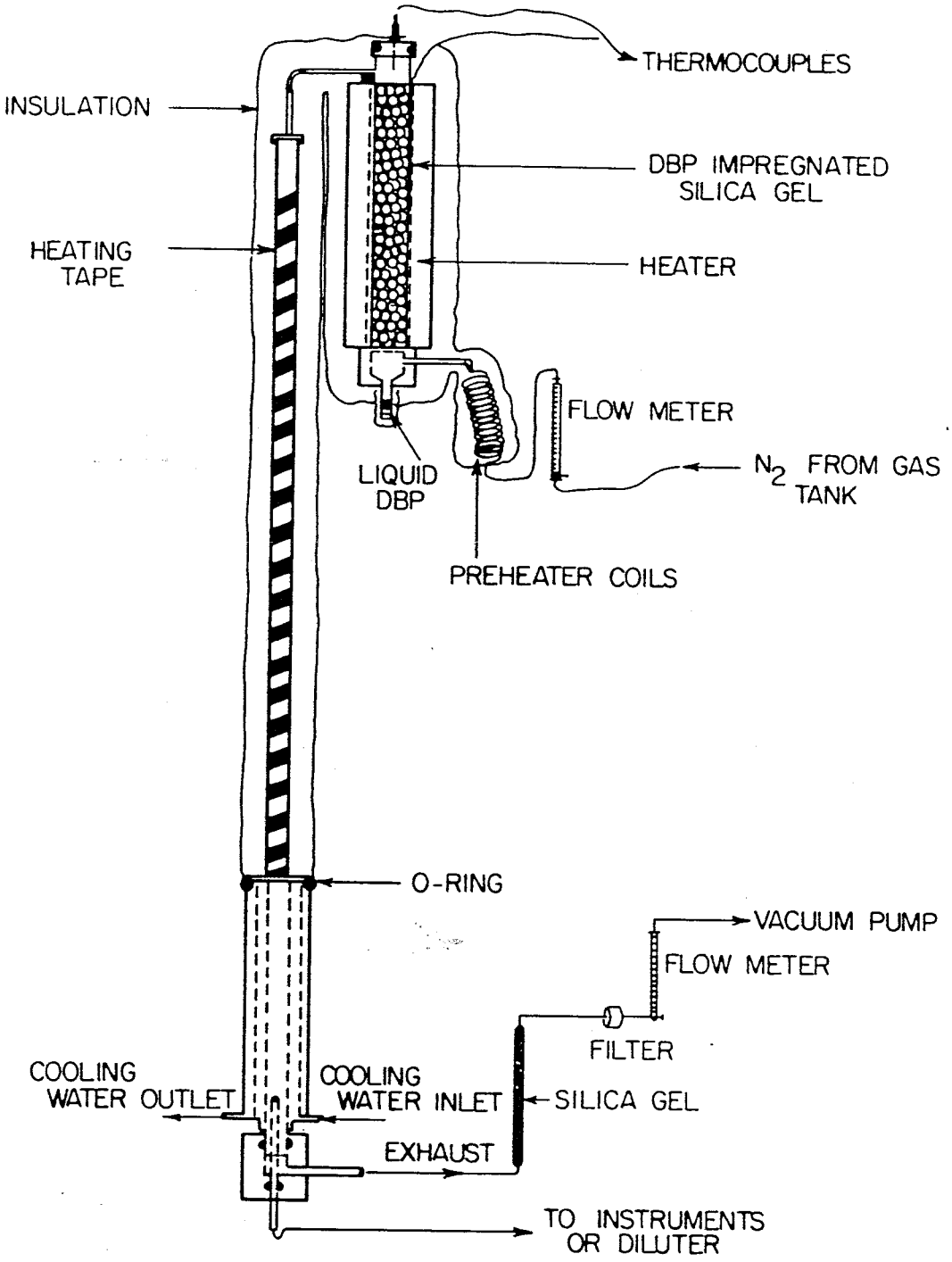
THERMOCOUPLES
INSULATION
DBP IMPREGNATED SILICA GEL
HEATING TAPE
HEATER
FLOW METER
LIQUID DBP
N_2 FROM GAS TANK
PREHEATER COILS
O-RING
VACUUM PUMP
FLOW METER
FILTER
COOLING WATER OUTLET
COOLING WATER INLET
SILICA GEL
EXHAUST
TO INSTRUMENTS OR DILUTER

Figure 1(a)

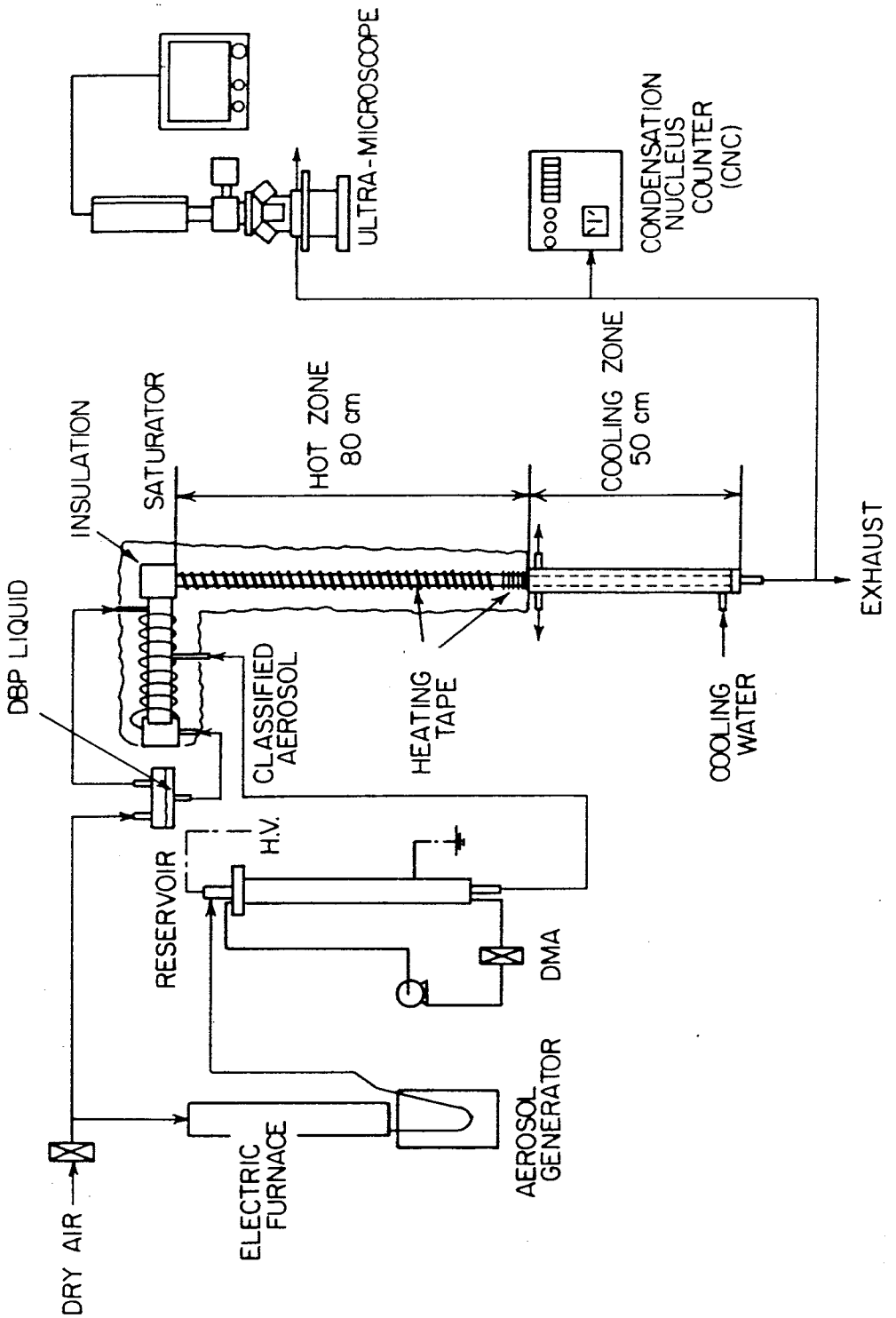
ULTRA-MICROSCOPE
CONDENSATION NUCLEUS COUNTER (CNC)
INSULATION
SATURATOR
HOT ZONE 80 cm
COOLING ZONE 50 cm
EXHAUST
DBP LIQUID
CLASSIFIED AEROSOL
HEATING TAPE
COOLING WATER
H.V.
RESERVOIR
DMA
AEROSOL GENERATOR
ELECTRIC FURNACE
DRY AIR

Figure 1(b)

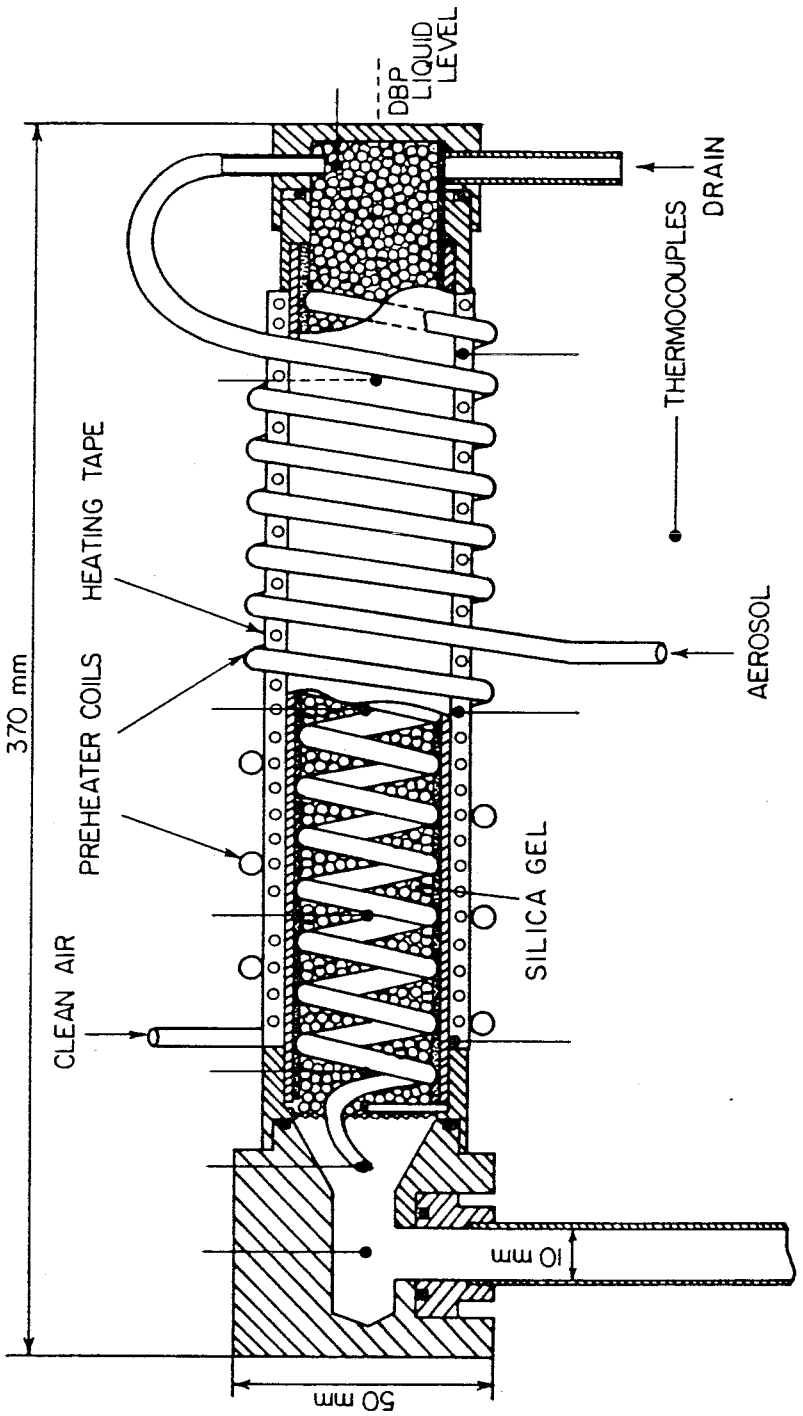
DBP LIQUID LEVEL
DRAIN
THERMOCOUPLES
HEATING TAPE
AEROSOL
370 mm
PREHEATER COILS
SILICA GEL
CLEAN AIR
10 mm
50 mm

Figure 2

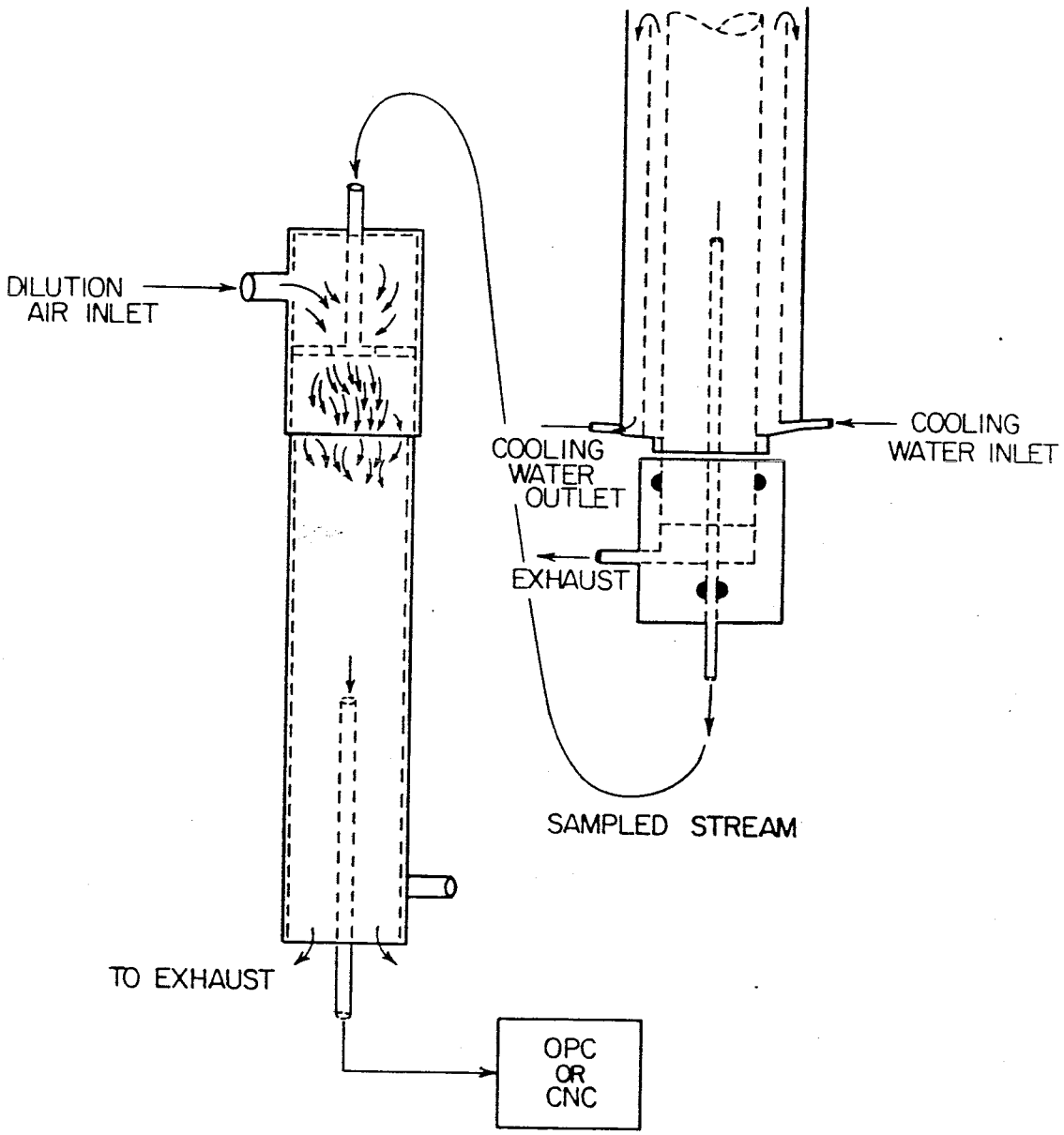
DILUTION
AIR INLET
COOLING
WATER
OUTLET
COOLING
WATER INLET
EXHAUST
SAMPLED STREAM
TO EXHAUST
OPC
OR
CNC

Figure 3(a)

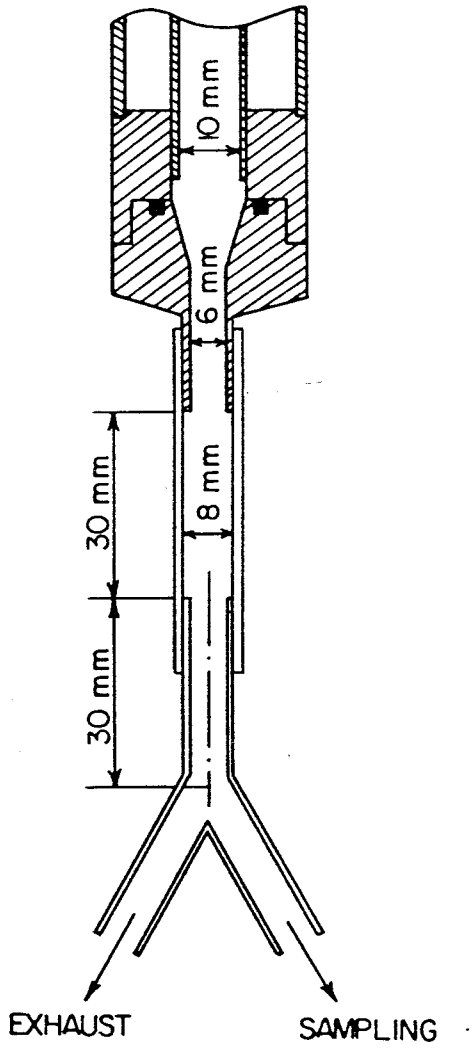

Figure 3(b)

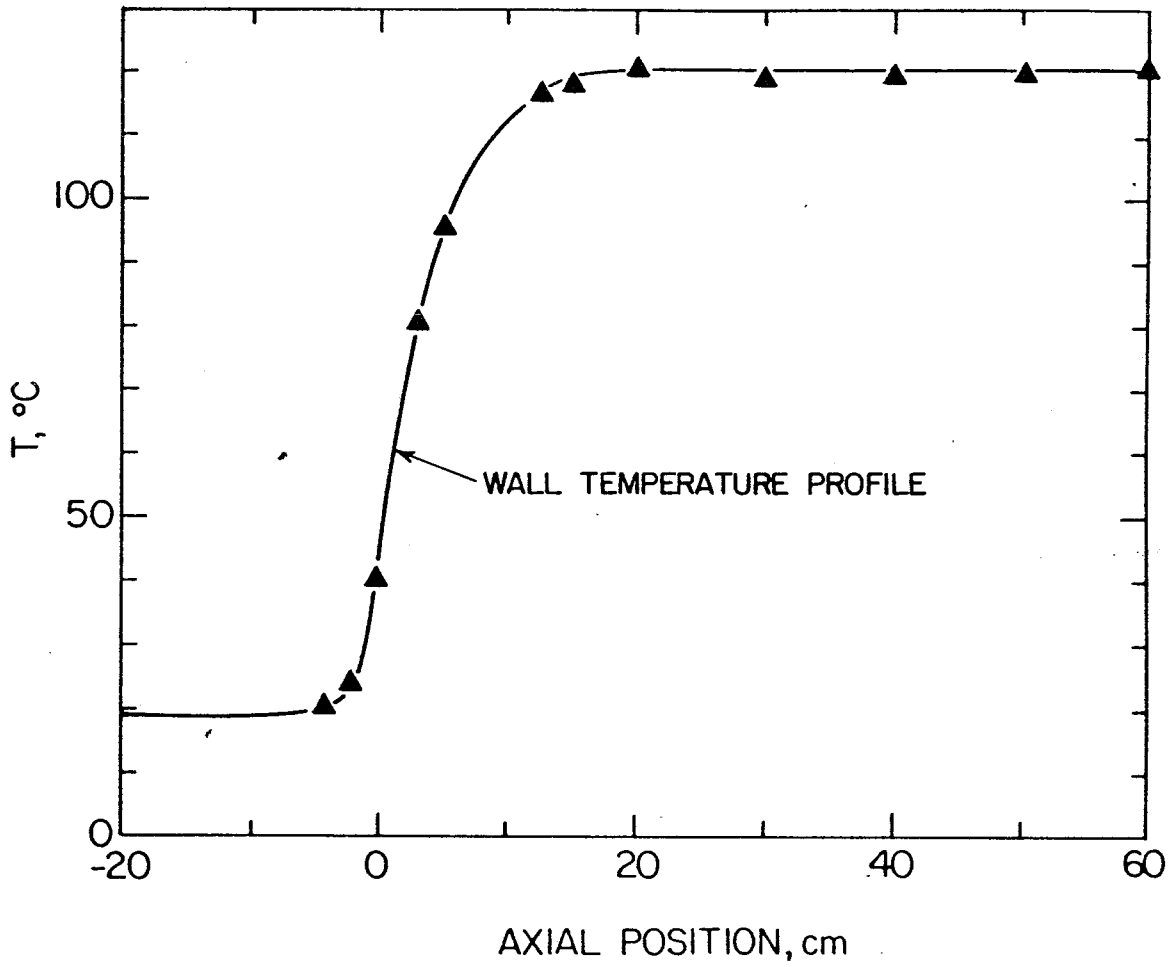
100
50
0
T, °C
WALL TEMPERATURE PROFILE
-20
0
20
40
60
AXIAL POSITION, cm

Figure 4(a)

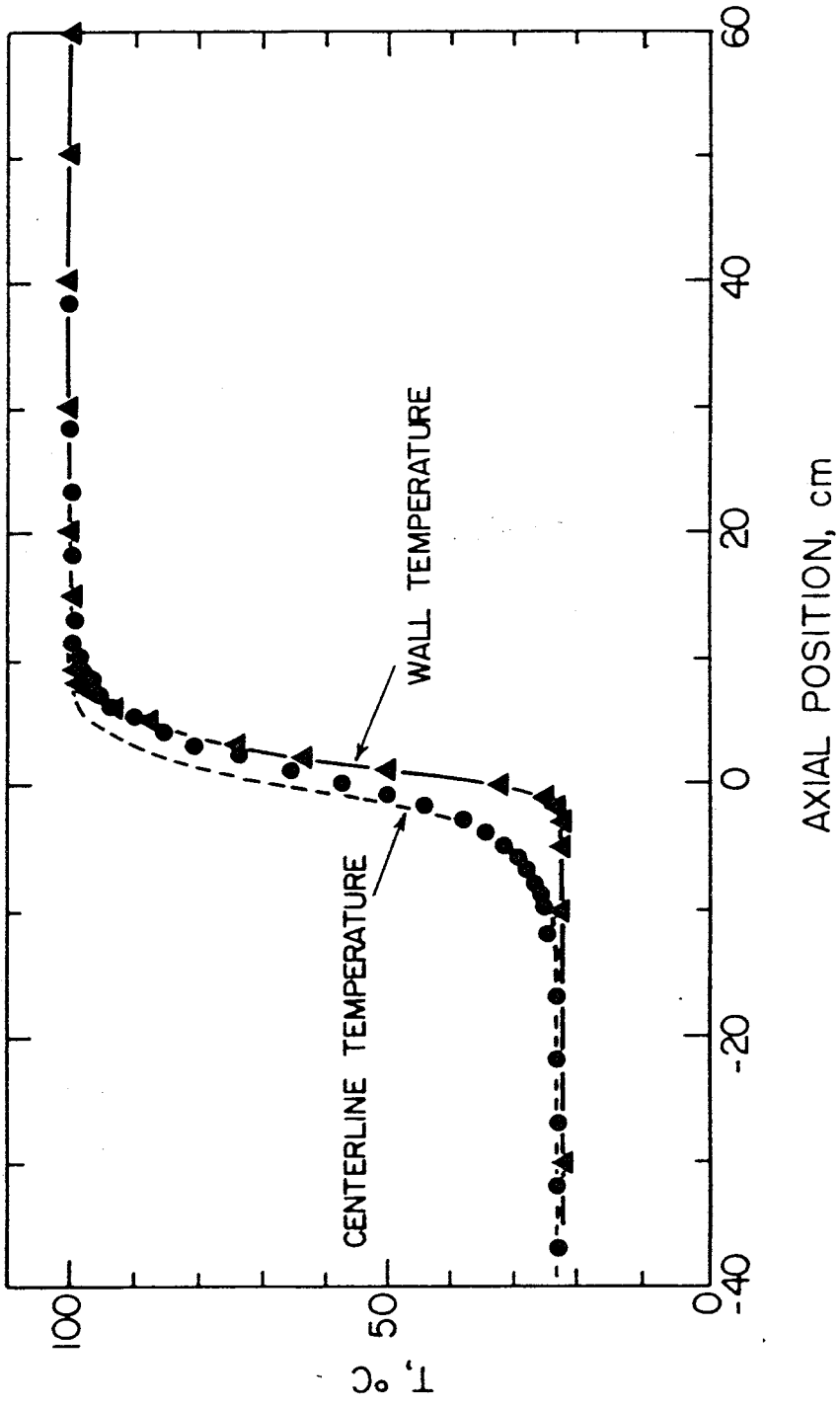
T, °C
100
50
0
-40
-20
0
20
40
60
AXIAL POSITION, cm
WALL TEMPERATURE
CENTERLINE TEMPERATURE

Figure 4(b)

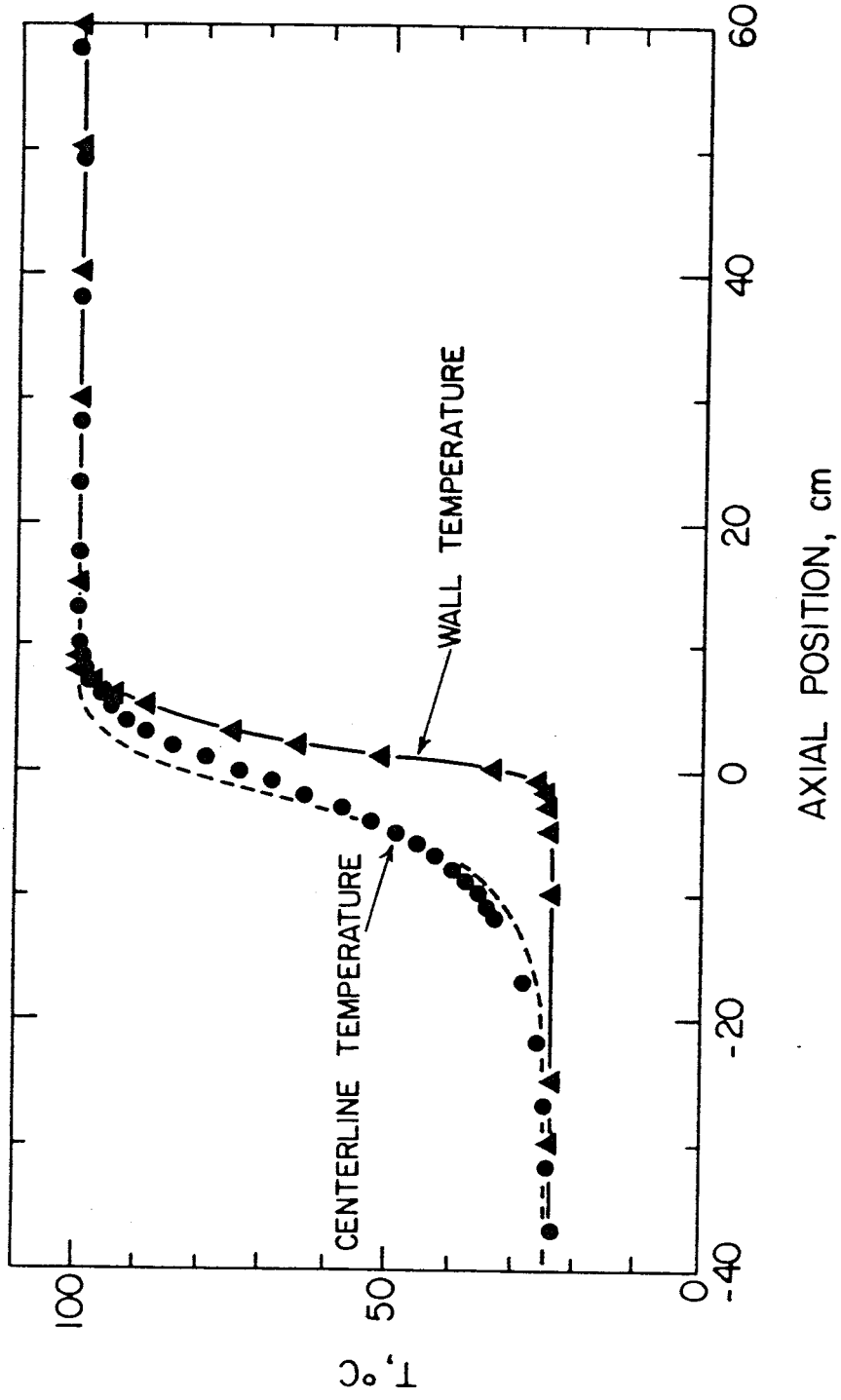
T, °C
100
50
0
-40
-20
0
20
40
60
AXIAL POSITION, cm
WALL TEMPERATURE
CENTERLINE TEMPERATURE

Figure 4(c)

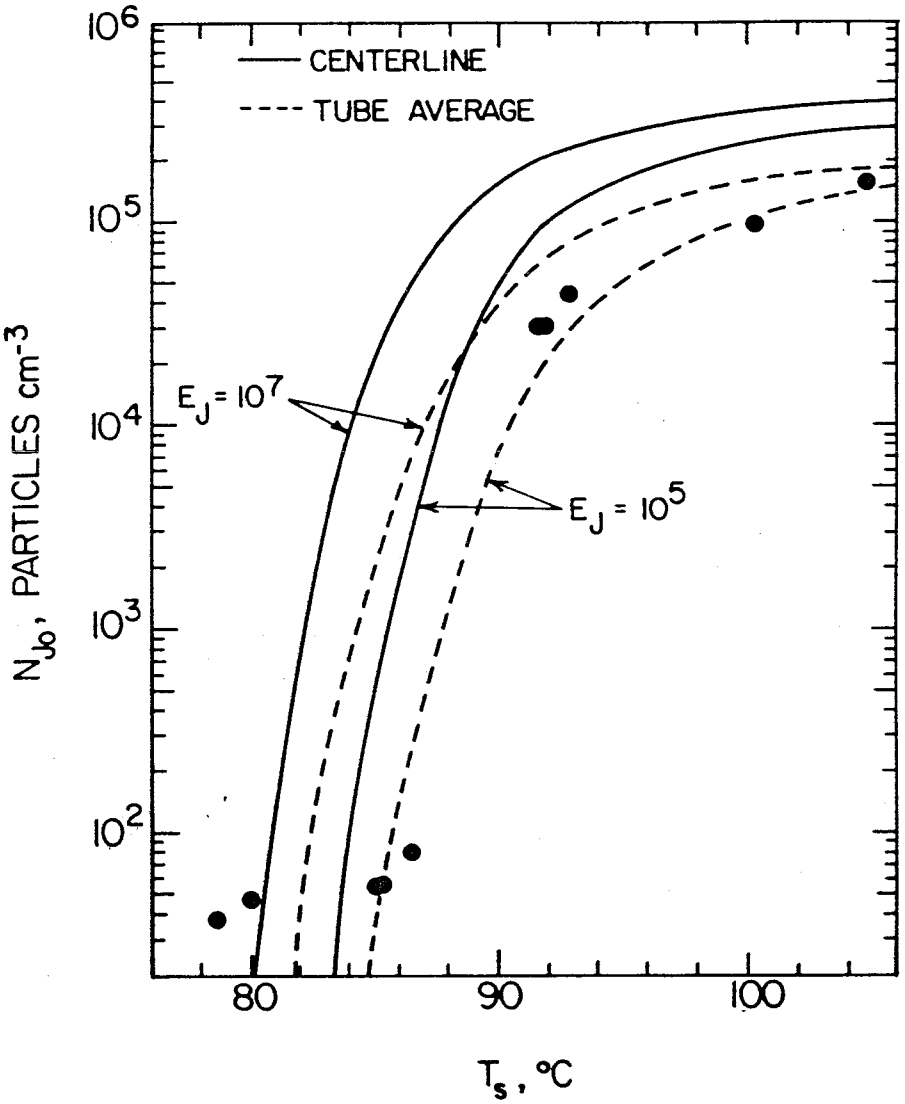
CENTERLINE
TUBE AVERAGE
$E_J = 10^7$
$E_J = 10^5$
N_{Jo}, PARTICLES cm^{-3}
T_s, °C
10^6
10^5
10^4
10^3
10^2
80
90
100

Figure 5

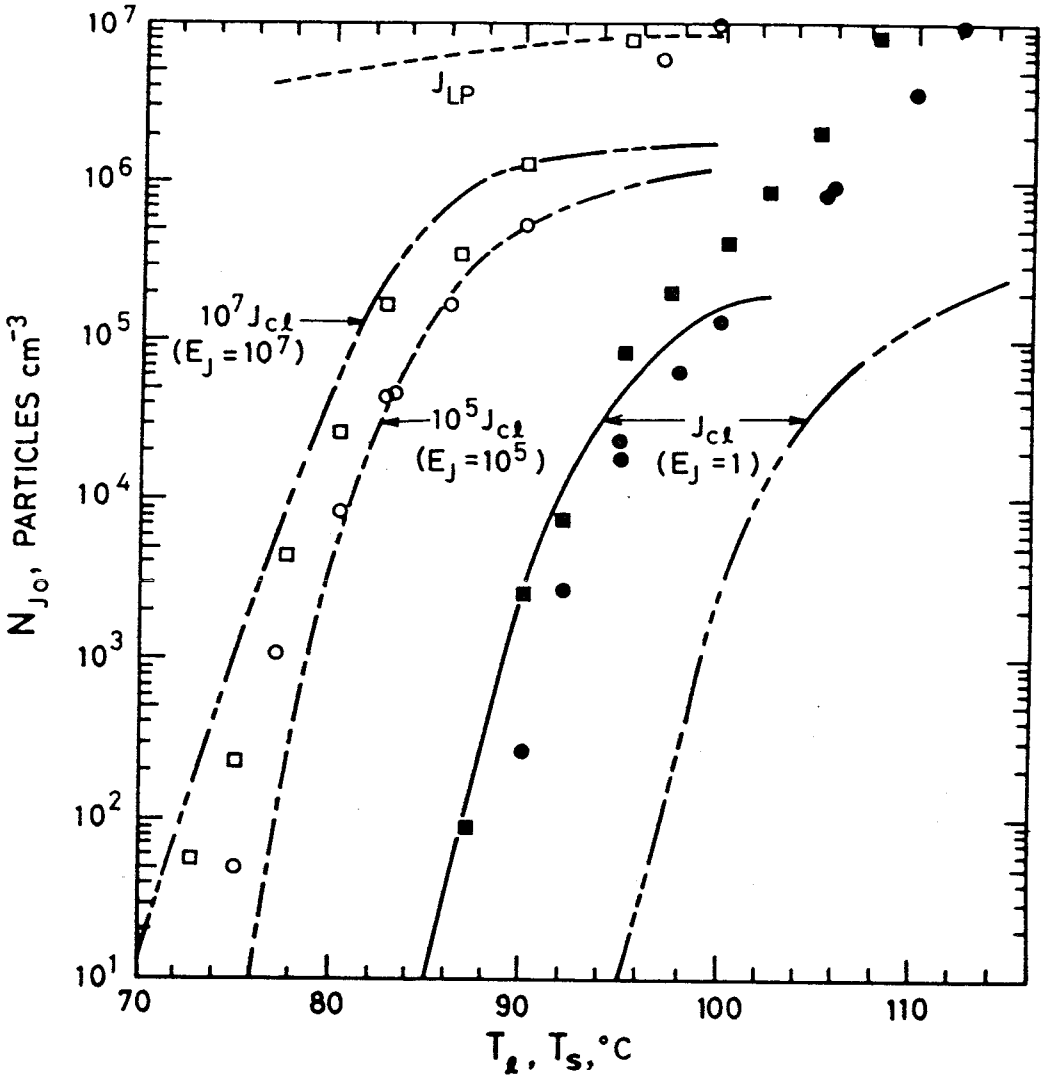

	experiment		calculation		
	Q, ℓ/min	T_{wf}, °C	$J_{c\ell}$	$E_J J_{c\ell}$	J_{LP}
○	0.5	8.5 – 8.9	——	– – – : $E_J = 10^5$ – – – : $E_J = 10^7$	– – –
□	1.0	8.7 – 9.3			
●	0.5	21.2 – 21.6	– – –		
■	1.0	20.9 – 21.6			

Figure 6

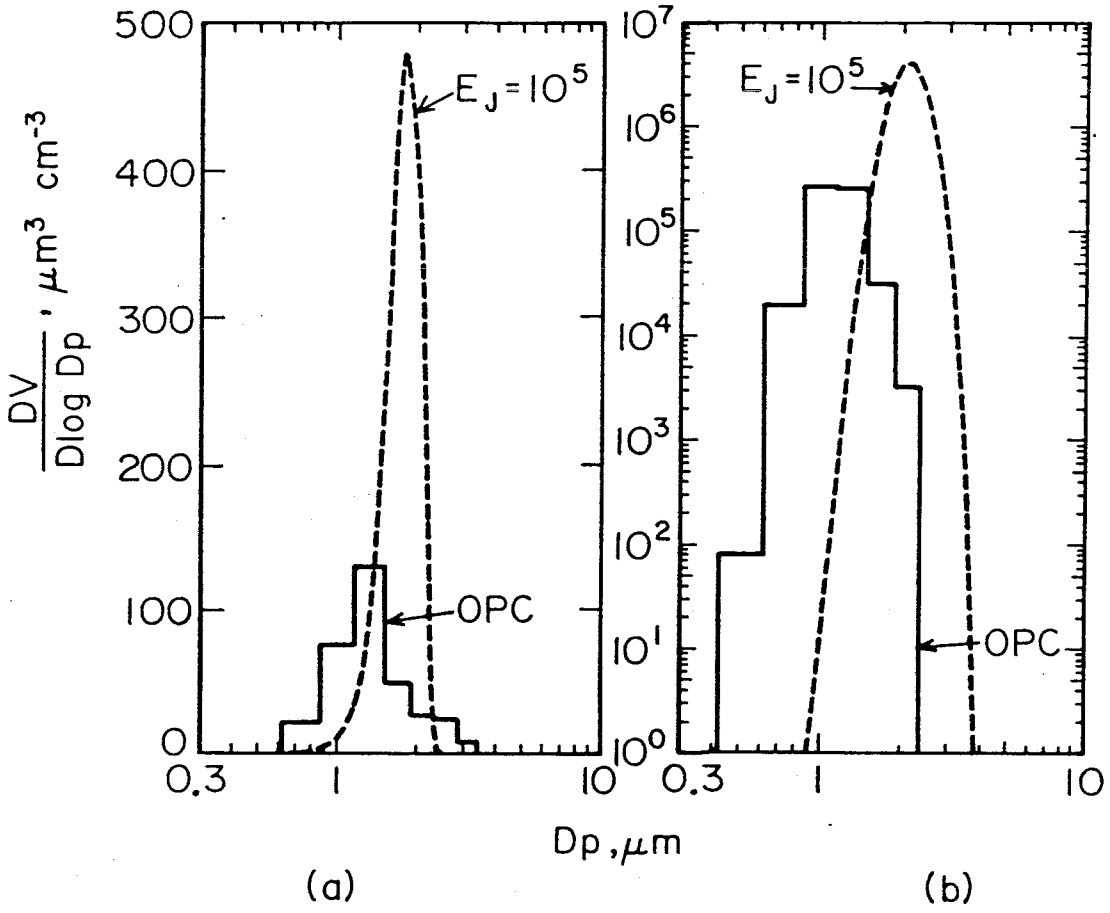
500
400
300
200
100
0
$\frac{DV}{Dlog\ Dp}$, $\mu m^3\ cm^{-3}$
$E_J = 10^5$
OPC
0.3
1
10
10^7
10^6
10^5
10^4
10^3
10^2
10^1
10^0
$E_J = 10^5$
OPC
0.3
1
10
Dp, μm
(a)
(b)

Figure 7

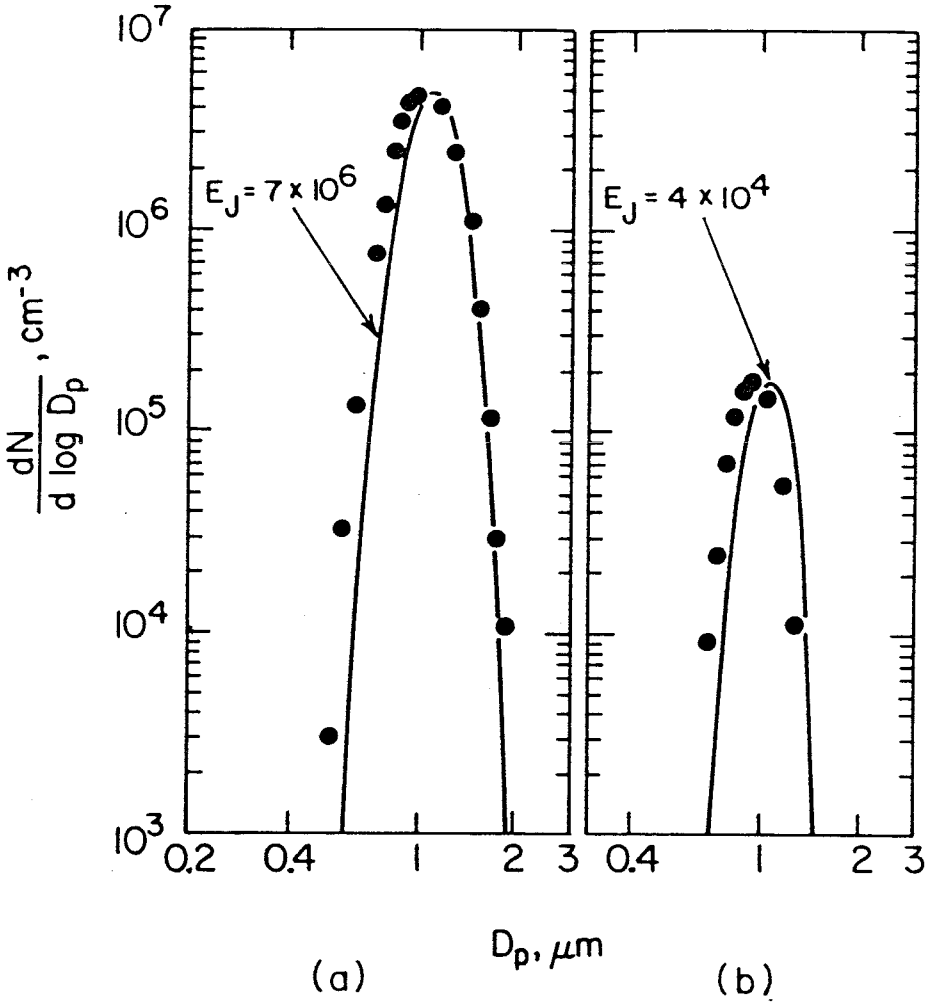
10^7
10^6
10^5
10^4
10^3
$\frac{dN}{d \log D_p}$, cm^{-3}
$E_J = 7 \times 10^6$
$E_J = 4 \times 10^4$
0.2
0.4
1
2
3
0.4
1
2
3
D_p, μm
(a)
(b)

Figure 8

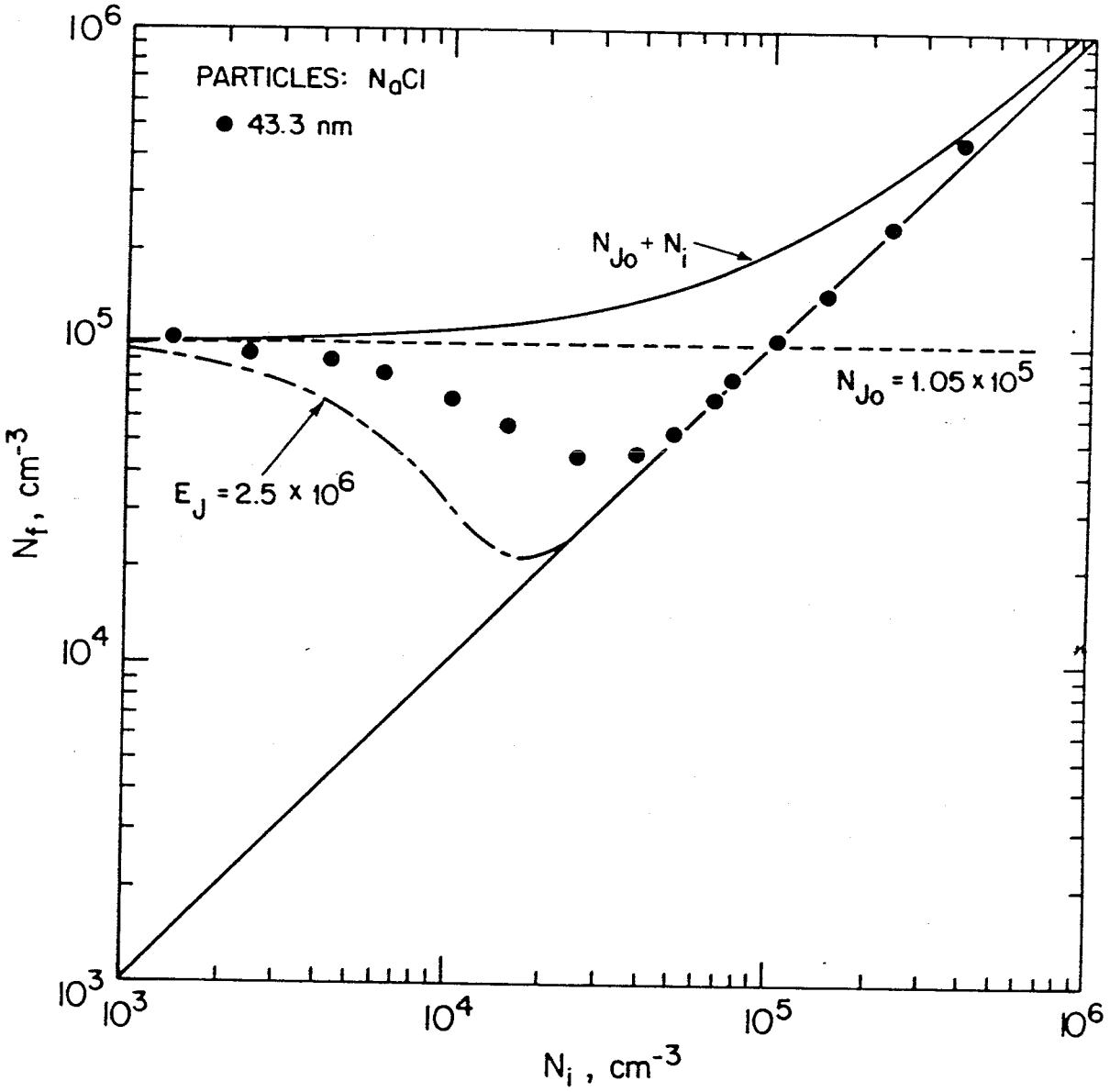
PARTICLES: NaCl
● 43.3 nm
$N_{Jo} + N_i$
$N_{Jo} = 1.05 \times 10^5$
$E_J = 2.5 \times 10^6$
N_f, cm^{-3}
N_i, cm^{-3}
10^3
10^4
10^5
10^6

Figure 9(a)

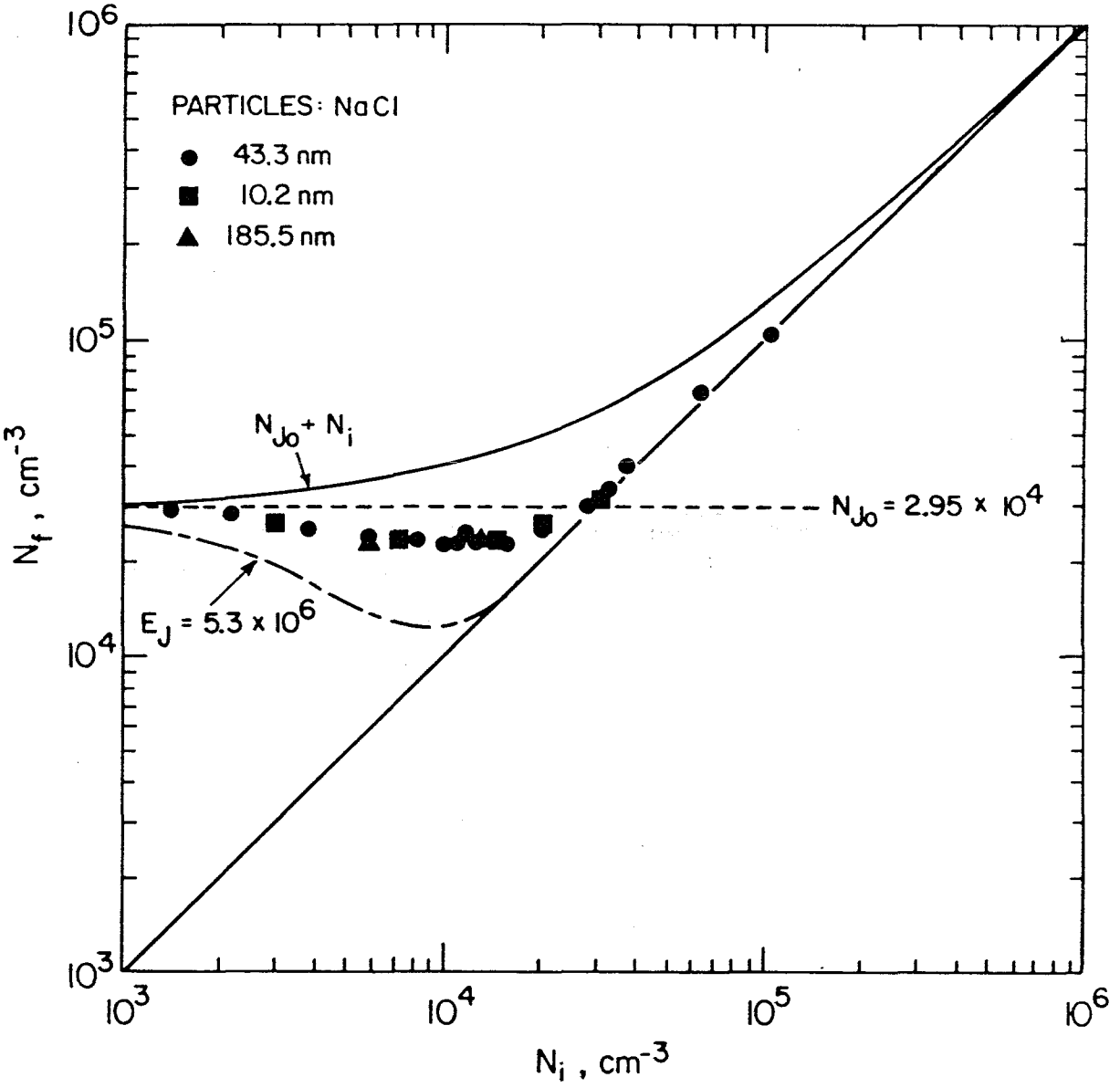
PARTICLES: NaCl
43.3 nm
10.2 nm
185.5 nm
$N_{Jo} + N_i$
$N_{Jo} = 2.95 \times 10^4$
$E_J = 5.3 \times 10^6$
N_f , cm^{-3}
N_i , cm^{-3}
10^3
10^4
10^5
10^6

Figure 9(b)

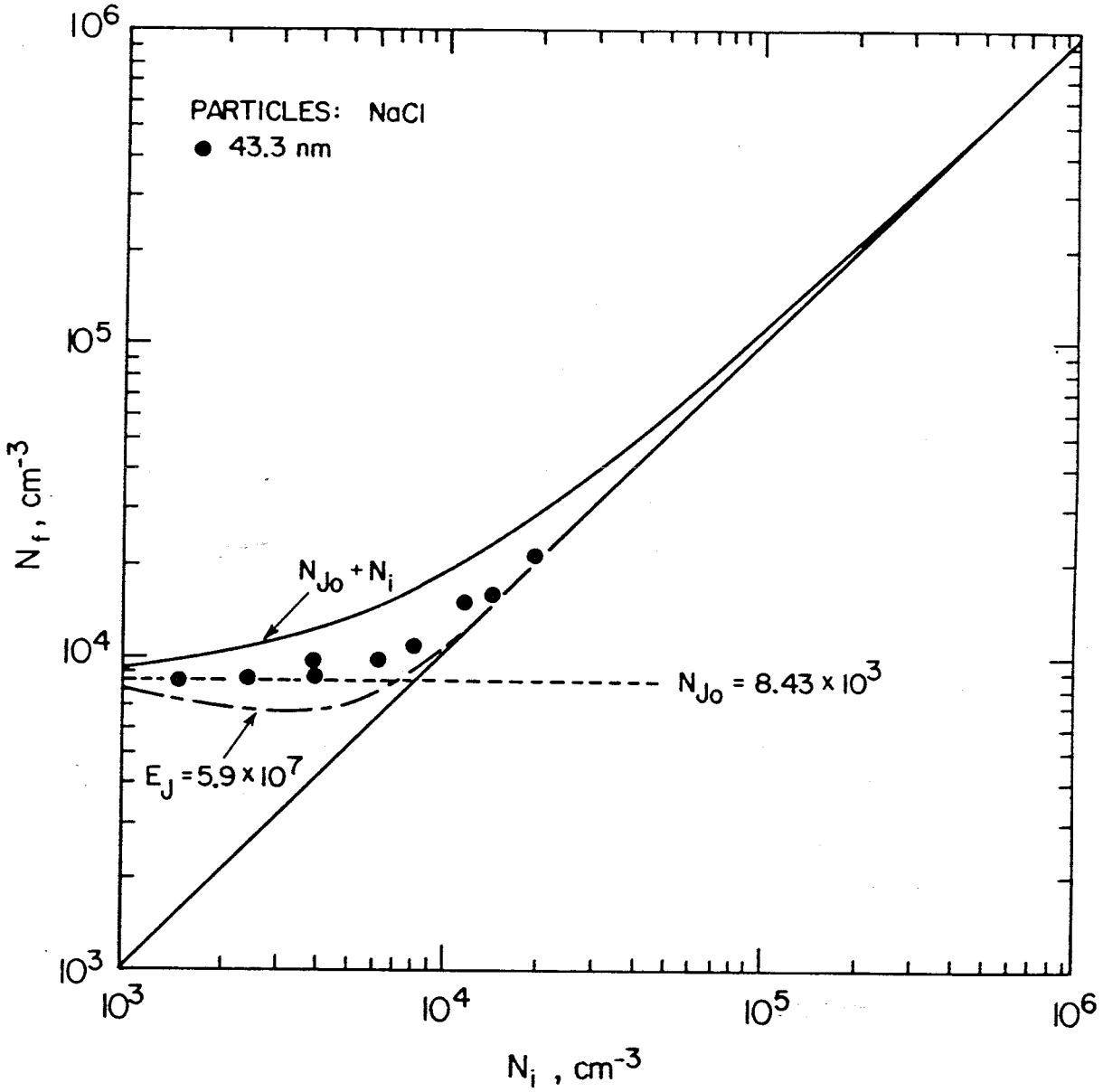
PARTICLES: NaCl
● 43.3 nm
$N_{Jo} + N_i$
$N_{Jo} = 8.43 \times 10^3$
$E_J = 5.9 \times 10^7$
N_f, cm^{-3}
N_i, cm^{-3}
10^3
10^4
10^5
10^6

Figure 9(c)

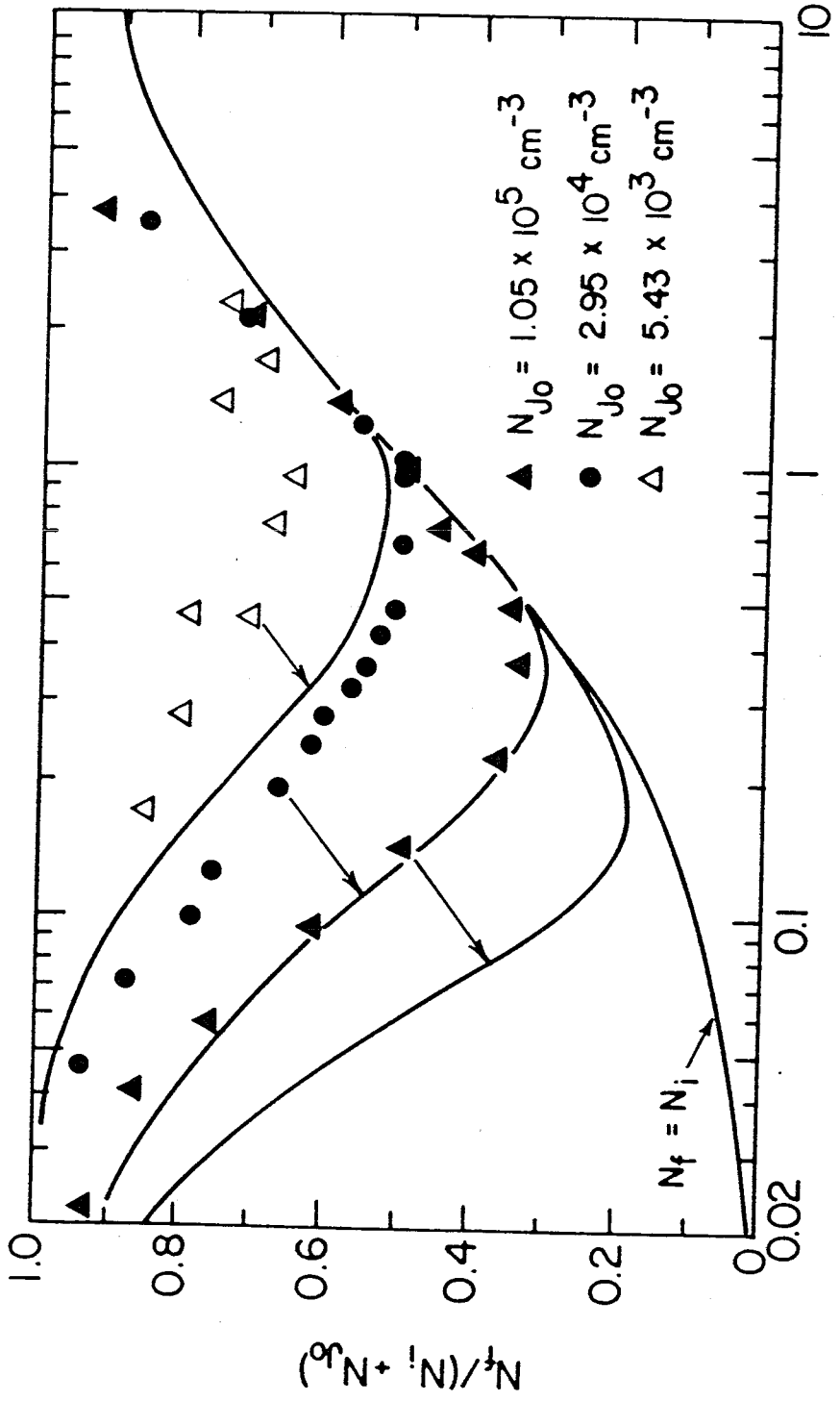
1.0
0.8
0.6
0.4
0.2
0
0.02
0.1
1
10
$N_f/(N_i + N_{Jo})$
N_i/N_{Jo}
$N_{Jo} = 1.05 \times 10^5\ cm^{-3}$
$N_{Jo} = 2.95 \times 10^4\ cm^{-3}$
$N_{Jo} = 5.43 \times 10^3\ cm^{-3}$
$N_f = N_i$

Figure 10

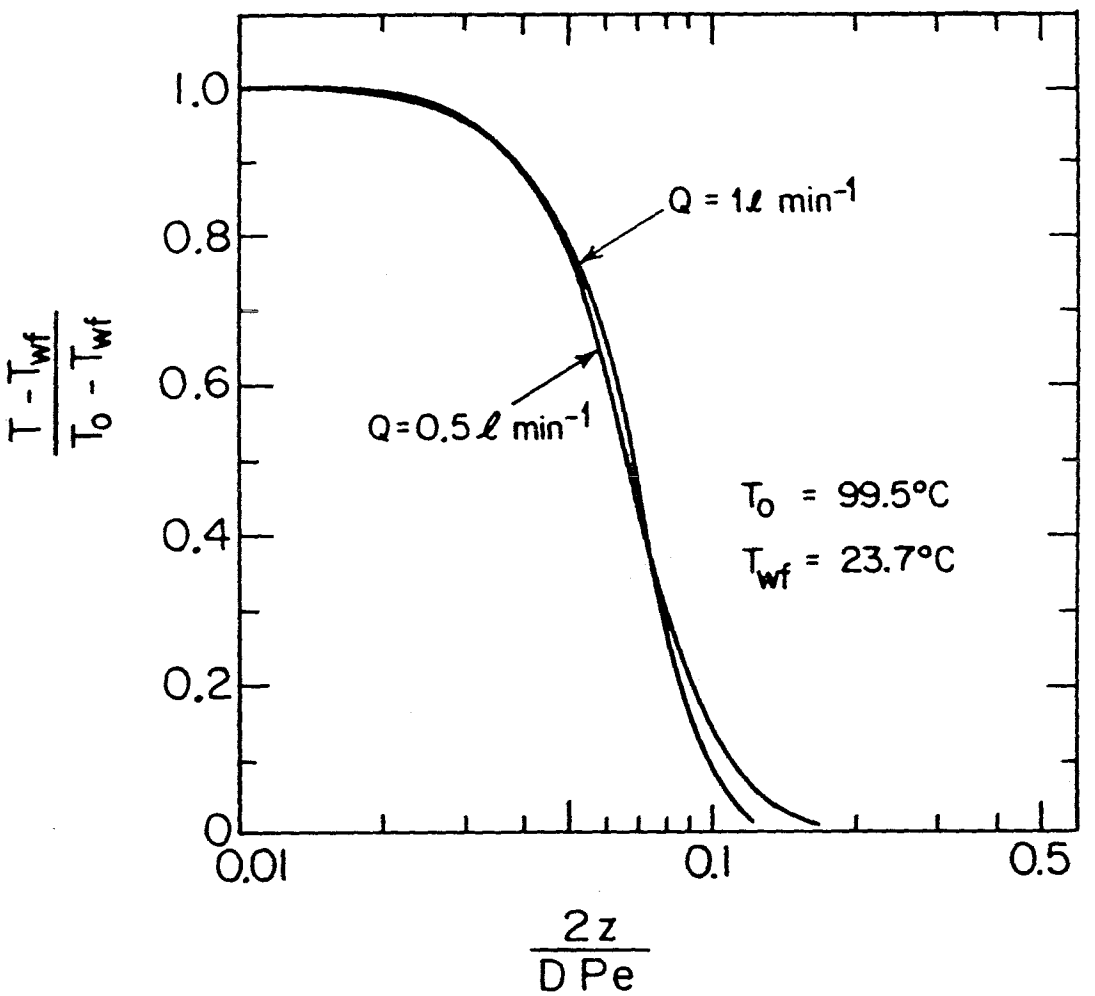
1.0
0.8
0.6
0.4
0.2
0
0.01
0.1
0.5
Q = 1ℓ min⁻¹
Q=0.5ℓ min⁻¹
T₀ = 99.5°C
T_wf = 23.7°C
(T - T_wf)/(T₀ - T_wf)
2z/(D Pe)

Figure 11

CHAPTER 3

THE GROWTH OF SILICON PARTICLES PRODUCED IN SINGLE STAGE AEROSOL REACTORS

ABSTRACT

The structures of silicon particles produced in a single stage, externally heated aerosol reactor are shown. Experimental results and simple model calculations indicate that the growth mechanism is not purely by vapor and small cluster deposition, but also by large cluster deposition and coagulation of like-sized particles. Results also suggest that, while growing dense refractory particles in a single stage reactor may be possible, it is extremely difficult to achieve. Use of the seed particles generated from a separate reactor is a more practical alternative.

1. Introduction

Engineering applications of ceramic materials place severe demands on the starting powders from which the parts are created. The properties of the ceramic parts, such as fracture toughness, are highly dependent on the building blocks, the powder materials from which they are made. Consolidation of large, dense particles tends to form green compacts with few large pores. If the powder contains agglomerates, large pores may be generated due to bridging. These large pores reduce the green density, and may cause substantial density variation across the compact. Large pores and inhomogeneous porosity in the green compact are a major cause of the highly variable structural properties of ceramic parts.

Furthermore, longer sintering times are required for complete densification of the large pores. If the pores are too large, complete densification of the compact may become impractical. Pores that remain after densification are the points of origin of cracks, causing parts to fail under stress far below those predicted for a homogeneous material.

Small ceramic precursor particles reduce sintering times and make smaller pore sizes attainable, although the range of possible improvement is limited since the handling of ultrafine particles is both difficult and expensive. Moreover, their high surface area to volume ratios makes such powders very susceptible to surface contamination. For these reasons, the finest ceramic powders in use today are about 0.1 μm diameter. Powders consisting of solid, roughly equiaxed, nonagglomerated, submicron particles with controlled size distribution are thought to be ideal for the production of uniform high density green compacts of ceramics and other powder based materials (1).

A variety of methods have been used to produce such powders. Solution methods such as the sol-gel process can produce highly uniform, nonagglomerated par-

ticles, although the range of composition is limited primarily to metal oxides (2,3). Synthesis by aerosol routes has also been used to produce high quality powders. Thermal plasma processes are used commercially to synthesize a broad range of powders for ceramics and other applications. Reasonably uniform silicon, silicon nitride, and silicon carbide have been generated by laser induced reactions (4,5). Oxide particles are produced by vapor phase oxidation of metal halides in flame synthesis (6-8). A variety of materials have been produced by externally heated aerosol reactors. High quality silicon powders have been obtained by the thermal pyrolysis of silane (9). The reaction of silane and ammonia in a heated tube produces silicon nitride (10). Spray pyrolysis is another class of aerosol process that has been applied to a broad spectrum of ceramic materials.

Vapor precursor powder synthesis begins with gas phase chemical reactions that produce condensible vapors from more volatile precursors. High supersaturations are readily achieved due to the low saturation vapor pressure of ceramic materials, so large numbers of particles are generated by homogeneous nucleation. These particles grow by the combined effects of vapor deposition (physical condensation and/or surface reaction), small molecular cluster deposition, and coagulation both with large clusters and similarly sized particles. Growth by vapor phase deposition is thought to produce dense, nonagglomerated particles. Growth by coagulation creates low density flocs unless the temperature is high enough that the agglomerates sinter completely. Thus, dense particles can be generated either by vapor and small cluster deposition or by sintering of agglomerates. The maximum size of dense particles that can be produced by the latter mechanism is limited for refractory materials because of the very high temperatures required for complete coalescence within the limited time available in aerosol reators. On the other hand, the growth of dense particles by vapor and cluster depostion can be achieved only if homogeneous

nucleation can be suppressed, an extremely difficult feat for refractory materials. Homogeneous nucleation of refractory materials generally generates large numbers of small particles, making coagulation a major contributor to particle growth.

Wu et al. (9) have proposed a method for the production of high quality powders by vapor-phase precursors using a single stage, multi-zone thermal reactor. Their recipe involves generating particles much smaller than the desired particle size by homogeneous nucleation while keeping the number concentration low enough to suppress growth by coagulation. The chemical reactions that lead to gas-to-particle conversion must then be carried out at gradually increasing but controlled rates such that the particles are grown by deposition of the reaction products and new particle formation is suppressed. Uniformly sized spherical silicon particles have been synthesized using this approach (9).

It can be shown that particle growth in these experiments was influenced by both vapor and cluster deposition and coagulation. The number concentration at the exit of the reactor was reported to be $N = 4.6 \times 10^9$ cm^{-3}. The residence time τ_R in the reactor was approximately 1.5 seconds. Assuming that the particles were mono-sized, the coagulation rate coefficient for 0.1 μm particles is on the order of $\beta = 1 \times 10^{-9}$ cm^3 s^{-1}. The characteristic time for coagulation estimated by $\tau_c = 2/\beta N_o$ is about 0.5 second, i.e., of the same order of the reactor residence time. The actual characteristic time for coagulation was probably shorter within the reactor because of the higher actual number concentration and the spread (the final concentration accounts only for those particles that remain after coagulation) of the size distribution of particles. Thus, it appears likely that coagulation contributed significantly to the particle growth in the experiment of Wu et al. (9). To produce the dense spherical particles reported, agglomerates produced during coagulation must have sintered completely. Given the high peak temperatures of

those experiments (1523 K), such sintering can not be ruled out.

For development of thermal reactor technologies for the synthesis of refractory ceramic materials, it is important that the mechanism of growth of the silicon particles be identified. The use of single stage, multi-zone reactors for the production of more refractory ceramic materials such as silicon nitride is feasible only if dense particles can be grown directly by vapor and cluster deposition since densification of agglomerate particles may not be complete within reasonable residence times at achievable temperatures.

In this work, the experiments of Wu et al. (9) were repeated with the temperature of the final zone kept low to minimize sintering of any agglomerates formed. If the particles do, in fact, grow by vapor and small cluster deposition, then solid particles should be obtained even at low peak temperatures. On the other hand, the low temperature should ensure that aggregate particles survive to reveal the role of coagulation in particle growth. These experiments were accompanied by simulation of particle formation and growth to substantiate the inferred growth mechanism.

2. Experimental Systems

Figure 1 shows the single stage reactor used in the first set of experiments. It consisted of a 1.1 cm i.d., 100 cm, with a total heated length of (55 cm). The first three zones were each 5 cm long, and were separated by 1 cm of insulation to insure smooth temperature profiles. These zones were heated with nichrome resistance wire heating elements to temperatures up to 1370 K. The final two zones were 20 and 15 cm long, respectively, capable of achieving temperatures as high as 1770 K using silicon carbide heating elements. Again, the zones were separated by insulation.

One percent silane in nitrogen was mixed with high purity nitrogen (99.996%)

that had been passed over hot copper shavings for additional oxygen removal. The ratio of the two flow rates was varied to control the initial silane concentration. The resulting mixture was introduced into the top of the reactor tube. The total flow rate was 1 l $min^{-1} \pm 6\%$ for all silane concentrations. The temperatures of the heating zones were controlled to achieve the wall temperature profile illustrated by the solid curve in Fig. 2. The profile used on the previous experiments on the same reactor by Wu et al. (9) is illustrated by the broken curve.

The concentrated aerosol stream exiting from the bottom of the reactor tube was cooled and diluted with high purity nitrogen that was transpired through a porous, sintered stainless steel tube (Fig. 2, insert). This served the dual purposes of reducing the particle number concentration and the gas temperature, minimizing loss by thermophoretic deposition onto the cold wall. The resulting aerosol mixture was further diluted with the recirculating dilution system shown in Fig. 3. The two dilution stages reduced the number concentration of particles to a level compatible with conventional aerosol intruments.

The size distributions of the product aerosol were measured using a differential mobility analyzer (DMA, TSI Model 3071) with a condensation nuclei counter (CNC, TSI Model 3020) as a detector. The basic working principle of the DMA is electrostatic classification of charged particles with an applied electric field. In the DMA aerosol particles are passed through a ^{85}Kr neutralizer where they acquire a bipolar charge distribution. The particles are then classified by their drift velocity in the electric field. Particles within a particular mobility range are extracted from the DMA with the CNC. Once the mobility distribution was obtained by making a series of number concentration measurements at different electric field strengths, the size distribtution was determined by inverting the data with the routine MICRON (11). The portions of the inverted distributions beyond that measurable by

the DMA were truncated, and the geometric mean diameters were computed based on the resultant distributions.

The DMA/CNC combination provides only information regarding the mobility equivalent size of the particles, i.e., the electrostatic force to aerodynamic drag ratio, not their morphologies. Particle samples collected on Teflon filters were dispersed in water and placed on grids for examination under a transmission electron microscope (TEM). Microscopic analysis revealed the nature of the primary particles that made up the agglomerates. Due to the agglomeration of particles during the TEM grid preparation, structures of single aggregates could not be obtained. If the particles were solid single spheres, the mean mobility diameter computed from the DMA/CNC measurements would be the same as the mean primary particle diameter measured by the TEM, but as will be shown below, the two sizes differed markedly.

Micrograghs of the product particles were also obtained using a thermophoretic TEM sampling probe. This probe (Fig. 4) allowed for direct collection of the particles exiting the reactor on the TEM grids. In the probe, the aerosol stream is heated, then impinged on a TEM grid that is mounted on the end of a copper rod. The rod is cooled in either liquid N_2 or ice water. This creates a sharp temperature gradient in the boundary layer, causing the particles to be driven from the hot gas to the cold grid by thermophoresis. The number of particles collected on the TEM grid can be controlled by controlling the temperature gradient and collection time. By keeping the number of particles per unit grid area (number density) low, structures of individual particles could be determined.

3. Experimental Results

Typical particle size distributions measured at the reactor outlet are shown

in Fig. 5. Duplicate measurements are presented for two different initial silane concentrations. For each reactant concentration, the size distributions agree closely in size and number. The general shapes of the the size distribtutions are similar in each case. Increasing the reactant concentration leads to larger apparent particle sizes.

The variation in the mean particle size with reactant concentration is shown in Fig. 6. Both the mean mobility equivalent diameters and the sizes determined by transmission electron microscope analysis of the particles collected by the Teflon filters are presented. The mobility equivalent particle size is 2 to 20 times higher than that determined by microscopy for the silane concentrations studied. This large discrepency indicates that the product particles are aggregates of the smaller structures. The mobility equivalent size increased significantly with initial silane concentration, while the fine structure or primary particle size remained relatively constant.

The thermophoretic sampling probe was used to examine the structure of individual particles. Figure 7a shows a typical particles collected during reaction of 0.17% silane. It is a chain agglomerate with a fine structure scale approximately 19 nm that was typical of the particles collected under nominal reactor operating conditions. From this structure, we may conclude that coagulation played a major role in the particle growth, leading to the formation of the aggregates. Furthermore, it is apparent that the particles have not fused completely within the 0.3 second residence time at the 1060 K peak temperature in the reactor.

Additional experiments were performed with higher peak temperatures to examine the possible role of particle fusion in the previous experiments of Wu et al. (9). Figures 7b and 7c show the particle structures that resulted when the peak temperature is raised to 1473 K. Aggregates like that shown in Fig. 7a have undergone

substantial, but not complete, coalescence. Hence, the dense particles previously reported with peak reactor temperatures of 1523 K likely resulted from coalescence of aggregate particles formed early in the reactor.

The product number concentration variation with reactant concentration is shown in Fig. 8. A 50-fold increase in the initial silane concentration resulted in a modest 35% increase in the total number concentration at the reactor outlet. This weak dependence of the number concentration with reactant loading is also consistent with the growth of particle primarily by coagulation. The number of particles predicted by the self-preserving particle size distribtution (12) for the silane concentration of 0.018%, assuming an average reactor temperature of 910 K, is 2.82×10^8 cm^{-3}, which is in close agreement with the measured value of 1.57×10^8 cm^{-3}. This further supports the arguments above.

4. Modelling of Aerosol Evolution

The particle structure observed with low temperature strongly suggests that coagulation played a crucial role in particle growth. A modeling effort was undertaken to substantiate this conclusion. Available models of aerosol dynamics do not fully describe the evolution of an aerosol system in which aggregates coalesce slowly. Most aerosol dynamics models assume that particles coalesce instantly upon agglomeration, so that all particles are dense spheres (Seinfeld, 1986) (13). For spherical particles, the diffusivities and collision cross sections are well known. The structures of non-coalescing particles can be predicted using diffusion-limited aggregation or cluster-cluster aggregation models (14,15), but data on diffusivities and collision cross sections are lacking. The influence of finite coalescence rates on particle growth has not been described theoretically. Thus, an approximate solution to the aerosol dynamic equation based on dense, spherical particles will be

employed, even though it provides an imperfect description of the aerosols examined in the present study.

The simplified reaction coagulation (SRC) model developed by Wu et al. (16) was used to simulate the aersol evolution. This is an integral model representing the aerosol size distribution with two modes. The first, called the fine or homogeneous nucleation mode, follows the evolution of fine particles and clusters. The second mode describes the behavior of the seed particles. In the original SRC model, mass is added to the fine mode directly from the reaction source. Here, a separate monomer balance is added to the model to better account for the condensation of the condensible vapors onto the particles. Mass is introduced into the fine mode by the self-coagulation of the monomers and by condensation of the monomers onto the fine particles (coagulation of the monomer with the fine particles), and is removed by the seed particles. Mass is added to the seed mode from both monomers and fine particles. The two modes are followed by the number and mass concentrations N_H and M_H, and N_S and M_S, respectively, where the subscript H represents the homogeneous nucleation or fine mode, and S the seed mode. For the present purposes, wall losses are neglected, and the aerosol and temperature are assumed to be uniformly distributed across the reactor tube. In addition, it is assumed that when two particles collide, they stick and form a single, dense new particle. A set of seven nonlinear differential equations is sufficient to follow the aerosol evolution:

$$\frac{d}{dz}(C_A u_z) = -R \qquad [1]$$

$$\frac{d}{dz}(N_1 u_z) = R\, N_{AV} - K_1 N_1^2 - K_{1H} N_1 N_H - K_{1S} N_1 N_S \qquad [2]$$

$$\frac{d}{dz}(N_H u_z) = \frac{1}{2} K_1 N_1^2 - \frac{1}{2} K_H N_H^2 - K_{HS} N_H N_S \qquad [3]$$

$$\frac{d}{dz}(M_H u_z) = m_1 K_1 N_1^2 + m_1 K_{1H} N_1 N_H - \bar{m}_H K_{HS} N_H N_S \qquad [4]$$

$$\frac{d}{dz}(N_S u_z) = -\frac{1}{2}K_S N_S \qquad [5]$$

$$\frac{d}{dz}(M_S u_z) = m_1 K_{1S} N_1 N_S + \bar{m}_H K_{HS} N_H N_S \qquad [6]$$

$$u_z \rho C_p \frac{dT}{dz} = \frac{4}{D_R} h_x (T_w - T), \qquad [7]$$

with initial conditions

$$N_H = M_H = 0 \qquad [8]$$

$$N_S = N_{So} \qquad [9]$$

$$M_S = M_{So} \qquad [10]$$

$$T = T_o \qquad [11]$$

at $z = z_o$, where K_1, K_{1H}, K_{1S}, K_H, K_{HS}, and K_S represent the coagulation coefficients and are computed using Fuchs' interpolation formula, and $\bar{m}_H$ is the average mass of a particle in the fine mode evaluated by

$$\bar{m}_H = \frac{M_H}{N_H}.$$

D_R, ρ, C_p, and u_z, are the reactor diameter, bulk gas density, thermal conductivity, and average velocity, respectively. T and T_w are the gas and wall temperatures. h_x is the average local heat transfer coefficient. N_{AV} is Avogadro constant, and R is the reaction rate.

The equations can be cast in a more familiar form with the use of the steady-state one-dimensional continuity equation,

$$\frac{d}{dz}(u_z \rho) = 0, \qquad [12]$$

to become:

$$u_z\rho\frac{d}{dz}(\frac{C_A}{\rho}) = -R \qquad [13]$$

$$u_z\rho\frac{d}{dz}(\frac{N_1}{\rho}) = R\ N_{AV} - K_1N_1^2 - K_{1H}N_1N_H - K_{1S}N_1N_S \qquad [14]$$

$$u_z\rho\frac{d}{dz}(\frac{N_H}{\rho}) = \frac{1}{2}K_1N_1^2 - \frac{1}{2}K_HN_H^2 - K_{HS}N_HN_S \qquad [15]$$

$$u_z\rho\frac{d}{dz}(\frac{M_H}{\rho}) = m_1K_1N_1^2 + m_1K_{1H}N_1N_H - \bar{m}_HK_{HS}N_HN_S \qquad [16]$$

$$u_z\rho\frac{d}{dz}(\frac{N_S}{\rho}) = -\frac{1}{2}K_S{N_S}^2 \qquad [17]$$

$$u_z\rho\frac{d}{dz}(\frac{M_S}{\rho}) = m_1K_{1S}N_1N_S + \bar{m}_HK_{HS}N_HN_S. \qquad [18]$$

The detailed decomposition kinetics of silane involves many elementary reactions. However, it has been accepted that the rate limiting step is (17)

$$SiH_4 + M \rightarrow SiH_2 + H_2 + M. \qquad [19]$$

First order kinetics was assumed in the model calculations. The following pseudo first order rate expression was used for conversions up to 1% (17):

$$\frac{d[SiH_4]}{dt} = 10^{15.18} \times e^{-28133/T}[M]^{1/2}[SiH_4]\ \text{moles}\,l^{-1}\,s^{-1}, \qquad [20]$$

where [M] is the total molar concentration of gas in the system (silane plus background gas) expressed in units of moles l^{-1}. For conversions from 1% to depletion of the reactant, a first order rate expression in silane reported by White et al. (17) was used. The rate constant for this range was

$$k = 10^{12.9} \times e^{-25768/T}\ s^{-1}. \qquad [21]$$

Back reactions due to H_2, which have been observed for conversions beyond 40%, were neglected.

Two approaches were used to simulate the aerosol evolution. In the first approach (approach A), the aerosol remains as a single mode (fine mode) throughout the simulation. In the second approach (approach B), the aerosol starts out with a single mode, the fine particles formed by homogeneous nucleation. Once the number concentration in the fine mode reaches a local maximum, the fine particles become seed particles, and the size distribution is represented by two modes. Calculations were performed for the experimental conditions studied. The wall temperature profile was assumed to vary lineary from the midpoint of one zone to the next. The reactor inlet and outlet were at room temperature.

5. Modelling Results

Figure 9(a) shows the predicted variation in the number concentration with axial position in the reactor for an initial silane concentration of 0.018%. Particles formation begins approximately 20 cm downstream of the reactor inlet. The number concentration rises rapidly, peaking at about 35 cm from the reactor inlet. At this point, the two representations of the particle dynamics diverge. The single mode description (approach A) shows a gradual decrease in the number concentration, the result of the competition between coagulation of the nuclei formed early in the reactor and the formation of new nuclei from monomers. Accelerating the reaction in the downstream region leads to a second brief burst of new particle formation. With the precursor depleted, coagulation dominates the aerosol dynamics in the region downstream of this second nucleation burst.

The two-mode representation of the aerosol dynamics (approach B) treats the particles formed early in the reactor as seed particles, and probes the ability of these seeds to suppress further new particle formation. The seed concentration decreases quickly due to coagulation, with additional fine particle formation increasing the total number concentration above that of the single mode description after a short

delay. The discontinuity seen in Fig. 9(a) results from the arbitrary splitting of the two modes and is not physically significant. The number of the fine particles rapidly reaches a limiting value beyond which the concentration decreases slightly due to the combined effects of new nuclei formation and loss of nuclei by coagulation with other nuclei and with the seed particles. Late in the process there is again a second burst in the fine particle formation. That event is followed by the rapid loss of all of the fine mode particles by coagulation with the seed particles. The small increase in the seed mode concentration near the reactor outlet is due to the cooling of the gas, resulting in an increase in the gas density, which increases the particle number concentration (the reactants are consumed completely in the hot zone between 20 cm and 80 cm from the reactor inlet). The number concentration predicts by the single mode model is approximately twice that by the two-mode model.

Firure 9(b) shows the variation the particle size. The single mode calculation shows a gradual increase in the particle size from atomic dimensions until late in the reaction, where the second burst of new particle formation occurs. At that point, the mean particle size decreases slightly. Particles are not expected to decrease in size. Rather, the decrease in the mean size results from fast production of large numbers of very small particles. The two-mode model eliminates this complicated computation artifact. The seed particles grow continuously. The fine particles are continously being formed and rapidly lost by coagulation with the seed particles. Thus, the apparent gradual decrease in the fine particle size after the initial nucleation burst is representative of the size to which the particles can grow before being lost to the seeds. During the second burst, the fine particles grow to their largest size, slightly smaller than 1 nm. The rapid scavenging of the fine particles by the seeds limits their growth to sizes far below the mean size.

Similar results for higher initial silane concentrations are presented in Figures

10(a)-(b) (0.10% SiH_4) and Figures 11(a)-(b) (0.71% SiH_4). The general trends are similar to those for 0.018% SiH_4, but the peak size of the fine particles predicted by the two-mode model decreases with reactant concentration while the ultimate size of the seed particles increases.

Figure 12 compares calculations and experimental observations of the variation in the final number concentration with reactant concentration. The measured values are substantially lower than the predicted, but the sensitivity of the number concentrtion to the precursor level is weak in both cases. Possible sources of discrepency are polydispersity (note that the two-mode model yields lower final number concentration than the single mode, monodisperse model), losses to the reactor wall, and particle structure. The collision cross sections of agglomerates particles are larger than those of dense spheres of comparable mass.

Figure 13 compares the number mean mobility equivalent size at the reactor outlet with predictions. The average size increases significantly with increasing silane concentration, and the agreement between the model calculations and the measured values is relatively good. This agreement may be fortuitous, however, because of the differences in the structures produced experimentally with low peak reactor temperatures and the spherical shape assumed in the models.

The average sizes predicted by the two-mode model are larger than those by the single mode. The predicted sizes are larger than the measured mean size for small silane concentrations, but are smaller for higher silane concentrations. This may be due to wall losses. At low silane concentrations, the particles produced are small and can not compete for the condensible vapors as efficiently as the larger particles formed at higher reactant concentrations. The particles generated at these temperatures are low density agglomerates; thus, as long as losses are not important, the measured mean sizes are expected to be larger than those computed based on

the assumption of spherical shape.

6. Conclusions

The present experimental results suggest that the dense silicon particles produced in a single stage multi-zone thermal reactor by Wu et al. (9) resulted not from vapor and cluster deposition on the nuclei generated early in the reaction, but rather by sintering of the agglomerates that had grown by coagulation of like sized particles. Model predictions further support this conclusion, indicating that coagulation plays a major role in particle growth throughout the reactor.

To eliminate coagulation of the "seed" particles formed by nucleation early in the reactor, the seed number concentration must be reduced to a sufficiently low level that the characteristic time for self-coagulation of those seed particles, when they are large, becomes long compared to the residence time in the active portion of the reactor. While this might be accomplished by allowing a long time for coagulation after seed formation, when the particles are still very small, the use of a separate reactor stage for seed particle formation would allow coagulation to be quenched by dilution as demonstrated by Alam and Flagan (18) in the growth of large particles.

Even though agglomerate particles were generated, their fine structure reveals that significant coalescence has taken place. The predicted fine particle size is below 1 nm in all cases. Most of the mass deposits on the seeds in the form of fine particles rather than monomers. The fine structure sizes range from 13 to 19 nm, indicating that the deposited material has coalesced substantially, although incompletely.

8. References

1. Bowen, H.K., *Mater. Sci. Eng.*, 44, 1 (1980).

2. Barringer, E.A., and Bowen, H.K., *Comm. Am. Ceram. Soc.* , C-199 (1982).

3. Gobet, J., and Matejevic, E., *J. Colloid Interface Sci.* , 100, 555 (1984).

4. Cannon, W.R., Danforth, S.C., Flint, J.H., Haggerty, J.S., and Marra, R.A., *J. Am. Ceram. Soc.*, 65, 324 (1982).

5. Cannon, W.R., Danforth, S.C., Haggerty, J.S., and Marra, R.A., *J. Am. Ceram. Soc.*, 65, 330 (1982).

6. Ulrich, G.D., *Combust. Sci. Technol.* , 4, 47 (1971).

7. Ulrich, G.D., Ines, B.A.M., and Subramanian, N.S., *Combust. Sci. Technol.* , 14, 243 (1976).

8. Ulrich, G.D., and Subramanian, N.A., *Combust. Sci. Technol.*, 17, 119 (1977).

9. Wu, J.J, Nguyen, H.V., and Flagan, R.C., *Langmuir* , 3, 266 (1987).

10. Prochazka, S., Greskovich, C., *Am. Ceram. Soc. Bull.*, 57, 579 (1978).

11. Wolfenbarger, K., Ph. D. Thesis, Caltech.

12. Lai, F.S., Friedlander, S.K., Pich, J., and Hidy, G.M., *J. Colloid Interface Sci.*, 39, 395 (1972).

13. Seinfeld, J.H., "*Air Pollution*," Wiley, New York (1986).

14. Meakin, P., and Witten, T.A., Jr., *Phys. Rev. A.* , 28, 2985 (1983).

15. Meakin, P., *J. Colloid Interface Sci.*, 112, 187 (1986).

16. Wu, J.J, Nguyen, H.V., Flagan, R.C., Okuyama, K., and Kousaka, Y., *AIChE Journal*, 34, 1249 (1988).

17. White, R.T., Espino-Rios, R.L., Rogers, D.S., Ring, M.A., and O'Neal, H.E. *Int. J. Chem. Kin.*, 17, 1029 (1985).

18. Alam, M.K., and Flagan, R.C., *Aerosol Sci. Technol.*, 5, 237 (1986).

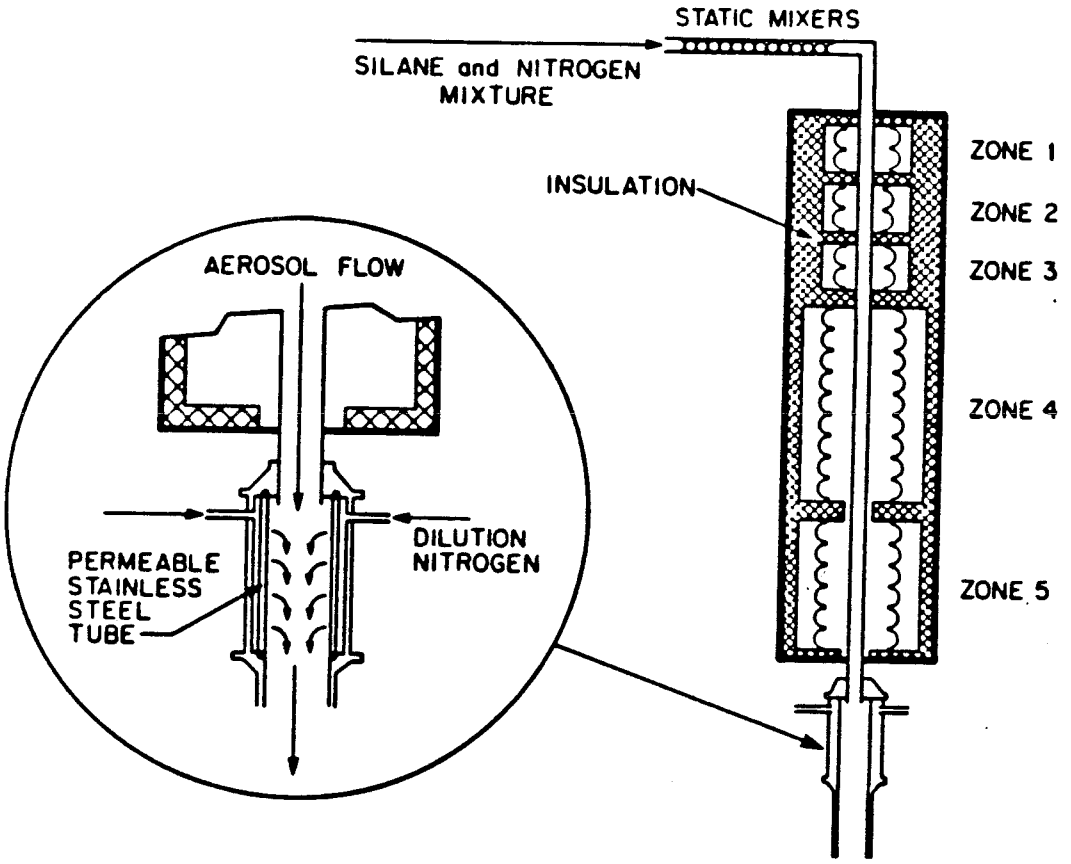

Figure 1. Schematic of the single stage, 5 zone aerosol reactor used in the experiment to produce silicon particles by silane pyrolysis, and the transpired wall system for the product dilution and cooling.

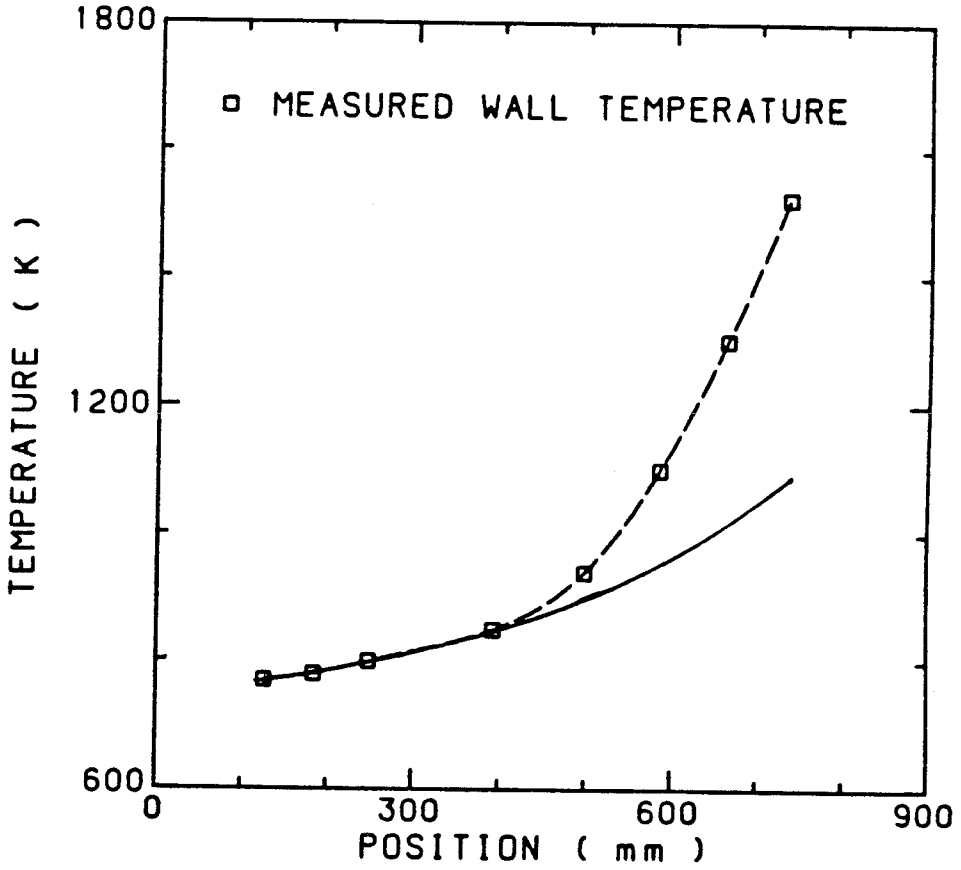

Figure 2. Measured wall temperature profiles.

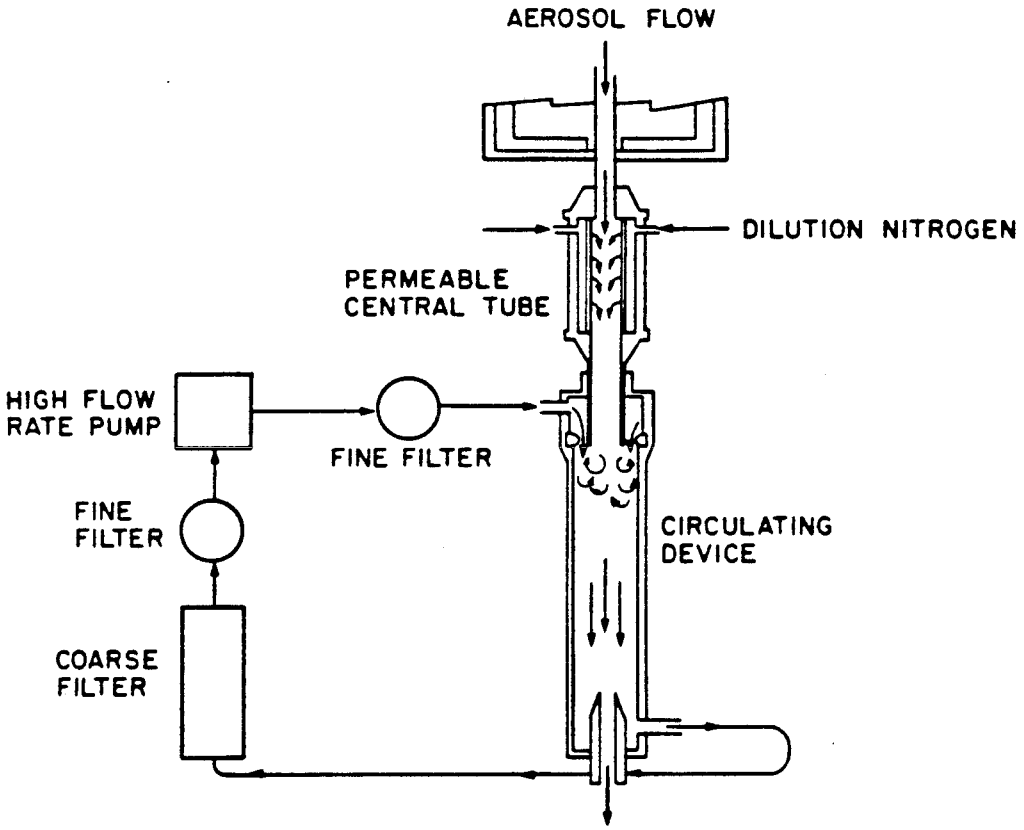

Figure 3. Schematic of the recirculating dilution system.

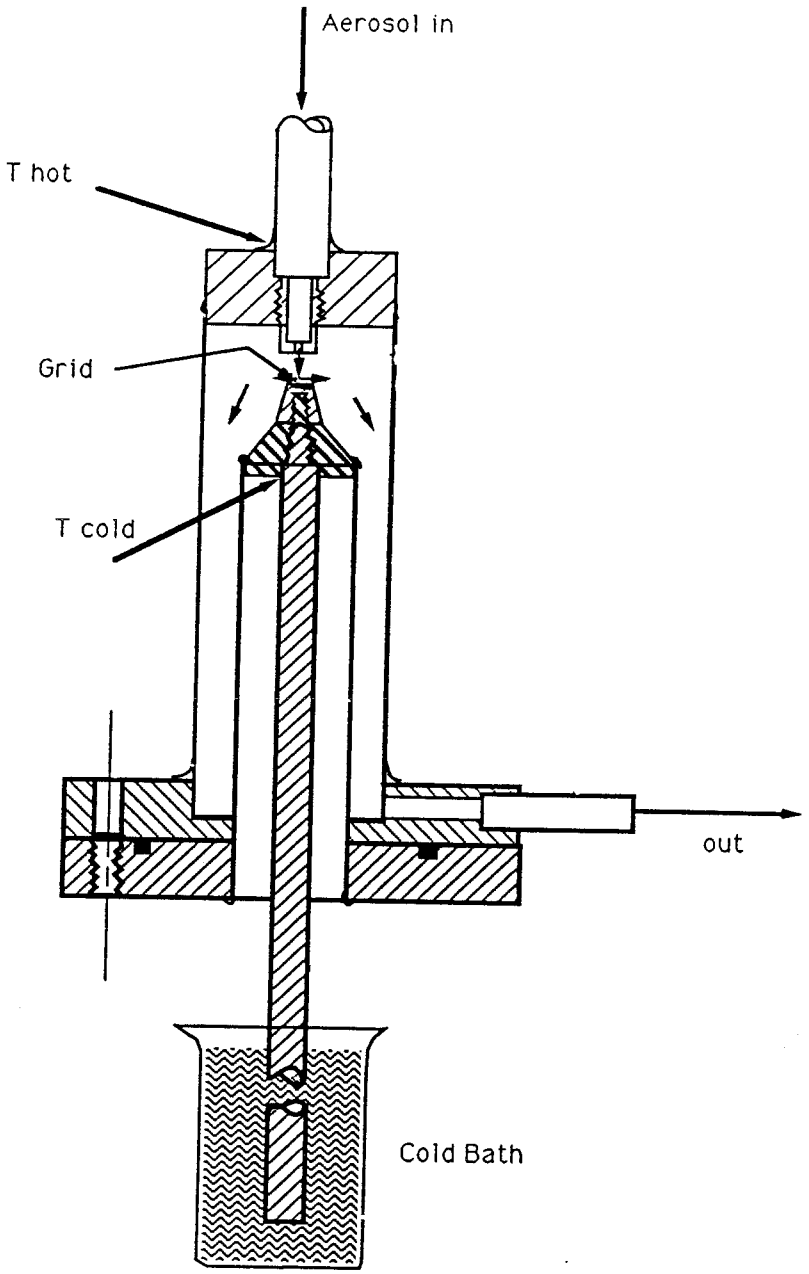

Figure 4. Schematic of the thermophoretic sampling probe used to obtain TEM images of individual particles.

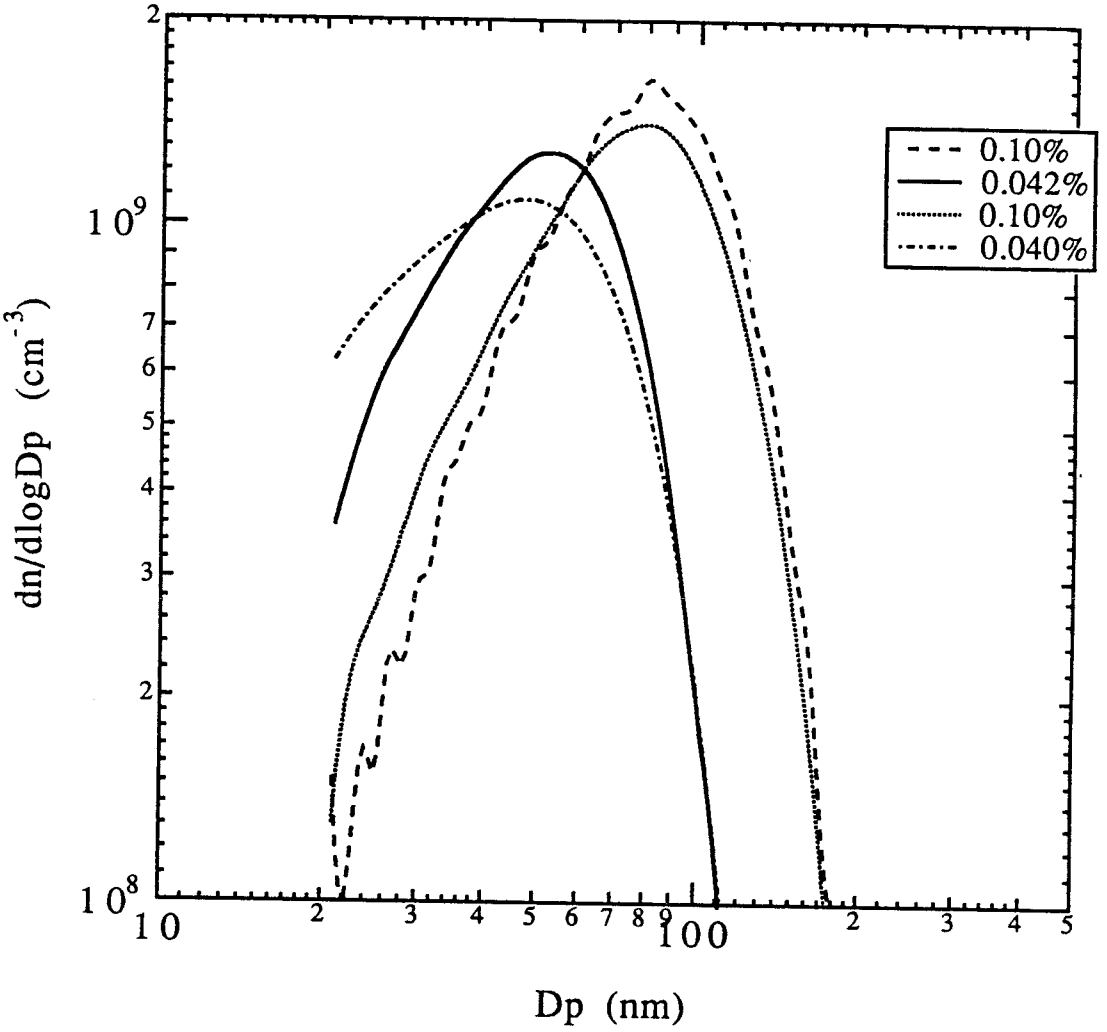

Figure 5. Size distributions for different initial SiH_4 concentrations. The inversions were carried out using the code MICRON.

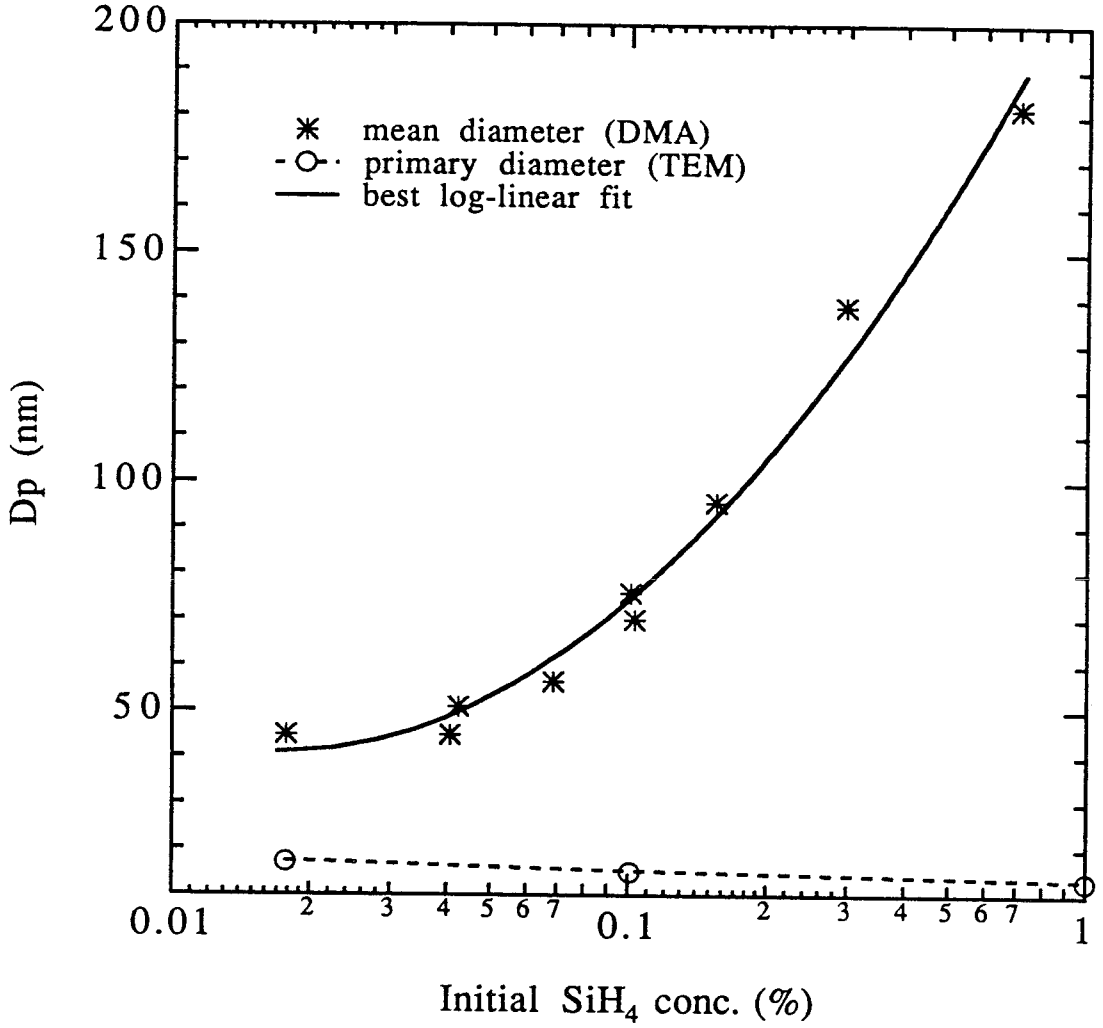

Figure 6. Variation in the particle mean size as a function of initial SiH_4 concentration. Shown are the mean mobility diameter, the best polynomial fit in terms of the natural log of silane concentration, and the primary particle size measured by TEM.

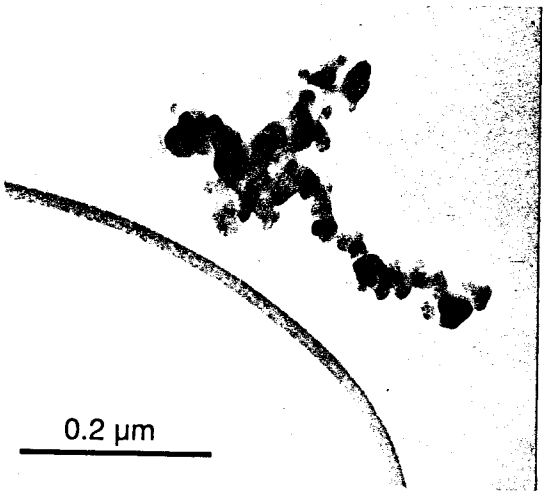

(a) 1073 K

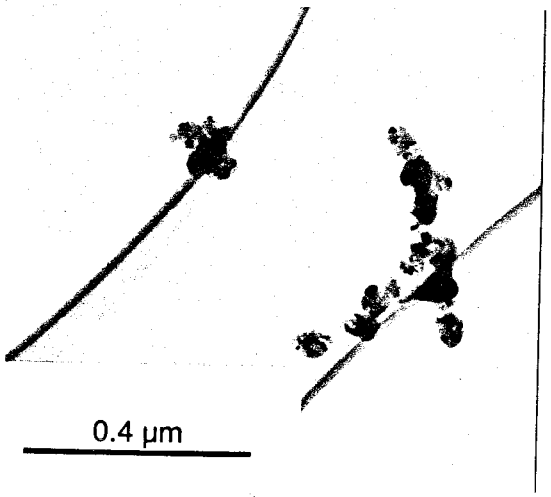

(b) 1273 K

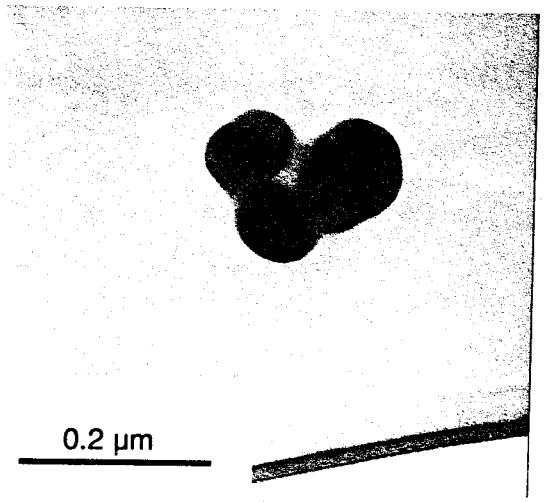

(c) 1473 K

Figure 7. TEM micrograghs of silicon particles produced with an initial SiH_4 concentration of 0.17% at a maximum peak temperature of (a) 1073 K; (b) and (c) 1473 K.

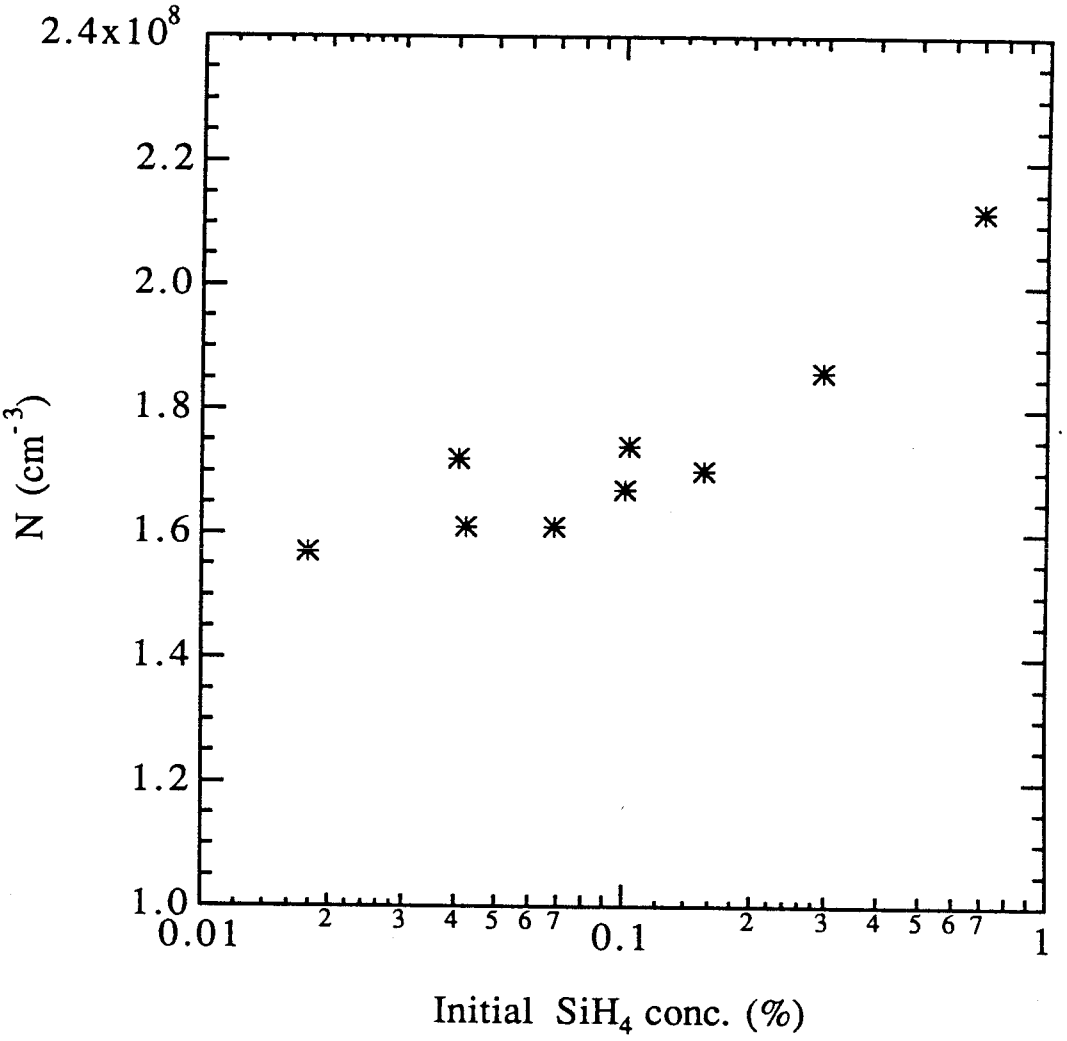

Figure 8. Particle number concentration measured at the reactor outlet using a TSI 3020 CNC as a function of initial SiH_4 concentration.

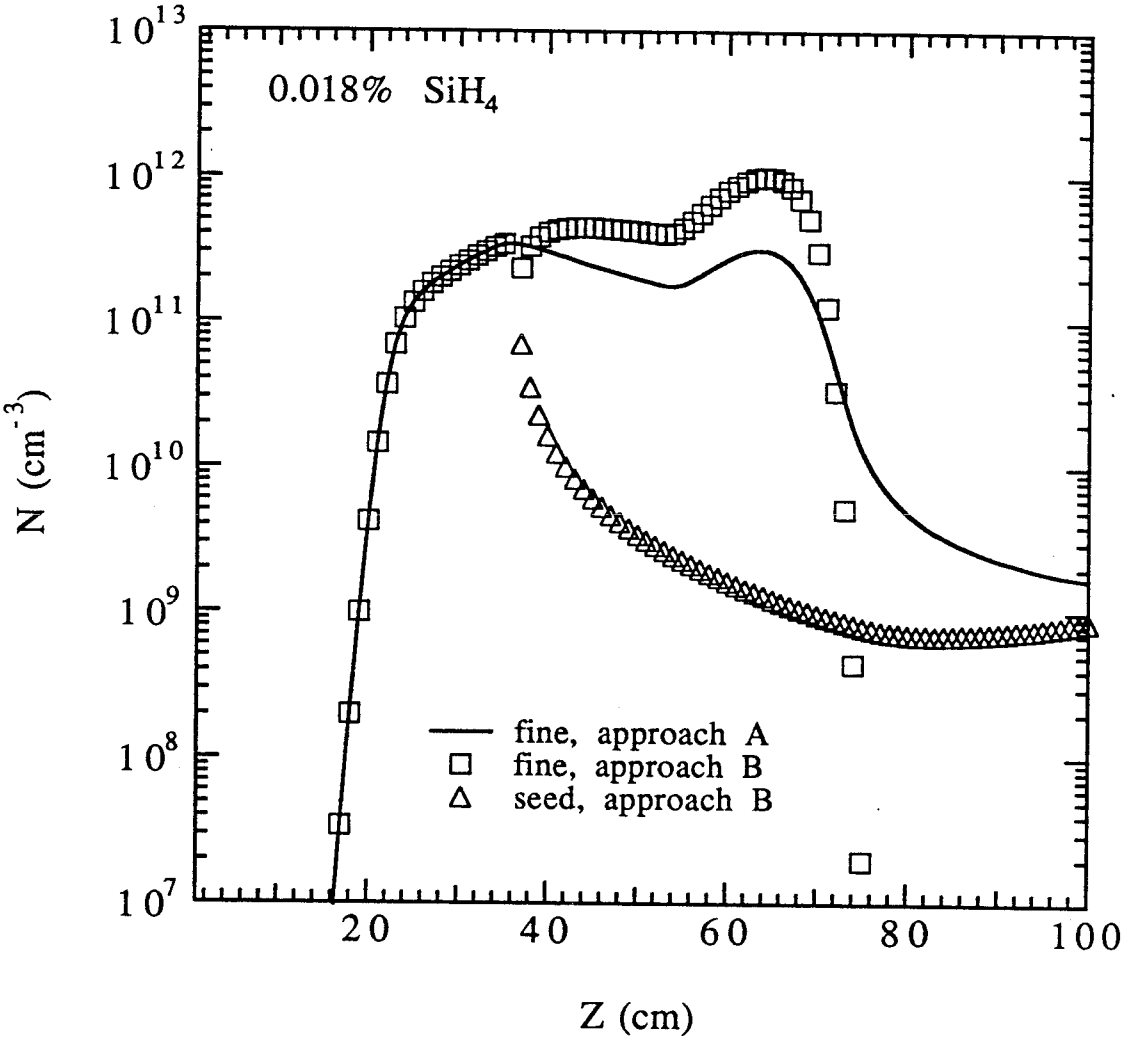

Figure 9(a). Predicted number concentration as a function of axial reactor position for 0.018% SiH_4 using approaches A (single mode), and B (two-mode).

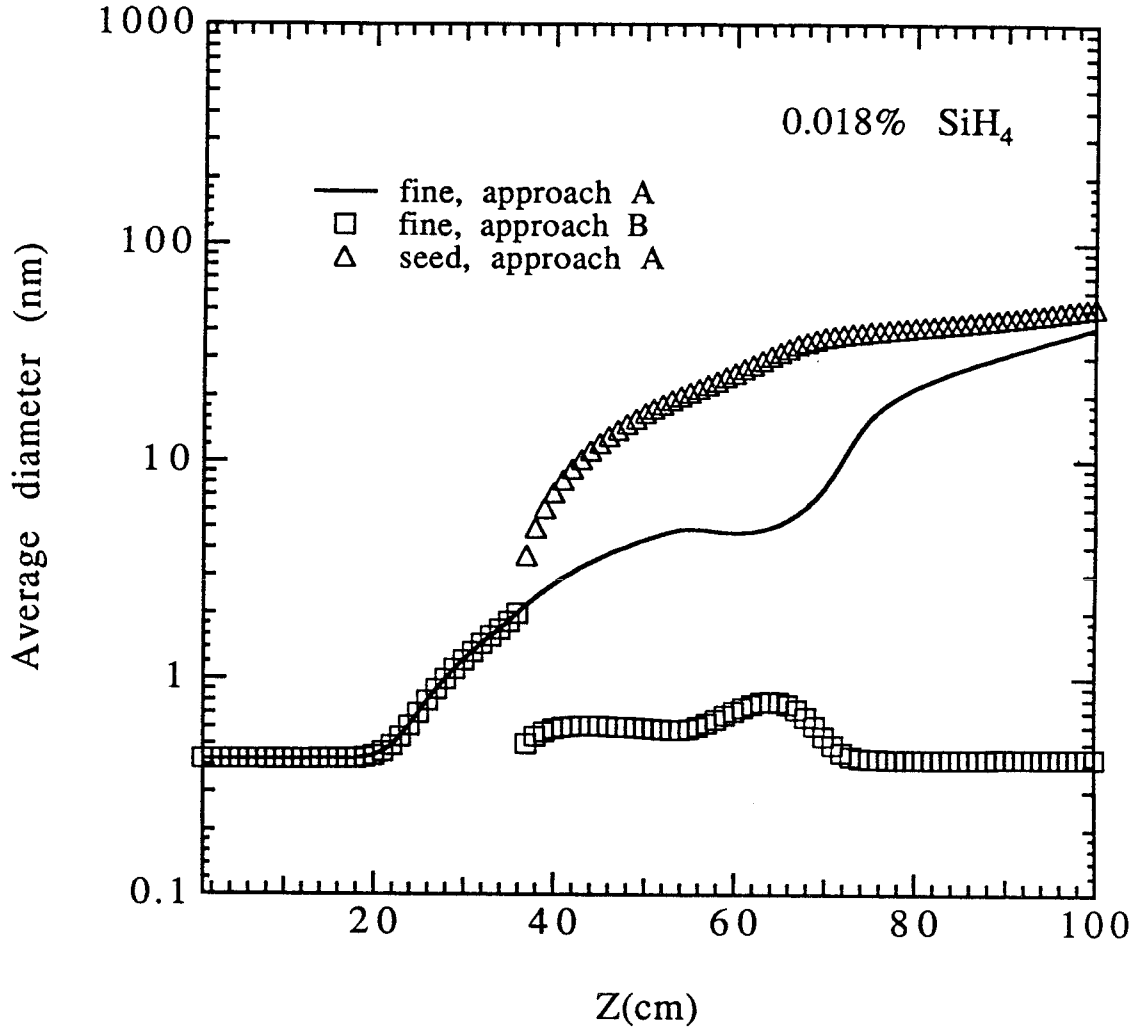

Figure 9(b). Predicted average particle sizes as a function of axial position for 0.018% SiH_4 using approaches A (single mode), and B (two-mode).

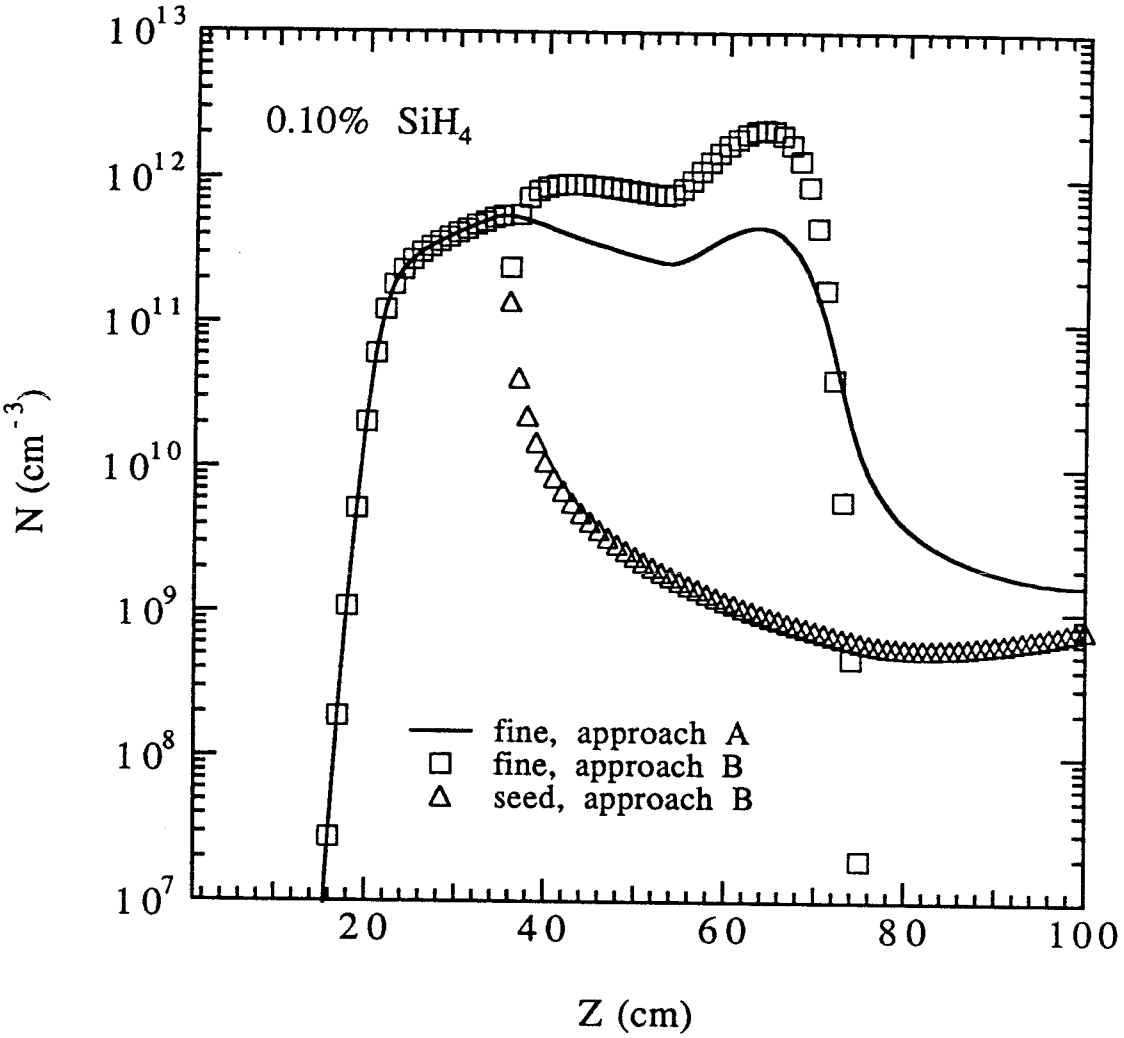

Figure 10(a). Predicted number concentration as a function of axial reactor position for 0.10% SiH_4 using approaches A (single mode), and B (two-mode).

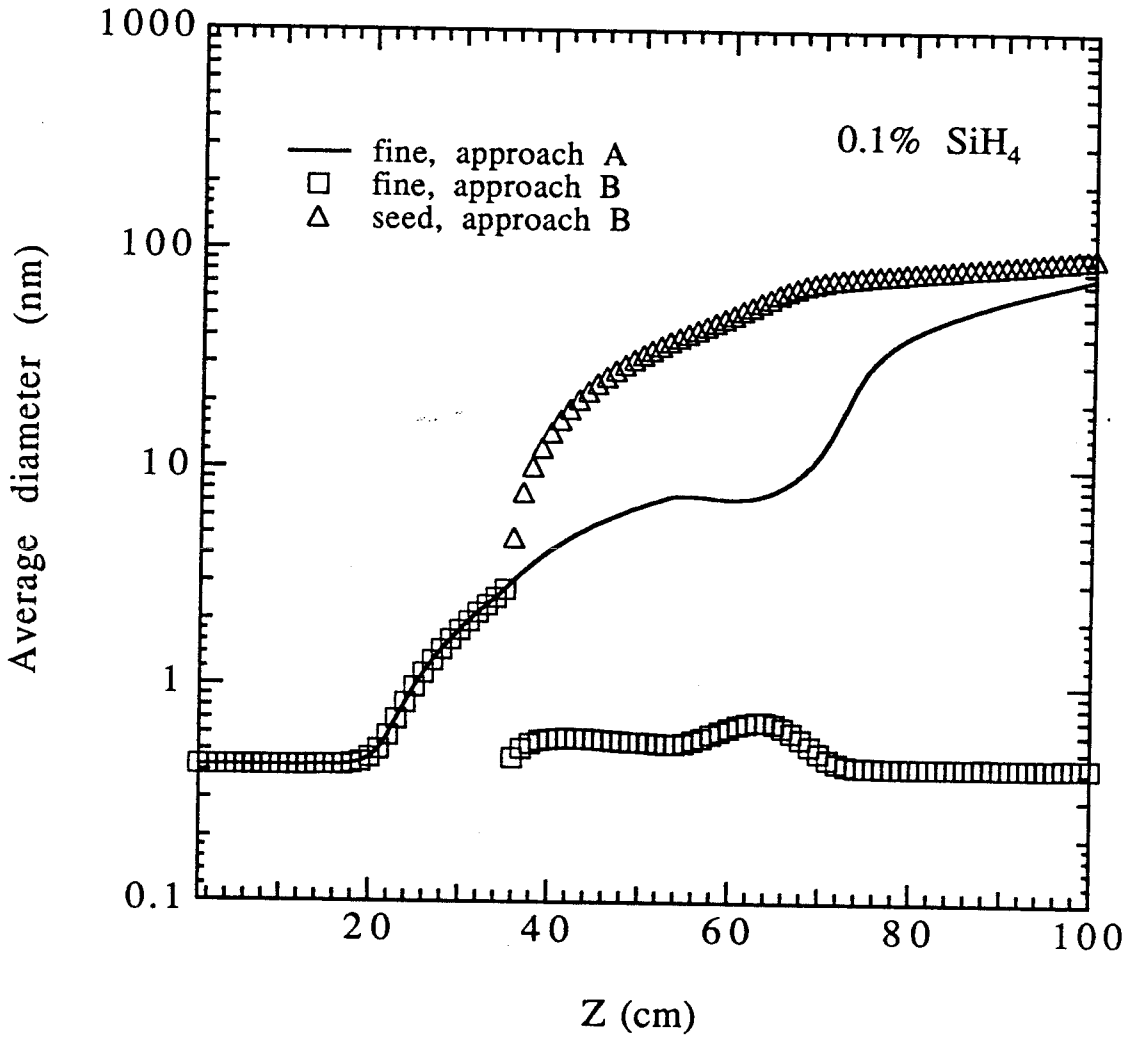

Figure 10(b). Predicted average particle sizes as a function of axial position for 0.10% SiH_4 using approaches A (single mode), and B (two-mode).

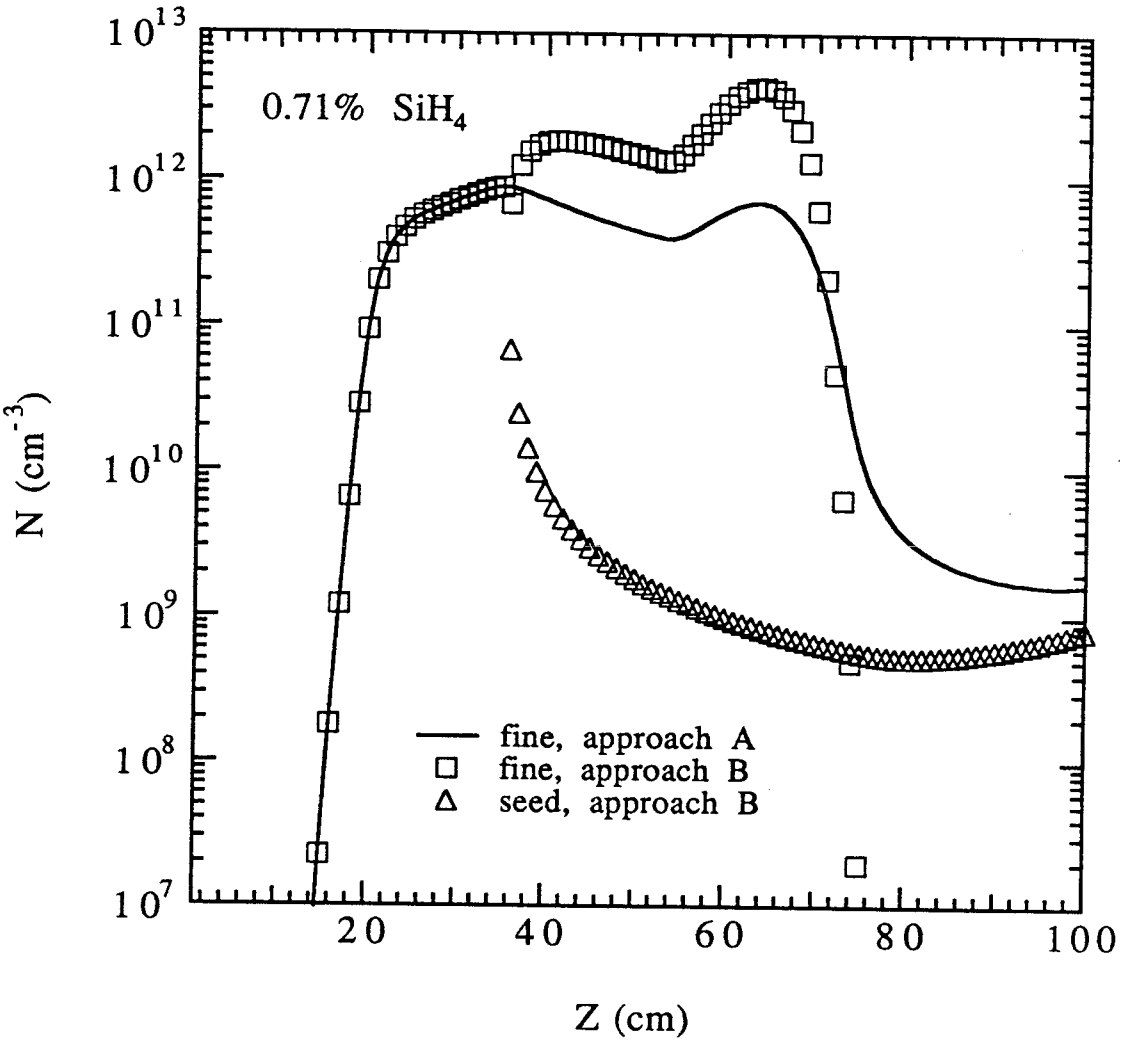

Figure 11(a). Predicted number concentration as a function of axial reactor position for 0.71% SiH_4 using approaches A (single mode), and B (two-mode).

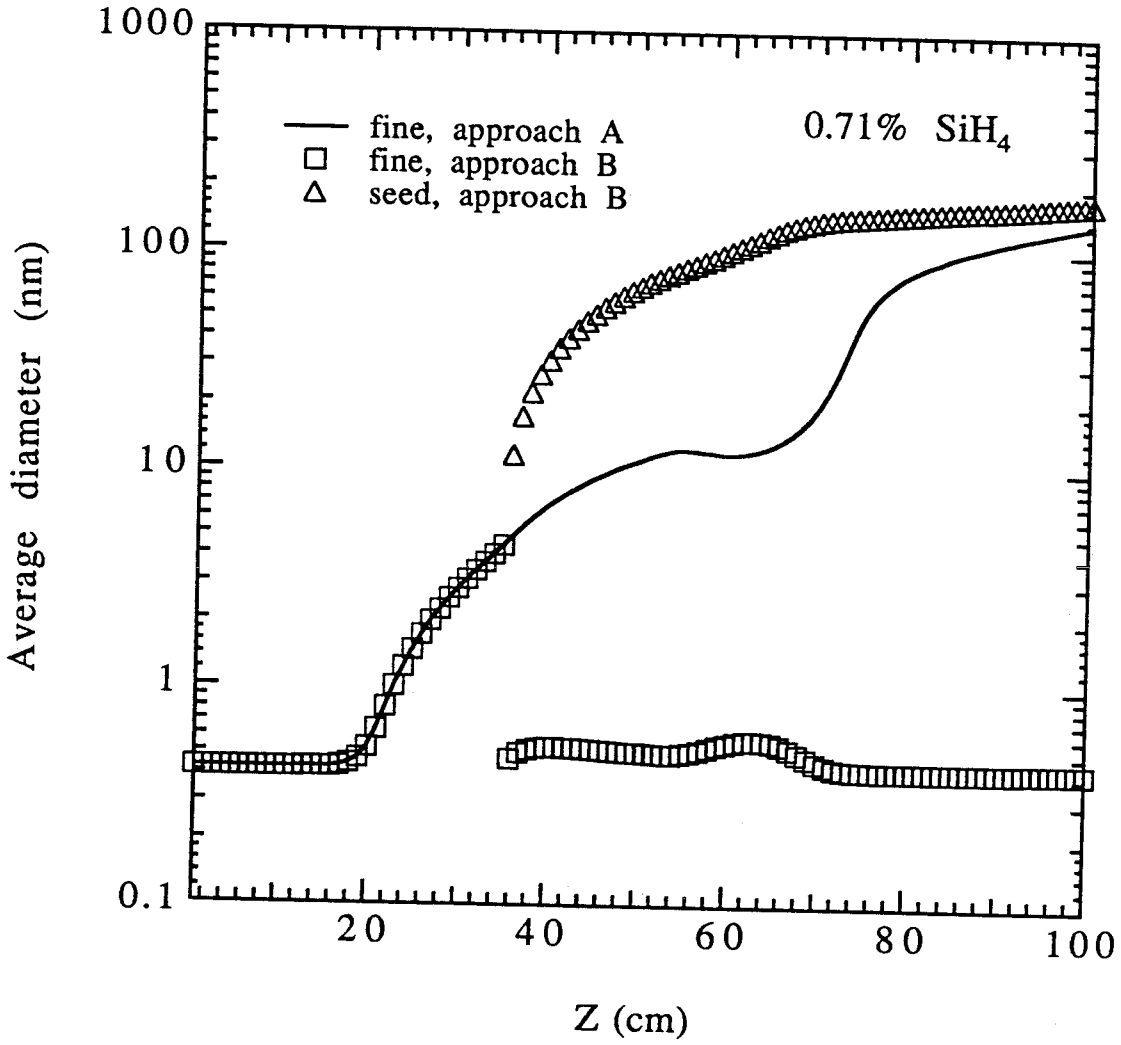

Figure 11(b). Predicted average particle sizes as a function of axial position for 0.71% SiH_4 using approaches A (single mode), and B (two-mode).

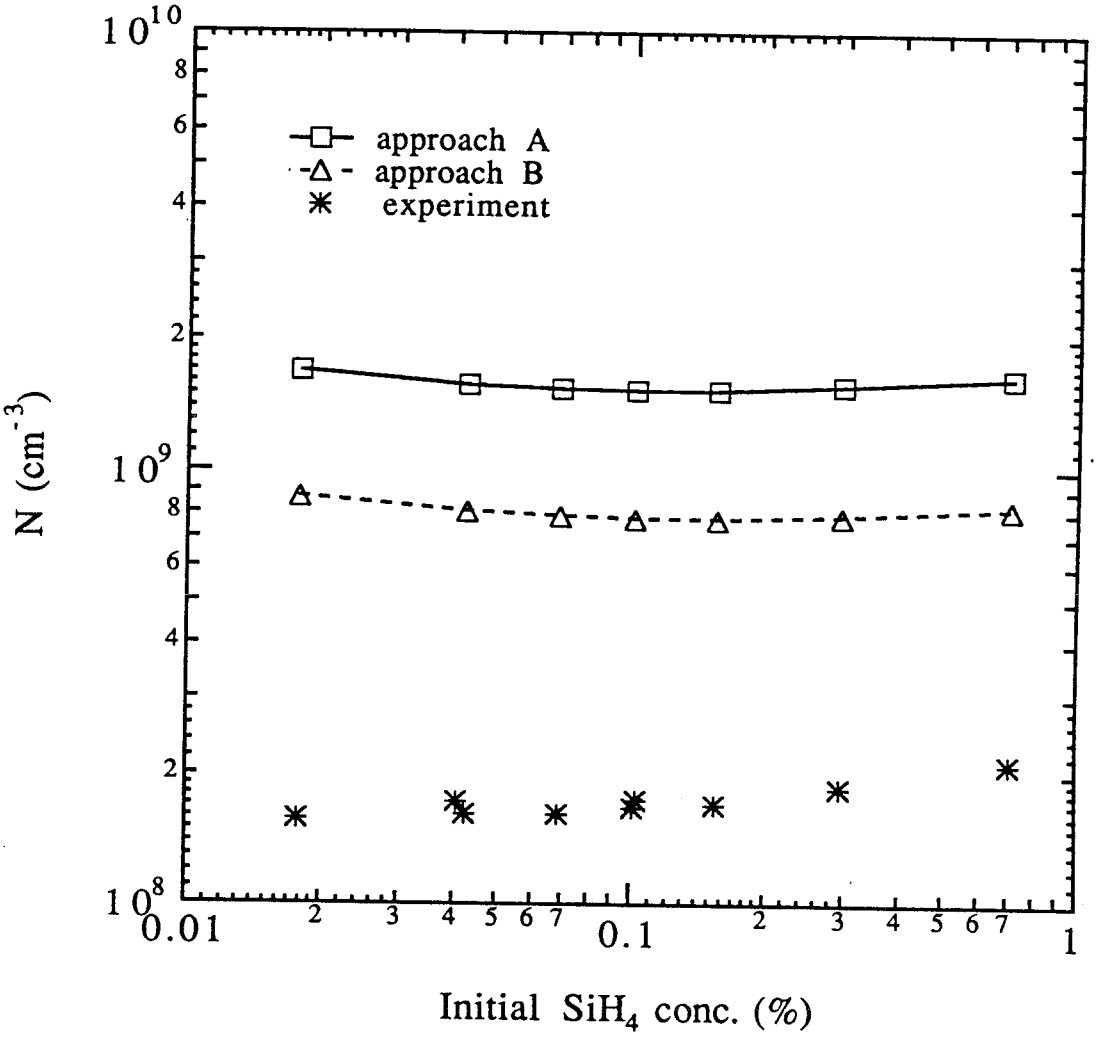

Figure 12. Comparison of the calculated and experimental number concentrations at the reactor outlet as a function of initial SiH_4 concentration.

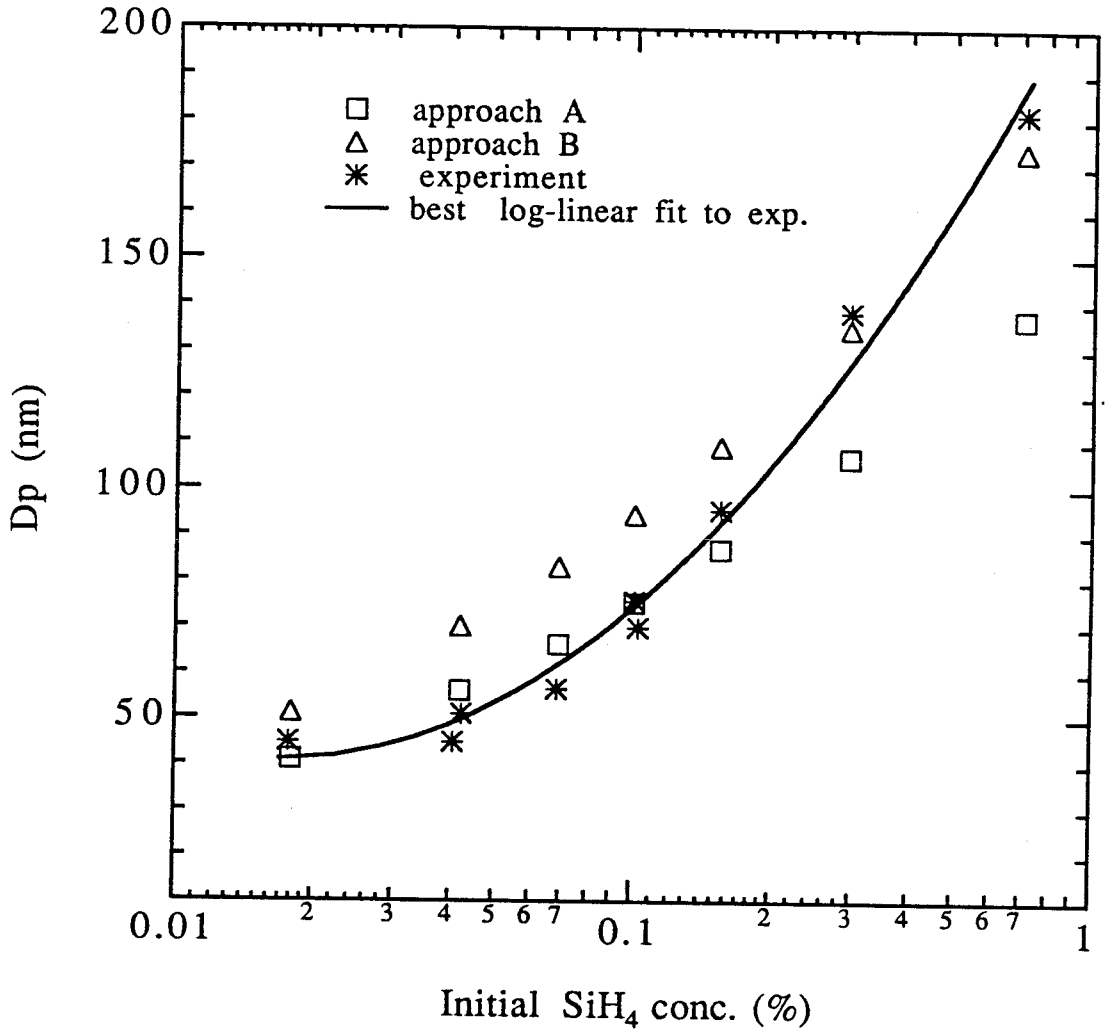

Figure 13. Comparison of the calculated and experimental average diameters as a function of initial SiH_4 concentration.

CHAPTER 4

AEROSOL REACTOR OPTIMIZATION USING THE SIMPLIFIED REACTION COAGULATION MODEL

ABSTRACT

The simulator-optimizer approach has been applied to the highly nonlinear reactor system to directly derive optimal temperature profiles that maximizes the growth of the seed aerosol while minimizes the size of the fine clusters formed, using a modified simplified reaction coagulation (SRC) model as the aerosol dynamic simulator. Optimization results indicate that if the seed sink is too small or the reactor length is too short, large cluster formation can not be suppressed regardless of the temperature profile used. A discrete SRC model has been developed to check the validity and accuracy of the SRC model predictions. The SRC model was found to be adequate for the derivation of the optimal temperature profiles, but for quantitative information, i.e., the absolute value of the mass fraction in the various modes, etc., a more accurate model should be used for the final computation once the optimal profile is found.

1. Introduction

Ceramic materials are generally not as reliable as required for demanding engineering applications. The ultimate strength of a ceramic material is directly related to the flaws formed during fabrication, and those flaws can frequently be traced to the starting powder (1). Under the best circumstances, the maximum flaw size is directly related to the sizes of the largest particles in the powder. Hence, very fine powders are receiving increasing attention for ceramic applications. Irregularly shaped particles introduce kinematic constraints to packing, so nonagglomerated particles of roughly spherical shape are thought to be optimal for ceramic applications.

For these reasons, efforts to produce ceramic materials suitable for demanding applications in engineering systems have focussed on the powders from which the ceramics are synthesized. A number of new chemical processes have been developed to produce the oxide, nitride, and carbide powders with controlled particle size distribution and morphology. Colloidal methods such as the sol-gel process can produce highly uniform, nonagglomerated particles, although the range of compositions is limited primarily to metal oxides (2,3). Interparticle forces can be manipulated in colloidal synthesis, with coulombic or steric repulsion being used to inhibit agglomerate formation. Aerosol routes can be used to generate a broader range of powders than is possible with present colloidal processing technology, but control of particle structure has proven to be considerably more difficult. Nonetheless, aerosol technologies such as plasmas and sprays (4,5) and reactions of gaseous precursors (6-9) have shown good potential for the production of high quality dispersed powders.

The use of gaseous precursors is particularly promising because the method can be applied to virtually any material that can be deposited by chemical va-

por deposition (CVD). Gas phase chemical reactions of these precursors generate condensible vapors from which particles are formed. Surface reactions may also contribute to particle growth. Due to the very low vapor pressures of the ceramic materials, generation of even very small quantities in the vapor phase leads to high supersaturation and subsequent formation of large numbers of fine particles by homogeneous nucelation. These particles grow by the combined effects of condensation, surface reactions, deposition of small clusters, and coagulation with like-sized particles. Agglomerates formed by coagulation may coalesce if the reactions take place at sufficiently high temperatures, for example, in a plasma reactor, or they may persist if the temperature is low enough that coalescence proceeds more slowly than coagulation. Because coagulation is a second order process, the high number concentrations generated by homogeneous nucleation almost invariably lead to rapid coagulation and the resulting formation of agglomerate particles.

In most vapor synthesis processes, particles are formed by homogeneous nucleation. As noted above, this leads to very high number concentrations and particle growth by coagulation. To minimize coagulation, the number concentration must be reduced. If the aerosol reactor were seeded with small particles, the reactions could conceivably grow those seeds by vapor deposition rather than by coagulation, provided homogeneous nucleation could be suppressed. The existence of particles in the reactor is a necessary but not sufficient condition for nucleation suppression in an aerosol reactor. Both heterogeneous condensation and homogeneous nucleation will occur unless the rates of gas phase reactions leading to condensible products are limited so the vapor deposition on the surfaces of growing particles prevents the development of the supersaturation levels required for homogeneous nucleation. Once homogeneous nucleation takes place in the synthesis of refractory powders, the number concentration will be large enough that coagulation will dominate the

growth process.

Alam and Flagan (10) demonstrated that, by severely constraining the reaction rates, seed particles could be grown at constant number concentration in the pyrolysis of silane to produce silicon particles. As the seed particles grow, their ability to scavenge condesible reaction products increases, so higher rates of reaction can be tolerated. Growth of large silicon particles from small seeds was achieved by gradually increasing the temperature along the length of the reactor, thereby taking advantage of this increase in the scavenging efficiency. The reactor was designed using the known decomposition kinetics of the silane precursor and an approximate model of nucleation suppression by aerosol particles.

Assuming the primary mechanism of particle growth in the silane pyrolysis reactor to be silicon monomer deposition, one might expect this rate-constrained seed growth to generate dense particles. Subsequent investigations of the structures of particles grown in this way revealed low density agglomerates, suggesting that the seed particles were grown by deposition of clusters rather than by monomer deposition, and further that the clusters were too large to sinter fully before additional deposition took place (11). One may speculate that the reaction rates would have to slowed even further to minimize the formation of such clusters and, thereby, to grow fully dense particles. Alternate approaches to reaction rate scheduling are needed to define the reactor operating conditions that would achieve this objective. No method has yet been proposed for direct determination of the optimal reactor design to meet these stringent requirements.

This study is a first attempt to apply optimization techniques to highly nonlinerar aerosol reactor systems to derive the reaction rate schedule that would produce high quality refractory powders under constraints of finite reactor volume,

throughput, residence time, initial seed size, seed number concentration, and initial reactant concentration.

2. Modelling of Aerosol Dynamics

Simulation of the full aerosol dynamics is essential to the design of an aerosol reactor. The evolution of an aerosol under the influences of homogeneous nucleation, condensation and evaporation, and coagulation is described by the so-called General Dynamic Equation (GDE). The most rigorous description is provided by the discrete form of the GDE in which the change in the concentrations of monomers, dimers, trimers, and all larger clusters is described by a separate ordinary differential equation for the number concentration of clusters of the appropriate size. Homogeneous nucleation is incorporated in this representation through the population balances on clusters smaller than the thermodynamically stable size, taking into account condensation and evaporation of monomers. Coagulation of clusters of all sizes can conceivably be followed using the discrete representation of the GDE, although the method is limited to the cluster sizes of fewer than a few hundred monomers in practice due to computational limitations.

To follow the dynamics of an aerosol system that extends over many orders of magnitude of particle mass, the discrete GDE is usually cast in integral form. The most common form of the continuous GDE (12) is

$$\begin{aligned}\frac{\partial n(v,t)}{\partial t} =& \frac{1}{2}\int_0^v K(v-\tilde{v})n(v-\tilde{v},t)n(\tilde{v},t)\,d\tilde{v} \\ &- \int_0^\infty K(\tilde{v},v)n(v,t)n(\tilde{v},t)\,d\tilde{v} \\ &- \frac{\partial}{\partial v}[I_o(v)n(v,t)] + J_o(v)\delta(v-v_o), \end{aligned} \qquad [2.1]$$

where $n(v,t)$ is the size distribution function, and $n(v,t)\,dv$ is defined as the number per unit volume having volumes in the range v to $v + dv$. $K(v,\tilde{v})$ is the coefficient of coagulation of two particles of volumes v and $\tilde{v}$. The term on the left-hand side describes the evolution of the aerosol with time. The first term on the right-hand side represents the formation of particles of volume v from the coagulation of particles smaller than v; the second term represents the coagulation of particles of volume v with other particles, forming particles with volume larger than v; and the third term is the net growth term, representing the change in the aerosol size distribution due to condensation, evaporation, chemical reaction, or phase transition (12). The fourth term represents the rate of particle formation by nucleation of condensible vapors. The delta function indicates that nucleation occurs at a critical volume v_o.

Numerical solution of the continuous GDE requires integration over the particle size distribution at each time step. While the numerical demands of this calculation are considerably less than the solution of the discrete GDE equations for particles ranging from monomer to hundreds of nanometers in size, they remain severe. Gelbard and coworkers (13) introduced the sectional approximation to the continuous GDE to overcome this difficulty. The sectional model represents the continuous particle size distribution function $n(v)$ as a histogram. Within each section, i.e., between v_i and v_{i+1}, the mass distribution is assumed to be constant. Balance equations were derived to conserve mass exactly as the populations of the various sections change through the action of condensation, evaporation, and coagulation. The rates of mass transfer between sections can be expressed as the products of the masses in the two sections and coagulation frequency function that is evaluated by integration of the integral terms of the continuous GDE over the appropriate limits. For isothermal systems, this integration must be performed only once for each pair

of sections, so the need for numerical integration over the particle size distribution function is eliminated. The integro-differential equation of the continuous GDE is reduced to a relatively small set of ordinary differential equations. Thus, the sectional model represents a major reduction in the computational demands with a relatively minor sacrifice in computational precision.

Both the continuous and sectional GDE solutions are suitable for particles that are much larger than the monomer, but do not account for the large differences between sizes of adjacent cluster sizes at the small end of the particle size spectrum. Gelbard and Seinfeld (14) addressed this issue with the development of the discrete-continuous model, a hybrid representation in which a discrete representation of the smallest clusters was coupled to the continuous representation of larger particles. Wu and Flagan (15) later adapted this approach to the development of a discrete-sectional model (DS). The discrete-sectional model accounts for both discrete particle size effects and the broad range of particle sizes that must be followed in aerosol reactors and other aerosol systems.

Although the sectional or discrete-sectional models offer major reductions in the computational demands over more exact representations, these methods are still too computer intensive for the present purpose of reaction rate schedule design since the optimization will require integration of the aerosol dynamic equations along the length of the reactor many times for a single design optimization. Further simplifications are needed to facilitate reactor design calculations.

Simple integral or moment models, although they cannot track the evolution of the size distribution, can describe the important features of the aerosol system with relatively little computational effort (16-18). Most of the moment models implemented have used the classical nucleation theory for the computation of the

particle generation rate. This is reasonable for atmospheric aerosol systems or systems in which the dimensionless source rate (the ratio of the monomer production rate to the rate of monomer-monomer collision at saturation vapor pressure) are smaller than or of order one. Due to the very low saturation vapor pressures of the refractory materials produced in aerosol reactors, the dimensionless source rates can exceed 10^8. This renders key assumptions in the classical nucleation theory invalid, notably the assumption of a steady-state distribution of subcritical clusters. The critical size computed based on this theory is estimated to be of atomic dimensions or smaller in some cases, indicating the absence of a thermodynamic (Gibbs free energy) barrier to particle formation. Under these conditions, even the smallest clusters are stable. Furthermore, most of the studies using these models neglected particle coagulation (a critical assumption for our present purposes) and were limited to isothermal systems (a more readily relaxed assumption). A similarity transformation is valid at long times when coagulation is the dominant growth mechanism, leading to the *so called* self-preserving particle size distribution function (19). This model is not appropriate for dense particle production, since coagulation without complete sintering to coalescence results in low density flocs.

A particularly simple model that retains the essential features of the general dynamic equation is the simplified reaction coagulation model (SRC). This model, which is described in detail below, follows the evolution of two modes of the particle size distribution: (*i*) homogeneously nucleated or fine particles; and (*ii*) seed particles. SRC model calculations of particle formation and growth in aerosol reactors have been compared with the more detailed predictions of the discrete-sectional model (20). The SRC model predictions agree reasonably well with those of the DS model, particularly when reaction is important relative to coagulation.

The advantages and disadvantages of the various aerosol dynamic models de-

scribed above are summarized in Table I. For the optimal reactor design problem addressed in this chapter, the aerosol dynamic equations must be integrated along the length of an aerosol reactor many times. Since many evaluations are necessary, a fast and fairly accurate model is needed. The SRC model meets these criteria and was chosen for this study.

2.1 The SRC Model

The SRC model describes the aerosol size distribtuion with two modes, the homogeneously nucleated or fine mode, and the seed mode. Each mode is represented by number, N and mass, M, concentrations, with the fine mode denoted by the subscript H, and the seed mode by the subscript S. In this study, the original SRC model was modified to include a separate balance for monomers. The temperature, reactant and aerosol concentrations were assumed to be uniform across the reactor tube. Wall losses were neglected, and the average cross sectional velocity was used. Using the SRC model, the entire aerosol system can be described by a set of seven nonlinear ordinary differential equations:

$$\frac{d}{dz}(C_A u_z) = -R \qquad [2.2]$$

$$\frac{d}{dz}(N_1 u_z) = R\ N_{AV} - K_1 N_1^2 - K_{1H} N_1 N_H - K_{1S} N_1 N_S \qquad [2.3]$$

$$\frac{d}{dz}(N_H u_z) = \frac{1}{2} K_1 N_1^2 - \frac{1}{2} K_H N_H^2 - K_{HS} N_H N_S \qquad [2.4]$$

$$\frac{d}{dz}(M_H u_z) = m_1 K_1 N_1^2 + m_1 K_{1H} N_1 N_H - \bar{m}_H K_{HS} N_H N_S \qquad [2.5]$$

$$\frac{d}{dz}(N_S u_z) = -\frac{1}{2} K_S N_S \qquad [2.6]$$

$$\frac{d}{dz}(M_S u_z) = m_1 K_{1S} N_1 N_S + \bar{m}_H K_{HS} N_H N_S \qquad [2.7]$$

$$u_z \rho C_p \frac{dT}{dz} = \frac{4}{D_R} h_x (T_w - T) \qquad [2.8]$$

with initial conditions

$$N_H = M_H = 0 \qquad [2.9]$$

$$N_S = N_{So} \qquad [2.10]$$

$$M_S = M_{So} \qquad [2.11]$$

$$T = T_o \qquad [2.12]$$

at z = z_o, where K_1, K_{1H}, K_{1S}, K_H, K_{HS}, K_S represent the coagulation coefficients and are computed using Fuchs' interpolation formula, and $\bar{m}_H$ is the average mass of a particle in the fine mode and is evaluated by

$$\bar{m}_H = \frac{M_H}{N_H}.$$

D_R, ρ, C_p, and u_z, are the reactor diameter, bulk gas density, thermal conductivity, and average velocity, respectively. T and T_w are the gas and wall temperatures. h_x is the average local heat transfer coefficient computed from the local Nusselt number for laminar flow. Because neither the reactor wall temperature nor the heat flux along the ractor tube is constant, an averaged Nusselt number of the two limiting cases was used, i.e., $N_u = 4$. N_{AV} is Avogadro constant, and R is the reaction rate.

On application of the steady state one dimensional continuity equation

$$\frac{d}{dz}(u_z \rho) = 0, \qquad [2.13]$$

Eqs. [2.2] to [2.7] become

$$u_z\rho\frac{d}{dz}(\frac{C_A}{\rho}) = -R \qquad [2.14]$$

$$u_z\rho\frac{d}{dz}(\frac{N_1}{\rho}) = R\ N_{AV} - K_1N_1^2 - K_{1H}N_1N_H - K_{1S}N_1N_S \qquad [2.15]$$

$$u_z\rho\frac{d}{dz}(\frac{N_H}{\rho}) = \frac{1}{2}K_1N_1^2 - \frac{1}{2}K_HN_H^2 - K_{HS}N_HN_S \qquad [2.16]$$

$$u_z\rho\frac{d}{dz}(\frac{M_H}{\rho}) = m_1K_1N_1^2 + m_1K_{1H}N_1N_H - \bar{m}_HK_{HS}N_HN_S \qquad [2.17]$$

$$u_z\rho\frac{d}{dz}(\frac{N_S}{\rho}) = -\frac{1}{2}K_S{N_S}^2 \qquad [2.18]$$

$$u_z\rho\frac{d}{dz}(\frac{M_S}{\rho}) = m_1K_{1S}N_1N_S + \bar{m}_HK_{HS}N_HN_S. \qquad [2.19]$$

The detailed chemical reaction mechanism and reaction kinetics of precursors used in aerosol reactors are rarely known. The actual chemical pathway usually involves many elementary reactions. However, in many cases and for the present purpose, it is sufficient to use the rate expression of the rate limiting step. For this study, the reaction was assumed to be first order,

$$R = -\frac{dC_A}{dt} = k_AC_A \qquad [2.20]$$

with an Arrhenius rate constant

$$k_A = Ae^{-E_R/R_gT}, \qquad [2.21]$$

where A is the preexponential factor, E_R is the activation energy, and R_g is the gas constant. Upon nondimensionalization with the dimensionless groups

$$\frac{1}{\Delta_1} = \frac{\tau_{res}}{\tau_{rxn}} = \frac{L_R/U_{ave}}{1/k_{Aave}}, \quad \frac{1}{\Delta_2} = \frac{\tau_{res}}{\tau_{11}} = \frac{L_R/U_{ave}}{2/K_{1o}N_{1o}},$$

$$\frac{1}{\Delta_3} = \frac{\tau_{res}}{\tau_{sc}} = \frac{L_R/U_{ave}}{1/k_{1So}N_{So}}, \quad \frac{1}{\Delta_4} = \frac{\tau_{res}}{\tau_\theta} = \frac{L_R/U_{ave}}{(\rho_{ave}\ C_{pave}\ D_R)/4h_{xave}},$$

$$\Gamma = \frac{\rho}{\rho_{ave}}, \quad \Gamma_o = \frac{\rho_o}{\rho_{ave}}, \quad \beta_A = \frac{k_A}{k_{Aave}}, \quad \beta_1 = \frac{K_1}{K_{1o}}, \quad \beta_{1H} = \frac{K_{1H}}{K_{1o}},$$

$$\beta_H = \frac{K_H}{K_{1o}}, \quad \beta_{1S} = \frac{K_{1S}}{K_{1So}}, \quad \beta_{HS} = \frac{K_{HS}}{K_{1So}},$$

$$\beta_S = \frac{K_S}{K_{1So}}, \quad \omega_H = \frac{\bar{m}_H}{m_1}, \quad \Omega = \frac{m_1 N_{1o}}{M_{total}},$$

$$X_A = \frac{C_A/\rho}{C_{Ao}/\rho_o}, \quad X_1 = \frac{N_1/\rho}{N_{1o}/\rho_o}, \quad X_H = \frac{N_H/\rho}{N_{1o}/\rho_o},$$

$$X_S = \frac{N_S/\rho}{N_{So}/\rho_o}, \quad X_{MH} = \frac{M_H/\rho}{M_{total}/\rho_o}, \quad X_{MS} = \frac{M_S/\rho}{M_{total}/\rho_o},$$

$$\xi = \frac{z}{L_R}, \quad \Xi = \frac{h_x}{h_{xave}}, \quad \zeta = \frac{C_p}{C_{pave}},$$

$$\Theta = \frac{T - T_o}{T_{ave} - T_o}, \quad \text{and} \quad \Theta_w = \frac{T_w - T_o}{T_{ave} - T_o},$$

where τ_{res} is the average reactor residence time, τ_{rxn} is the characteristic reaction time, τ_{11} is the characteristic monomer-monomer collision time, τ_{sc} is the characteristic scavenging time of the seed mode, and τ_θ is the characteristic time for heat transfer, we obtain

$$\frac{dX_A}{d\xi} = \frac{1}{\Delta_1}\beta_A X_A \Gamma \qquad [2.22]$$

$$\frac{dX_1}{d\xi} = \frac{1}{\Delta_1}\beta_A X_A \Gamma - \frac{2}{\Delta_2}\beta_1 X_1^2 \Gamma^2/\Gamma_o - \frac{1}{\Delta_2}\beta_{1H} X_1 X_H \Gamma^2/\Gamma_o - \frac{1}{\Delta_3}\beta_{1S} X_1 X_S \Gamma^2/\Gamma_o \qquad [2.23]$$

$$\frac{dX_H}{d\xi} = \frac{1}{\Delta_2}\beta_1 X_1^2 \Gamma^2/\Gamma_o - \frac{1}{\Delta_2}\beta_H X_H^2 \Gamma^2/\Gamma_o - \frac{1}{\Delta_3}\beta_{HS} X_H X_S \Gamma^2/\Gamma_o \qquad [2.24]$$

$$\frac{dX_{MH}}{d\xi} = \frac{1}{\Delta_2}\Omega\beta_1 X_1^2 \Gamma^2/\Gamma_o + \frac{1}{\Delta_2}\Omega\beta_{1H} X_1 X_H \Gamma^2/\Gamma_o - \frac{1}{\Delta_3}\Omega\ \omega_H \beta_{HS} X_H X_S \Gamma^2/\Gamma_o \qquad [2.25]$$

$$\frac{dX_S}{d\xi} = -\frac{1}{2}\frac{1}{\Delta_3}\beta_S X_S^2 \Gamma^2/\Gamma_o \qquad [2.26]$$

$$\frac{dX_{MS}}{d\xi} = \frac{1}{\Delta_3}\Omega\beta_{1S}X_1 X_S\ \Gamma^2/\Gamma_o + \frac{1}{\Delta_3}\Omega\ \omega_H\beta_{HS}X_H X_S\Gamma^2/\Gamma_o \qquad [2.27]$$

$$\frac{d\Theta}{d\xi} = \frac{1}{\Delta_4}\frac{\Xi}{\zeta}(\Theta_w - \Theta). \qquad [2.28]$$

This set of nonlinear ordinary differential equations were solved using the ODE solver package EPISODE.

3. Optimization

3.1 The Physical Problem

In a chemical plant, it is often of interest to find the temperature control stategy that will maximize the output of a certain chemical product, while suppressing the production of other by-products. For ceramic powder synthesis in an aerosol reactor, the ultimate goal is to produce uniformly sized, semi-equiaxed (roughly spherical), dense, noagglomerated particles.

To achieve this objective the formation of large numbers of fine particles by homogeneous nucleation must be suppressed. While the formation of small numbers of seeds *in situ* may be possible, the extreme sensitivity of the nucleation rate to the monomer production rate makes single stage reactor design and control exceedingly difficult. Nucleation suppression and growth of high quality powder can be achieved more readily using seed particles produced from a separate reactor. If the seed particles can be grown purely by vapor deposition with no stable new particles being generated, and with little self-coagulation of the seed particles, then the resulting powder would be expected to consist of dense, nonagglomerated particles. Unless the source rate is kept so low that very long residence time will be needed for appreciable seed growth, stable clusters will always be present in significant concentrations, making cluster deposition an important growth mechanism.

Figure 1 illustrates the role of clusters in the growth of a solid particle. As a cluster deposits onto the seed particle, it begins to undergo structural rearrangment governed by solid state diffusion. If the driving force for coalescence is large, the cluster may completely sinter into the seed particle before another one arrives, and the particle may remain fully dense throughout the growth process. If, on the other hand, the cluster is only partially sintered when a new cluster arrives, an agglomerate will be formed. Therefore, whether or not solid, dense particles are generated depends on the two time scales, that of coalescence $\tau_{coalescence}$ and that of arrival to the surface $\tau_{arrival}$. If $\tau_{coalescence} << \tau_{arrival}$, dense particles result; but if $\tau_{coalescence} >> \tau_{arrival}$, low density agglomerates result. Thus, suppression of new particle formation is necessary, but may not be sufficient to ensure the production of dense particles; the number of large clusters that would coalesce slowly must be limited as well.

In terms of the SRC model, the reactor design objective becomes maximizing the amount of mass scavenged by the seed particles while minimizing that in the fine mode. It is very important to minimize the mass in the fine mode at all times, since a large fraction of mass in the fine mode means large clusters will be formed. This might be achieved by adding the reactant continuosly along the reactor tube, with a fixed reactor temperature. Since the reaction rate is only linearly dependent on the reactant concentration while exponentially dependent on the temperature, suppression of cluster formation by this method is very difficult. The more sensitive or effective control variable is the reactor temperature.

3.2 Mathematical Statement of Optimization

Our problem falls under the general class of lumped parameter systems and can be formulated as follows: Find the control variable schedule $\mathbf{u}(z)$ that maximizes

(or minimizes the negative thereof) an objective function $I(\mathbf{u}(z))$, i.e.,

$$\max_{\mathbf{u}(z)} \quad I(\mathbf{u}(z)) \tag{3.1}$$

subject to the governing set of ordinary differential equations for the state variables

$$\frac{d\mathbf{x}(z)}{dz} = \mathbf{f}(\mathbf{x}(z), \mathbf{u}(z)), \tag{3.2}$$

with initial conditions

$$\mathbf{x}(z_o) = \mathbf{x_o}, \tag{3.3}$$

and equality and inequality constraints

$$\mathbf{h}(\mathbf{x}, \mathbf{u}) = \mathbf{0} \tag{3.4}$$

$$\mathbf{g}(\mathbf{x}, \mathbf{u}) \leq \mathbf{0}, \tag{3.5}$$

where, in this case, $\mathbf{x}(z)$, the vector of the state variables, represents the reactant, fine mode, and seed mode concentrations, etc., and $\mathbf{u}(z)$, the vector of control variables, represents the reactor temperature which we would like to determine optimally. The scalar objective function $I(\mathbf{u})$ is a function of the state variables at the reactor outlet and the path within the reactor, i.e.,

$$I(\mathbf{u}(z)) = \mathbf{G}(\mathbf{x}(z_f)) + \int_{z_o}^{z_f} \mathbf{F}(\mathbf{x}(z), \mathbf{u}(z))dz. \tag{3.6}$$

3.2.1 Control Vector Iteration Procedures

The equality and inequality constraints [3.4] and [3.5] add considerable complexity to the optimization problem. If the problem involves only simple bounds on the control variable of the form

$$\mathbf{u}_l \leq \mathbf{u} \leq \mathbf{u}_p, \tag{3.7}$$

and no other equality or inequality constraints are imposed, the necessary conditions for optimality can be shown to be (21,22)

$$\frac{\partial \mathbf{H}}{\partial \mathbf{u}} = \mathbf{0} \tag{3.8}$$

on the unconstrained portion of the path, and $\mathbf{H}$ be at the maximum on the constrained portion of the path, where $\mathbf{H}$ is the Hamiltonian defined by

$$\mathbf{H} = \mathbf{F}(\mathbf{x}, \mathbf{u}) + \lambda^{\mathbf{T}} \mathbf{f}(\mathbf{x}, \mathbf{u}). \tag{3.9}$$

Here λ is the time dependent Lagrange multiplier, and is defined by

$$\frac{d\lambda^{\mathbf{T}}}{dz} = -\frac{\partial \mathbf{H}}{\partial \mathbf{x}} \tag{3.10}$$

and

$$\lambda_i(z_f) = \frac{\partial \mathbf{G}}{\partial x_i} \tag{3.11}$$

for the state variables not specified at $z = z_f$ (21,22). The optimality conditions for the case with the equality and inequality constraints can be found in Bryson and Ho (22) and will not be presented here.

We are faced with a very difficult two-point boundary value problem where the initial conditions for $\mathbf{x}$ are given at $z = z_o$ and the initial conditions for λ at $z = z_f$. One of the methods that can be used to solve the problem is the control vector iteration procedures (21). This technique makes use of the fact that the change in the objective function due to perturbations in the control variables can be expressed as

$$\delta I = \int_{z_o}^{z_f} \left[\sum_i \frac{\partial \mathbf{H}}{\partial u_i} \delta u_i(z) \right] dz. \qquad [3.12]$$

If the control variable profile $u_i(z)$ is not optimal, the maximum improvement in I can be made by choosing $\delta u_i(z)$ to be corrected in the gradient direction at each z. By choosing

$$\delta u_i(z) = \epsilon \frac{\partial \mathbf{H}}{\partial u_i}, \qquad \epsilon > 0 \qquad [3.13]$$

one obtains

$$\delta I = \epsilon \int_{z_o}^{z_f} \left[\sum_i \left(\frac{\partial \mathbf{H}}{\partial u_i} \right)^2 \right] dz > 0, \qquad [3.14]$$

which guarantees that $\delta I > 0$ for values of ϵ small enough that the linear approximation made in deriving the optimality conditions is not violated.

With these results, optimization is achieved by the following iterative procedures:

(1) Guess $\mathbf{u}_g(z)$, $0 \leq z \leq z_f$.

(2) Integrate the state Eqs. [3.2] forward in z using the values of $\mathbf{u}_g(z)$ to generate $\mathbf{x}_g(z)$, $0 \leq z \leq z_f$.

(3) With these values of $\mathbf{u}_g(z)$ and $\mathbf{x}_g(z)$, integrate the adjoint Eqs. [3.10] backward in z to produce $\lambda(z)$, $0 \leq z \leq z_f$.

(4) Correct $\mathbf{u}_g(z)$ using Eqs. [3.13] with an arbitrary value of ϵ. Compute I for the new values of $\mathbf{u}(z)$.

(5) If $I(\mathbf{u}(z)) > I(\mathbf{u}_g(z))$, double ϵ and repeat step (4); if $I(\mathbf{u}(z)) < I(\mathbf{u}_g(z))$, half ϵ and repeat step (4). Do this until a concave function $I(\epsilon)$ is achieved.

(6) Fit the results to a quadratic $I(\epsilon)$ and find the value at which $I(\epsilon)$ is maximum, i.e., find ϵ_{opt}.

(7) Update $\mathbf{u}_g(z)$ by

$$\mathbf{u}_g^{new} = \mathbf{u}_g^{old} + \epsilon_{opt} \frac{\partial \mathbf{H}}{\partial \mathbf{u}} \qquad [3.15]$$

and return to step (2).

(8) Iterate until convergence.

At first glance this method seems very attractive, since one can use the state (model) equations directly in the optimization procedures. However, as can be seen, the control vector procedures require storage of the values of the state variables along z for use in the backward integration to evaluate λ, which, again, must be stored in order to compute the correction for δu_i. For a set of equations that are not very stiff, where one can use a relatively large fixed stepsize for both the forward and backward integration, this is not a problem. One can store the values at fixed intervals with little storage space required to accomplish the task.

For a very stiff set of nonlinear equations, as in aerosol models, where variable step sizes must be used for fast and accurate integration, this method presents a problem. A very small step size means large storage allocation is needed. Variable step sizes mean the forward integration steps along z are different from the backward

steps, and interpolation of the state, control, and adjoint variables is necessary. In addition, the equations for the adjoint variable λ requires the evaluation of partial derivatives of the state equations (see Eqs. [3.10], [3.9], and [3.2]). Some of the partial derivatives cannot be evaluated analytically, and must be approximated by finite differences. This adds to the errors and instability in the integration. Furthermore, some of the partial derivatives are singular at the end points due to physical constraints. Nonlinear constraints on the state and control variables further complicate the procedures. Moreover, changes in the objective function, constraints, or model require complete modification of the optimization code since the state and the adjoint equations are coupled, making this technique very inflexible.

3.2.2 The Simulator-Optimizer Approach

A simpler approach is to decouple the state or dynamic equations from the optimization procedures, and use a separate, proven, and efficient nonlinear program solver as the optimizer (23). In this method (Fig. 2), values of the objective function, gradients, and constraints are supplied to the optimizer, when required, using the simulator. To the optimizer, the simulator is just another routine supplying the necessary information for it to do its job, which is to find the values of the control variables that maximize or minimize the objective function. The job of the simulator is to compute the objective function and constraints given the values of the control variables. This technique has the advantage of arbitrary specification of the objective function and constraints, so long as they can be computed. Furthermore, changes to the simulator can be made easily, independent of the optimizer (23). The relative ease of implementation and versatility of this method make it well suited for aerosol reactor optimization.

3.3 Aerosol Reactor Optimization

The simulator-optimizer (SO) method was used for the derivation of optimal reactor conditions in this study. The similator for the aerosol reactor was the SRC model. The control variable is the reactor temperature. The problem involves a tubular reactor consisted of a tube externally heated by a series of heaters or zones, each of which can be controlled (Fig. 3). Given the reactor size (diameter and length), initial reactant concentration, total flow rate, activation energy for the reaction rate constant, and seed particle number concentration and size, the goal is to find the temperatures of the zones that will maximize a certain objective with or without constraints. Thus, the variables to the optimizer are the zone temperatures. Note that the continuous control function $\mathbf{u}(z)$ is now reduced to a finite number of control variables u(z_1), u(z_2), ... u(z_{N_z}), where N_z is the number of zones. The reactor wall temperature was assumed to vary linearly from the midpoint of one zone to the next. The reactor and the gas are at room temperature at the reactor inlet, i.e., at $z = 0$. The lengths of the zones and the number were specified in the problem statement and not optimized directly. The gradients were computed by perturbation (Fig. 4). Central difference was used to ensure adequate accuracy. The bounds on the temperatures were such that the reaction rate constant could not be less than 10^{-3}s^{-1} and more than 100s^{-1}. This restrained the optimizer from choosing unrealistically low or high temperatures, causing problems with the simulator. The optimizer used was the nonlinear problem solver NPSOL from the Systems Optimization Laboratory of Standford University (24).

4. Optimization Results

Calculations were performed for a model product material with a molecular weight $M_W = 28.09$ g mol^{-1} (silicon), and density $\rho_s = 3.44$ g cm^{-3} (silicon nitride) in nitrogen carrier gas at a concentration of $C_{Ao} = 10^{-7}$ mol cm^{-3}. The reactor

consisted of five zones, each 0.2 m in length, with a diameter $D_R = 2$ cm. The total flow rate was 1500 cm^3 s^{-1}, and the first order rate constant used was $k_A = 10^{13} \times e^{-24056/T}$ s^{-1}.

4.1 Simple Objective Function Without Constraints

The optimization was first carried out for a simple objective function and no constraints. The objective here was to grow the seed particles as large as possible in the available residence time, i.e., maximize the final mass fraction in the seed mode, $I_1 = X_S$. Fig. 5(a) shows the plot of three gas temperature profiles along the reactor length (normalized) for an initial seed concentration $N_{So} = 10^7$ cm^{-3} and size $d_{So} = 100$ nm for three different initial guesses; the corresponding optimal zone temperatures are tabulated in Table II. All of the initial guessed wall temperature profiles were flat, i.e., all of the zones had the same initial temperatures. In each case, the reactor temperature rises from room temperature to about 800 K, decreases slightly, then increases again. The beginning of the profile is the same for all three cases. The curve for the initial guess temperature of 875 K differs from the other calculations in the region from $Z/L_R = 0.5$ to $Z/L_R = 0.8$. All three profiles show a final rapid increase in temperature from $Z/L_R = 0.8$ to the end of the reactor.

Figure 5(b) is the corresponding plot of the fraction of the reactant mass converted to the fine and seed modes versus reactor position. In all cases, a large fraction of the mass goes into the fine mode before being scavenged by the seed particles. Most of the mass is deposited in the seed mode late in the reaction. The differences in the peak mass of fraction in the fine between the three profiles amount to about 3%. The maximum fine mode mass fractions are about 33%. The 875K initial guess indicates a slightly lower final mass fraction (98.6%) then the other two (99.95%).

Figures 5(c) and 5(d) show the normalized fine mode number concentration, N_H/N_{1o}, and the average mode diameters versus reactor position, respectively, for the initial guess of 950K. There is a burst of fine particle formation early in the reaction. The number concentration decreases midway, increases again, and finally drops rapidly. The initial burst generates many small particles. These particles then grow as the reaction slows and the number decreases. The high number concentration near the reactor outlet, and the corresponding small average size of the particles in the fine mode indicates that small clusters are lost to the seeds as fast as they are formed and do not grow significantly late in the reaction. Similar behaviors were obtained for the other two initial guesses.

Calculations performed for different initial seed number concentrations and sizes are tabulated in Table III(A) and (B). The final mass fraction in the seed mode increases with increasing seed number concentration at a fixed seed size and initial precursor concentration, and with increasing seed size at a fixed seed number concentration.

4.2 Objective Functions With Constraints

As seen from the results presented above for a simple objective function without constraints, although the optimum values of the objective function are very close for different initial guesses, the details of the temperature profile can be quite different, i.e., the profiles are not unique. More important is the very high peak mass in the fine mode. We would like to lower this peak as much as possible to reduce the number of large clusters formed. An objective funtion that not only maximizes the final mass fraction in the seed mode, but also minimizes the peak mass in the fine mode at any point in the reactor is $I_2 = X_S - X_{Hmax}$. An additional constraint that 99.99% of the precursor must be reacted by the exit of the reactor, i.e., $X_{CA} \leq 10^{-4}$,

was imposed to insure that the optimizer would not choose the path to react only a small amount of the precursor in order to maximize I_2. This is important in practice since many reactants and byproducts are either too reactive or harmful to permit significant carry-over, so their concentrations must be limited to a safe level.

Figures 6(a) and (b) show the temperature profiles and the mass fraction versus reactor length for the same conditions as in Figs. 5(a) - (d), but with the new objective function and constraint. It is clear that the profiles are almost identical for all three different initial guesses. Furthermore, the peak mass in the fine mode is reduced by half, from 33% to 17%. The final mass fraction of the seed mode is, however, slightly lower than before, reduced from 99.9% to 98%. It can be seen from Fig. 6(c) that the qualitative behavior is the same as that shown in Fig. 5(c), but the magnitudes of the various peaks in the number concentration are different. The dip in the temperature and the number concentration of the fine mode early in the reactor is sharper, while the latter peak in the concentration is higher for the present case. Note that the peak mass fraction is lower, but extends longer along the reactor to near the reactor exit.

Figures 7(a) and (b) are plots of temperature and mass fraction versus reactor position, respectively, for $N_{So} = 10^8$ cm^{-3}. The solid lines represent the results using I_1 and the dashed line using I_2 as the objective function. With I_1, the optimal profile is not unique. Any guessed profile that results in complete reaction within a fraction of length from the reactor exit is also an optimal profile, since the number of seed particles are so high that they can scavenge all of the mass by coagulation. Shown here are the results for the initial guessed wall temperature profile of 875 K. With I_2, a totally different temperature profile was obtained. Both cases result in 100% of the mass scavenged by the seed mode. However, the peak mass fraction in the fine mode is about 18% when optimized with objective function I_1 compared

to a fraction of a percent with I_2. The final seed particle number concentration, in this case, is reduced by about 25% by self-coagulation.

Using the objective function I_2, the effects of residence time on the resulting temperature profile and the the particle evolution were evaluated. The results are shown in Figs. 8(a) - (d). Except for the reactor zone lengths, all conditions were the same as that of Figs. 6(a) - (d). The length of the first zone in each case was 0.2 m. The lengths of the remaining zones were varied from 0.4 m to 0.8 m. The temperature overshoot near the beginning of the reactor disappears and the temperature during the early stages of reaction decreases with increasing zone, and, thus, reactor length. The trend after the initial peak is a gradual increase in the temperature followed by a rapid increase near the reactor outlet. The peak mass in the fine mode also decreases with increasing reactor length, from approximately 17% to 1% (Fig. 8(b)). The mass scavenged by the seed particles exceeds that of the fine mode much earlier in the reactor as the length increases. The reduction in the seed number concentration due to self-coagulation, however, increases with increasing reactor length, from 3.8% for zone length $\Delta Z_{zone} = 0.2$ m to 7.7% for $\Delta Z_{zone} = 0.8$ m.

Calculations using the objective function I_2 for different initial seed sizes are recorded in Table III(B) along with the results using I_1. Under these conditions, I_2 has no effect on the optimal temperature profile, the final mass fraction of the seed mode, and the peak mass fraction in the fine mode.

From the results, we see that a simple objective function of maximizing only the final mass of the seed mode may not yield unique solutions, particularly if the time scale for scavenging is short compared to the reactor residence time, i.e., Δ_3 is very small. With this simple objective function, no constraint is placed on

the path of maximization. When the sink is very large (very high seed number concentration and/or large seed size), it can scavenge all of the mass by coagulation within available residence time. Thus, any temperature profile that causes all of the reactant to be consumed relatively early in the reactor is an optimal solution. When the sink is too small to scavenge all of the mass available, the path that maximizes I_1 (maximizing the mass in the seed mode, no constraints) is the same as that which optimizes I_2 (maximizing the mass in the seed mode while minimizing the peak mass in the fine mode) because the only way to get as much mass into the seed mode as possible is by minimizing the mass in fine mode at all times. It should be noted that when the sink is very small, and the reactor residence time is very short, there is no way for the seed particles to collect all of the mass available regardless of the temperature profile used.

Increasing the initial seed concentration or size increases the capacity of the seed particles to scavenge, resulting in an increase in the final mass fraction in the seed mode and a decrease in the peak mass fraction in the fine mode. Higher activation energy forces the reactor to operate at higher temperatures which reduces the average residence time, thereby reduces the final mass fraction in the seed mode and increases the peak mass fraction in the fine mode.

Placing constraints on the path, like limiting the peak mass in the fine mode and the concentration of the precursors at the reactor outlet, reduces the solution domain. For most of the cases studied, the sink is small enough that only one solution is possible. It can be envisioned that with a very large sink, Δ_3 small, only the temperature profile in the first half of the reactor may be unique, requiring very slow reactions initially until the seed particles grow sufficiently and until most of the precursors are reacted. Once the reaction approaches completion or the sink grows sufficiently, the temperature has no further effect on the objective function.

If no other constraints are active, the profile can take any form, and, thus, loses its uniqueness. However, the lack of uniqueness in this case does not alter the growth mechanism during the important stages of growth, when control of the growth path is most critical.

More important is the the physical significance of choosing the right objective function with proper constraints on the path to control the quality of the powders produced. Without minimizing the mass in the fine mode, large clusters may be produced in high numbers that will likely result in the formation of low density flocs. Even with the minimization of the peak mass in the fine mode under conditions ensuring that all the mass will be scavenged by the seed particles within the available residence time, if the sink is too small, large clusters will be formed and the particles generated may not be dense. This means there is a minimum (critical) sink mass required to both suppress new particle formation and allow growth by vapor and small cluster deposition which result in dense particles. Below this critical mass, the sink is unable to suppress the production a high number of large clusters, and low density aggregates result. This physical picture is consistent with, and may explain the experimentally observed low density agglomerates resulting even when the seed particles were grown under constant apparent number concentration.

5. The Discrete SRC Model

The SRC model is a very simplified representation of the General Dynamic Equation. While its solution provides important insights into the dynamics of aerosol powder synthesis reactors, it offers an incomplete picture of the fine particle evolution. The characteristic particle size for each mode is the number mean diameter. No information regarding the polydispersity of the mode is generated. The production of fine particles by monomer-monomer agglomeration reduces the mean

size of the fine mode, but physically increases the breadth of the size distribution. The growth of the larger nuclei present when new nuclei are formed will be enhanced by increased coagulation among the nuclei. Consequently, the downward shift in the mean size of the nuclei (fine particles) may be accompanied by an increased tendency to form low density aggregates due to the increase in the maximum size in the large diameter tail of the fine mode distribution. The SRC model does not treat any of this detail in aerosol evolution.

Additional computational artifacts may arise due to the size dependence of the coagulation rate coefficient. In the free molecular limit, the coagulation rate coefficient for particles of widely disparate sizes is $K_{HS} \propto Dp_H^{-3/2}$. Thus, reducing the mean size in the fine mode leads to an increase in the predicted flux of the fine particles into the seed mode.

On the other hand, the flux of monomer into the fine mode by condensation (coagulation of the monomers with the fine particles) is $\propto N_1 N_H D p_H^2$. This means that the higher the number concentration and the larger the average particle size, the larger the flux of monomers into the fine mode. To reduce this flux, both the number concentration and the average size of the particles in the fine mode need to be reduced. The number concentration can be reduced by both self-coagulation and coagulation with the seed particles. The reduction by self-coagulation increases the average particle size, while that by coagulation with the seeds has no net effect on the average size. As self-coagulation reduces the number of fine particles from N_{Hi} to N_{Hf}, the mean particle size increases from D_{Hi} to $D_{pHf} = D_{pHi}(N_{Hi}/N_{Hf})^{1/3}$. The net result of this process is a decrease in the flux of the monomers to the fine mode by condensation from $N_1 N_{Hi} D_{pHi}^2$ to $N_1 N_{Hi}^{2/3} N_{Hf}^{1/3} D_{pHi}^2$. This also leads to a decrease in the flux of fine particles to the seed mode because of both the decrease in the number concentration and the increase in the average size ($K_{HS} \propto D_{pH}^{-3/2}$).

If the fine particles are allowed to exist at high number concentration, they will continue to grow by condensation. By scavenging the condensible vapors, they not only grow larger, but in doing so, also reduce the mass flux to the seed mode by reducing the coagulation coefficient with the seed particles and the amount of vapor available. If the growth is significant, the fine particles will not coalesce completely upon agglomeration. Therefore, reduction of the number concentration in the fine mode by self-coagulation is physically advantageous in maximizing the mass in the seed mode and minimizing the mass in the fine mode, as long as this occurs while the fine particles are still very small so that complete coalescence is achieved.

The overshoots and subsequent decrease seen in some of the optimal temperature profiles produce both the physically consistent phenomena and the artifacts. An important question that needs to be addressed is this: Are the details in the temperature profile predicted from the optimization physically real or are they mathematical artifacts due to the limitation of the SRC model? In particular, is the temperature overshoot in the early region of the reactor needed to meet the reactor design objectives, or is it an artifact of the aerosol dynamics model?

To help answer this question, an extended SRC model was derived, called the discrete SRC (DSRC) model. This model expands the current single monomer balance in the discrete sizes to arbitrary number of discrete sizes. In the SRC model, any cluster larger than a monomer is considered a particle in the fine mode; whereas in the DSRC model, only clusters bigger than n-mers are considered to be in the fine mode. Here n represents the number of the discrete sizes. The expansion of the discrete sizes reduce the effect of decreasing the average particle size in the fine mode due to an increase in the number concentration of the monomers. The dimensionless form of the DSRC model equations are:

$$\frac{dX_A}{d\xi} = \frac{1}{\Delta_1}\beta_A X_A \Gamma \qquad [5.1]$$

$$\frac{dX_1}{d\xi} = \frac{1}{\Delta_1}\beta_A X_A \Gamma - \frac{2}{\Delta_2} X_1 \sum_{i=1}^{n} \beta_{1i} X_i \Gamma^2/\Gamma_o - \frac{1}{\Delta_2}\beta_{1H} X_1 X_H \Gamma^2/\Gamma_o - \frac{1}{\Delta_3}\beta_{1S} X_1 X_S \Gamma^2/\Gamma_o \qquad [5.2]$$

$$\frac{dX_i}{d\xi} = \frac{1}{\Delta_2}\sum_{l=1}^{i-1} \beta_{i-l\,l} X_{i-l} X_l \Gamma^2/\Gamma_o - \frac{1}{\Delta_2} X_i \sum_{l=1}^{n} \beta_{il} X_l \Gamma^2/\Gamma_o - \frac{1}{\Delta_2}\beta_{iH} X_i X_H \Gamma^2/\Gamma_o - \frac{1}{\Delta_3}\beta_{iS} X_i X_S \Gamma^2/\Gamma_o, \quad i \geq 2 \qquad [5.3]$$

$$\frac{dX_H}{d\xi} = \frac{1}{\Delta_2}\sum_{\substack{i,l=1 \\ i+l>n}}^{n} \beta_{il} X_i X_l \Gamma^2/\Gamma_o - \frac{1}{\Delta_2}\beta_H X_H^2 \Gamma^2/\Gamma_o - \frac{1}{\Delta_3}\beta_{HS} X_H X_S \Gamma^2/\Gamma_o \qquad [5.4]$$

$$\frac{dX_{MH}}{d\xi} = \frac{1}{\Delta_2}\Omega \sum_{\substack{i,l=1 \\ i+l>n}}^{n} (i+l)\beta_{il} X_i X_l \Gamma^2/\Gamma_o + \frac{1}{\Delta_2}\Omega\, X_H \sum_{i=1}^{n} i\,\beta_{iH} X_i \Gamma^2/\Gamma_o - \frac{1}{\Delta_3}\Omega\,\omega_H \beta_{HS} X_H X_S \Gamma^2/\Gamma_o \qquad [5.5]$$

$$\frac{dX_S}{d\xi} = -\frac{1}{2}\frac{1}{\Delta_3}\beta_S X_S^2 \Gamma^2/\Gamma_o \qquad [5.6]$$

$$\frac{dX_{MS}}{d\xi} = \frac{1}{\Delta_3}\Omega\, X_S \sum_{i=1}^{n} i\,\beta_{iS} X_i\, \Gamma^2/\Gamma_o + \frac{1}{\Delta_3}\Omega\,\omega_H \beta_{HS} X_H X_S \Gamma^2/\Gamma_o \qquad [5.7]$$

$$\frac{d\Theta}{d\xi} = \frac{1}{\Delta_4}\frac{\Xi}{\zeta}(\Theta_w - \Theta), \qquad [5.8]$$

where

$$\beta_{il} = \frac{K_{il}}{K_{1o}}, \quad \beta_{iH} = \frac{K_{iH}}{K_{1o}}, \quad \text{and} \quad \beta_{iS} = \frac{K_{iS}}{K_{1so}}.$$

The DSRC model is a more rigorous solution to the GDE than the SRC model. However, the computational time required with the DSRC is orders of magnitude higher than with the SRC because of the many more equations that must be solved. This renders optimization calculations using the DSRC impractical. The main purpose here is to determine the effects of the number of discrete sizes on the reactor simulation results and the validity of the optimal profiles derived using the SRC model.

6. DSRC Model Results

Figures 9(a) - (c) show the cluster distribution and the number concentration and the average size in the fine mode (labelled fine mode) at three different reactor positions for the conditions in Figs. 6(a)-(d), but with the flat temperature profile depicted by the solid curve in Fig. 7(a). There is a sharp fall off in the number concentration with cluster size. The predicted number concentration in the fine mode decreases, while the average size increases, with increasing number of discrete sizes early in the reactor ($z/L_R = 0.2$). At this reactor position, there are significant differences between the results computed with the SRC model ($n = 1$) and with the DSRC model. The results for all n converge to the same point later in the reaction (Figs. 9(b)-(c)), and the final predictions are the same, independent of the number of discrete sizes used. This is expected because, in this case, the temperature is high and the reaction is completed quickly. Early in the reactor, clusters are generated at high concentrations. Once the reaction is complete, the number concentrations of the clusters decrease rapidly due to self-coagulation and scavenging by the fine and the seed particles. At this point on, the clusters have little effect on the size and concentration in the fine mode.

Figures 10(a)-(c) represent the results for same conditions as in Figs. 9(a)-(c),

but with the optimal temperature profile depicted by the solid curve in Fig. 6(a). Here, the differences between $n = 1$ and $n = 40$ are large, but those between $n = 30$ and $n = 40$ are small except near the entrance where the cluster distribution is beginning to develop. This is because in this case the reaction is carried out more gradually and growth by cluster deposition is important throughout the particle evolution process (note that the number concentrations of the clusters are higher than those in Figs. 9(a)-(c)).

The corresponding plots of number concentration and mass fraction in the fine and the seed mode as a function of reactor position are shown in Figures 11 and 12, respectively. The SRC model considerably overpredicts the amount of mass scavenged by the seed particles. As expected, the error is reduced with increasing number of discrete sizes used.

It appears that the SRC model's predictions are worse when growth by vapor and small cluster deposition is important. The question is, thus, are the profiles derived using the SRC model really the optimums?

Calculations performed using the DSRC model with 30 discrete sizes for selected optimal conditions predicted by the SRC model are tabulated in Table IV. Again, the SRC model overpredicts the amount of mass scavenged by the seed particles, and underpredicts the peak mass fraction in the fine mode. The absolute errors are large for low seed concentration (conditions of Figs. 6(a)-(d) and 7(a)-(d)), but are much smaller high seed concentration (conditions of Figs. 8(a)-(b)) and long reactor length (conditions of Figs. 9(a)-(d)).

The ultimate objective with optimization is, again, to derive conditions that would produce dense particles. This requires minimizing the amount of mass in the fine mode at all times, since this determines the size of the fine particles under-

going self-coagulation. Higher peak mass in the fine mode implies that larger fine particles will result before they are scavenged by the seed particles. The crucial test, therefore, is whether the profiles generated by the SRC model are those that result in minimum peak mass without significantly reducing the final mass in the seed mode.

To check the integrity of the SRC model in deriving the optimal temperature profiles, the optimal profile for conditions in Figs. 7(a)-(d) was changed and calculations were undertaken using the DSRC model. Two different wall temperature profiles were chosen based on the recipe proposed by Wu et al. (24). The zone temperatures and the corresponding mass fractions are recorded in Table V along with the optimal results for comparison. The initially isothermal profile produces the worst results, significantly lower final seed mass and much higher peak mass in the fine mode compared to the optimized profile. Slightly more mass is converted to the seed particles with the gradually increasing temperature profile, but the peak mass in the fine mode is significantly higher. This suggests that while the SRC model does not provide the correct absolute values of the mass fraction in the two modes, it does correctly predict the profile that would result in the lowest peak mass in the fine mode. It also implies that if the sink is weak, then to minimize the peak mass in the fine mode at any time in the reactor, the reaction must be slowed and less product material will be deposited in the seed mode.

The computation time is orders of magnitude higher for the more detailed DSRC compared to the SRC model, especially near optimal or at optimal conditions. This is because a slower, nearly constant source rate generates a significant number concentration of monomers and clusters throughout the reactor, causing the equations to remain stiff throughout the reactor. When the reaction is very fast and coagulation is dominant, the computational requirement by the DSRC model

is reduced, but is still much more than that required by the SRC model. Thus the SRC model can be used to obtain a first approximation of the optimal conditions. With these conditions, a more detailed and accurate model should be implemented for quantitative information.

7. Conclusions

An optimization technique was applied to the highly nonlinear aerosol reactor system to directly derive optimal temperature profiles that maximize growth of a seed aerosol and minimize the size of the fine clusters formed. The results indicate that if the reactor residence time is too short or the sink is too small, large cluster formation cannot be suppressed regardless of the temperature profile used. With a sink that is too small to effectively scavenge the condensible vapors, slowly reacting the precursor at first and later accelerating the reaction may not lead to deposition of most of the material on the seed particles. A larger seed sink can be used to suppress large cluster formation, but the number concentration of the seeds must be kept at a level where self-coagulation is not important. Optimization calculations are, therefore, crucial in the initial reactor design to ensure adequate residence time for growth by monomer and small cluster deposition.

The objective function used must constrain the evolution of the particles to such a path that the formation of large clusters is minimized. Without such constraints, low density flocs will most likely result due to growth by coagulation of like-sized particles.

The SRC model is adequate for the derivation the optimal profiles, but for quantitative information, i.e., the absolute magnitudes of the mass fractions, etc., a more accurate model should be used for the final computation once the optimal profile is found. Neither the SRC nor any of the more detailed models that are

presently available can directly describe the structural evolution and morphology of the particles. To determine conditions that will produce dense, nonagglomerated particles, descriptions of morphological changes need to be developed and incorporated into the aerosol dynamic model.

9. References

1. Bowen, H.K., *Mater. Sci. Eng.*, 44, 1 (1980).
2. Barringer, E.A., and Bowen, H.K., *Comm. Am. Ceram. Soc.* , C-199 (1982).
3. Gobet, J., and Matejevic, E., *J. Colloid Interface Sci.* , 100, 555 (1984).
4. Fauchias, P., Bourdin, E., Coudert, J.F., and McPherson, R., *Topics in Current Chemistry. Vol. 107: Plasma Technology*, S. Veprek and M. Venurgopalan, Eds. Springer Verlag, 59 (1983).
5. Kagawa, M., Kikuchi, M., Syono, Y., and Nagae, T., *J. Am. Ceram. Soc.*, 66, 751 (1983).
6. Cannon, W.R., Danforth, S.C., Flint, J.H., Haggerty, J.S., and Marra, R.A., *J. Am. Ceram. Soc. 65*, 65, 324 (1982).
7. Cannon, W.R., Danforth, S.C., Haggerty, J.S., and Marra, R.A., *J. Am. Ceram. Soc.*, 65, 330 (1982).
8. Wu, J.J, Nguyen, H.V., and Flagan, R.C., *Langmuir* , 3, 266 (1987).
9. Prochazka, S., Greskovich, C., *Am. Ceram. Soc. Bull.*, 57, 579 (1978).
10. Alam, M.K., and Flagan, R.C., *Aerosol Sci. Technol.*, 5, 237 (1986).
11. Wu, J.J., and Flagan, R.C., *J. Appl. Phys.*, 61, 1365 (1987).
12. Flagan, R.C., and Seinfeld, J.H., "*Fundamentals of Air Pollution Engineering*," Prentice Hall (1988).
13. Gelbard, F., Tambour, Y., and Seinfeld, J.H., *J. Colloid Interface Sci.*, 76, 541 (1980).
14. Gelbard, F., and Seinfeld, J.H., *J. Computing Physics*, 28, 357 (1978).
15. Wu, J.J., and Flagan, R.C., *J. Colloid Interface Sci.*, 123 [2], 339 (1988).

16. Friedlander, S.K., *Ann. New York Acad. Sci.*, 404, 354 (1983).

17. Pratsinis, S.E., Kodas, T.T., Dudukovic, M.P., and Friedlander, S.K., *Ind. Eng. Chem. Process Des. Dev.*, 25, 634 (1986).

18. Warren, D.R., and Seinfeld, J.H., *Aerosol Science and Technology*, 3, 135 (1984).

19. Lai, F.S., Friedlander, S.K., Pich, J., and Hidy, G.M., *J. Colloid Interface Sci.*, 39, 395 (1972).

20. Wu, J.J, Nguyen, H.V., Flagan, R.C., Okuyama, K., and Kousaka, Y., *AIChE Journal*, 34, 1249 (1988).

21. Ray, W.H., and Szekely, J., "*Process Optimization*," Wiley and Sons (1973).

22. Bryson, A.E., Jr., and Ho, Y.C., "*Applied Optimal Control*," Blaisdell (1969).

23. Dardo, M., Ph.D. Thesis, University of Wisconsin (1985).

24. Gill, P.E., Murray, W., Saunders, M.A., and Wright, M.H., "*User's Guide for NPSOL*," Stanford University (1986).

TABLE I

Advantages and Disadvanages of Various Aerosol Models

Model	Advantages	Disadvantages
Discrete-continuous	very accurate	computationally intensive
Sectional	ideal for low source rate systems, good for representing large particles	not good for high source rate systems
Discrete-sectional	accurate	fair computational requirements
Moment models	relatively simple, fast	fair accuracy, not good for high source rate systems,
Self-preserving size distribution	fast and simple	limited to coagulation dominant systems
Simplified reaction coagulation (SRC)	very fast, good for optimization problems where many calculations are required	fair accuracy

TABLE II

Optimal Zone Temperatures Predicted by the SRC for Different Initial Guesses

Initial guess	zone1	zone2	zone3	zone4	zone5
950	811	791	796	833	911
875	824	783	821	793	949
750	823	746	789	818	946

TABLE III(A)

Mass Fractions Predicted by the SRC Model for Different Initial Seed Concentrations

N_{So} (cm^{-3})	10^5	10^6	10^7
$X_S(\%)$	1.38	13.62	99.99
$X_{Hmax}(\%)$	98.28	85.9	31.82

$D_{So} = 100\text{nm}$, $E/R = 24056\,\text{K}^{-1}$, $I_1 = X_S$

TABLE III(B)

Mass Fractions Predicted by the SRC Models for Different Initial Seed Diameters

D_{So} (nm)	50	500	1000
$X_S^\star$ (%)	14.31	37.75	75.46
$X_{Hmax}^\star$ (%)	85.26	61.91	24.37

$N_{So} = 10^6\,\text{cm}^{-3}$, $E/R = 20000\,\text{K}^{-1}$, $I_2 = X_S - X_{Hmax}$

* Results for I_1 are the same

TABLE IV

Comparison of the Mass Fractions (%) Predicted by the SRC and DSRC ($n = 30$) Models

Figures	X_S (SRC)	X_{Hmax} (SRC)	X_S (DSRC)	X_{Hmax} (DSRC)
5(a) - (d) (I_1)	100	31.82	78.04	41.08
6(a) - (d) (I_2)	98.1	16.0	72.19	33.57
7(a) - (b) Solid (I_1)	100	18.21	99.99	24.84
7(a) - (b) Dashed (I_2)	100	0.12	99.99	2.51
8(a) - (d) Solid (I_2)	98.1	16.0	72.19	33.57
8(a) - (d) Dashed (I_2)	100	2.59	90.54	18.61
8(a) - (d) Dashed-Dotted (I_2)	100	0.66	99.99	5.02

TABLE V

Mass Fractions (%) Predicted by the SRC and DSRC ($n = 30$) Models for Different Wall Temperature Profiles

Z1...Z2..Z3..Z4..Z5	X_S (SRC)	X_{Hmax} (SRC)	X_S (DSRC)	X_{Hmax} (DSRC)
*820 746 786 821 917	98.1	16.0	72.19	33.57
825 825 825 825 949	—	—	62.44	63.12
791 796 811 833 917	—	—	72.19	45.80

* Optimal Profile Computed Using I_1

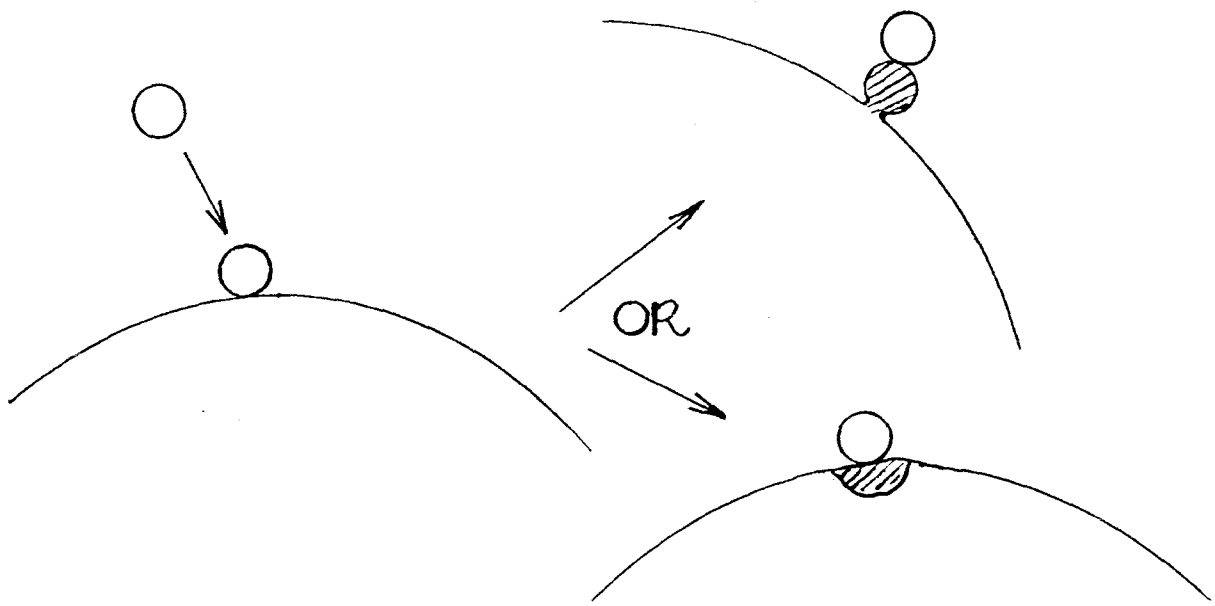

$$\tau_{\text{coalesce}} >> (\pi a^2 \frac{N_c \overline{C_c}}{4})^{-1} : \text{Agglomerate particle}$$

$$\tau_{\text{coalesce}} << (\pi a^2 \frac{N_c \overline{C_c}}{4})^{-1} : \text{Dense particle}$$

Figure 1. Schematic describing the role of clusters in the growth of solid particles.

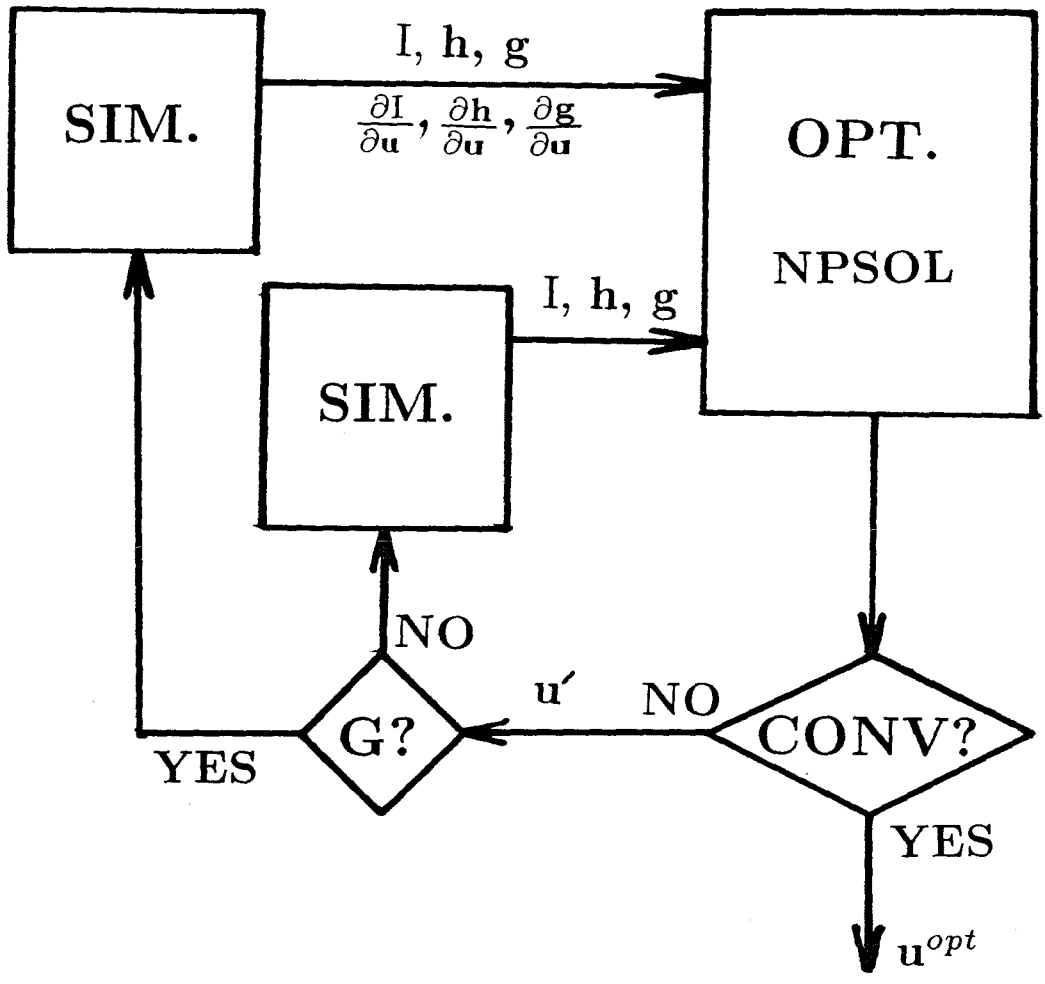

Figure 2. Schematic of the simulator-optimizer method.

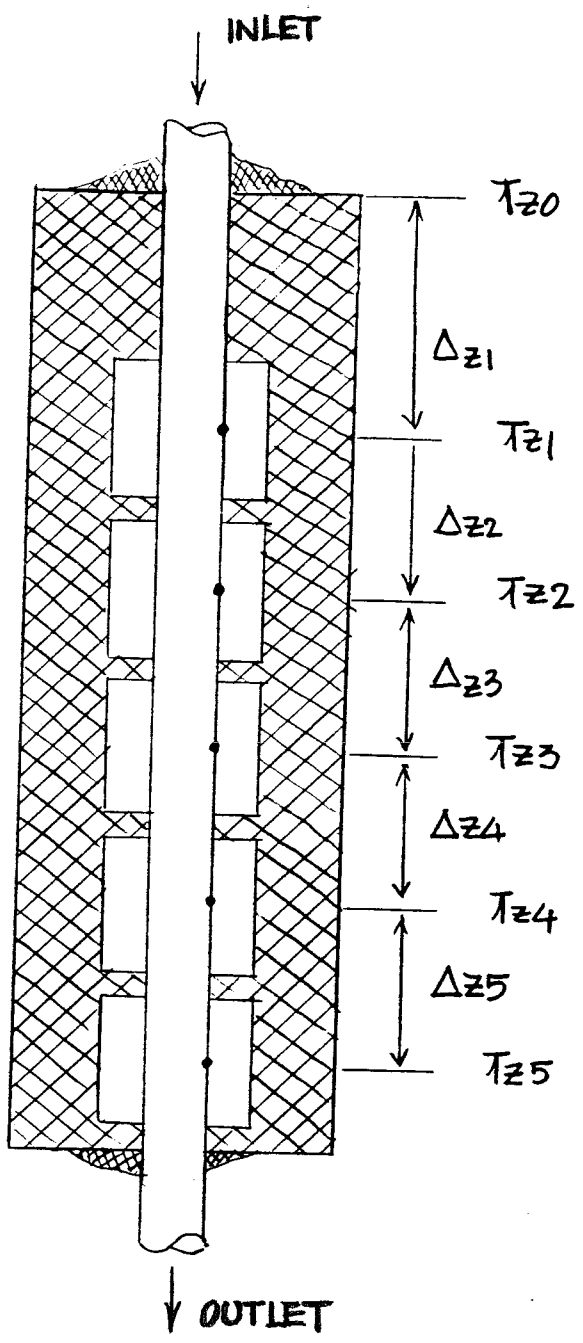

Figure 3. Schematic of the five zone reactor and the wall temperature positions used in the optimization.

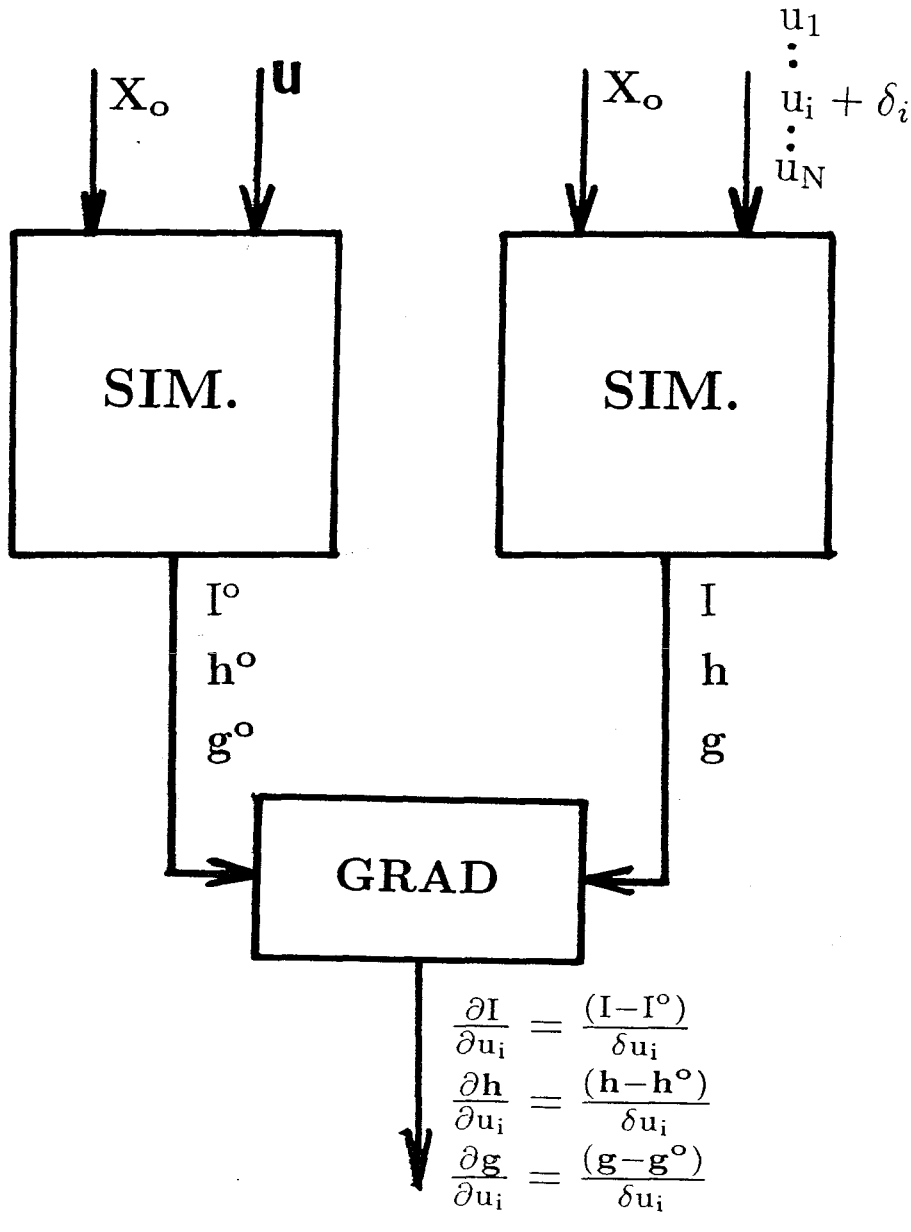

Figure 4. Perturbation scheme used to compute the gradients in the optimization.

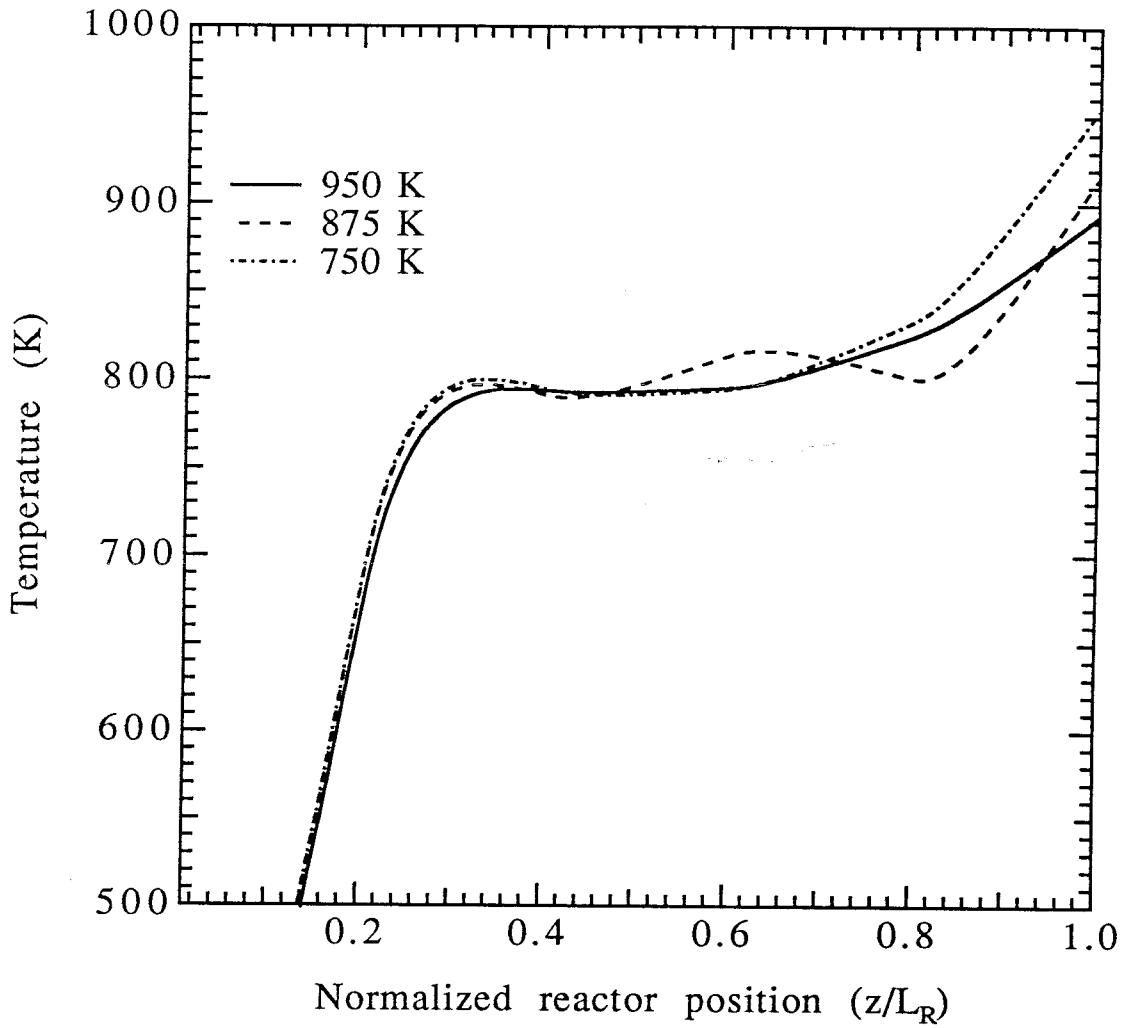

Figure 5(a). Optimal gas temperature profiles for an initial seed concentration $N_{so} = 10^7$ cm^{-3} and size $d_{So} = 100$ nm, reactor length $L_R = 1$ m, for three different initial guesses, obtained using the objective function I_1.

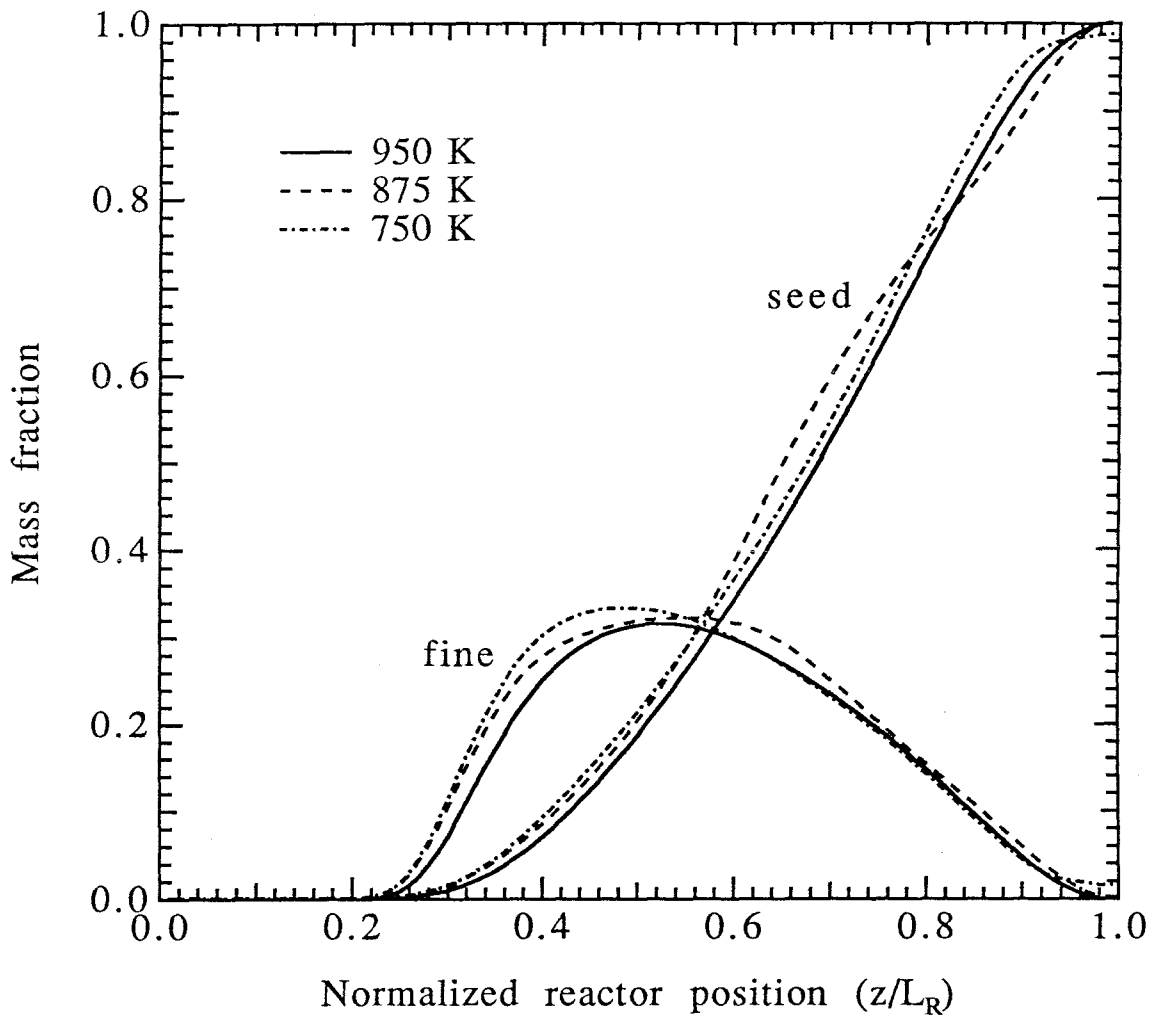

Figure 5(b). Mass fractions of the fine and seed modes as a function of normalized reactor position for an initial seed concentration $N_{so} = 10^7$ cm^{-3} and size $d_{So} = 100$ nm, reactor length $L_R = 1$ m, for three different initial guesses, obtained using the objective function I_1.

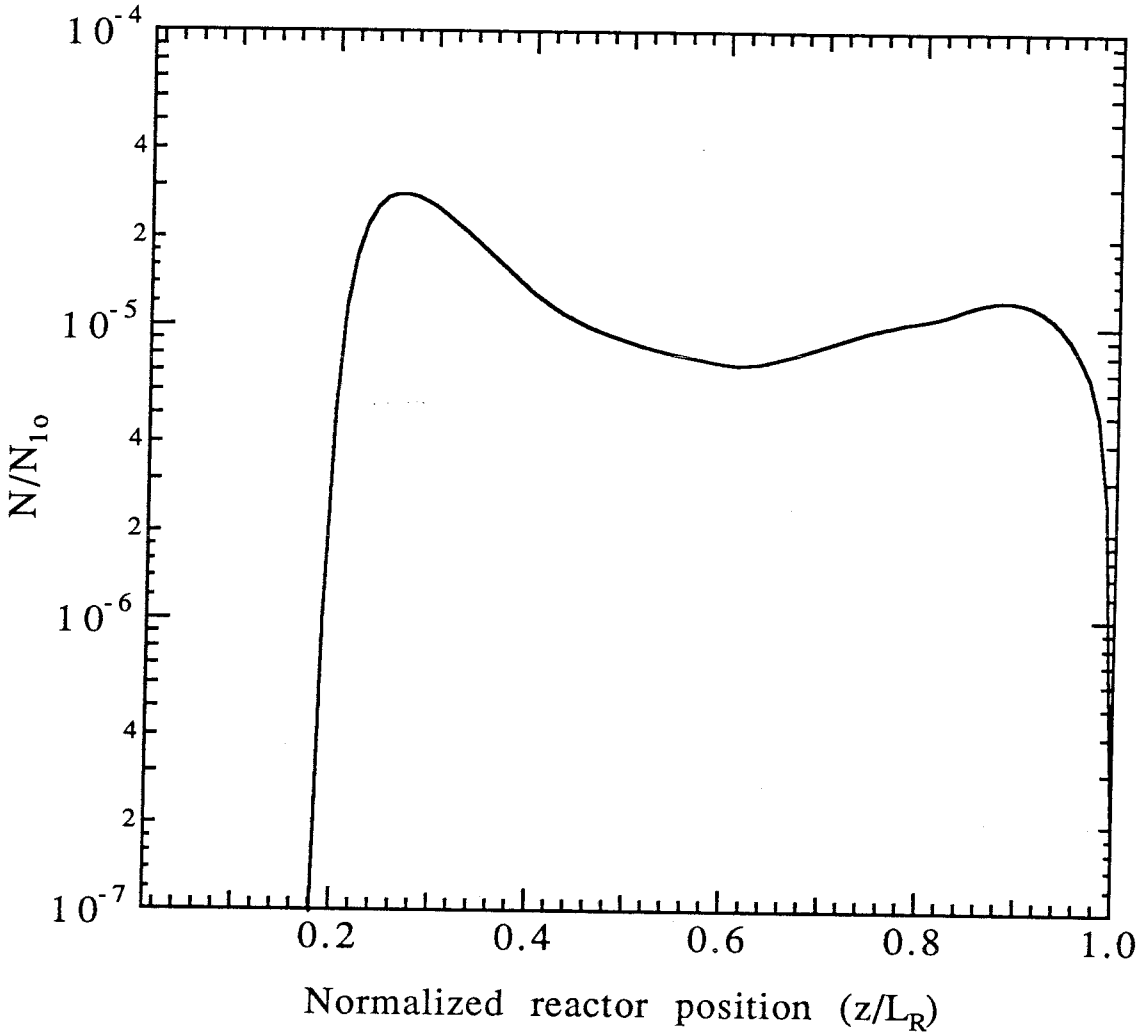

Figure 5(c). Fine mode number concentration normalized by the maximum monomer concentration N_H/N_{1o} as a function of normalized reactor position for an initial seed concentration $N_{so} = 10^7$ cm^{-3} and size $d_{So} = 100$ nm, reactor length $L_R = 1$ m, for the initial guess of 950 K, obtained using the objective function I_1.

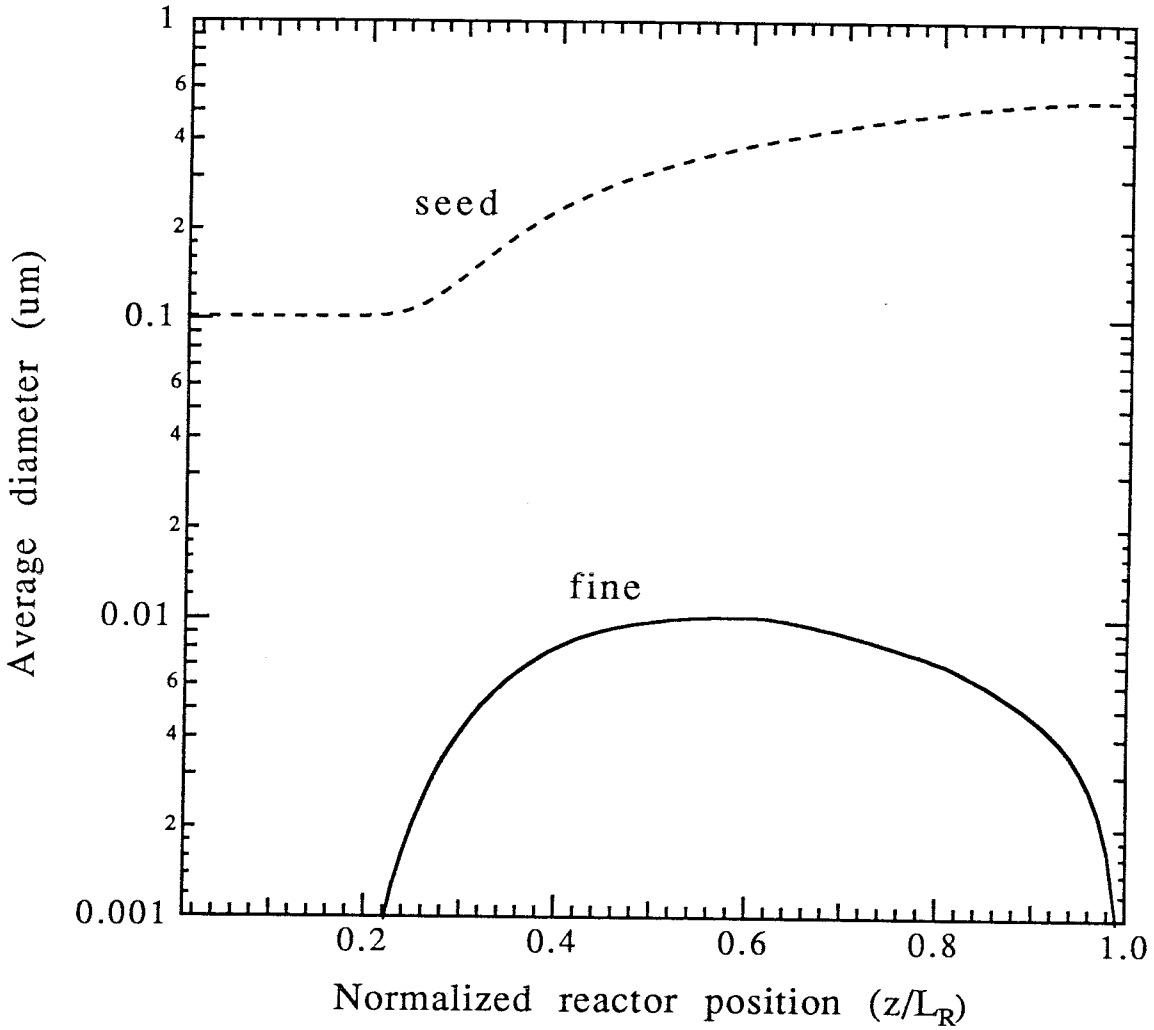

Figure 5(d). Average diameters in the fine and seed modes as a function of normalized reactor position for an initial seed concentration $N_{so} = 10^7$ cm^{-3} and size $d_{So} = 100$ nm, reactor length $L_R = 1$ m, for the initial guess of 950 K, obtained using the objective function I_1.

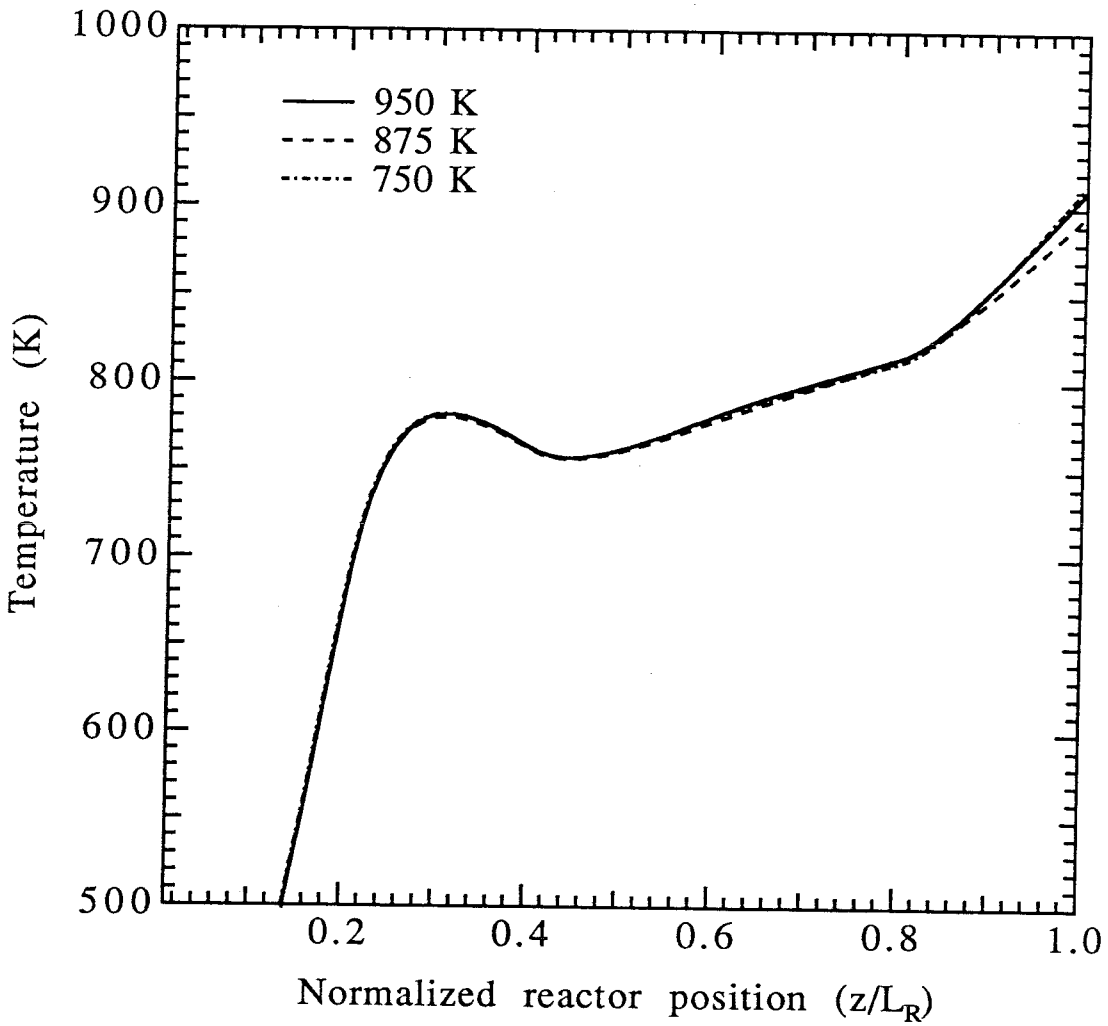

Figure 6(a). Optimal gas temperature profiles for an initial seed concentration $N_{so} = 10^7$ cm^{-3} and size $d_{So} = 100$ nm, reactor length $L_R = 1$ m, for three different initial guesses, obtained using the objective function I_2.

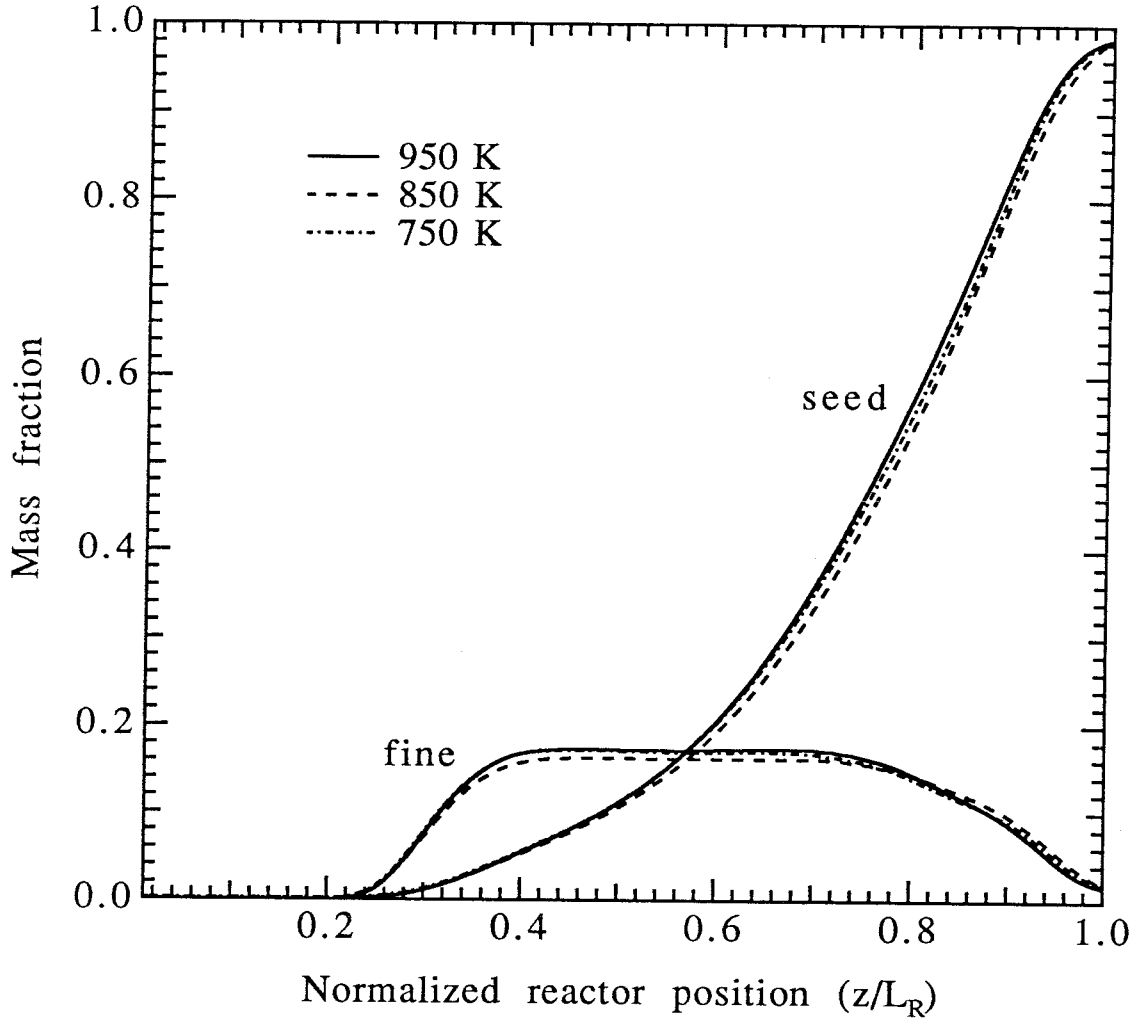

Figure 6(b). Mass fractions of the fine and seed modes as a function of normalized reactor position for an initial seed concentration $N_{so} = 10^7$ cm^{-3} and size $d_{So} = 100$ nm, reactor length $L_R = 1$ m, for three different initial guesses, obtained using the objective function I_2.

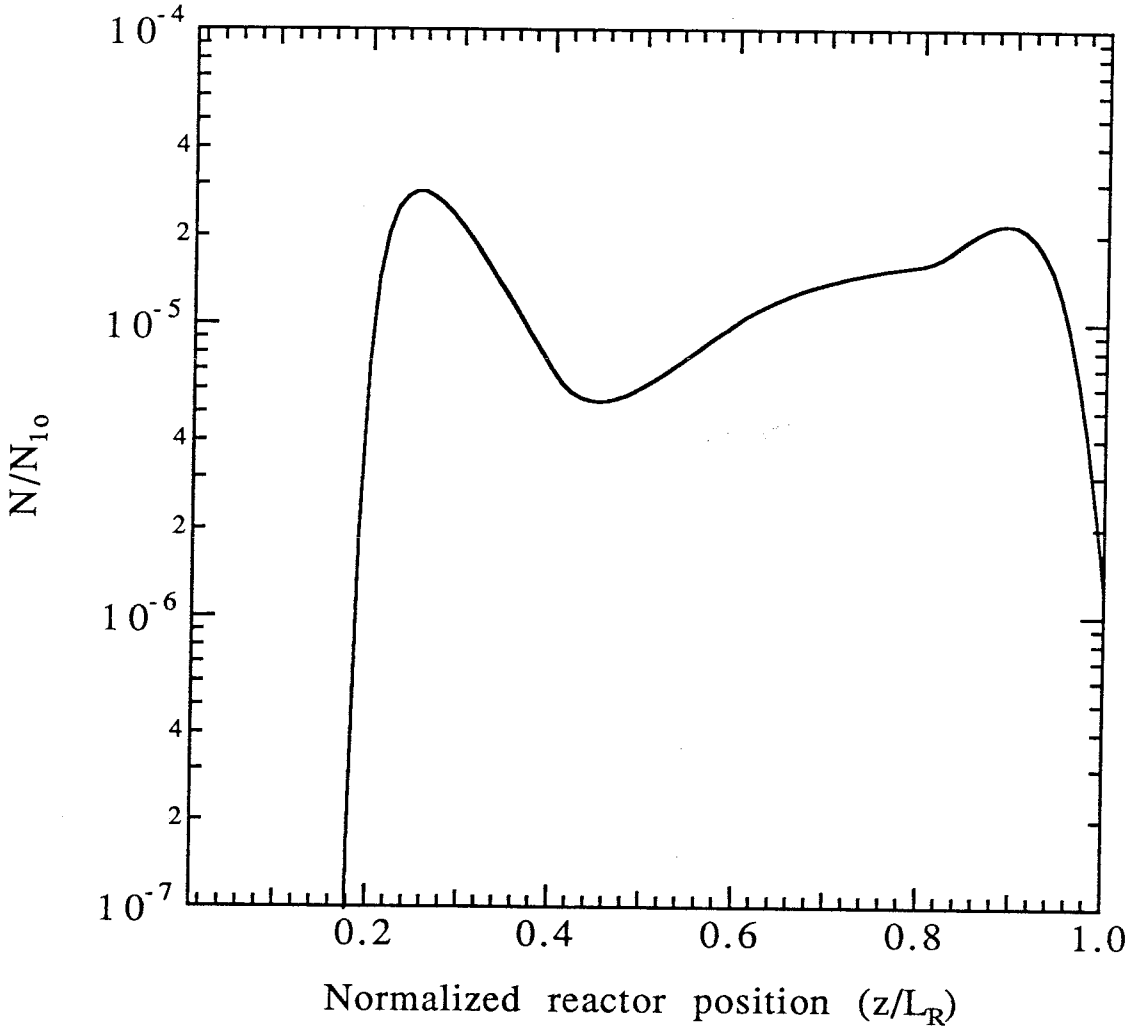

Figure 6(c). Fine mode number concentration normalized by the maximum monomer concentration N_H/N_{1o} as a function of normalized reactor position for an initial seed concentration $N_{so} = 10^7$ cm^{-3} and size $d_{So} = 100$ nm, reactor length $L_R = 1$ m, for the initial guess of 950 K, obtained using the objective function I_2.

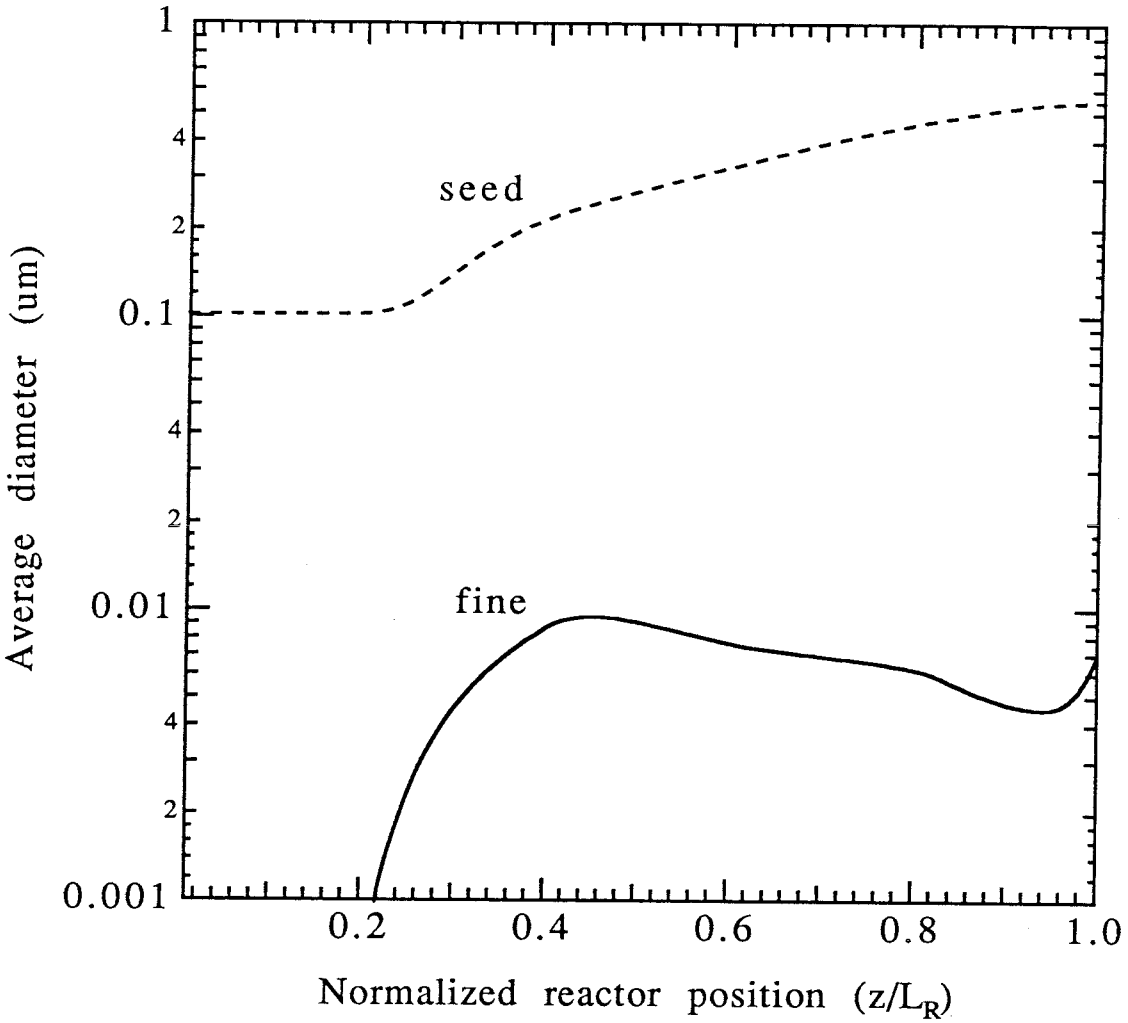

Figure 6(d). Average diameters in the fine and seed modes as a function of normalized reactor position for an initial seed concentration $N_{so} = 10^7$ cm^{-3} and size $d_{So} = 100$ nm, reactor length $L_R = 1$ m, for the initial guess of 950 K, obtained using the objective function I_2.

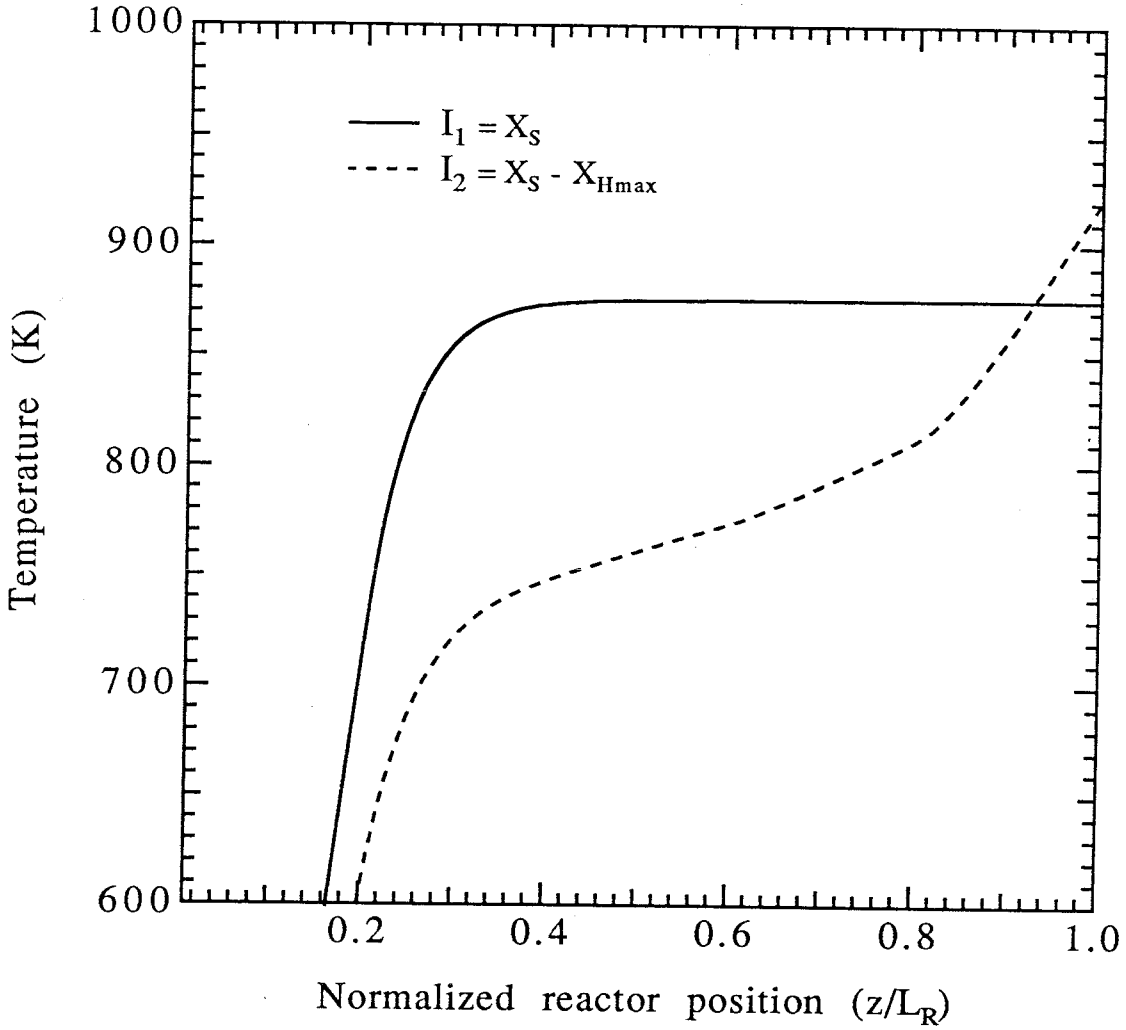

Figure 7(a). Comparison of the optimal gas temperature profiles for an initial seed concentration $N_{so} = 10^8$ cm^{-3} and size $d_{So} = 100$ nm, reactor length $L_R = 1$ m, obtained using the objective functions I_1 and I_2.

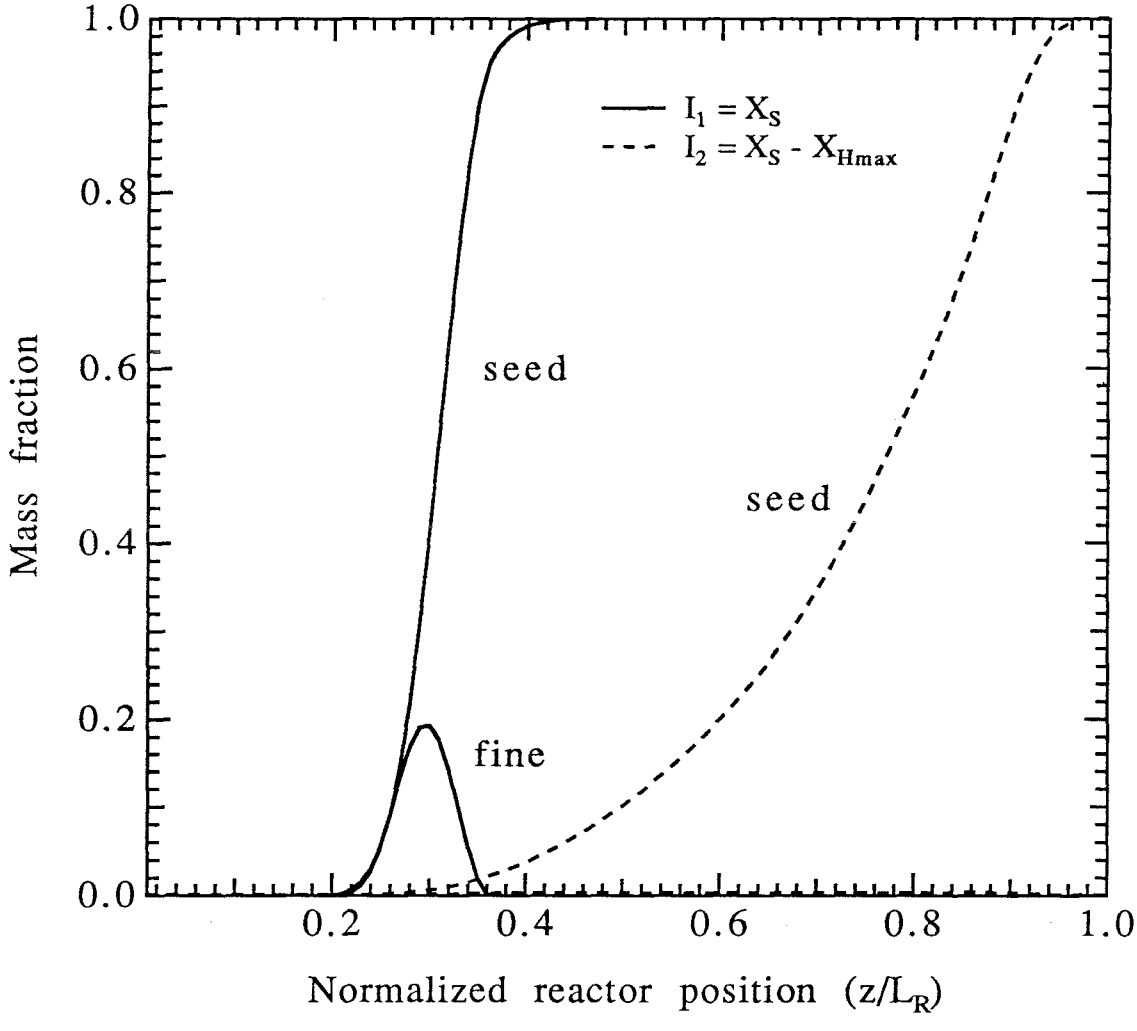

Figure 7(b). Comparison of the mass fractions of the fine and seed modes as a function of normalized reactor position for an initial seed concentration N_{so} = 10^8 cm^{-3} and size d_{So} = 100 nm, reactor length L_R = 1 m, obtained using the objective functions I_1 and I_2.

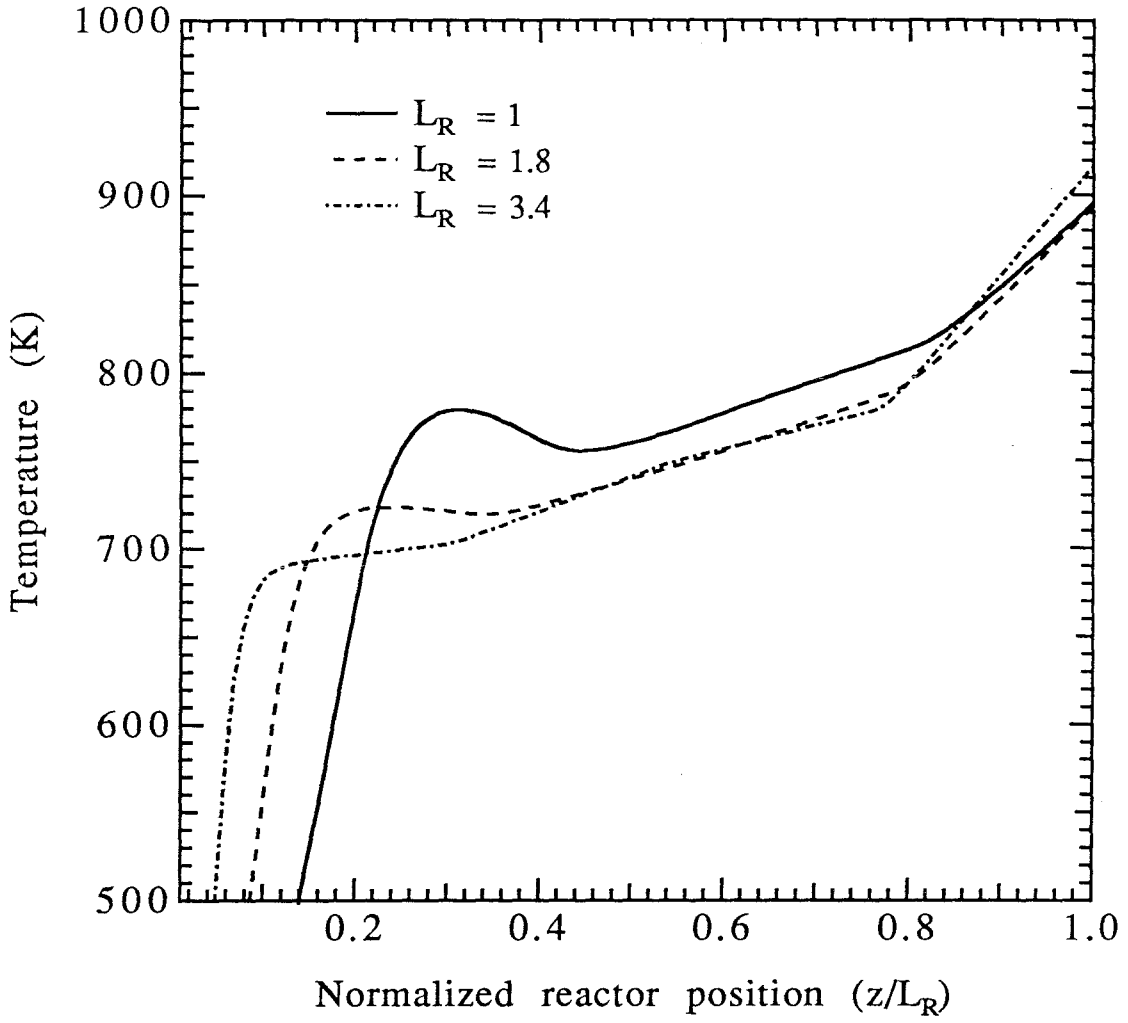

Figure 8(a). Optimal gas temperature profiles for an initial seed concentration N_{so} = 10^7 cm^{-3} and size d_{So} = 100 nm, for three different reactor lengths, obtained using the objective function I_2.

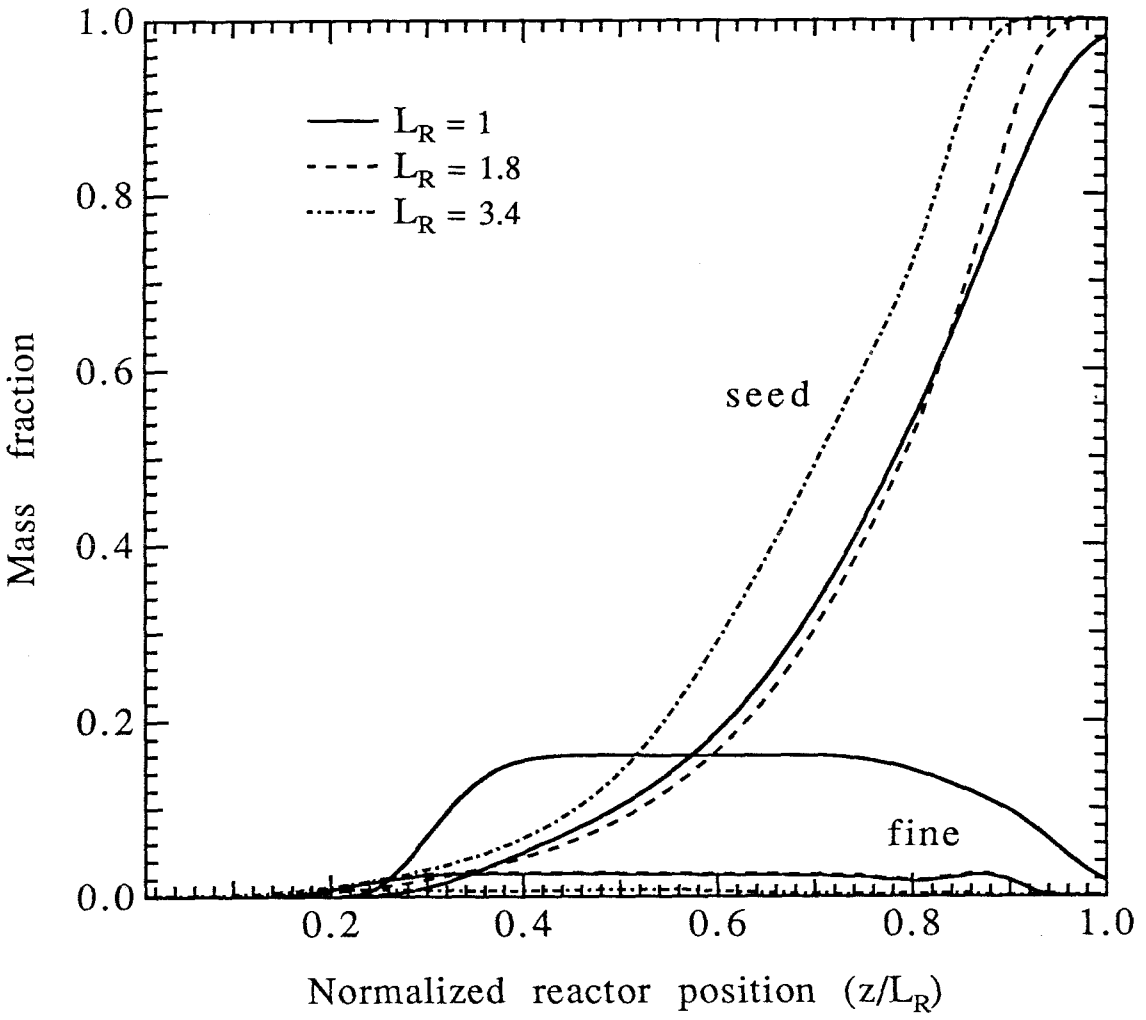

Figure 8(b). Mass fractions of the fine and seed modes as a function of normalized reactor position for an initial seed concentration $N_{so} = 10^7$ cm^{-3} and size $d_{So} = 100$ nm, for three different reactor lengths, obtained using the objective function I_2.

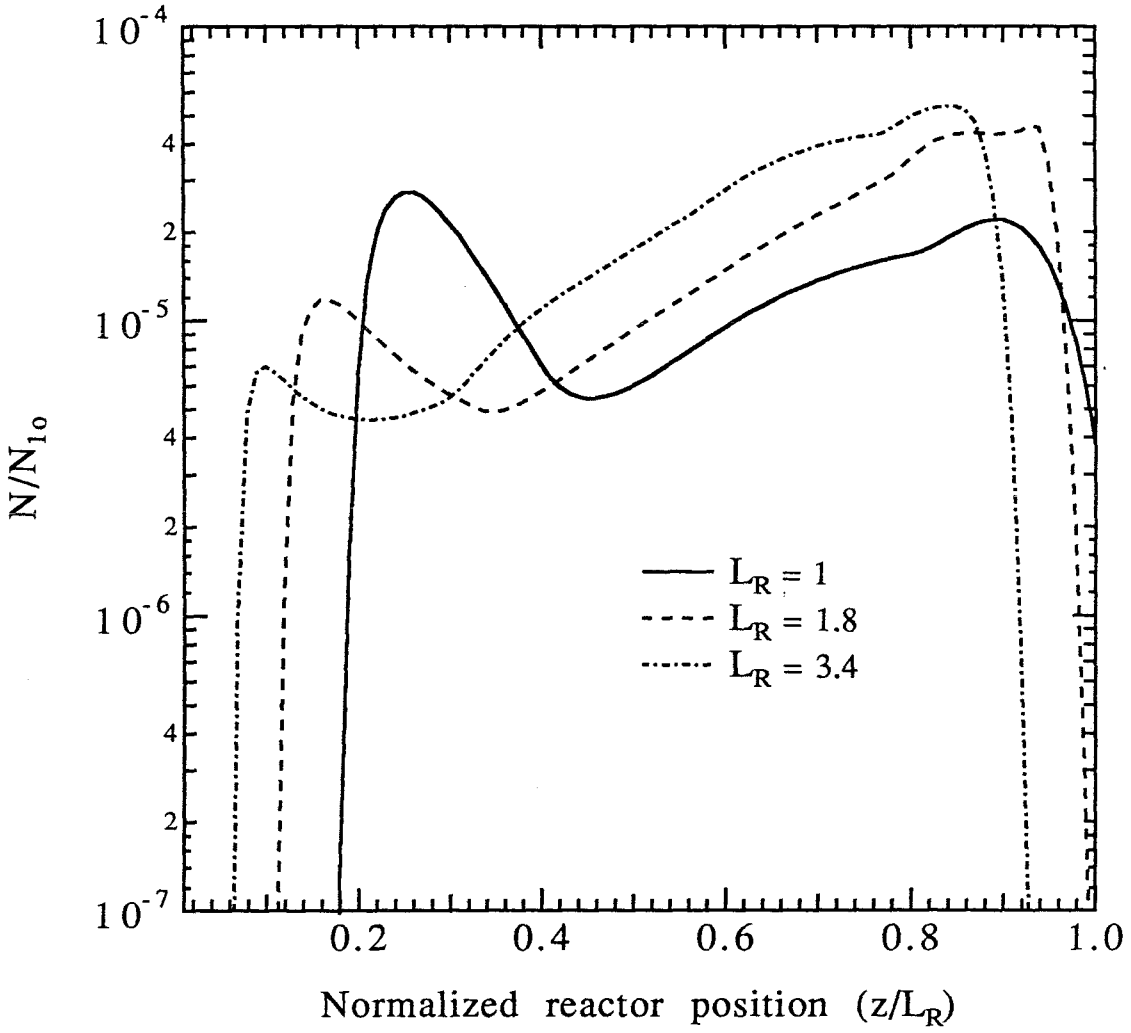

Figure 8(c). Fine mode number concentration normalized by the maximum monomer concentration N_H/N_{1o} as a function of normalized reactor position for an initial seed concentration $N_{so} = 10^7$ cm^{-3} and size $d_{So} = 100$ nm, for three different reactor lengths, obtained using the objective function I_2.

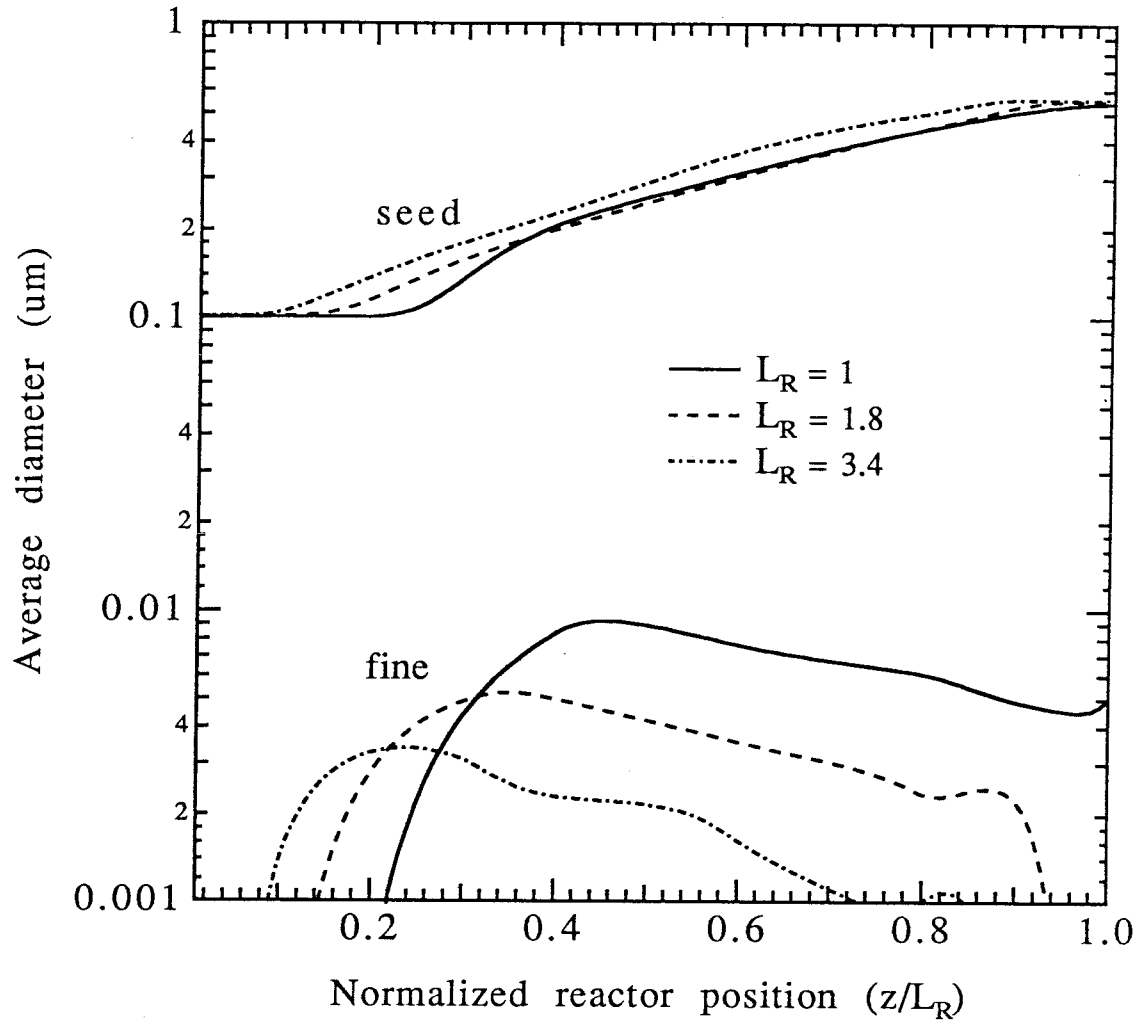

Figure 8(d). Average diameters in the fine and seed modes as a function of normalized reactor position for an initial seed concentration $N_{so} = 10^7$ cm^{-3} and size $d_{So} = 100$ nm, for three different reactor lengths, obtained using the objective function I_2.

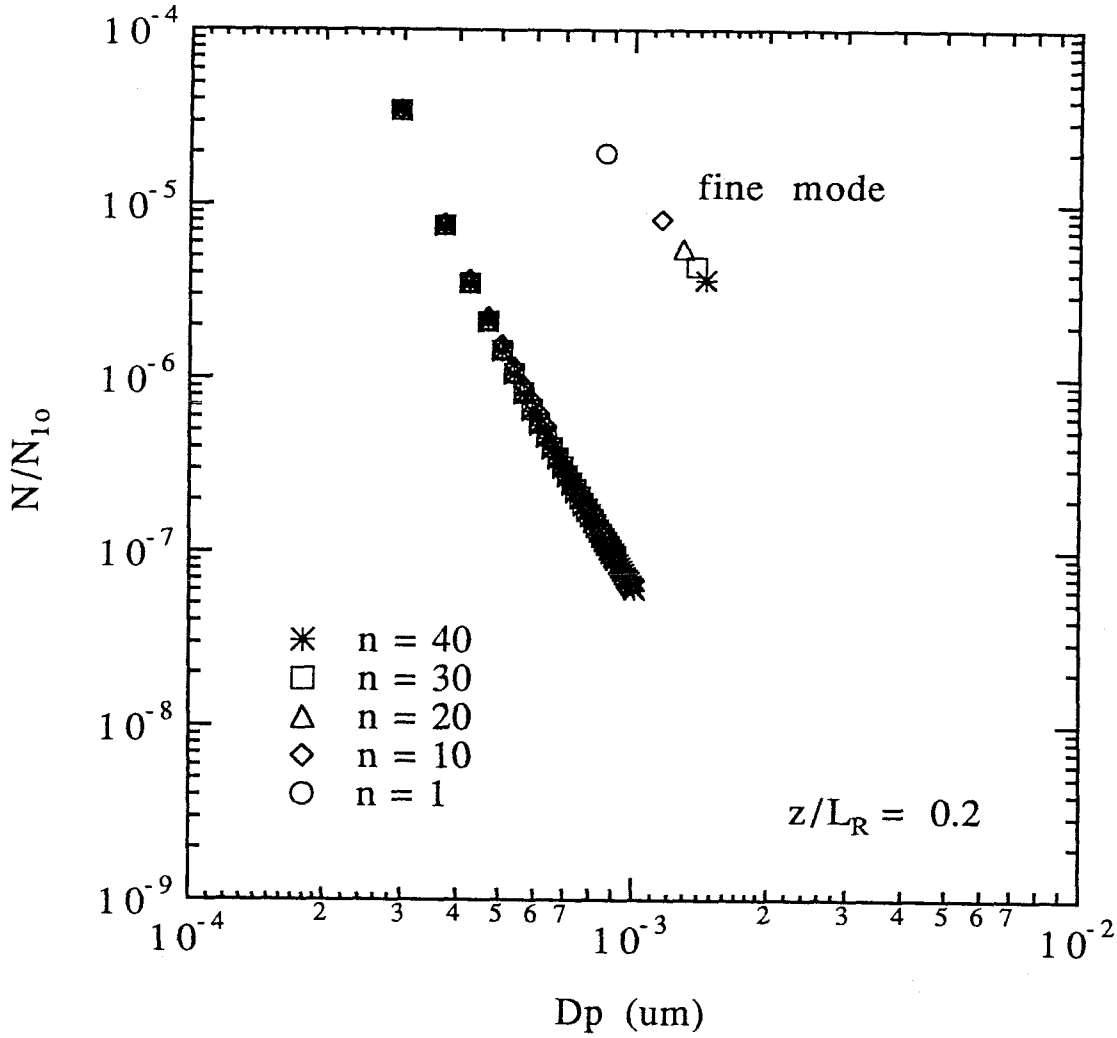

Figure 9(a). Cluster distribution and the number concentration and average size of the particles in the fine mode computed using the DSRC model with different numbers of discrete sizes, n, at $Z/L_R = 0.2$ for an initial seed concentration $N_{so} = 10^7$ cm^{-3} and size $d_{So} = 100$ nm, and the solid temperature profile shown in Fig. 7(a).

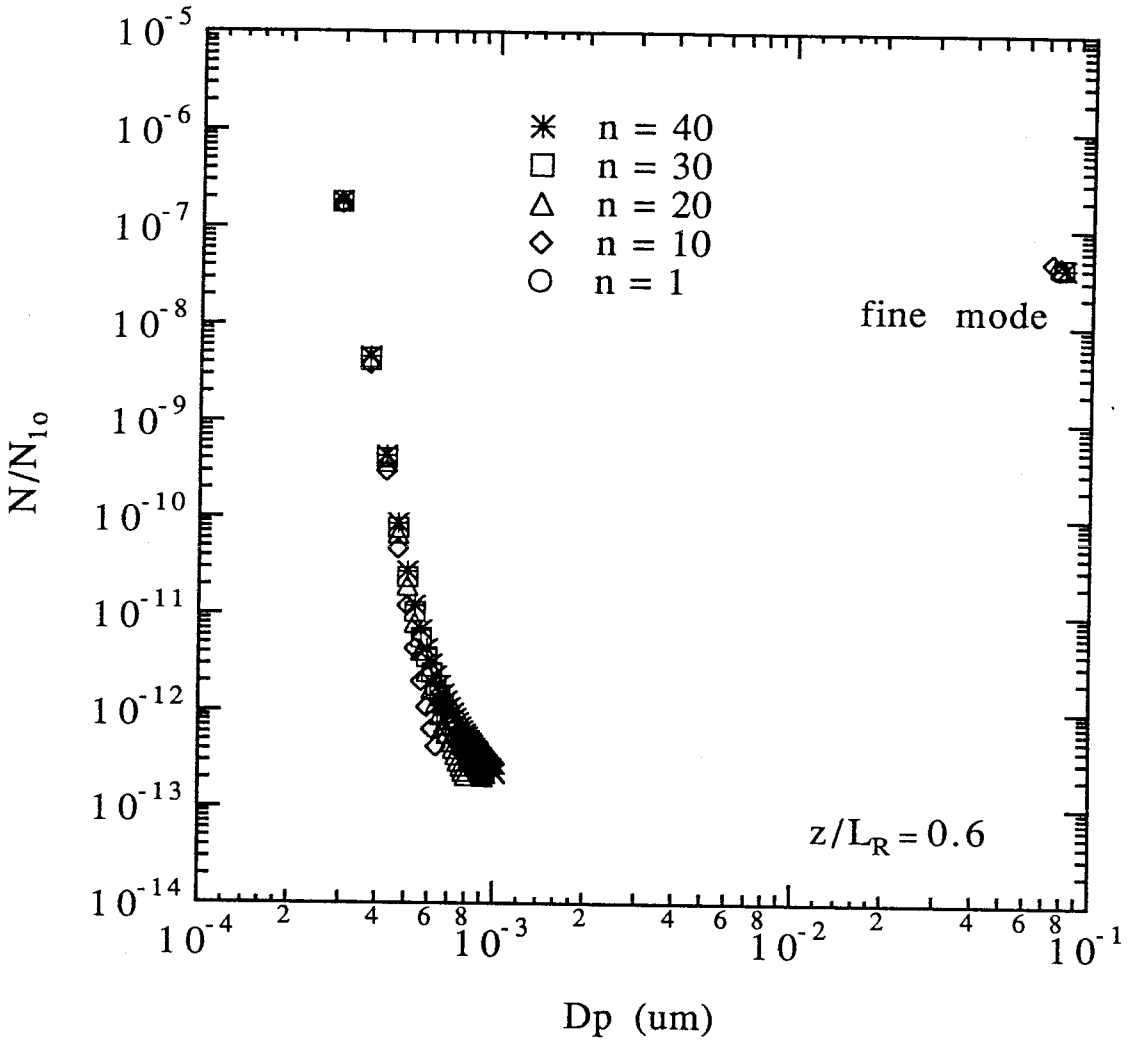

Figure 9(b). Cluster distribution and the number concentration and average size of the particles in the fine mode computed using the DSRC model with different numbers of discrete sizes, n, at $Z/L_R = 0.6$ for an initial seed concentration $N_{so} = 10^7$ cm^{-3} and size $d_{So} = 100$ nm, and the solid temperature profile shown in Fig. 7(a).

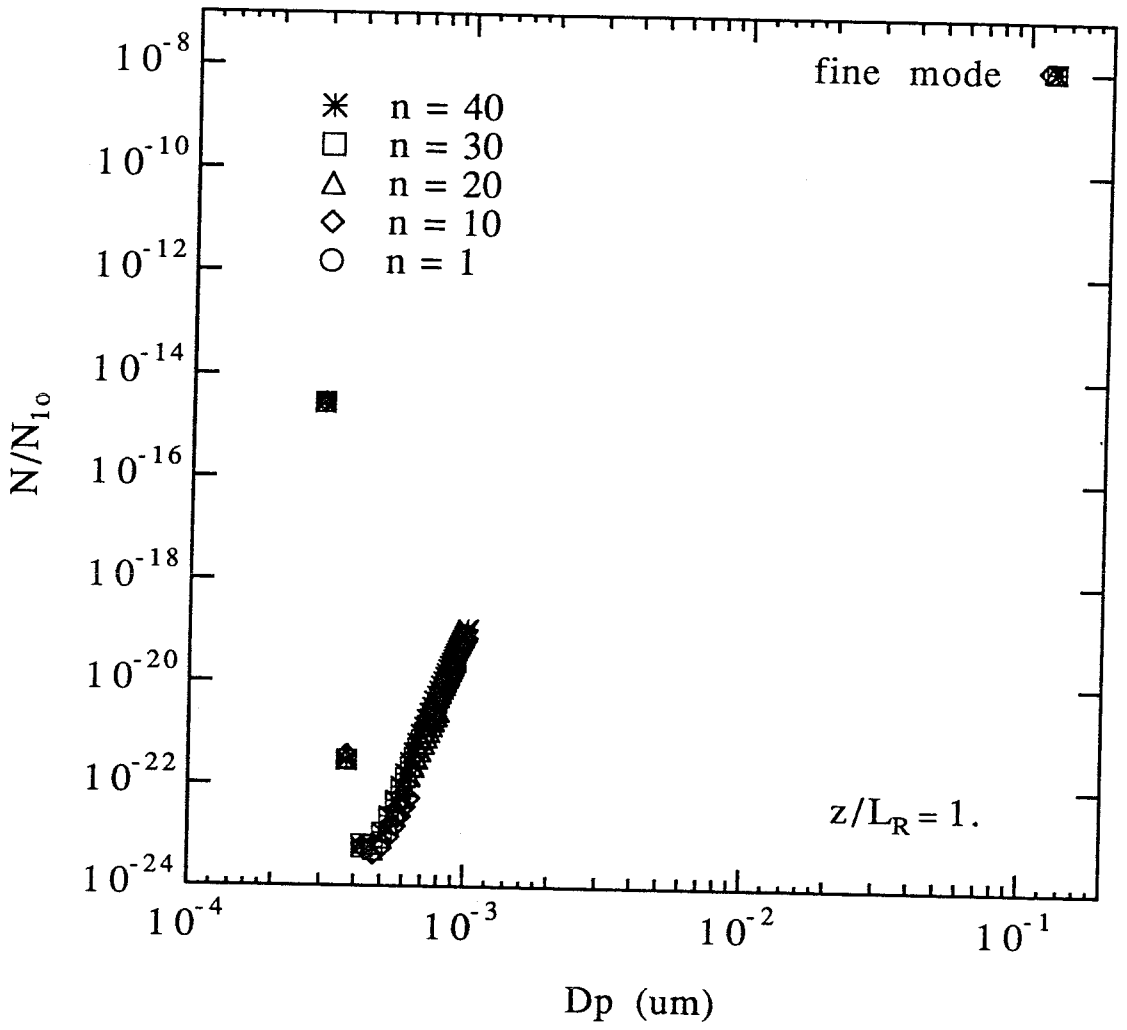

Figure 9(c). Cluster distribution and the number concentration and average size of the particles in the fine mode computed using the DSRC model with different numbers of discrete sizes, n, at $Z/L_R = 1.0$ for an initial seed concentration $N_{so} = 10^7$ cm^{-3} and size $d_{So} = 100$ nm, and the solid temperature profile shown in Fig. 7(a).

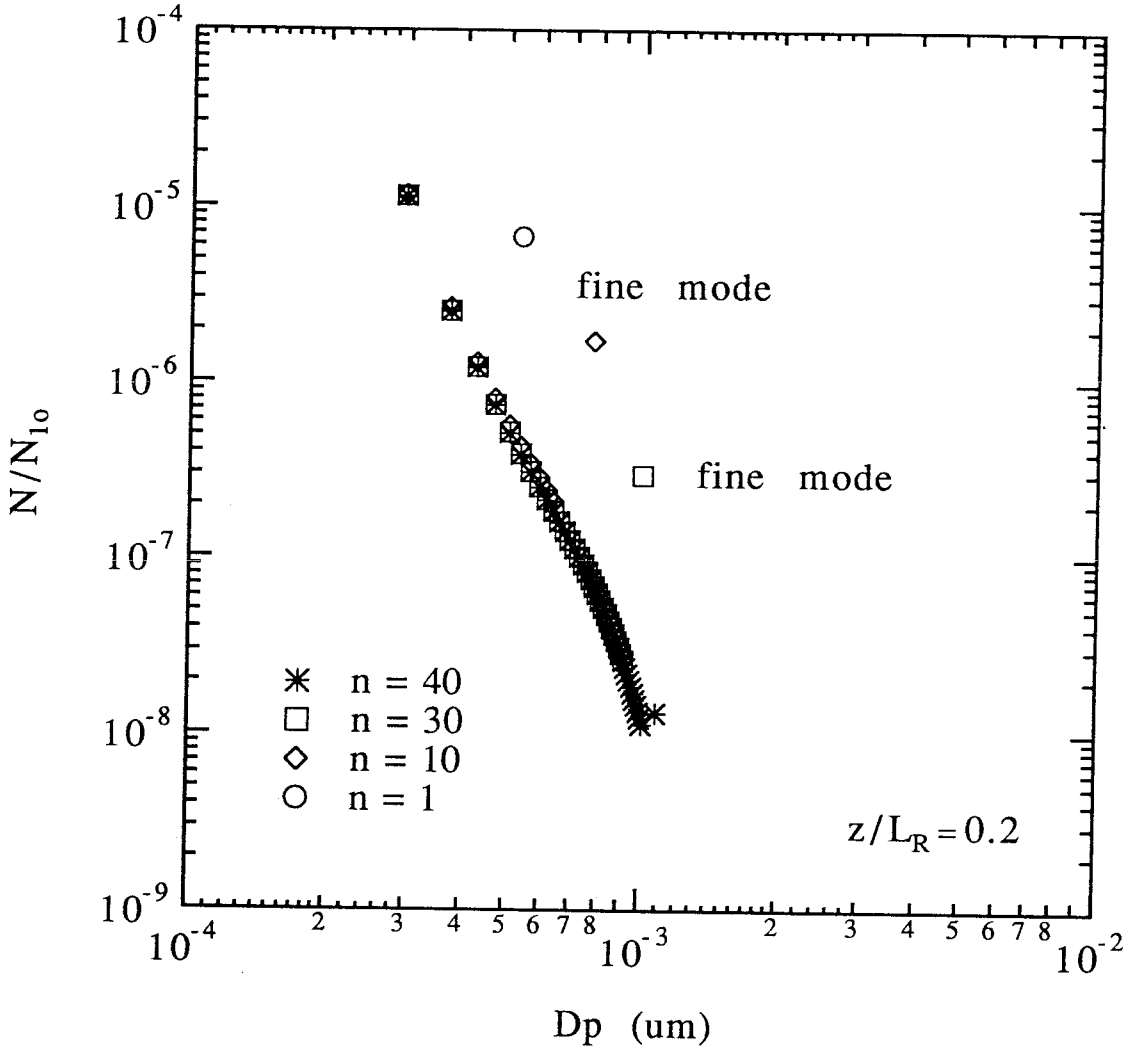

Figure 10(a). Cluster distribution and the number concentration and average size of the particles in the fine mode computed using the DSRC model with different numbers of discrete sizes, n, at $Z/L_R = 0.2$ for an initial seed concentration $N_{so} = 10^7$ cm^{-3} and size $d_{So} = 100$ nm, and the solid temperature profile shown in Fig. 6(a).

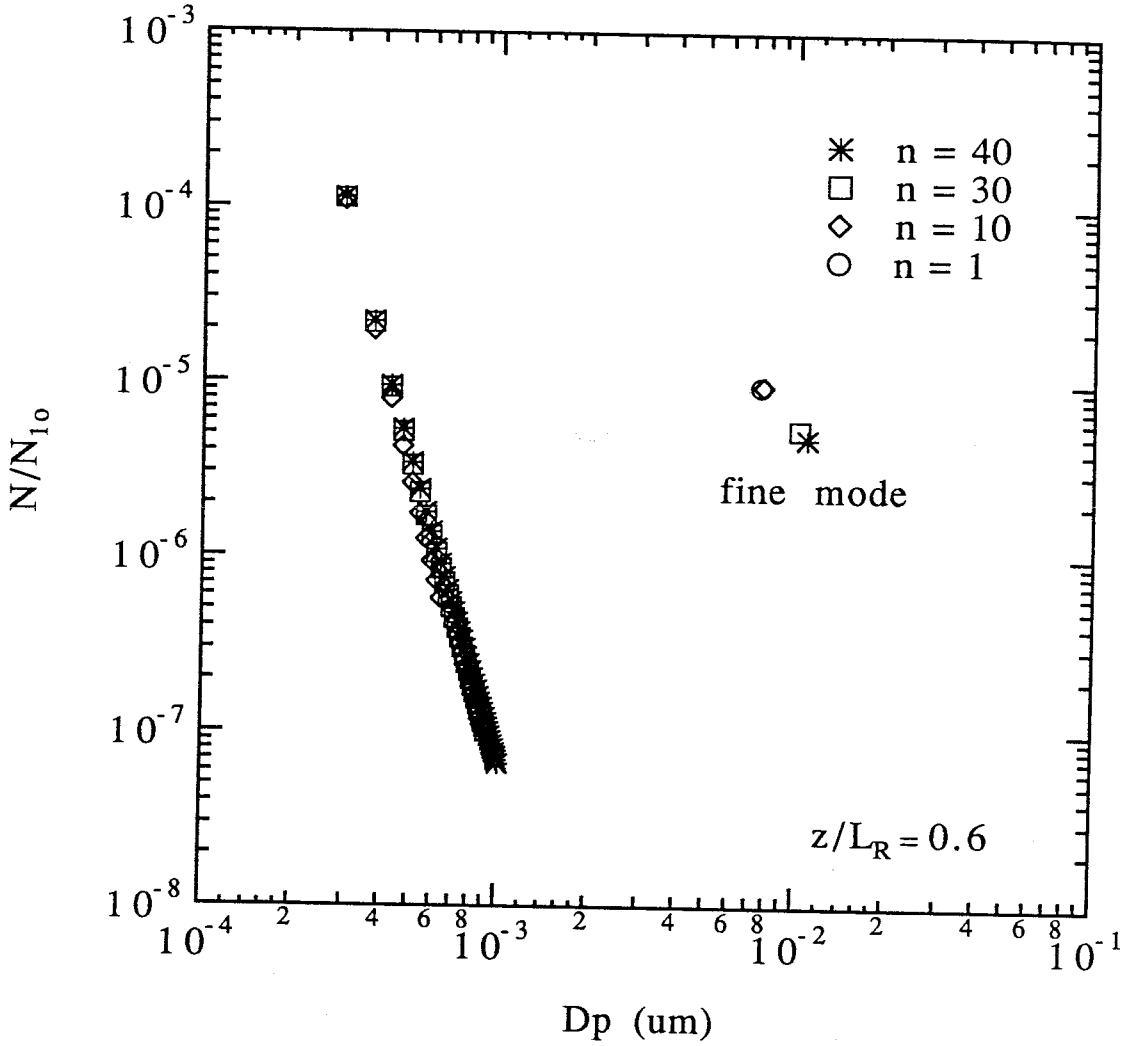

Figure 10(b). Cluster distribution and the number concentration and average size of the particles in the fine mode computed using the DSRC model with different numbers of discrete sizes, n, at $Z/L_R = 0.6$ for an initial seed concentration $N_{so} = 10^7$ cm^{-3} and size $d_{So} = 100$ nm, and the solid temperature profile shown in Fig. 6(a).

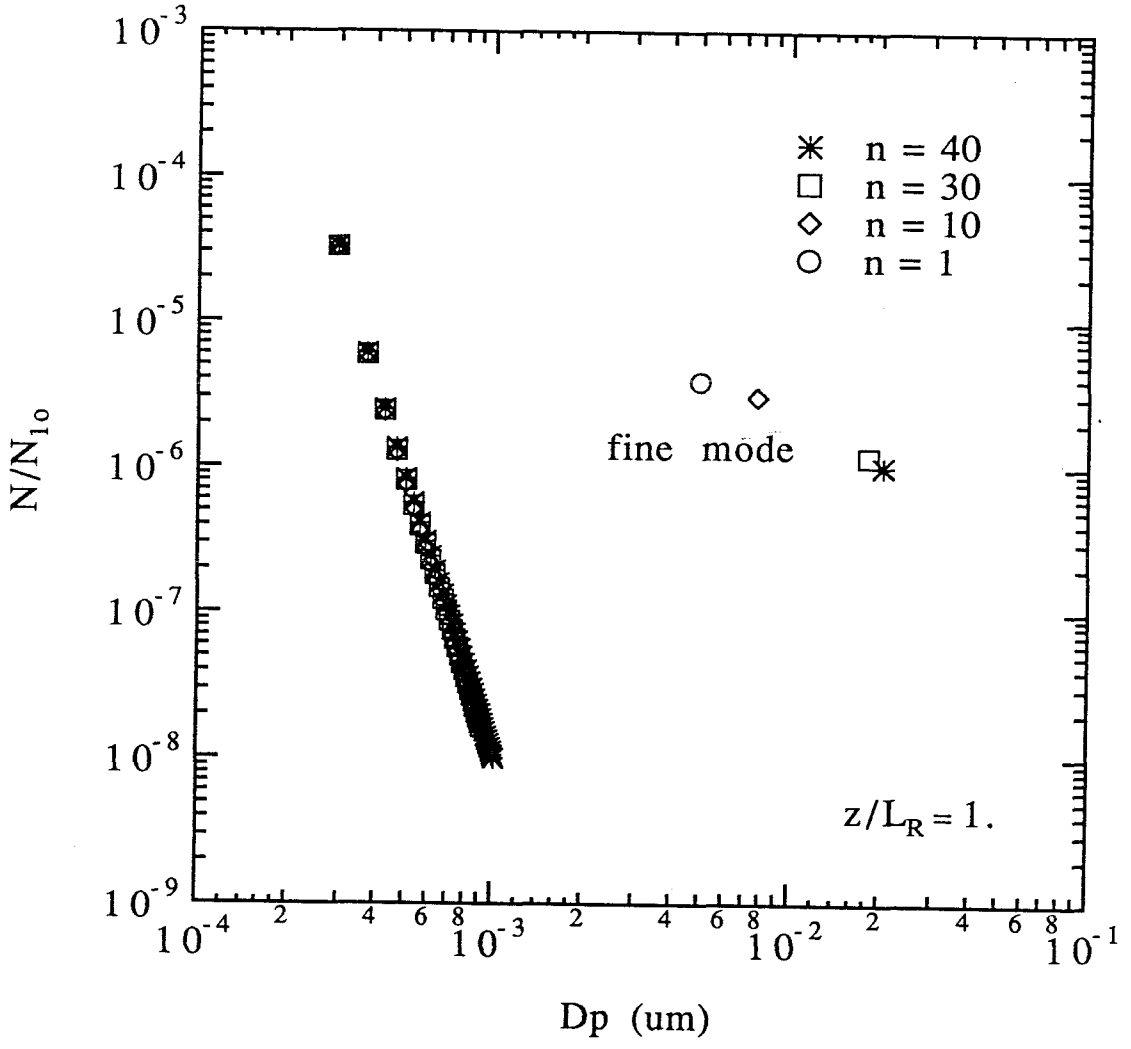

Figure 10(c). Cluster distribution and the number concentration and average size of the particles in the fine mode computed using the DSRC model with different numbers of discrete sizes, n, at $Z/L_R = 1.0$ for an initial seed concentration $N_{so} = 10^7$ cm^{-3} and size $d_{So} = 100$ nm, and the solid temperature profile shown in Fig. 6(a).

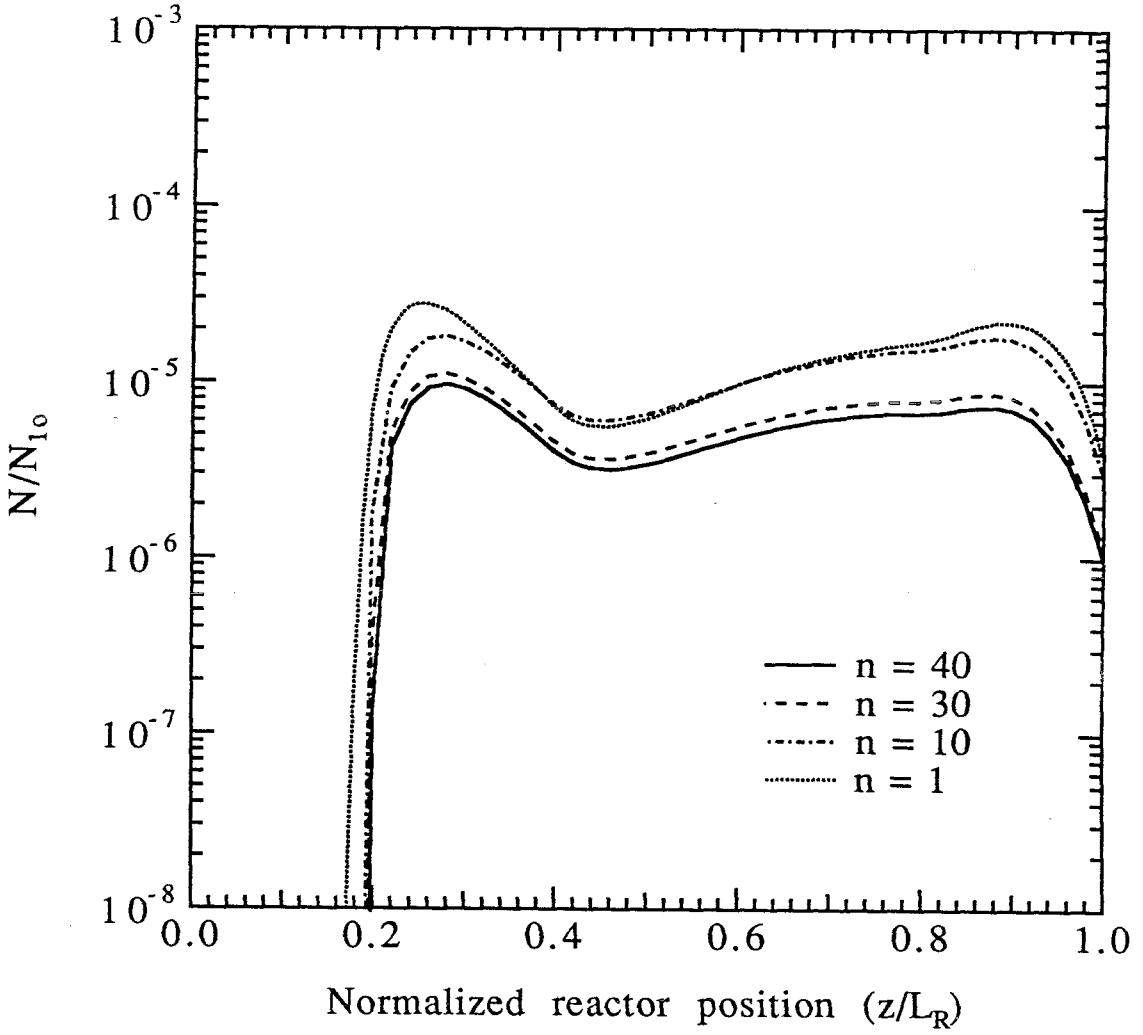

Figure 11. Normalized number concentration in the fine mode as a function of normalized reactor position computed using the DSRC model with different numbers of discrete sizes, n, for an initial seed concentration $N_{so} = 10^7$ cm^{-3} and size $d_{So} = 100$ nm, and the solid temperature profile shown in Fig. 6(a).

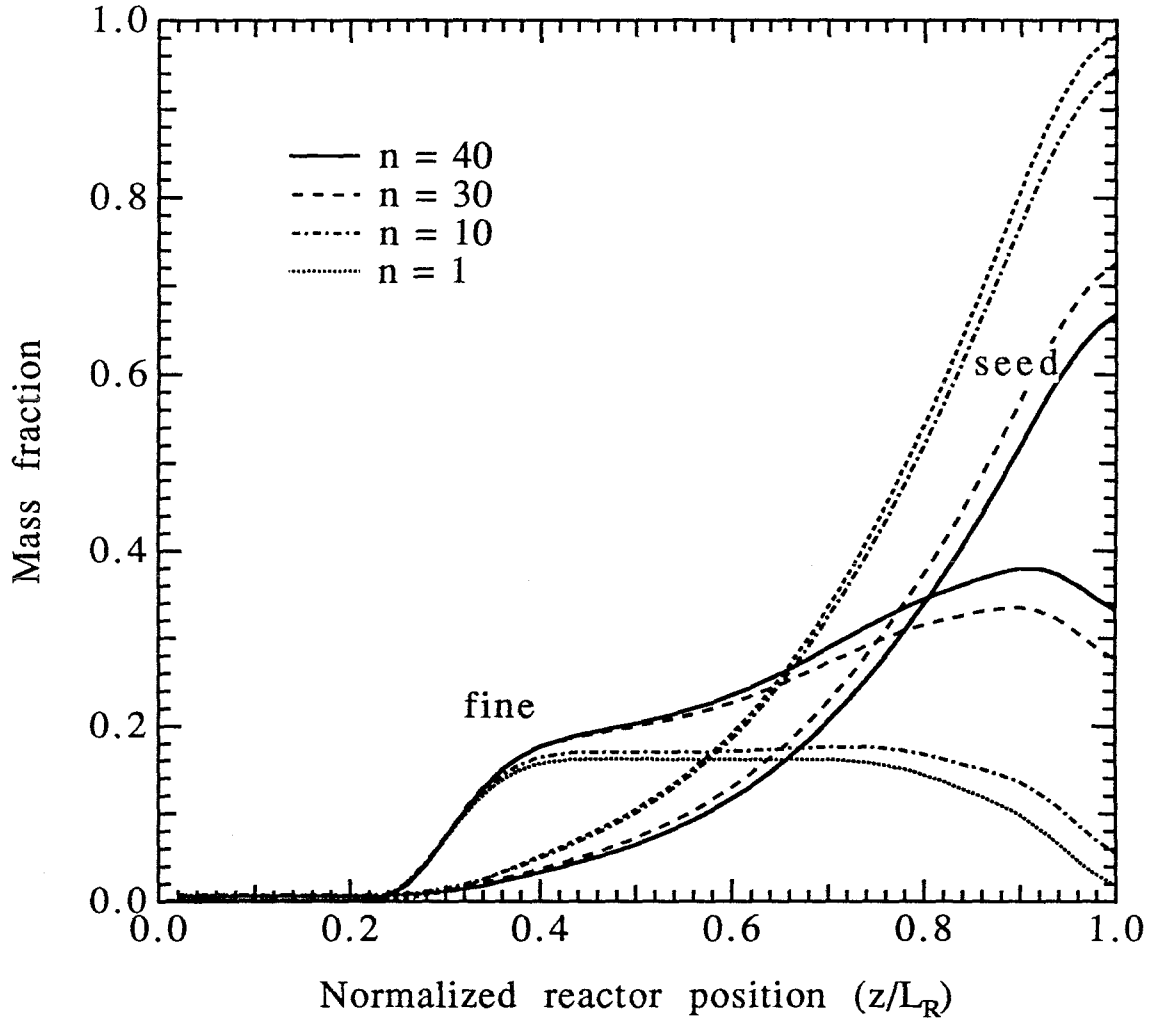

Figure 12. Mass fractions in the fine and the seed modes as a function of normalized reactor position computed using the DSRC model with different numbers of discrete sizes, n, for an initial seed concentration $N_{so} = 10^7$ cm^{-3} and size $d_{So} = 100$ nm, and the solid temperature profile shown in Fig. 6(a).

CHAPTER 5

CONCLUSIONS

Homogeneous and heterogeneous nucleation in a laminar flow aerosol generator has been studied experimentally using dibutylphthalate vapors. The results were found to be consistent with those predicted by the classical theory of homogeneous nucleation when the rates were multiplied by an enhancement factor of $10^5 - 10^7$. NaCl particles were used to probe the suppression of homogeneous nucleation due to the presence of seed nuclei. It was found that the extent of suppression depends on the seed particle number concentration.

Experiments have been performed to determine the mechanism of dense particle formation in a single stage multi-zone reactor reported by previous researchers. From the mobility measured size distributions and TEM analysis, it was determined that coagulation plays a major role in particle growth in such systems, and that the dense particles produced resulted from the sintering of low density aggregates formed by the agglomeration of like-sized particles produced early in the reactor. Calculations using a modified simplified reaction coagulation model are consistent with the experimental results. They also suggest that to produce dense particles, the concentration of the "seed" nuclei produced early in the reaction process must be allowed to reduce to a level that coagulation is no longer important before these seeds grow significantly. Continued growth of the seed nuclei at high concentrations results in incomplete coalescence upon coagulation and low density agglomerates are formed.

An optimization technique was applied to the highly nonlinear aerosol reactor system to directly derive optimal temperature profiles that maximizes seed growth and minimizes the formation of large clusters. The results indicate that if the sink is too small or the reactor residence time is too short, large cluster formation can not be suppressed regardless of the temperature profile used. For production of dense, nonagglomerated particles, the objective function and constraints must be chosen

such that the formation of large clusters is minimized. Without such constraints, growth by coagulation of like-sized particle will most likely occur resulting in the formation of low density aggregates.

A more detailed discrete SRC model was derived and the effects of small clusters on the average size and the number concentration of particles in the fine mode were evaluated. It was found that the SRC model considerably overpredicts the mass scavenged by the seed mode. The SRC model, however, is adequate for the derivation of optimal profiles. Once the optimal profile is found, a more accurate model should be used to obtain quantitative information.

Neither the SRC nor any of the more rigorous aerosol dynamic model that are presently available can desrcibe accurately the structural evolution and morphology of the partiles. In order to determine conditions that will produce dense, noagglomerated refactory particles, description of morphological changes must be developed and incorporated into the dynamic model.

APPENDIX A

A METHOD FOR THE SYNTHESIS OF SUBMICRON PARTICLES

with

J.J. Wu, and R.C. Flagan

Published in

Langmuir

3, 266 (1987)

A Method for the Synthesis of Submicron Particles†

Jin Jwang Wu,‡ Hung V. Nguyen,§ and Richard C. Flagan*‡

Division of Engineering and Applied Science and Department of Chemical Engineering, California Institute of Technology, Pasadena, California 91125

Received August 11, 1986. In Final Form: December 17, 1986

Powder synthesis by thermally induced vapor-phase reactions in aerosol reactors is described. The powders generated by this technique consist of high-purity, spherical, nonagglomerated, and uniformly sized particles in the 0.1-μm size range. Most of the particles are crystalline spheres. A theoretical examination based on the discrete–sectional model is presented. The comparison shows that the calculated size distribution of the final product from the aerosol reactor is fairly consistent with that observed experimentally.

Introduction

Powders having uniform submicron particles of spherical shape and that are free from agglomerates, of controlled size distribution, and of high purity are required to produce very uniform and dense compacts of the starting materials, a critical step in the processing of ceramics and other powder-based materials.[2] A variety of methods are presently being used to generate these starting powders. Extreme uniformity of particle size can be achieved by solution synthesis,[3,4] but this technique is applicable to a limited range of compositions. Highly uniform powders of silicon, silicon carbide, and silicon nitride have recently been generated by laser-induced pyrolysis of silane.[5,6]

Thermally induced vapor-phase reactions have also been used to produce a variety of powders. Oxide particles are produced by vapor-phase oxidation of metal halides in externally heated furnaces[7] and in flames.[8-10] Silicon nitride powders have been synthesized by reaction of ammonia and silane in a heated tube.[11] A common feature of these processes is the rapid production of condensible reaction intermediates and products by gas-phase reactions leading to the formation of large numbers of very small particles. The residence time is generally long enough for appreciable growth by coagulating and, since this growth takes place at high temperatures, for sintering of the agglomerates. This results in low-density flocs that make subsequent processing of the powder difficult. Low-density flocs are known to leave inherently large pores in the compacts that lead to large defects which reduce the tensile strength of the ceramic products.

The production of uniformly sized, nonagglomerated, spherically shaped solid particles by gas-phase chemical reactions is limited to the growth-dominant domain and is possible only under special conditions. The first step is to form particles by homogeneous nucleation, a process that generally leads to very high number concentrations of very fine particles. These particles can grow by Brownian coagulation or by chemical and/or physical vapor deposition. The former results in the formation of the aforementioned low-density flocs and a relatively broad size distribution. The latter, vapor deposition on existing particles, leads to dense particles with a narrow size distribution. Vapor deposition can dominate over coagulation only when the particle concentration is low since coagulation is a second-order process. It is, however, very difficult to prevent the formation of large numbers of particles by homogeneous nucleation when condensible low vapor pressure refractory species are generated by gas-phase chemical reactions, even when there may be already many particles present in the system.

To produce powders with the desired characteristics, it is, therefore, necessary to generate particles much smaller than the desired powder size by homogeneous nucleation while keeping the particle number concentration low enough to suppress growth by coagulation; then carry out the gas-phase chemical reactions gradually at such a rate that the particles can grow by deposition of the reaction products and the formation of new particles is suppressed. As the particles grow by vapor deposition, they deplete the condensible reaction products, thereby depressing the tendency to nucleate.

To date most aerosol reactor development has been empirically based, in spite of serious attempts to develop predictive models. The theoretical description of refractory particle formation and growth presents as serious a challenge as the experimental developments. A major difficulty is the high condensible vapor source rate that rapidly results in very high supersaturation. Warren et al.[23] showed that when the dimensionless source rate (defined as the ratio of the source rate of condensible vapor over the collision rate of vapor molecules) exceeds unity, the classical nucleation theory is not valid since new particle formation would take place on a time scale that is shorter than the time required to establish the steady-state cluster distribution on which the classical theory is based. The small critical nucleus size that the classical theory predicts for nucleation of refractory vapors casts further doubt upon the applicability of the classical theory to these systems. To optimize an aerosol reactor for the synthesis of refractory powders, the ability to predict quantitatively the evolution of the particle size distribution is essential.

In this paper we describe and demonstrate a method for the synthesis of uniformly sized spherical particles by thermally induced chemical reactions and introduce an aerosol kinetic model developed specifically to deal with high source rates typical of aerosol reactor operations. The

† Presented at the symposium on "Fine Particles: High Temperature Synthesis", 60th Colloid and Surface Science Symposium, Atlanta, GA; June 15–18, 1986; G. Mulholland, Chairman.

‡ Division of Engineering and Applied Science.

§ Department of Chemical Engineering.

(1) Wu, J. J.; Flagan, R. C., submitted for publication in *J. Colloid Interface Sci.*
(2) Bowen, H. K. *Mater. Sci. Eng.* **1980**, *44*, 1.
(3) Barringer, E. A.; Bowen, H. K. *J. Am. Ceram. Soc.* **1982**, *65*, C-199.
(4) Gobet, J.; Matijevic, E. *J. Colloid Interface Sci.* **1984**, *100*, 555.
(5) Cannon, W. R.; Danforth, S. C.; Flint, J. H.; Haggerty, J. S.; Marra, R. A. *J. Am. Ceram. Soc.* **1982**, *65*, 324.
(6) Cannon, W. R.; Danforth, S. C.; Haggerty, J. S.; Marra, R. A. *J. Am. Ceram. Soc.* **1982**, *65*, 330.
(7) Suyama, Y.; Kato, A. *J. Am. Ceram. Soc.* **1976**, *59*, 146.
(8) Ulrich, G. D. *Combust. Sci. Technol.* **1971**, *4*, 47.
(9) Ulrich, G. D.; Ines, B. A. M.; Subranmanian, N. S. *Combust. Sci. Technol.* **1976**, *14*, 243.
(10) Ulrich, G. D.; Subranmanian, N. S. *Combust. Sci. Technol.* **1977**, *17*, 119.
(11) Prochazka, S.; Greskovich, C. *Am. Ceram. Soc. Bull.* **1978**, *57*, 579.

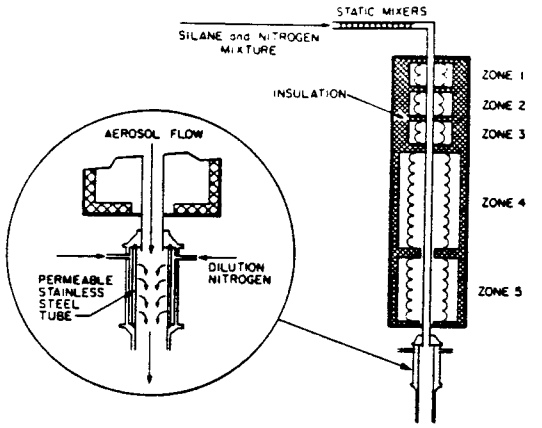

Figure 1. Schematic of the five-zone aerosol reactor in which silicon particles were generated by silane pyrolysis and the transpired wall system for product dilution and cooling.

ability of this model to predict the evolution of refractory aerosols produced by gas-phase chemical reactions is demonstrated by the comparison of calculations with experimental observations of particle formation and growth in a silane pyrolysis, fine particle synthesis reactor.

Particle Synthesis

The synthesis of uniform particles of 0.1-μm diameter requires the use of small numbers of much smaller particles as seeds to be grown by vapor deposition. While the mechanism of silicon formation from silane is not fully understood, the rate-limiting step is generaly thought to be the unimolecular decomposition of silane, $SiH_4 \rightarrow SiH_2 + H_2$.[12-16] The activation energy for this reaction is 60 kcal/mol, and the rate can be manipulated by temperature control. A single-stage reactor[17] was designed as to assure that the initial reaction rate can be kept very low, to severely limit the size and number concentration of particles generated by nucleation.

The single-stage reactor, illustrated in Figure 1, consisted of a 12 mm i.d., 850 mm long quartz tube that was heated in five separate zones. The first three heating zones were 50 mm long and were separated by 10 mm of low-density insulation. The remaining zones were 150 mm long and, again, were separated by insulation. By ramping the temperature along the length of the flow reactor, the rate of reaction was accelerated and seeds were grown by vapor deposition.

Electronic grade silane (Union Carbide, 99.99%) was thoroughly mixed with high-purity nitrogen (further purified and dried by passing over hot copper) by a series of static mixers (Luwa, Inc.). The resulting atmospheric pressure mixture of silane in nitrogen with controlled mole fraction was introduced into the upper end of the reactor tube. The first reaction zone was heated to 770 K, a temperature at which silane decomposed sufficiently slowly that only a small number of particles were generated by

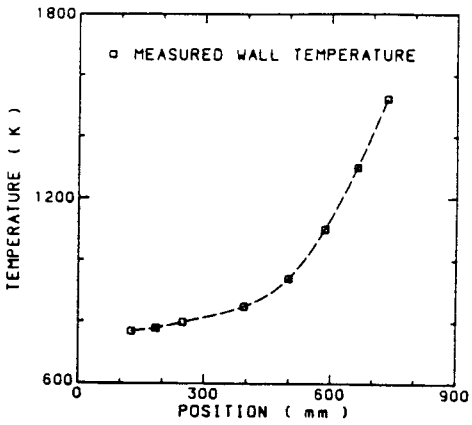

Figure 2. Measured temperature profile of the reactor wall.

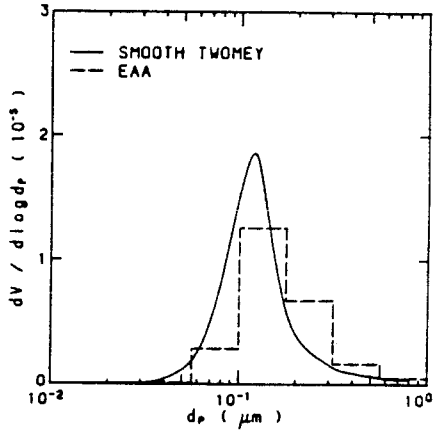

Figure 3. Volume distributions of the product aerosol. The histogram is the raw data obtained from the EAA. Also shown is an estimate of the actual particle size distribution obtained by applying a modified Twomey algorithm[18] to correct for cross sensitivities in the EAA instrument response function.

homogeneous nucleation. The temperature of the reactor wall was gradually increased to accelerate the reactions as the particles grew and became more effective at scavenging the condensible vapors and, therefore, at inhibiting nucleation. The temperature at the end of the fourth heating zone was 1100 K, as illustrated in Figure 2, sufficiently hot that complete decomposition was assured. In the remaining length of the reactor, provisions were made to heat the wall to temperatures as high as 1523 K to facilitate control of the structure and crystalline state of the particles.

The high concentration aerosol leaving the reactor was diluted with nitrogen before measurements by conventional aerosol instruments were made. The dilution system, shown in Figure 1, served the dual purposes of reducing the number concentration of particles and of minimizing thermophoretic losses of hot aerosol to the cooled reactor wall. This was accomplished by transpiring nitrogen diluent through the wall of a sintered stainless steel tube.

The size distribution and number concentration of the product aerosol were measured by using a TSI Model 3030 electrical aerosol size analyzer and an Environment One condensation nuclei counter. Teflon membrane filters (Milipore) were used to collect powder samples for studies

(12) Purnell, J. H.; Walsh, R. *Proc. R. Soc. London* **1966**, *293*, 543.
(13) Newman, C. G.; O'Neal, H. E.; Ring, M. A.; et al. *Int. J. Chem. Kinet.* **1979**, *11*, 1167.
(14) Hogness, T. R.; Wilson, T. L.; Johnson, W. C. *J. Am. Chem. Soc.* **1936**, *58*, 108.
(15) Neudorfl, P.; Jodhan, A.; Strausz, O. P. *J. Phys. Chem.* **1980**, *84*, 338.
(16) White, R. T.; Ring, M. A.; O'Neal, H. E. *Int. J. Chem. Kinet.* **1985**, *17* (10), 1029.
(17) Wu, J. J.; Flagan, R. C.; Gregory, O. J. *Appl. Phys. Lett.* **1986**, *49*, 82.

Figure 4. TEM micrograph of the crystalline silicon particles produced by rate-controlled thermal decomposition of silane.

of particle morphology by transmission electron microscopy, crystal structure by X-ray and electron diffraction, particle density by helium displacement measurements, and surface area measurements by the BET method.

Particle Characterization

An on-line EAA measurement of the silicon aerosol size distribution is shown in Figure 3. The histogram represents the raw data from channels 4–11 of the EAA, and the smooth curve is an estimate of the actual particle size distribution obtained by using the smooth Twomey algorithm which corrects for cross sensitivities in the EAA instrument response function.[18] The total number concentration of the product aerosol was $4.6 \times 10^{15}/m^3$ with a modal diameter of 0.1 μm. The total number concentration measured by the CNC was about 2.5 times higher.

The product silicon powders were brown in color, indicative of high-purity silicon.[19] A typical electron micrograph, Figure 4, shows the uniformly sized particles. The average diameter measured from the micrograph was consistent with the EAA measurements. The structure of these particles consisted of diamond cubic grains with dimensions of 50 nm showing extensive twinning and stacking faults. The twins extend across the entire diameter, suggesting the transformed planar front upon the amorphous to crystalline phase transformation. The twinned regions appear to be randomly oriented, as would be expected for particles that underwent independent processing in the aerosol phase. X-ray peak broadening was used to estimate the average crystallite size. The Bragg peak broadening as a function of the magnitude of the wave vector was calculated by taking into account Rachinger's and Stoke's corrections. The result (Figure 5) indicates that the dominant contribution to the line broadening was not from stress but from small crystal size.

The apparent surface area of the collected powder by nitrogen adsorption and interpreted by the BET isotherm was 25 m^2/g, and the helium density measurement was 2.3 g/cm^3, corresponding very closely to the 0.1-μm size estimated from more direct measurements. The latter results strongly suggest that the number of particles smaller than those included in the EAA measurement was small. Particles ranging from 0.05 to 0.5 μm had been generated by varying the silane concentration and temperature profile.

Theory

When gas-phase chemical reactions generate low vapor pressure species in excess of their equilibrium vapor pressure, the vapors may deposit on existing surfaces or,

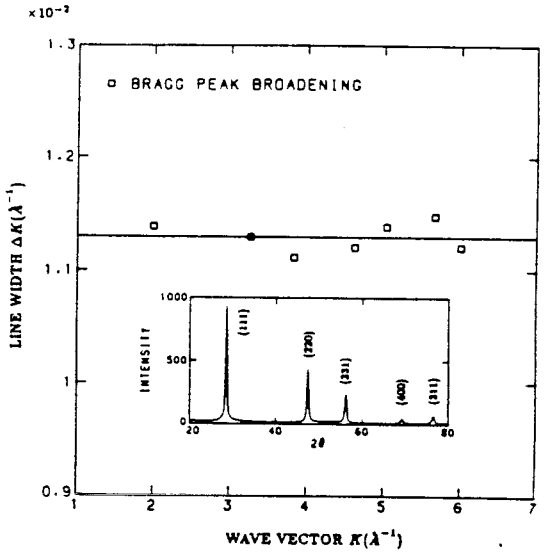

Figure 5. Bragg peak broadening as a function of the magnitude of the wave vector. The insert is the copper Kα X-ray pattern of the produced silicon powder.

if large excesses of condensible species are produced, form new particles by homogeneous nucleation. The classical theory of homogeneous nucleation developed by Volmer, Becker, Doring, and Zeldovich around the 1930's is the most common approach for treating homogeneous nucleation (VBDZ theory). The rate of formation of new particles is represented by

$$J = S^2 n_{sat}{}^2 2\nu_1 \left(\frac{\sigma}{2\pi m_1}\right)^{1/2} \exp\left(\frac{-16\pi\sigma^3\nu_1{}^3}{3k^3T^3 \ln^2 S}\right) \quad (1)$$

Equation 1 expresses the rate of formation of new particles as a function of the local saturation ratio of the vapor, S, and the local temperature, T. The particles formed have a surface tension, σ, molecular volume, ν_1, molecular mass, m_1, and number concentration of saturated vapor n_{sat}.

The clasical model was derived from a combination of thermodynamic and kinetic theories, incorporating a number of questionable assumptions. It ascribes macroscopic thermodynamic properties, such as surface tension and bulk chemical potential, to microscopic clusters of only a few molecules (the so-called capillary approximation). The existing alternative statisticomechanical theories, such as Lothe–Pound[20] and Reiss, Katz, and Cohen,[21] inevitably suffer from many of the same problems associated with the extrapolation of macroscopic properties to molecular clusters and generally do not seem to outperform the classical theory in experimental tests.[22]

The starting point in the classical nucleation theory is a system of monomers in a supersaturated gas phase. Such a system is inherently unstable—leading ultimately to clusters of unbounded size. However, the concept of thermodynamic pseudoequilibrium is then introduced with a constraint allowing some fixed maximum cluster size. This helps to bring the power and elegance of thermodynamics to bear upon a dynamic system. Once the free energy barrier to nucleation, arising from surface energy,

(18) Markowski, G. R. *Aerosol Sci. Technol.*, in press.
(19) Moulsen, A. J. *J. Mater. Sci.* **1979**, *14*, 1071.
(20) Lothe, J.; Pound, G. M. *J. Chem. Phys.* **1962**, *36*, 2080.
(21) Reiss, H.; Katz, J. L.; Cohen, E. R. *J. Chem. Phys.* **1968**, *48*, 5553.
(22) Springer, G. S. "Homogeneous Nucleation In Advances in Heat Transfer", Academic Press, New York, 1980.

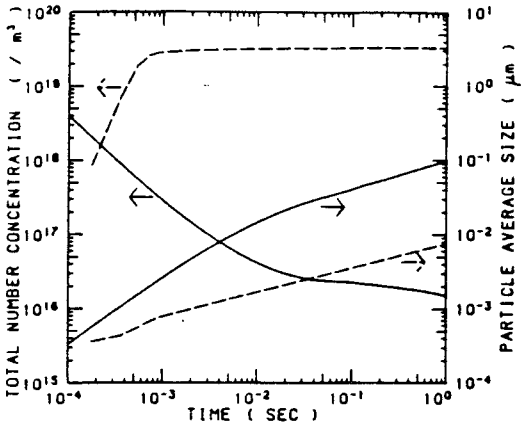

Figure 6. Comparison of the aerosol evolution predicted by the SNM model[23] (dashed curves) vs. the kinetic model[1] (solid curves).

is overcome and a cluster exceeds the critical size, further growth is increasingly favored. The critical size is simply the least thermodynamically favored cluster size, lying at the peak of the activation energy curve for nucleation. The hypothetical, pseudoequilibrium state is only valid when the time scale for generating saturated vapor molecules is much longer than that for binary collisions of saturated vapor molecules. This is what we call low source rate nucleation processes. Warren, and Seinfeld[23] had shown how one can predict a final number concentration of particles that will be formed at low vapor source rate, i.e.,

$$\tilde{R}_s = \frac{R_s}{\tilde{R}_\beta} = \frac{R_s}{n_{sat}{}^2 \beta_1 s_1 / 4} \leq 1 \qquad (2)$$

where $\tilde{R}_s$, the dimensionless source rate, is the ratio of the characteristic vapor source rate (R_s) to the rate of monomer–monomer collisions in the saturated vapor ($\tilde{R}_\beta$).

For many of the chemical reaction systems, e.g., powder synthesis reactors or CVD systems, the source generation rate is very high, and the pseudo-steady-state assumption is not valid. All the steady-state models of nucleation break down, as the cluster population will not be in steady state with either the monomers or the stable particles. In that case, the "critical nucleus", calculated on the basis of a macroscopic surface energy, may be of atomic dimensions, or even smaller. That means that the bulk energy of association is large enough to make any surface energy term negligible. Under such conditions, the formation and growth of particles of the condensed phase may be determined primarily by the kinetics of collisions in the gas phase among molecular clusters and aerosol particles.

To examine the evolution of aerosol in the powder synthesis reactor, one can describe the dynamics of coagulation between the molecular clusters and aerosol particles by[24]

$$\rho \frac{d}{dt}\left(\frac{N_1}{\rho}\right) = R_s - \sum_{j=1}^{\infty} \beta_{1j} N_1 N_j \qquad (3)$$

$$\rho \frac{d}{dt}\left(\frac{N_i}{\rho}\right) = \frac{1}{2}\sum_{j=1}^{i-1} \beta_{i-j,j} N_{i-j} N_j - \sum_{j=1}^{\infty} \beta_{ij} N_i N_j \qquad i \geq 2 \qquad (4)$$

Where R_s in (3) is the source rate of the condensible vapors, which is a function obtained from gas-phase chemical reactions. N_i is the number concentration of particles containing i–mers. ρ is the density of the gas. The aerosol concentrations, N_i/ρ, are described in terms of mass unit since the temperature of the system is allowed to change.

Fuchs' interpolation expression of the Brownian coagulation coefficients, β_{ij}, between the clusters and the aerosol, without considering interparticle forces, is adopted for the simulation.[25]

$$\beta_{ij} = 2\pi(D_i + D_j)(d_i + d_j)\left[\frac{d_i + d_j}{d_i + d_j + 2g_{ij}} + \frac{8(D_i + D_j)}{\bar{v}_{ij}(d_i + d_j)}\right]^{-1} \qquad (5)$$

$$D_i = \frac{kT}{3\pi d_i \eta}\left[1 + Kn_i\left(1.257 + 0.4\exp\left(-\frac{1.1}{Kn_i}\right)\right)\right] \qquad (6)$$

$$g_{ij} = (g_i^2 + g_j^2)^{1/2} \qquad (7)$$

$$g_i = \frac{1}{3d_i l_i}[(d_i + l_i)^3 - (d_i^2 + l_i^2)^{3/2}] - d_i \qquad (8)$$

$$l_i = \frac{8D_i}{\pi \bar{v}_i} \qquad (9)$$

$$\bar{v}_i = (8kT/\pi m_i)^{1/2} \qquad (10)$$

β_{ij} is highly dependent on the particle diameters d_i and d_j. D is the particle diffusivity, usually determined from the Stokes–Einstein expression which includes the Millikan slip correction factor. Kn_i is the Knudsen number defined as $Kn_i = 2\lambda/d_i$, where λ is the mean free path of the vapor molecules. k is the Boltzmann constant. T is the absolute temperature. η is the viscosity of the medium, and m_i is the mass of the particle.

The aerosol systems of interest here extend from the monomer and smallest clusters to micron particles. Description of the aerosol evolution in terms of discrete cluster sizes (eq 3 and 4) over this size range requires the simultaneous solution of an extremely large number of ordinary differential equations. On the other hand, the use of a continuous representation of the particle size distribution introduces unacceptable approximations at small cluster sizes since the discrete differences between the small clusters (monomer, dimer, trimer, etc.) cannot be taken into account. A discrete–sectional representation of the particle size distribution has recently been developed by Wu and Flagan[1] to overcome these difficulties with minimal approximation.

This model, which allows the examination of particle nucleation and growth by coagulation and vapor deposition even when the monomer source rate is very high, is an extension of the sectional model of Gelbard et al.[26] The aerosol size spectrum is separated into two parts. The first part of the spectrum, starting from the monomer, is described by the number of concentration, N_i, of particles containing i monomers, where $1 \leq i \leq k$, since number concentration is more appropriate for smaller particles. The second part is described by the mass, Q_l, of the divided sections of the rest of the space. Assuming constant aerosol density, it is convenient to represent the particle size of this part with x, defined as the logarithm of the mass of the particle $x = \ln v$. For each section l ($1 \leq l \leq M$), whose size range is defined by $x_{l-1} \leq x < x_l$, the aerosol mass per

(23) Warren, D. R.; Seinfeld, J. H. *Aerosol Sci. Technol.* **1984**, *3*, 135.
(24) Gelbard, F.; Seinfeld, J. H. *J. Colloid Interface Sci.* **1979**, *68*, 363.
(25) Fuchs, N. A. *The Mechanics of Aerosol*, Pergamon: New York, 1964.
(26) Gelbard, F.; Tambour, Y.; Seinfeld, J. H. *J. Colloid Interface Sci.* **1980**, *76*, 541.

unit volume is given $Q_l = \int_{x_{l-1}}^{x_l} e^x n(x)\,dx$. The parameter k, the dividing point between the two parts, is chosen on the basis of the required accuracy of the distribution of small clusters.[1]

The governing equations of coagulation, (3) and (4), of an aerosol in the aerosol reactor system in terms of discrete–sectional representations become

$$\rho \frac{d}{dt}\left(\frac{N_1}{\rho}\right) = R_s - \sum_{i=1}^{k} \beta_{1i} N_1 N_i - [\sum_{r=1}^{M} {}^1\bar{\beta}_{1r} Q_r] N_1 \quad (11)$$

$$\rho \frac{d}{dt}\left(\frac{N_i}{\rho}\right) = \frac{1}{2}\sum_{j=1}^{i-1} \beta_{i-j\,j} N_{i-j} N_j - \sum_{j=1}^{k} \beta_{ij} N_i N_j - [\sum_{r=1}^{M} {}^1\bar{\beta}_{ir} Q_r] N_i \qquad 2 \le i \le k \quad (12)$$

$$\rho \frac{d}{dt}\left(\frac{Q_l}{\rho}\right) = \frac{1}{2}\sum_{i=1}^{l-1}\sum_{j=1}^{l-1} {}^1\beta_{ij} Q_i Q_j - [\sum_{i=1}^{l-1} {}^2\bar{\beta}_{il} Q_i] Q_l - \frac{1}{2} {}^3\bar{\beta}_{ll} Q_l^2 - [\sum_{i=l+1}^{M} {}^4\bar{\beta}_{il} Q_i] Q_l - [\sum_{i=1}^{k} {}^2\bar{\beta}_{il} N_i] Q_l + \sum_{i=1}^{k}\sum_{r=1}^{l-1} {}^3\bar{\beta}_{ir\,l} N_i Q_r + \frac{1}{2}\sum_{i=1}^{k}\sum_{j=1}^{k} {}^4\bar{\beta}_{ij\,l} N_i N_j \qquad 1 \le l \le M \quad (13)$$

Where N_i, as mentioned earlier, is the number concentration of particles with i–mers and Q_l is the mass concentration of section l with size range from x_{l-1} to x_l. ${}^1\bar{\beta}_{ir}$, ${}^2\bar{\beta}_{il}$, ${}^3\bar{\beta}_{ir\,l}$, and ${}^4\bar{\beta}_{ij}$ are the discrete–sectional coagulation coefficients[1] to account for the interactions of particles between the discrete and sectional regimes. ${}^1\beta_{ij\,l}$, ${}^2\beta_{il}$, ${}^3\beta_{ll}$, and ${}^4\bar{\beta}_{il}$ are the inter- and intrasectional coagulation coefficients derived by Gelbard et al.[26] to account for the interactions of particles inside the sectional regions.

In the limit of very narrow sections, (11)–(13) reduce to the exact representation of the particle and cluster population. The aerosol evolution in the reactor can be simulated by solving (11)–(13) with appropriate initial conditions. For the present purposes, the initial condition is taken to be particle-free gas at the temperature of the reactor inlet. The simulation then extends from the first inception of stable nuclei through growth to the final particle sizes.

Predictions of Submicron Powder Synthesis

Warren et al. developed the SNM aerosol model which assumes that the aerosol is formed according to the classical nucleation theory and then grown by condensation.[23] Nucleation is triggered by a continuously reinforced vapor input at a constant rate or an initial burst of condensible vapors. The aerosol is assumed to be monodisperse with a characteristic diameter calculated on the basis of mass balance. The model neglects the interaction between the molecular clusters and the particles and is applicable for dimensionless source rate for $\bar{R}_s \le 1$.

Simulations based on both the SNM model and the discrete–sectional kinetic model were performed with the corresponding experimental conditions. The reaction mechanisms and kinetics of White et al.[16] were adopted for the simulation. The simulation time step, t, was assumed to be z/u, where z is the differential length along the reactor, and u is the plug flow velocity which is a function of the gas temperature. The input source rate for the simulations is a function of time and is derived from White's kinetics and the experimental temperature–time history. The critical nucleus size was assumed, in the SNM model, to be of atomic dimension since the calculated critical size based on the macroscopic physical properties[27]

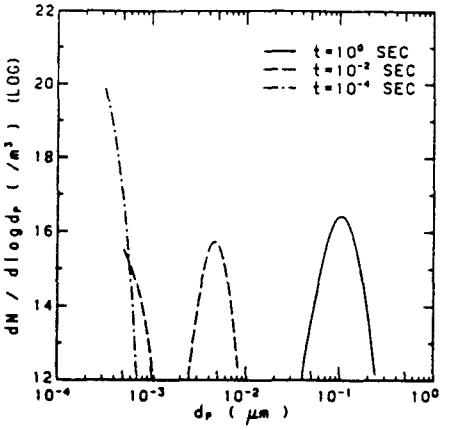

Figure 7. Simulated aerosol size distribution at different times corresponding to the experimental conditions.

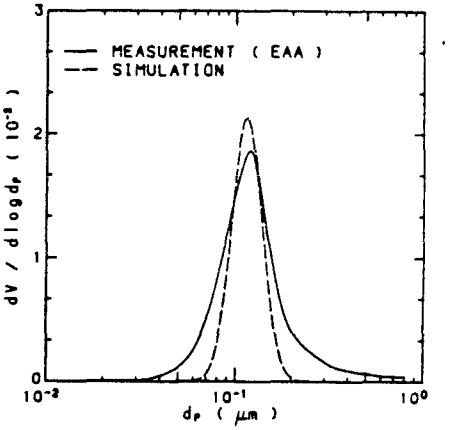

Figure 8. Comparison of the output silicon size distribution measured at the outlet of reactor and that calculated by the kinetic model.

was much smaller than the atomic size of silicon. The aerosol evolution predicted by the SNM model is depicted by the dashed curves in Figure 6. A burst of nucleation occurred immediately after the reactions started due to the extremely low equilibrium vapor pressure. The number concentration eventually leveled off because nucleation was quenched by condensation, and coagulation was neglected. The simulated aerosol evolution based on the kinetic model is described by the solid curves in Figure 6, with the corresponding size distributions at different times shown in Figure 7. One can see from Figure 6 that the average size increased and the number concentration decreased due to the cluster–particle interactions, clearly indicating that a more detailed representation of the particle size distribution than is possible with the SNM model or any model that considers only one mode in the particle size distribution. Figure 7 shows that a brief burst of nucleation provided the seeds for subsequent rapid particle growth by vapor deposition. The total number did not change appreciably, but the mean particle size was increasing with time. The calculated final size distribution based on the kinetic model, shown in Figure 8, is fairly

(27) Yaws, C. L.; et al. *Process Feasibility Study in Support of Silicon Material Task I*, DOE/JPL 954343-81/21, 1981.

consistent with that observed experimentally. The final mean particle diameter was about 0.1 μm, consistent with the measurements from the EAA and the TEM micrographs and that estimated from BET surface area. The broader size distribution observed experimentally may result in part from the distribution of residence times and time–temperature histories in the laminar flow reactor and from the resolution limitations of the EAA.

Conclusions

Submicron particles are of great interest because they offer excellent possibilities in the production of powder catalysts, ceramics, electronic devices, etc. To generate high-quality ceramics, the particles should be uniformly sized, be approximately spherical in shape, and contain few agglomerates. Conventional powder synthesis processes based on gas-phase chemical reactions have difficulty achieving these criteria. High reaction rates generate large numbers of very small particles. These particles then coagulate, resulting in a relatively broad size distribution and, in most cases, significant quantities of partially sintered agglomerates. This paper describes a new type of aerosol reactor capable of producing particles that much more closely approach the ideal powder.

The production of uniformly sized particles by gas-phase chemical reactions is achieved by promoting growth of a relatively small number of small particles by vapor deposition, while maintaining the number concentration low enough that coagulation does not occur at an appreciable rate. The rate of gas-phase reactions leading to the formation of condensible species is initially very low, leading to the formation of a relatively small concentration of very small particles. Continued reaction promotes the growth of these nuclei by vapor deposition, provided the reaction proceeds slowly enough to avoid the formation of large numbers of particles in a second burst of nucleation. This requires a delicate balance to grow the seeds appreciably within the limited residence time that can be tolerated in gas flow reactors. Initially, when the particles are small, the rate of reaction must be very slow since the particles are not very effective at scavenging condensible vapors and, thereby, suppressing nucleation. As the particles grow, higher reaction rates can be tolerated without nucleation. In contrast to particle growth by coagulation, the size distribution narrows as particles are grown by vapor deposition. Growth by vapor deposition not only results in a relatively narrow particles size distribution, it also minimizes the formation of agglomerates.

This process was demonstrated in the production of silicon particles by the thermal decomposition of silane. Variation of the reaction rate was achieved by ramping the temperature along the length of a laminar flow reactor. By this means, spherical silicon particles of 0.1-μm mean diameter were generated. The particles were predominantly crystalline and were readily separable into individual spheres.

The design of aerosol reactors capable of producing uniform and nonagglomerated particles requires an understanding of the dynamics of particle formation and the kinetics of the gas-phase reactions that lead to the production of condensible vapors. The particulate materials of interest generally have very low equilibrium vapor pressures, so even slow rates of production of condensible vapors lead to such high saturation ratios that the classical theory of homogeneous nucleation cannot be applied. At high supersaturations, key assumptions in the classical nucleation theory are violated, specifically (i) the steady-state cluster distribution and (ii) the growth of clusters by monomer addition rather than through cluster–cluster aggregation. Numerous studies have shown that the nucleation rate can exceed that predicted by the classical theory by several orders of magnitude. This discrepency has been dealt with in some cases by the introduction of an enhancement factor ranging from 10^4 to 10^8. A more satisfying approach is the direct solution of the cluster balance equations, beginning with the monomer and extending to the ultimate particle size. This approach is computationally intractable by using the discrete representation of the particle size distribution, and serious errors are introduced in the use of the continuous representation to describe the small clusters that play such an important role in determining the rate of new particle formation. To overcome these difficulties, we have used a discrete–sectional model that minimizes the approximation in simulation of the dynamics of small clusters while incorporating a computationally efficient algorithm to describe the dynamics of the larger particles.

Predictions made by using this model together with previously published descriptions of the silane pyrolysis kinetics and the experimental temperature time histories are in reasonable agreement with experimental observations of the mean particle size and number concentration. The predicted distributions are somewhat narrower than observed. The causes of this discrepency have not been elucidated but may be, at least in part, the result of applying a plug flow simulation to a fully developed laminar pipe flow.

The discrete–sectional model is a powerful approach to the simulation of aerosol dynamics since the role of small clusters is accurately simulated, at least within the accuracy of the descriptions of cluster and particle properties and the chemical source rates. For the present calculations, we have assumed that the particles are, at all times, dense spheres and that the cluster surface free energy equals that of the bulk material.

Acknowledgment. This work was supported by the Program in Advanced Technologies of the California Institute of Technology. The provision of the X-ray diffractonmeter from Professor William L. Johnson is greatly appreciated.

Registry No. SiH_4, 7803-62-5; Si, 7440-21-3.

APPENDIX B

EVALUATION AND CONTROL OF PARTICLE PROPERTIES IN AEROSOL REACTORS

with

J.J. Wu, R.C. Flagan, K. Okuyama, and Y. Kousaka

Published in the

AIChE Journal

34, 1249 (1987)

Evaluation and Control of Particle Properties in Aerosol Reactors

The production of powders by aerosol routes spans a wide range of operating temperatures depending on the type of aerosol reactors used. The dominant mechanism of particle growth and evolution depends highly on the rate at which the reactions producing the condensible species are carried out. Numerical solutions of the discrete-sectional aerosol general dynamic equation that accounts for the interactions of the discrete clusters were obtained for conditions representative of the different types of aerosol reactors used for powder production today. Simplified reaction and coagulation equations that give fast and useful prediction of the evolution of aerosols associated with chemical reactions were derived, and a simple reaction-coagulation model was developed. The effects of reaction rate, initial vapor concentration, residence time, seed particles, and temperature profile on the properties of fine particles produced by gas-phase chemical reactions were evaluated using both models. Results show good agreement between the two.

Jin Jwang Wu, Hung V. Nguyen, Richard C. Flagan
Div. of Engineering and Applied Science
California Institute of Technology
Pasadena, CA 91125

Kikuo Okuyama, Yasuo Kousaka
Department of Chemical Engineering
University of Osaka Prefecture
Osaka, Japan

Introduction

Fine powders have become increasingly important in a number of high technology industries, particularly in ceramics. As the applications of the powders become more severe, so do the demands placed on the powder properties. Bowen (1980) suggested that an ideal powder used in fine ceramics should consist of roughly spherical, nonagglomerated, uniformly-sized particles preferably in the submicron-size range and with controlled chemical composition. Powder production from gaseous precursors has long been technologically important for such commodities as carbon black, fume silica, titanium dioxide, oxide ceramics, and magnetic powders. The technologies for the synthesis of particles, however, have been primarily empirical developments aiming at controlling various powder properties such as particle size and size distribution, internal porosity, extent of agglomeration, and material phase.

Aerosol reactors used for powder synthesis usually operate at elevated temperatures. Since the reaction rates depend exponentially on temperature, it is useful to classify the chemical processes in terms of the heat source. Flame or combustion systems, which have been used to synthesize carbon black and other powders, operate at temperatures in the range from 1,500 to 3,000 K. The reaction rates at these temperatures are very high and the reactions are completed on the order of milliseconds. An early technological application of plasmas is in powder synthesis (Fauchais et al., 1983). Plasmas can achieve the high temperatures needed for the synthesis of refractory materials, but require some optimal cooling schedule to control nucleation and reduce agglomeration upon collection. Powders that have been produced by plasmas include oxides, carbides, nitrides, borides, and pure elemental species. Laser-induced chemical reaction also has been used to synthesize fine powders (Cannon et al., 1982a,b). The heating rate in laser systems can be as high as 10^6 $K \cdot s^{-1}$. Peak temperatures measured optically range from 1,400 to 1,600 K. The particles form rapidly in a "flame" produced by the laser heating with the number concentration peaking and decaying by coagulation within a few tenths of a millisecond. The total time in the laser beam is about 2 ms. Finally, thermal processes for powder synthesis induce reaction by an external heat source. The powders produced by this route can be much coarser than those generated in flame processes. One of the oldest applications of this technique is in the production of carbon blacks (Walker, 1963). Other examples include the decomposition of metal alkoxides or silane gas to produce fine powders at relatively low temperatures (Okuyama et al., 1986; Wu et al., 1986, 1987a).

Correspondence concerning this paper should be addressed to R. C. Flagan.
Jin Jwang Wu is presently with IBM, T. J. Watson Research Center, Yorktown Heights, NY 10598.

The elementary processes involved in the formation and growth of particles from gaseous precursors include: 1) gas-phase chemical reactions; 2) surface reactions; 3) homogeneous nucleation; 4) heterogeneous condensation; 5) coagulation; and 6) coalescence or fusion. The differences in the properties of particles produced in the various reactors can be traced back to the differences in the relative importance of these processes. The reactions in high-temperature processes, i.e., plasma, laser, and flame reactors, are carried out at such a rate that high supersaturation levels are achieved, resulting in rapid nucleation of high number concentrations of very small particles. These particles then grow by coagulation. The end result, for temperatures below the melting point, is a powder consisting of low-density flocs. The rapid cooling of the particles in plasma and laser reactors to temperatures well below the sintering temperature should, in principle, minimize the formation of low-density agglomerates. On the other hand, slow chemical reaction rates that allow vapor and cluster deposition on the surfaces of existing particles to play a more important role in particle growth than coagulation should also lead to the production of uniformly-sized particles with minimal agglomeration.

The advances in aerosol physics and chemistry now have made feasible theoretical descriptions of the dynamical processes involved in particle formation and growth in chemical synthesis reactors. Although most of the research has been concentrated in the studies of aerosols in the environment, applications to powder synthesis in aerosol reactors have begun to gain increasing emphasis. A major problem confronted is that the chemical reaction mechanisms as well as many physical and chemical properties needed to describe the evolution of particles in aerosol systems are not known. The key features regarding the behavior of different reactor systems, however, can be extracted, without detailed knowledge of the reaction chemistry or shapes of the generated agglomerates, by using available aerosol models appropriate for these high source rate reactors. By focussing on the nucleation, vapor and cluster deposition, and coagulation, we can gain understanding on the behaviors and relationships between the various aforementioned reactor systems used for powder synthesis today. This study examines the effect of reaction rate, initial vapor concentration, residence time, and seed particles on the distributions of fine particles using two models. The results show that growth of refractory particles in a high source rate operation is dominated by coagulation that results in a broad particle-size distribution. Control of the reaction rate is the most effective way to suppress nucleation of new particles and to grow uniformly-sized particles.

Models of Particle Production Processes

Figure 1 illustrates the physical processes involved in particle formation from the gas phase. Gaseous precursors react to produce vapor molecules. If the vapor reaches sufficient level of supersaturation, ultrafine primary clusters are formed by homogeneous nucleation. Larger secondary particles are formed by the coagulation of clusters and by the simultaneous heterogeneous condensation of vapor molecules onto the clusters. If seed particles are introduced into the system, they may scavenge a considerable amount of condensible vapor and clusters, thereby reducing the potential for new particle formation.

Friedlander (1983) presented a theoretical model for aerosol formation by chemical reactions in the absence of coagulation in batch and flow aerosol reactors. Assuming that the classical theory of homogeneous nucleation is valid, four coupled nonlinear ordinary differential equations were derived to describe the time evolution of the total number concentration and total surface area of the aerosol, the first moment of the aerosol-size distribution (mean particle diameter), and the saturation ratio in the system.

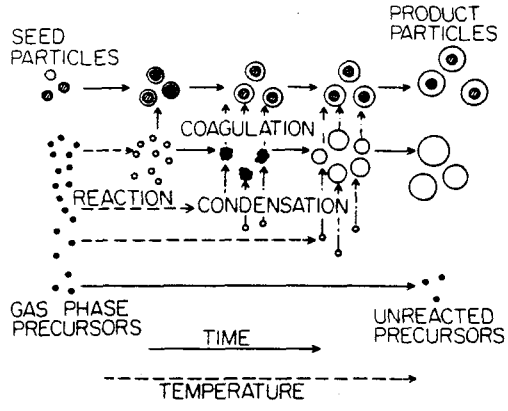

Figure 1. Processes contributing to particle formation from gas-phase chemical reactions.

The classical theory of homogeneous nucleation assumes that particles are formed by the successive addition of monomers to the clusters. The time scale for this process is assumed to be such that a steady-state cluster distribution is established. Using thermodynamic principles, one can determine a critical cluster size, below which the Gibbs free energy of the clusters increases with size and the clusters are thermodynamically unstable. Beyond this size, the free energy decreases with size so continued growth of the clusters is thermodynamically favorable. The critical cluster size, which is a function of the surface tension and the saturation ratio (the ratio of the actual partial pressure to the saturation vapor pressure), is often computed to be of atomic dimensions for aerosol reactor systems. The monomer production rates in these systems are extremely high, with dimensionless source rates (the ratio of the rate of monomer production to the rate of monomer-monomer collision at saturation vapor concentration) on the order of 10^{10}. Warren and Seinfeld (1984) have shown that in order for the steady-state cluster population approximation to be valid, the dimensionless source rate must be smaller than unity. It is clear that the steady-state assumption of the classical theory of homogeneous nucleation breaks down under conditions of powder synthesis systems, and a dynamical model accounting for the interactions of the clusters is needed.

As shown in Figure 1, particles range in size from the clusters containing small number of monomers to large particles. These particles evolve as a result of cluster-cluster, cluster-particle, and particle-particle collisions, as well as individual cluster and particle growth due to the accretion of vapor molecules.

Discrete-sectional (D-S) model

The dynamic behavior of the monomers, clusters, and aerosol particles in the formation processes is described by the aerosol General Dynamic Equation (GDE) (Gelbard and Seinfeld, 1979). The GDE can be expressed in the discrete form, separately representing monomers, dimers, trimers, etc., or in terms

of a continuous particle-size distribution function. The former approach is well suited to the description of small clusters, but is cumbersome for modelling the growth of large particles. The latter approach is useful for describing the evolution of large particles, but inaccurately represents the small clusters. A discrete–sectional GDE was developed to overcome the numerical problems in modeling aerosol formation and growth under high source rate conditions (Wu and Flagan, 1987c). In the discrete–sectional GDE the aerosol size spectrum is separated into two parts. The smaller clusters, varying rapidly with time, are described by the number concentrations of discrete particle sizes, n-mers. The large clusters and aerosol particles are followed in terms of the mass concentrations of ranges in cluster size called sections. Monomer formation is described as a chemical source term. The aerosol size distribution changes with time due to the combined effects of coagulation and evaporation over the entire clusters and aerosol size spectrum. Since the dynamics of the small clusters are followed explicitly, it is not necessary to use the classical nucleation theory to describe new particle formation.

In this study, the following assumptions were made:

- Evaporation of monomers from clusters or particles can be ignored because of the very low saturation vapor pressure of the particulate materials.
- Particle deposition onto surrounding walls is negligible.
- Surface reactions can be neglected.
- When two particles collide, a single new spherical particle is formed. Its mass is equal to the combined mass of the two smaller particles.
- Particles are spherical and electrically neutral.
- Particles and vapor are uniformly distributed throughout the system.

The discrete–sectional GDE to describe the aerosol evolution with a chemical reaction source for monomers is a coupled set of ordinary differential equations,

$$\rho \frac{d}{dt}\left(\frac{N_1}{\rho}\right) = S_0 - \sum_{i=1}^{k} \beta_{1i} N_1 N_i - \left[\sum_{r=1}^{M} {}^{1}\overline{\beta}_{1r} Q_r\right] N_1 \qquad (1)$$

$$\rho \frac{d}{dt}\left(\frac{N_i}{\rho}\right) = \frac{1}{2}\sum_{j=1}^{i-1} \beta_{i-j,j} N_{i-j} N_j - \sum_{j=1}^{k} \beta_{ij} N_i N_j - \left[\sum_{r=1}^{M} {}^{1}\overline{\beta}_{ir} Q_r\right] N_i, \quad 2 \le i \le k \qquad (2)$$

$$\rho \frac{d}{dt}\left(\frac{Q_l}{\rho}\right) = \frac{1}{2}\sum_{i=1}^{l-1}\sum_{j=1}^{l-1} {}^{1}\overline{\beta}_{ijl} Q_i Q_j - \left[\sum_{i=1}^{l-1} {}^{2}\overline{\beta}_{il} Q_i\right] Q_l - \frac{1}{2} {}^{3}\overline{\beta}_{ll} Q_l^2 - \left[\sum_{i=l+1}^{M} {}^{4}\overline{\beta}_{il} Q_i\right] Q_l - \left[\sum_{i=1}^{k} {}^{2}\overline{\beta}_{il} N_i\right] Q_l + \sum_{i=1}^{k}\sum_{r=1}^{l-1} {}^{3}\overline{\beta}_{ir} N_i Q_r + \frac{1}{2}\sum_{i=1}^{k}\sum_{j=1}^{k} {}^{4}\overline{\beta}_{ijl} N_i N_j, \quad 1 \le l \le M \qquad (3)$$

where

N_i = number concentration of clusters with i-mers

Q_l = mass concentration of aerosol particles in section l

ρ = density of the gas

k = dividing size between the discrete and sectional regimes

M = total number of sections

S_0 = generation rate of monomers by a chemical reaction

β_{ij} = Brownian coagulation coefficient of spherical particles with i- and j-mers

Fuchs' interpolation formula that expresses the coagulation rate function for the whole range of Knudsen numbers from the free molecule to the continuum regime was used. The enhancement of the coagulation rate due to van der Waals forces highly depends on the Hamaker constant used (Alam, 1987); since we could not accurately estimate the Hamaker constant, the effect of van der Waals forces was not included in the simulation. ${}^{1}\overline{\beta}_{ir}$, ${}^{2}\overline{\beta}_{il}$, ${}^{3}\overline{\beta}_{irl}$, and ${}^{4}\overline{\beta}_{ijl}$ are the discrete–sectional coagulation coefficients accounting for the interactions of particles between the discrete and sectional regimes. ${}^{1}\overline{\beta}_{ijl}$, ${}^{2}\overline{\beta}_{il}$, ${}^{3}\overline{\beta}_{ll}$, ${}^{4}\overline{\beta}_{il}$ are the inter- and intrasectional coagulation coefficients (Gelbard and Seinfeld, 1980) to count the interactions of particles inside the sectional regime.

Simplified reaction–coagulation (SRC) model

The discrete-sectional model can relatively accurately describe the evolution of the entire particle-size distribution. The sectional representation makes it relatively efficient computationally, at least by comparison with solving the integro-differential equation that results from using the continuous particle-size distribution. Nonetheless, the computational demands of this method can be severe in the face of the many calculations required for reactor design and optimization studies. A simpler model can be derived, which gives valuable information regarding the domain of operation of aerosol reactors. This simplied model (SRC model) can be used to indicate whether a given set of reactor conditions would result in growth or nucleation dominant operation. In this model, the aerosol-size distribution is represented by two modes. The first, called the nuclei mode, follows the evolution of the fine particles and clusters. The second, called the seed mode, describes the evolution of the seed particles. Mass is added to the nuclei mode from the reaction source, and is removed by the seed particles. Both the nuclei and the seed modes are monitored by the number and mass concentrations N_H and M_H, and N_S and M_S, respectively. Four differential equations are sufficient to describe the aerosol system,

$$\rho \frac{d}{dt}\left(\frac{N_H}{\rho}\right) = S_0 - K_H N_H^2 - K_{HS} N_H N_S \qquad (4)$$

$$\rho \frac{d}{dt}\left(\frac{M_H}{\rho}\right) = S_0 - \overline{m}_H K_{HS} N_H N_S \qquad (5)$$

$$\rho \frac{d}{dt}\left(\frac{N_S}{\rho}\right) = -K_S N_S^2 \qquad (6)$$

$$\rho \frac{d}{dt}\left(\frac{M_S}{\rho}\right) = \overline{m}_H K_{HS} N_H N_S \qquad (7)$$

with initial conditions

$$N_H = M_H = 0 \qquad (8)$$

$$N_S = N_{S_0} \tag{9}$$

$$M_S = M_{S_0} \tag{10}$$

K_H, K_{HS} and K_S represent the global coagulation coefficients of the two modes, i.e.,

$$K_H = \frac{1}{2}\beta(\bar{d}_H, \bar{d}_H), \quad \bar{d}_H = \sqrt[3]{\frac{6M_H}{\pi\rho_p N_H}}$$

$$K_S = \frac{1}{2}\beta(\bar{d}_S, \bar{d}_S), \quad \bar{d}_S = \sqrt[3]{\frac{6M_S}{\pi\rho_p N_S}}$$

$$K_{HS} = \beta(\bar{d}_H, \bar{d}_S), \quad \bar{m}_H = \frac{\pi}{6}\bar{d}_H^3\rho_p$$

Note that the SRC model can only predict the average particle size of each of the two modes, not the size distribution.

The chemical reaction kinetics in aerosol reactors are rarely known. For present purposes we have assumed that the rate of production of condensible vapors is first order in reactant concentration,

$$r_p = \rho\frac{dC_p/\rho}{dt} = -\rho\frac{dC_A/\rho}{dt} = k_A C_A \tag{11}$$

where

C_p = concentration of condensible vapors

C_A = concentration of the reactant gas

k_A = reaction rate constant

The generation rate of monomer in an isothermal reactor is then

$$S_0(v_1, t) = r_p N_{AV} = (k_A C_{A0} e^{-k_A t})N_{AV} \tag{12}$$

where C_{A0} is the initial concentration of the reactant gas, and N_{AV} is Avogadro's number. The time required for complete reaction is estimated as $5/k_A$. This is the time when 99.3% of the reactant is converted to products. Obviously, if the reaction mechanisms and kinetics are known for the system of interest, S_0 should be replaced accordingly.

Particle Formation and Growth in Isothermal Reactors

The case of constant source rate reactors has been examined by Friedlander (1983). Operation at a constant source rate requires continuous adjustment of the reactor temperature to increase the rate constant as the reactants are consumed. This increase must be such that it precisely balances the loss of the reactants and is in general difficult. As we will see later, the optimal operating conditions for powder production may be such that neither the rate constant nor the reaction rate remains invariant. We begin our examination of powder synthesis with the simpler case of an isothermal reactor. In this case, the reaction rate constant stays fixed. The reaction rate, however, decreases with time due to the depletion of the reactants. For the examples considered in this section, the physical properties will be those corresponding to the production of TiO_2 by the thermal decomposition of titanium tetraisopropoxide (Okuyama et al., 1986),

$$Ti(OC_3H_7)_4 \rightarrow TiO_2 + 4C_3H_6 + 2H_2O$$

The reaction is assumed to be first order in $Ti(OC_3H_7)_4$.

Homogeneously-generated particles

Figures 2a–b show the evolution of the particle-size distributions for values of the reaction rate constant, k_A, of 0.01, and 100 s^{-1}, respectively. Figure 2c presents the results for the case of instantaneous decomposition of the precursor, $k_A \gg 100\ s^{-1}$, which leads to particle growth purely by coagulation. The initial reactant concentration in each case is 5.25×10^{-10} mol · cm^{-3}. The reaction temperature is 600°C. Prior to depletion of the reactant vapors by thermal decomposition, there exist large differences in the evolution of the particle-size distributions. After

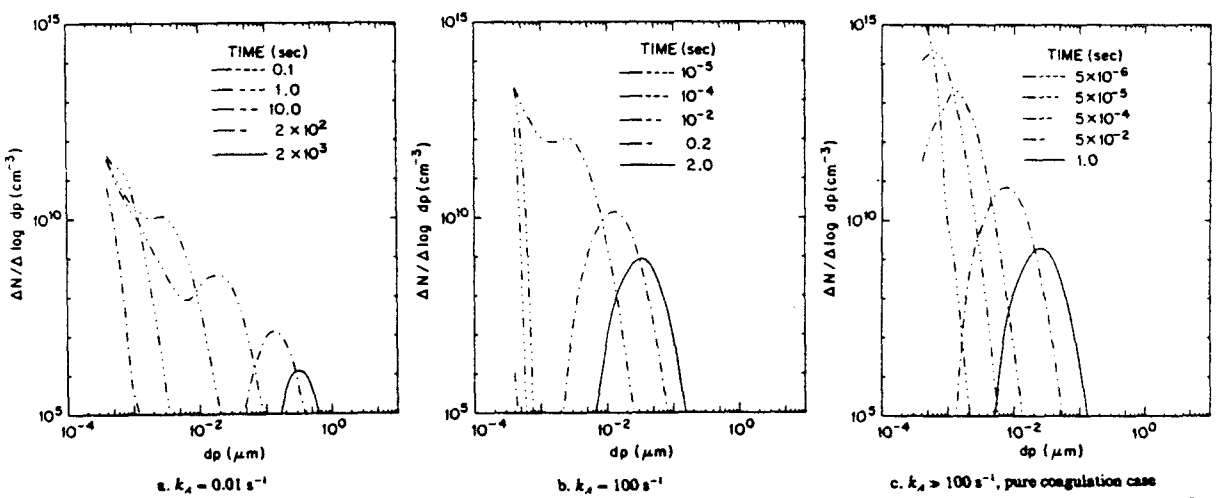

a. $k_A = 0.01\ s^{-1}$ b. $k_A = 100\ s^{-1}$ c. $k_A \gg 100\ s^{-1}$, pure coagulation case

Figure 2. Evolution of the TiO_2 particle-size distributions with an initial TTIP concentration of 5.25×10^{-10} mol · cm^{-3}.

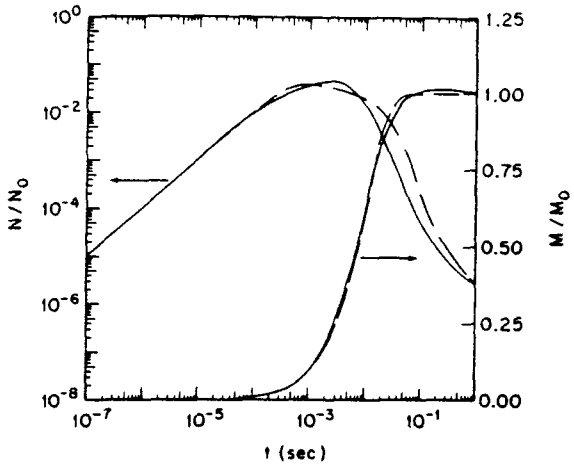

Figure 3. Comparison of the total normalized number and mass concentrations from the D-S (—) and SRC (– – –) models for an initial TTIP concentration of 5.25×10^{-10} mol · cm^{-3} and $k_A = 100$ s^{-1}.

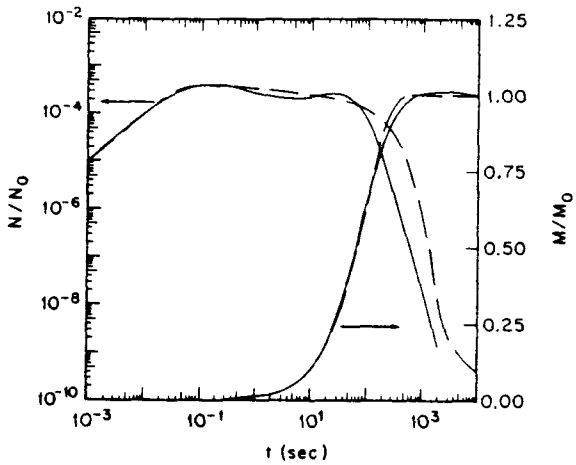

Figure 4. Comparison of the total normalized number and mass concentrations from the D-S (—) and SRC (– – –) models for an initial TTIP concentration of 5.25×10^{-10} mol · cm^{-3} and $k_A = 0.01$ s^{-1}.

sufficient time has elapsed, Brownian coagulation becomes dominant causing the size distributions to approach the self-preserving distribution function (Wang and Friedlander, 1967). Slower reactions take longer time to finish. The final size distributions show the effects of residence time on the average particle size and the spread of the size distribution.

The SRC model does not predict the size distribution, but can be used to examine the number and mass concentrations, and mean particle size. Figures 3 and 4 show the comparison of the results from the D-S and SRC models. The number concentrations shown are normalized by N_0, the maximum monomer concentration, and the mass concentrations by M_0, the total mass concentration of the condensible species, TiO_2, based on the initial precursor concentration. We compare here the zeroeth and the third moments of the particle-size distribution as a function of time for fast ($k_A = 100$ s^{-1}) and slow ($k_A = 0.01$ s^{-1}) reactions. Both Figures 3 and 4 show that the two models give very similar results from $t = 0$ to $t = \tau_{rxn}$, where $\tau_{rxn} = 1/k_A$. Since chemical reaction dominates during this time interval, narrow cluster-size distributions result. The difference between the number concentrations predicted by the two models increases from $t = \tau_{rxn}$ to $t = 10\tau_{rxn}$ because of the competition between coagulation and chemical reaction that produces a bimodal distribution during this period, Figure 2a. Reaction approaches completion and slows down after $t = 5\tau_{rxn}$. Coagulation causes the large clusters to grow, forming aerosol particles in an accumulation mode. For $t > 10\tau_{rxn}$, reaction is insignificant, and coagulation completely dominates the aerosol evolution, bringing it back to a single-mode aerosol. As the aerosol returns to a single mode, the difference gradually reduces, but increases again for $t \gg 10\tau_{rxn}$. This is because the SRC model uses a monodisperse approximation for the two modes. Its predicted coagu-

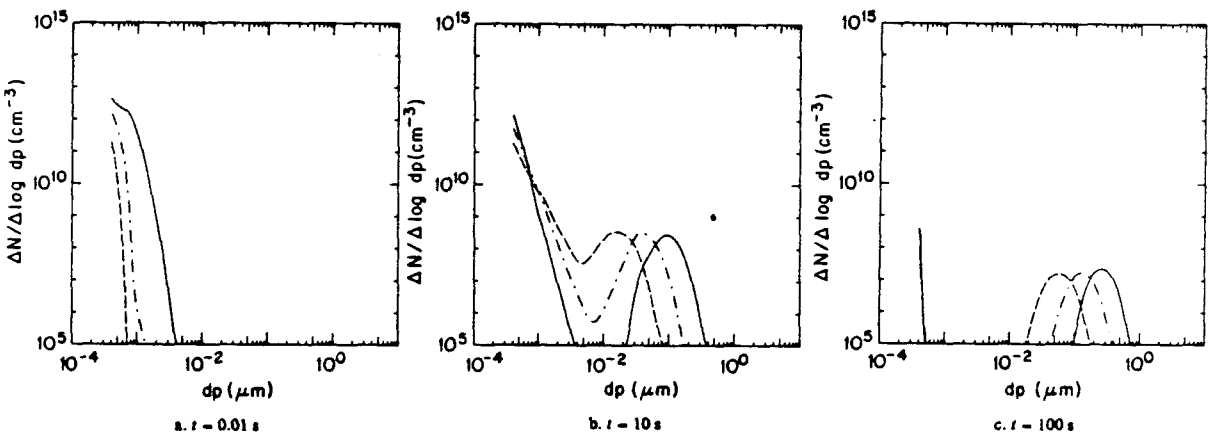

Figure 5. Evolution of the particle-size distributions.
$k_A = 0.1$ s^{-1} and initial concentrations of TTIP of 5.25×10^{-9} mol · cm^{-3} (—); 5.25×10^{-10} mol · cm^{-3} (– · – · –); and 5.25×10^{-11} mol · cm^{-3} (– – –).

lation rates are smaller than those from the more detailed D-S model, causing the difference between the two models to increase when integrated over time. Since the mass of the clusters is relatively small, the discrepancy between the mass concentrations is also small.

Figures 5a–c show the effects of the initial vapor concentration on the evolution of the aerosol-size distribution calculated using the D-S model for $k_A = 0.1\ s^{-1}$. The shapes of the size distributions are very similar to each other. The average particle size at a given time increases with increasing initial vapor concentration.

From the above calculations, we observe that coagulation plays an important role in the evolution of refractory aerosols produced in isothermal systems. The reason for the lack of dependence of the ultimate shape of the particle-size distribution on the reaction rate is that large numbers of particles are produced in the initial nucleation burst. Since the second-order coagulation process is very important at such high number concentrations, it dominates once the reaction is completed.

Growth of seed particles

Supermicron-size particles can be grown in typical aerosol reactor residence times if seed particles are introduced along with the gaseous reactants, provided the reaction rate is limited to favor seed growth by vapor and/or cluster deposition instead of allowing nucleation of new stable particles (Alam and Flagan, 1986). Wu and Flagan (1987b) have shown that very small changes in reactor operation can make the difference between successful growth of the seed particles and runaway nucleation. Important features of the growth of seed particles can be seen using the aerosol models. We begin with seed particle growth at fixed rate constants.

Figures 6a–c represent the normalized number and mass concentrations, and number-averaged diameter, respectively, calculated for an initial TTIP concentration of 5.25×10^{-10} mol · cm^{-3}, a 0.03 μm monodisperse seed aerosol concentration of $3 \times 10^7\ cm^{-3}$, and $k_A = 0.1\ s^{-1}$. The solid lines represent the results calculated using the D-S model. The number and mass concentrations here are normalized total concentrations, since the D-S model does not allow tracking of the seed and nucleated particles separately. The dashed and dashed-dotted lines represent the seed and nucleated particles, respectively, calculated by the SRC model. The normalized number and mass concentrations calculated by these two models, Figures 6a–b, for seed growth dominant conditions, show excellent agreement.

Figures 6a–c show that it is possible to grow seed particles while suppressing nucleation, provided the reaction is sufficiently slow. The time to complete the reaction is long, on the order of 100 s or longer. An aerosol reactor with such residence time would be very large. Increasing the reaction rate would decrease the required residence time and reactor volume, but could easily result in runaway nucleation. Consider what would happen if seed particles were introduced into a high source rate reactor. This is illustrated in Figures 7a–c for $k_A = 100\ s^{-1}$. It is apparent that the seed particles do not begin to grow until reaction is nearly completed. Instead, the fast reaction leads to the production of a large number of small nuclei that grow by coagulation. Only at long times do they begin to coagulate with the seed particles to an appreciable extent. Thus, the seed particles have little effect if the reaction rate is too high. Obviously, there is a middle ground between these two cases. However, there are better approaches for the growth of seed particles.

Particle Growth in Nonisothermal Reactors

Alam and Flagan (1986) demonstrated that seed particles could be grown to supermicron sizes with limited residence times if the reaction rate is initially low and gradually accelerated as the particles grow and scavenge condensible reaction products at increasing rates. The ability of a growing seed aerosol to suppress nucleation in a reactor with a reaction rate that increases with time is illustrated by the number (dashed lines) and mass (solid lines) distributions shown in Figure 8. In all cases, the reaction rate profiles are designed to ensure complete reaction within a 50-s residence time. Like the constant rate case, the linear rate variation, Figures 8a–b, results in new particle formation and a broad, coagulation dominated aerosol. Figures 8c–d clearly demonstrate that nucleation can be eliminated

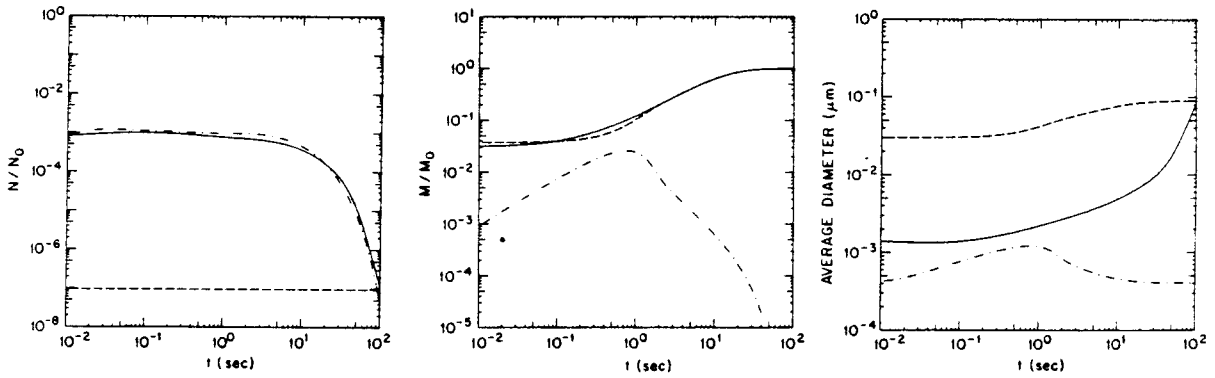

a. Total number concentration normalized by N_0. b. Total mass concentration normalized by M_0. c. Number averaged particle diameter.

Figure 6. Comparison of the results from the D-S and SRC models for an initial TTIP concentration of 5.25×10^{-10} mol · cm^{-3}, 0.03-μm seed particle concentration of $3 \times 10^7\ cm^{-3}$, and $k_A = 0.1\ s^{-1}$.

— results from the D-S model.
– – – seed particles from the SRC model.
– · – · new particles from the SRC model.

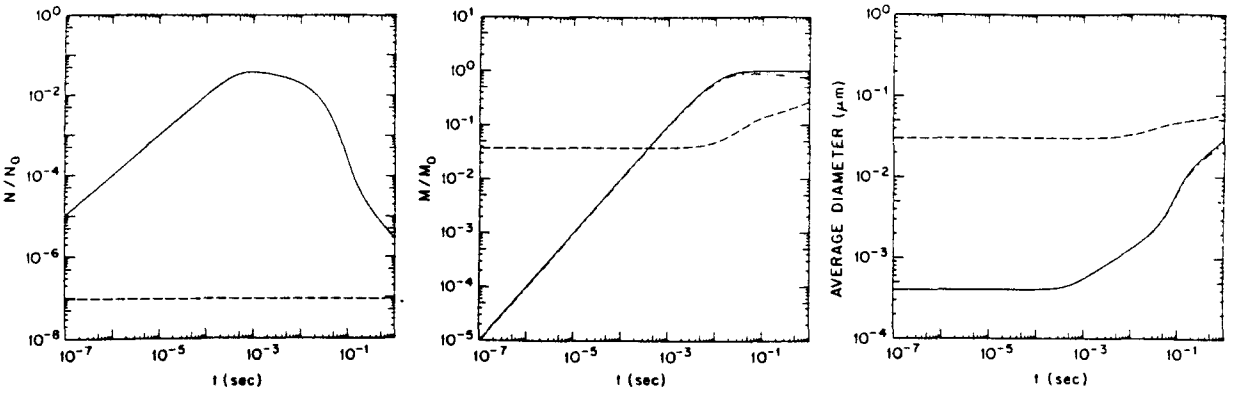

a. Total number concentration normalized by N_o. b. Total mass concentration normalized by M_o. c. Number averaged particle diameter.

Figure 7. Results from the SRC model for the case with 3×10^7 cm^{-3} of 0.03-μm seed particles, initial TTIP concentration of 5.25×10^{-10} mol · cm^{-3}, and $k_A = 100$ s^{-1}.

— without seed particles.
– – – seed particles.
– · – · nucleated particles.

effectively if the initial rate is very low and the rate is accelerated as the particle grows.

Submicron particles of relatively uniform size can be grown in a single-stage reactor without the introduction of seeds by beginning the reaction at a very low rate, allowing a small fraction of the precursor to produce seed nuclei *in situ* by homogeneous nucleation. The reaction rate is slowly accelerated to promote growth by vapor and cluster deposition as the small particles grow and become increasingly effective vapor scavengers. This technique has been demonstrated experimentally and theoretically by Wu et al. (1986, 1987a) in the production of uniformly-sized silicon particles by silane pyrolysis. The gradual increase in the reaction rate was achieved by increasing the temperature along the length of a tubular reactor. Their calculations were carried out using the rate expression for the rate-limiting step reported by Purnell and Walsh (1966), $SiH_4 + M \rightarrow SiH_2 + H_2 + M$. The nucleating and condensing species were assumed to be elemental silicon. The evolution of the particle-size distribution (Wu et al., 1987a) is shown in Figure 9. We see that the concentrations of small clusters are high initially, but decrease rapidly by coagulation. The slow reaction allows the condensible products to be scavenged by the seed nuclei before the small clusters can grow to clusters too large to effectively diffuse to the existing seed particles. As a result, the particles grow appreciably at a relatively constant number concentration. Comparison of the particle-size distributions in Figure 9 and those in Figures 2a–c shows that the size distribution is substantially narrower when growth is by vapor and cluster deposition rather than coagulation.

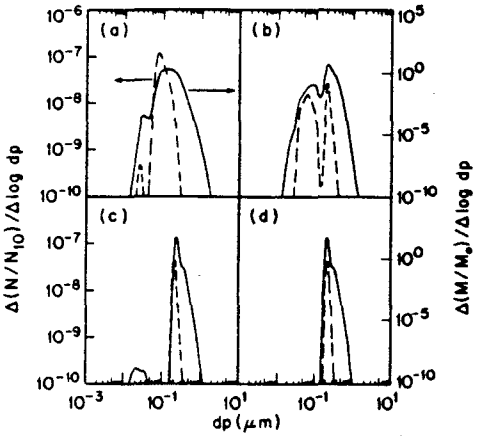

a. $k_A = 0.1$ s^{-1}.
b. $k_A = 0.05 + 0.002t$ s^{-1}.
c. $k_A = 0.033 + 0.0013t + 0.00004t^2$ s^{-1}.
d. $k_A = 0.025 + 0.001t + 0.00006t^2$ s^{-1}.

Figure 8. Particle number and mass distributions, starting with an initial TTIP concentration of 5.25×10^{-10} mol · cm^{-3} and 0.205-μm seed particle concentration of 2.44×10^6 cm^{-3} at time $t = 50$ s.

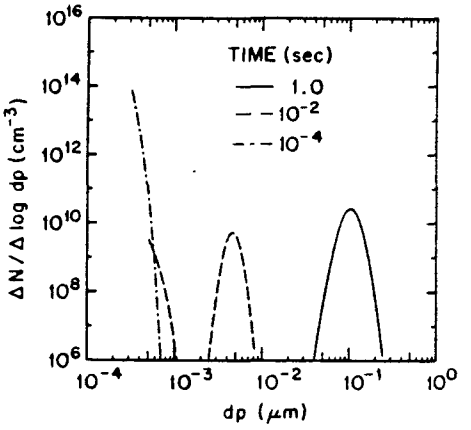

Figure 9. Aerosol size evolution starting with an initial vapor concentration of 5.25×10^{-7} mol · cm^{-3} and a gradually increasing reaction rate (After Wu et al., 1987a).

Conclusion

The reaction rates in aerosol systems used to synthesize fine particles commercially, namely thermal, flame, and plasma reactors, can vary over orders of magnitude. However, the physical processes that control the particle evolution in all these systems are the same, namely reaction and coagulation.

Two models for aerosol evolution in powder synthesis were described. Numerical solutions to the general dynamic equation for aerosols that takes into account the discrete nature of the small cluster sizes, while remaining practical for the description of the growth of large particles, were obtained using the discrete–sectional model. An approximate method that follows the growth of both seed and homogeneously-nucleated particles was developed. The results from the simplified reaction-coagulation model were shown to agree closely with those of the more exact model for a wide range of reactor operating conditions. Hence, it is a useful tool for the preliminary characterization of reactor operation under a particular set of operating conditions.

Using these models, several features of aerosol reactor operation have been demonstrated. Growth of refractory particles in either a high source rate or a constant source rate operation is dominated generally by coagulation that results in broad particle-size distributions that do not differ appreciably from one system to another regardless of the initial reactant concentration. Seed particles can be grown in isothermal reactors, but the rate must be very low, leading to unrealistically long residence times. On the other hand, if the rate is initially kept low and accelerated as the seed nuclei grow and become more effective at scavenging condensible reaction products and small clusters, the formation of new stable particles by homogeneous nucleation can be effectively suppressed. The particles can thus be grown significantly. Uniformly-sized submicron particles also can be synthesized in a single-stage reactor without the use of externally produced seed particles. This can be accomplished by initially reacting a small amount of reactants at a very small rate to produce seed nuclei *in situ*. The reaction rate can then be increased gradually to insure growth by deposition and complete consumption of the reactants in available residence time.

Acknowledgment

This work was supported in part by the Program in Advanced Technologies of the California Institute of Technology, sponsored by Aerojet General, General Motors, GTE, and TRW.

Literature Cited

Alam, M. K., and R. C. Flagan, "Controlled Nucleation Aerosol Reactors: Production of Bulk Silicon," *Aerosol Sci. and Technol.* **5**(2), 237 (1986).

Alam, M. K., "The Effect of van der Waals and Viscous Forces on Aerosol Coagulation," *Aerosol Sci. and Technol.* **6**, 41 (1987).

Bowen, H. K., "Basic Research Needs on High Temperature Ceramics for Energy Applications," *Mat. Sci. Engr.*, **44**, 1 (1980).

Cannon, W. R., S. C. Danforth, J. H. Flint, J. S. Haggerty, and R. A. Marra, "Sinterable Ceramic Powders from Laser-Driven Reactions: I. Process Description and Modeling," *J. of the Amer. Ceramic Soc.*, **65**(7), 324 (1982a).

Cannon, W. R., S. C. Danforth, J. S. Haggerty, and R. A. Marra, "Sinterable Ceramic Powders from Laser-Driven Reactions: II. Powder Characteristics and Process Variable," *J. of the Amer. Ceramic Soc.*, **65**(7), 330 (1982b).

Fauchais, P., E. Bourdin, J. F. Coudert, and R. McPherson, "High Pressure Plasmas and Their Application to Ceramic Technology," in *Topics in Current Chemistry, Plasma Technology IV*, S. Veprek and M. Venugopalan, Eds., Springer-Verlag, Berlin, 59 (1983).

Friedlander, S. K., "Dynamics of Aerosol Formation by Chemical Reaction," *Annals New York Academy of Science*, 354 (1983).

Gelbard, F., and J. H. Seinfeld, "The General Dynamic Equation of Aerosols," *J. Colloid and Interf. Sci.*, **68**, 363 (1979).

Gelbard, F., Y. Tambour, and J. H. Seinfeld, "Sectional Representations for Simulating Aerosol Dynamics," *J. Colloid and Interf. Sci.*, **76**, 541 (1980).

Okuyama, K., Y. Kousaka, N. Tohge, S. Yamamota, J. J. Wu, R. C. Flagan, and J. H. Seinfeld, "Production of Ultra-Fine Metal Oxide Particles by Thermal Decomposition of Metal Alkoxide Vapors," *AIChE J.*, **32**(12), 2010 (1986).

Purnell, J. H., and R. Walsh, "The Pyrolysis of Monosilane," *Proc. R. Soc. London*, **293**, 543 (1966).

Walker, Jr., P. L., "Ultrafine Carbon," in *Ultrafine Particles*, W. E. Kuhn, H. Lamprey, and C. Sheer, Eds., Wiley, New York, 297 (1963).

Wang, C. S., and S. K. Friedlander, "The Self-Preserving Particle Size Distribution for Coagulation by Brownian Motion," *J. Colloid and Interf. Sci.*, **24**, 170 (1967).

Warren, D. R., and J. H. Seinfeld, "Nucleation and Growth of Aerosol from a Continuously Reinforced Vapor," *Aerosol Sci. and Technol.*, **3**, 135 (1984).

Wu, J. J., and R. C. Flagan, "Submicron Silicon Powder Production in an Aerosol Reactor," *Appl. Phys. Letters*, **49**(2), 82 (1986).

Wu, J. J., H. V. Nguyen, and R. C. Flagan, "A Method for the Synthesis of Submicron Particles," *Langmuir*, **3**, 266 (1987a).

Wu, J. J., and R. C. Flagan, "Onset of Runaway Nucleation in Aerosol Reactors," *J. Appl. Phys.* **61**(3), 1365 (1987b).

Wu, J. J., and R. C. Flagan, "A Discrete–Sectional Solution to the Aerosol Dynamic Equation," *J. Colloid and Interf. Sci.*, in press (1987c).

Manuscript received Nov. 2, 1987, and revision received Apr. 7, 1988.

APPENDIX C

EXPERIMENTAL CONTROL OF ULTRAFINE TiO_2 PARTICLE GENERATION FROM THERMAL DECOMPOSITION OF TITANIUM TETRAISOPROPOXIDE VAPOR

with

K. Okuyama, J. Jeung, Y. Kousaka, J.J. Wu, and R.C. Flagan

Published in

Chemical Engineering Science

44 [6], 1369 (1989)

EXPERIMENTAL CONTROL OF ULTRAFINE TiO_2 PARTICLE GENERATION FROM THERMAL DECOMPOSITION OF TITANIUM TETRAISOPROPOXIDE VAPOR

KIKUO OKUYAMA,* JI-TAEK JEUNG and YASUO KOUSAKA
Department of Chemical Engineering, University of Osaka Prefecture, Osaka 591, Japan

and

HUNG V. NGUYEN, JIN JWANG WU‡ and RICHARD C. FLAGAN
Division of Engineering and Applied Science, California Institute of Technology, 138-78, Pasadena, CA 91125, U.S.A.

(*Received* 17 *February* 1988; *accepted* 14 *November* 1988)

Abstract—The generation of ultrafine TiO_2 particles by the thermal decomposition of titanium tetraisopropoxide (TTIP) vapor was carried out experimentally using a well-controlled cylindrical furnace. The effects of the initial vapor concentration of the TTIP vapor, the reaction temperature, the temperature profile of the furnace and properties of seed particles on the particle size distribution of produced aerosol particles were examined to control the generation of particles. The observed trends agreed semi-quantitatively with the simulation results obtained by solving the discrete-sectional aerosol dynamic equation accounting for Brownian coagulation and generation of monomer by chemical reaction.

INTRODUCTION

The process of the synthesis of powder from a vapor phase consists of physical vapor deposition (PVD) and chemical vapor deposition (CVD). Many of the synthesis methods for powder are based on aerosol processes (gas-to-particle conversion process), that is, the formation and growth of solid or liquid particles in the supersaturated vapor produced physically or chemically. The production of fine particles from gaseous reactants has long been an important technology. Carbon, fume silica, TiO_2 powder, oxide ceramics, and magnetic powders are but a few of the materials that have been produced over the past several decades. The technologies for the synthesis of powders have been primarily empirical developments designed to control such properties of the particles as particle size and size distribution, particle morphology, extent of agglomeration, internal porosity, and material phase.

Of fine particles of diameter less than a few microns, ultrafine particles (below about 0.1 μm in diameter) are of interest and considerable effort is being expended to produce ultrafine powders of metals, metal oxides, and other metallic compounds at the present stage. Ultrafine particles have different microscopic physical properties from those of bulk material because the number of atoms or molecules on the particle surface becomes comparable to that inside the particles, and are receiving increased attention today due to their importance in a number of high-technology industries.

*Author to whom correspondence should be addressed.
‡Present address: T. J. Watson Research Center, IBM, Yorktown Heights, NY 10598, U.S.A.

Typical methods preparing fine or ultrafine powders by a CVD process are classified into the following types: (1) combustion or flame process; (2) plasma technology; (3) laser-driven reaction; (4) thermal reaction using electrical furnace; and (5) gas evaporation method, which is a typical method belonging to the PVD process. In the particle production process, particles must be produced in a carefully controlled reaction system. The ideal particles used as the material need a controlled approximately equiaxed and controlled composition, a very narrow particle size distribution in the submicron size range, and are available in a largely unagglomerated state. The elementary processes involved in the formation and growth of particles from gaseous precursors include: (1) gas phase chemical reactions, (2) surface reactions, (3) homogeneous nucleation, (4) heterogeneous condensation, (5) coagulation, and (6) coalescence or fusion. The differences in the properties produced in various reactions can be traced back to the differences in the relative importance of these processes. So far, the control of particle properties has been mainly made empirically, but the science of aerosol physics and chemistry has made major advances that now make possible a theoretical description of particle synthesis reactions and corresponding improvements in particle synthesis technology. Much of the aerosol research has, however, been developed in the study of aerosols in the environment and has only recently been applied to the problems of powder synthesis in the chemical processes and material industries (Friedlander, 1983).

In this paper, the production of ultrafine TiO_2 particles by the thermal decomposition of titanium tetraisopropoxide (TTIP) vapor was carried out ex-

perimentally using well-controlled furnaces. The high-temperature processes promote very rapid gas phase chemical reactions. The high supersaturation quickly achieved leads to rapid nucleation, and the particles then grow by Brownian coagulation. If the temperature during this growth process is below the melting point of the particle material, low-density agglomerates are formed. These agglomerates may, over time, sinter or fuse together. If the chemical reactions proceed more slowly, vapor deposition on the surface of existing particles can dominate over the formation of stable new particles. Accordingly, in the experiments, the effects of the initial vapor concentration, reaction rate, properties of seed particles, and temperature profile on the properties of fine particles produced by gas phase chemical reactions were examined. Then the discrete-sectional aerosol general dynamic equation (GDE) accounting for coagulation and generation of monomer by chemical reaction was solved numerically under typical conditions. The obtained simulation results were compared with the observed results.

PARTICLE PRODUCTION EXPERIMENT

Experimental apparatus

The experimental system [similar to that used by Okuyama *et al.* (1986), except with better controlled furnaces] consists of a drying column, a vaporizer, tubular furnaces, a particle size magnifier, a differential mobility analyzer, and a mixing-type condensation nucleus counter.

TTIP liquid was maintained in a heated glass container serving as the vapor source. Clean nitrogen gas passed through the glass container, and left saturated with the TTIP vapor. It was then mixed with another nitrogen stream having a temperature higher than that of the vapor to avoid condensational loss before entering the reaction furnace. The TTIP vapor was thermally decomposed to produce supersaturated TiO_2 vapor. Ultrafine primary metal oxide clusters were produced by homogeneous nucleation. Larger secondary particles were formed by agglomeration of the clusters and simultaneous condensation of vapor molecules onto the clusters.

The analysis of particle size and number concentration of ultrafine aerosol from the furnace outlet was carried out by two different methods in a suspended state as described in a previous paper (Okuyama *et al.*, 1986). The minimum measurable particle size by this method is about 0.003 μm in diameter.

Figure 1(a) shows the tubular furnace consisting of a 35 mm i.d. stainless steel tube having a 490-mm length. The reactor had five heating zones, each 90 mm in length, which were separated by 10 mm of low-density insulation. Each of the heating zones was controlled by a temperature controller to within ±3°C. $T1$–$T5$ indicate the controlled wall temperatures of the five heating zones. The nitrogen gas containing the TTIP vapor was introduced with a flow rate of $Q1$ and the slightly higher temperature nitrogen gas was added with a flow rate of $Q3$. In order to prevent thermophoretic deposition of small particles in the hot reactant flow onto the cool wall of the sampling system, the aerosol was diluted by transpiring gas through a porous tube as used by Wu and Flagan (1986). By blowing room temperature nitrogen gas through the wall of the diluter at a flow rate of $Q4$, the particles were transported away from the vicinity of the wall with high-temperature gradients that would otherwise lead to substantial losses.

In the second reactor furnace consisting of a 35 mm i.d., 620-mm stainless steel tube as shown in Fig. 1(b),

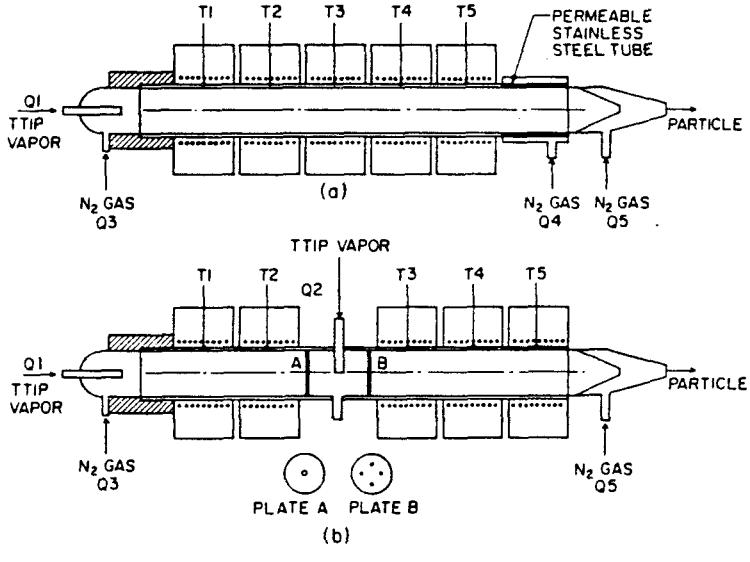

Fig. 1. Schematics of the furnaces used in the experiments: (a) for experiments with no added vapor stream Q_2, (b) for seeded experiments with added vapor stream Q_2.

the reactive vapor was introduced into the furnace at a flow rate of $Q1$, and was mixed with added vapor at a flow rate of $Q2$ after passing through the 260-mm heating zone and the first orifice (plate A). In the first two heating zones, small particles were generated by homogeneous nucleation. These particles were then used as seed nuclei (condensation nuclei), mixed with the additional TTIP vapor stream and passed through the second orifice (plate B) and the remaining 330-mm heating zone. The first orifice has a single 3-mm hole, while the second orifice has four 1.5 mm diameter holes. The distance between the orifices was 30 mm.

In the experiments, the concentration of the introduced TTIP vapor, the temperature profile of the furnace, and the amount of vapor added additionally were changed.

Experimental results

Temperature profiles. Since the furnace temperature governs the rate of the thermal decomposition of the TTIP vapor and TiO_2 particle formation, the temperature profile was measured at the center of the furnace by introducing a thermocouple probe. Figure 2 shows the steady-state centerline temperature profiles for three cases. The values of $T1$–$T5$ indicate the wall temperatures of the heating zone.

Changes in properties of generated particles. Figures 3–5 show the experimental results for the size distribution of TiO_2 particles obtained using the furnace shown in Fig. 1(a). The number concentrations were normalized by the measured total number concentration N_t corresponding to their respective run. Figure 3 shows the size distribution of the TiO_2 particles generated as a function of furnace temperature. In this series of experiments, the temperature of the evaporating alkoxide liquid was 40°C, and the flow rate $Q1$ of the carrier gas containing the vapor was 10 $cm^3\,min^{-1}$. The nitrogen gas was added at a flow rate of 1990 $cm^3\,min^{-1}$. The residence time of gas in the furnace was about 14 s. It is noted that the particles were generally less than 100 nm (0.1 μm). Since a higher concentration of TiO_2 vapor can be

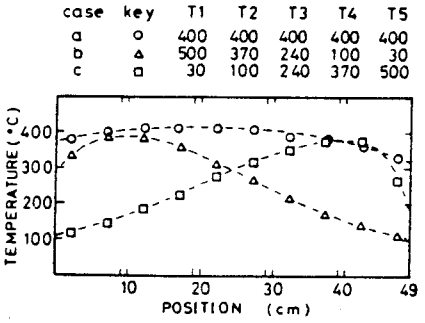

Fig. 2. Measured centerline temperatures for experiments using the reactor furnace shown in Fig. 1(a) with the corresponding results shown in Fig. 5. The corresponding wall temperatures are listed as $T1$, $T2$, $T3$, $T4$ and $T5$ with their respective symbols.

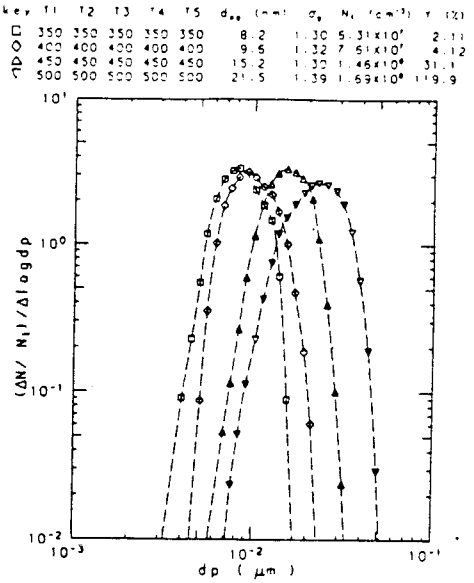

Fig. 3. Measured normalized size distributions of the TiO_2 aerosol: $Q1 = 10\ cm^3\,min^{-1}$, $Q3 = 1990\ cm^3\,min^{-1}$, $Q4 = 1000\ cm^3\,min^{-1}$, and $Q5 = 0\ cm^3\,min^{-1}$.

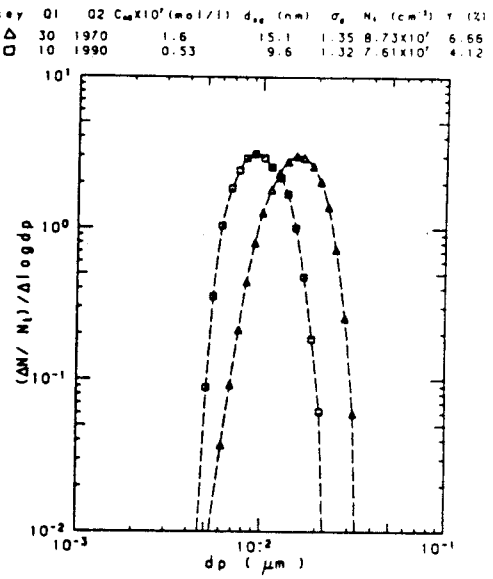

Fig. 4. Measured normalized size distributions of the TiO_2 aerosol; $Q1$ of 30 and 10 $cm^3\,min^{-1}$ corresponding to △ and □, respectively. $Q4 = 1000\ cm^3\,min^{-1}$, $Q5 = 0\ cm^3\,min^{-1}$, $T1$–$T5 = 400$°C.

obtained from the thermal decomposition at a higher temperature, the particles shifted to larger sizes as the reaction temperature was increased. TiO_2 particles were not generated by homogeneous nucleation for furnace temperatures lower than 300°C. The values of Y shown in the last column of table in Fig. 3 indicate the percentage conversion of the TTIP vapor to TiO_2

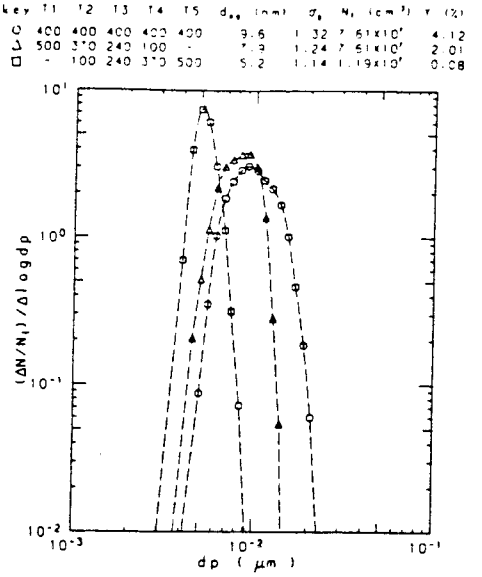

Fig. 5. Measured normalized size distributions of the TiO_2 aerosol obtained using furnace of Fig. 1(a) for the constant, increasing, and decreasing wall temperature profiles shown in Fig. 2: $Q1 = 10\ cm^3\ min^{-1}$, $Q3 = 1990\ cm^3\ min^{-1}$, $Q4 = 1000\ cm^3\ min^{-1}$, and $Q5 = 0\ cm^3\ min^{-1}$.

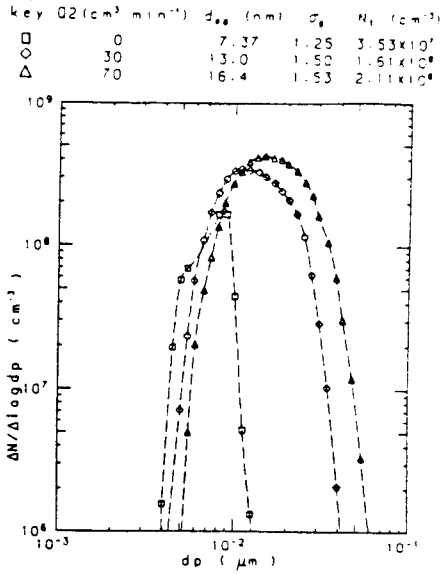

Fig. 6. Measured size distributions of the TiO_2 aerosol: $Q1 = 70\ cm^3\ min^{-1}$, $Q3 = 1930\ cm^3\ min^{-1}$, $Q5 = 1000\ cm^3\ min^{-1}$, $T1$–$T5 = 400$°C.

particles. The vapor quantity in the carrier gas was calculated assuming that complete thermal decomposition was achieved and that the carrier gas left the evaporator saturated with the TTIP vapor. Conversion to the aerosol phase was computed from the volume concentration of the product aerosol with the density assumed to be that of the oxide particles. As can be seen, the percentage of vapor converted to aerosol ranged from about 2% to above 100% depending on the reactor temperature used. The low yield at low reactor temperatures may have resulted from incomplete thermal decomposition and depositional loss by Brownian diffusion in the reactor. Those exceeding unity (100%) may be attributed to the assumption of the particles being solid dense spheres. The widths of the particle size distributions, the geometric standard deviation (σ_g), are found to be almost similar.

Figure 4 shows the changes in the size distribution of the TiO_2 aerosol due to changes in the feed vapor concentration of the TTIP. In this experiment, the TTIP vapor was generated at 40°C. The flow rates of the carrier gas were 10 and 30 $cm^3\ min^{-1}$, and the nitrogen gas was added at 1990 and 1970 $cm^3\ min^{-1}$, correspondingly, to maintain a total flow rate in the furnace of 2000 $cm^3\ min^{-1}$. The temperature of the furnace was maintained at 400°C. It is clearly seen that the particles grew larger as the concentration of the alkoxide vapor, C_{Ao}, was increased.

Figure 5 shows the changes in the size distribution of TiO_2 particles under constant-, increasing- and decreasing-temperature profiles. The centerline temperature profiles in the experiment were those shown

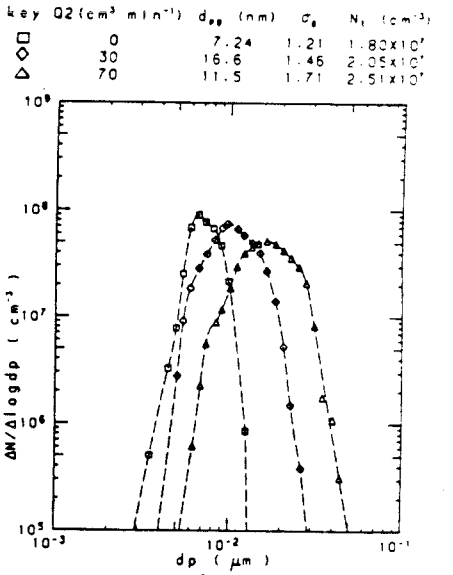

Fig. 7. Measured size distributions of the TiO_2 aerosol: $Q1 = 70\ cm^3\ min^{-1}$, $Q3 = 1930\ cm^3\ min^{-1}$, $Q5 = 1000\ cm^3\ min^{-1}$, $T1$ and $T2 = 400$°C, $T3$–$T5 = 200$°C.

in Fig. 2. The particles produced in the increasing-temperature profile were smaller with a narrower size distribution than those produced in the increasing and nearly constant temperature profiles. The low values of Y again suggest that the thermal decomposition was not completed before leaving the final zone and/or the depositional loss was much greater for smaller particles.

Figures 6 and 7 show the particles size distributions obtained using the furnace shown in Fig. 1(b). In the

experiment corresponding to Fig. 6, the temperature of all the heating zones was 400°C. The alkoxide vapor was produced at 40°C. The flow rate of the vapor carrying gas was 70 $cm^3 min^{-1}$ and the nitrogen gas was added at 1930 $cm^3 min^{-1}$. The flow rate of vapor added before the third heating zone was varied between 0, 30 and 70 $cm^3 min^{-1}$. The residence time in the first two heating zones was about 7.5 s, and that for the last three zones was about 9.5 s. The particle number concentrations and sizes were larger than those without the addition of vapor after the second heating zone, increasing with increasing added vapor flow rate. This is believed to be the result of additional homogeneous nucleation in the last three zones due to the added vapor.

Figure 7 shows the changes in the size distribution of TiO_2 particles with the temperature of the first two heating zones kept at 400°C, and that of the following three heating zones at about 200°C. It can be seen that, by the addition of vapor after the second heating zone, the total particle number concentration increased only slightly with increasing flow rate of the added vapor, while the particle size distribution shifted to larger sizes. In this case, seed particles were produced in the first two heating zones by homogeneous nucleation and grew by vapor and cluster deposition which dominated over homogeneous nucleation in the three heating zones because of the low chemical reaction rates resulting from the low furnace temperatures.

SIMULATION OF AEROSOL EVOLUTION IN FURNACE

In the furnace, the TTIP vapor is thermally decomposed to produce TiO_2 vapor molecules. If the supersaturation of TiO_2 vapor reaches a sufficient level, ultrafine primary TiO_2 clusters are formed by homogeneous nucleation. Larger secondary particles are formed by the agglomeration of clusters by the simultaneous heterogeneous condensation of vapor molecules onto clusters. If seed particles are introduced into the system, they may scavenge a considerable amount of condensable vapor and clusters. In this particle generation process, particles may vary in size, ranging from vapor monomers, cluster (collection of molecules) to larger particles. In many chemically reacting systems where the rate of vapor formation is very large and the saturated vapor pressure of condensable species is very low, the evolution of these particles occurs as a result of cluster–cluster, cluster–particle and particle–particle collisions, or individual cluster and particle growth due to accretion of vapor molecules. The dynamic behavior of the monomers, clusters, and aerosol particles in the formation process is described by the aerosol GDE (Friedlander, 1977; Gelbard and Seinfeld, 1979; Seinfeld, 1986). A discrete-sectional GDE was developed to overcome the numerical problems in modeling aerosol formation and growth under high source rate conditions, and to eliminate the dependence on the classical theory of homogeneous nucleation (Wu and Flagan, 1988). In the discrete-sectional GDE, the particle size spectrum is separated into two parts. The smaller clusters varying rapidly with time are described by number concentration and discrete distribution. The larger clusters and particles are modeled by mass concentration in sections. Monomers are generated by chemical reaction.

In the simulation of the discrete-sectional GDE, the following assumptions are made: (1) The velocity profile of gas in the furnace is flat, and the residence time corresponds to the ratio of the length from the inlet of the furnace to the average flow rate of gas. (2) Evaporation of monomer from cluster or particles can be ignored because of the very low values of the saturation vapor pressure of the particulate materials. (3) Particle deposition onto the surrounding wall is negligible. (4) When two particles collide, a single new spherical particle is formed. Its mass is equal to the combined mass of the two smaller particles. (5) Particles are spherical and electrically neutral. (6) Particles and vapor are uniformly distributed throughout the system. The thermal decomposition of titanium alkoxide vapor takes place in the furnace according to the following reaction:

$$Ti(OC_3H_7)_4 \rightarrow TiO_2 + 4C_3H_6 + 2H_2O. \quad (1)$$

As seen from the above reaction, the thermal decomposition will produce water vapor and gaseous propylene with metal oxide. In the case of the formation of TiO_2 particles, Kanai *et al.* (1985) suggested the thermal decomposition rate of TTIP was approximated by the 0.5-order reaction and that the formation was catalyzed by the TiO_2 deposit on the wall. However, the detailed reaction mechanism of eq. (1) has not been clear until now. It is apparent that comprehensive models of particle formation, growth, and structure evolution in particle synthesis reactions cannot be expected in the near future. The details of the reaction chemistry or the shape of the agglomerates generated will not be considered, the focus instead being on the nucleation, vapor deposition, and coagulation processes. In the calculation, the thermal decomposition of alkoxide vapor is assumed to be expressed as a first-order reaction, when the chemical reaction rate r_p can be given by $r_p = dC_p/dt = -dC_A/dt = k_A C_A$, where C_p is the concentration of condensable vapor (TiO_2 molecules), C_A is the concentration of the TTIP vapor and k_A is the reaction rate constant. The physical properties used in the model calculations and the detailed simulation methods are described in the papers by Okuyama *et al.* (1986) and Wu *et al.* (1988). The termination time of the thermal decomposition of vapor is given by $10/k_A$. It is the time when 99.3% of the reactant is converted to products by the thermal decomposition.

Figure 8 shows the simulation results for the evolution of the particle size distribution for different reaction rate constants k_A. After the chemical reaction was terminated at time 10 s for changes in reaction rate constants of 1 and 10 s^{-1}. Brownian coagulation dominates the following aerosol growth and the resulting particle size distributions become similar. As

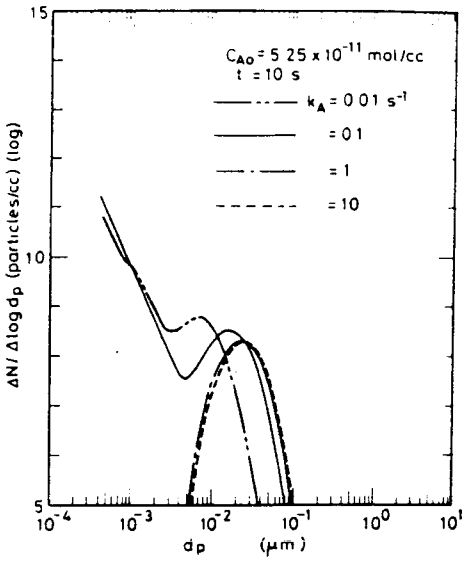

Fig. 8. Evolution of the TiO_2 particle size distributions with an initial TTIP concentration of 5.25×10^{-11} mol cm^{-3} for various reaction rate constants.

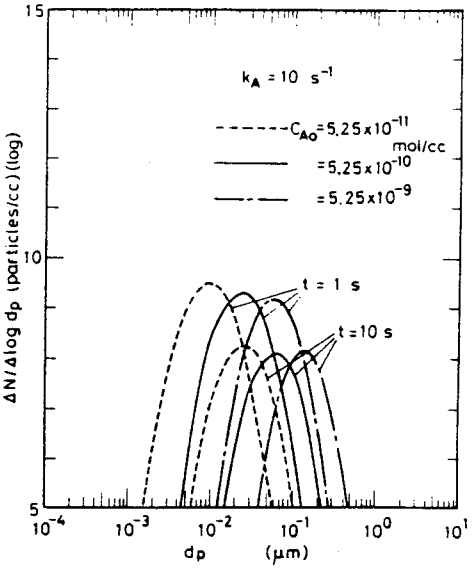

Fig. 10. Evolution of the particle size distributions with k_A = 10 s^{-1} for various initial concentrations of TTIP.

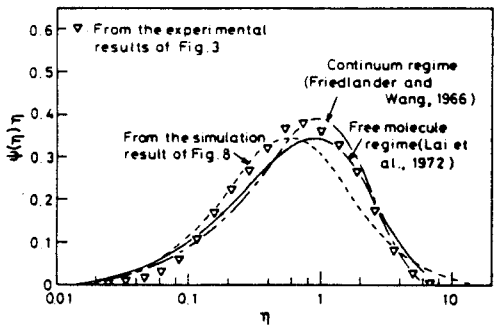

Fig. 9. Comparison of the self-preserving (asymptotic) size distributions obtained by simulation and experiment in the present study with the distributions given by Lai *et al.* (1972) (——, free molecule regime), and Friedlander and Wang (1966) (— – —, continuum regime).

seen from these results, there exist large differences in the changes of particle size distributions. Since a higher concentration of TiO_2 vapor can be obtained from the thermal decomposition at a higher temperature, the particle size distribution shifts to larger sizes as the reaction temperature is increased. This tendency agrees well with the experimental results of Fig. 3.

Particle size distributions of aerosols undergoing Brownian coagulation asymptotically approach equilibrium states as time proceeds. Namely, the shapes of asymptotic distributions after a long period resemble each other, irrespective of initial size distributions. These asymptotic distributions at the equilibrium state correspond to the self-preserving distribution (SPDF). Friedlander *et al.* obtained the self-preserving distribution function for Brownian coagulation in a continuum regime (Friedlander and Wang, 1966) and in a free molecule regime (Lai *et al.*, 1972). The self-preserving distribution function $\psi(\eta)$ and the variable η are related to the particle size distribution function $n(v, t)$ and particle volume v by eq. (2):

$$\psi(\eta) = n(v, t)\, V/N^2, \quad \eta = v/\bar{v} = Nv/V \qquad (2)$$

where $\bar{v}$ is the average particle volume, N the total particle number concentration, and V the total volume concentration.

The correlation of $\psi(\eta)\eta$ and η is shown in Fig. 9. The one point dashed line shows the SPDF derived by Friedlander and Wang (1966) in a continuum regime and the solid line the SPDF derived by Lai *et al.* (1972) in a free molecule regime. The broken line shows the SPDF transformed from the numerical solutions of particle size distribution for $k_A = 10\ s^{-1}$ and $t = 10$ s in Fig. 8, and the triangle points indicate the SPDF transformed from the experimental particle size distribution denoted by the key ▽ for the furnace temperature of 500°C in Fig. 3. Since the agreement among them is approximately good, the particle size distribution of aerosols formed by the fast chemical reaction of gas can be evaluated from the self-preserving distribution function as time proceeds.

Figure 10 shows the effect of the initial vapor concentration introduced into the particle production system. At the outlet of the furnace, the shapes of the size distributions are found not to change, but the average sizes tend to increase with the initial vapor concentration as shown in the experimental results of Fig. 4.

Figure 11 shows the change in size distribution of seed particles under two different reaction rates. Here, monodisperse particles 0.2 μm in diameter and 2.4×10^6 cm^{-3} in number concentration are introduced

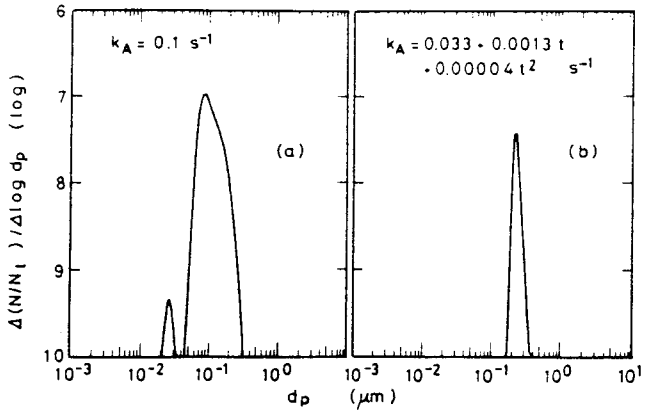

Fig. 11. Particle size distribution, starting with an initial TTIP concentration of 5.25×10^{-10} mol cm^{-3} and 0.20-μm seed particle concentration of 2.4×10^6 cm^{-3} at time 50 s: (a) $k_A = 0.1$ s^{-1}, (b) $k_A = 0.033 + 0.0013t + 0.00004t^2$ s^{-1}.

initially as seed particles. Figure 10(a) with $k_A = 0.1$ s^{-1} clearly shows that fresh newly nucleated particles overwhelm the growth of seed particles. It is, however, evident from Fig. 10(b) with a lower reaction rate of $k_A = 0.033 + 0.0013t + 0.00004t^2$ that nucleation of new particles can be quenched with a low and gradually increasing reaction rate. This trend is consistent with the experimental results of Figs 6 and 7. It is seen that the use of seed particles does not guarantee that particles can be grown by vapor and cluster deposition since nucleation can still exist in the presence of seeds.

It is extremely difficult to obtain the simulation results which will be able to be accurately compared with the experimental results because the dependence of the reaction rate constant k_A on the temperature is unknown and the diffusive loss of vapor and particles is not considered. The accurate evaluation of the reaction mechanism and the simulation of diffusion equation including particle formation and growth will enable one to explain the experimental results under various conditions.

CONCLUSIONS

The production of fine TiO_2 particles by thermal decomposition of TTIP vapor verified the feasibility of controlling the properties of the final product aerosol by changing the temperature profile, initial vapor concentration, and seed particle conditions. The experimental results are qualitatively consistent with the predictions by the discrete-sectional aerosol GDE. The results show that: (1) a higher inlet precursor concentration leads to a larger final mean particle diameter for a given reactor temperature, (2) a gradually increasing temperature profile produces a narrower particle size distribution compared to a decreasing- or constant-temperature profile, and (3) seed growth is dominant over the formation of new particles at low reaction rates.

Acknowledgements—This work was supported by National Science Foundation Grant ATM-8503103, Saneyoshi Research Fund and Grant-in-Aid for Scientific Research 62470110.

REFERENCES

Friedlander, S. K., 1977, *Smoke, Dust and Haze*, p. 196. John Wiley, New York.

Friedlander, S. K., 1983, Dynamics of aerosol formation by chemical reaction *Ann. N.Y. Acad. Sci.* 354–382.

Friedlander, S. K. and Wang, C. S., 1966, The self-preserving particle size distribution for coagulation by Brownian motion. *J. Colloid Sci.* **22**, 126.

Gelbard, F. and Seinfeld, J. H., 1979, The general dynamic equation of aerosols. *J. Colloid Interface Sci.* **68**, 363–382.

Gelbard, F., Tambour, Y. and Seinfeld, J. H., 1980, Sectional representations for simulating aerosol dynamics. *J. Colloid Interface Sci.* **76**, 541–556.

Kanai, T., Komiyama, H. and Inoue, H., 1985, TiO_2 particles by chemical vapor deposition–particle formation mechanism and chemical kinetics. *Kagaku Kogaku Ronbunshu* **11**, 317.

Lai, F. S., Friedlander, S. K., Pich, J. and Hidy, G. M., 1972, The self-preserving particle size distribution for Brownian coagulation in the free-molecule regime. *J. Colloid Interface Sci.* **39**, 395.

Okuyama, K., Kousaka, Y., Tohge, N., Yamamota, S., Wu, J. J., Flagan, R. C. and Seinfeld, J. H., 1986, Production of ultra-fine metal oxide particles by thermal decomposition of metal alkoxide vapor. *A.I.Ch.E. J.* **32**, 2010–2019.

Seinfeld, J. H., 1986, *Atmospheric Chemistry and Physics of Air Pollution*. Wiley–Interscience, New York.

Wu, J. J. and Flagan, R. C., 1986, Submicron silicon powder production in an aerosol reactor. *Appl. Phys. Lett.* **49**, 82.

Wu, J. J. and Flagan, R. C., 1988, A discrete-sectional solution to the aerosol dynamic equation. *J. Colloid Interface Sci.* **123**, 339.

Wu, J. J., Nguyen, H. V., Flagan, R. C., Okuyama, K. and Kousaka, Y., 1988, Evaluation and control of particle properties in aerosol reactors. *A.I.Ch.E. J.* **34**, 1249.